NASA-CR-197204

NASw-4435

IN-18-CR
26188
P-270

# ASPOD
# Modifications of 1993-1994

Dr. Kumar Ramohalli

Edited by Jennifer J. Jackson

N95-12698

(NASA-CR-197204) ASPOD
MODIFICATIONS OF 1993-1994 Final
Report (USRA) 270 p

Unclas

G3/18 0026188

# Table of Context

1. Summary 1

2. Acknowledgments 2

3. Introduction 3

1. The Tilt Table 4

2. ASPOD Solar Cutting Array Design Project
   Preliminary Report

3. ASPOD Solar Cutting Array Design Project
   Final Report

4. Controls for Robotic Arm

5. Proposed Redesign for ASPOD's Solar Tracking Device

6. Autocad drawings of this years design

# Summary

ASPOD, Autonomous Space Processors for Orbital Debris, provides a unique way of collecting the space debris that has built up over the past 37 years. For the past several years, ASPOD has gone through several different modifications. This year's concentrations were on the solar cutting array, the solar tracker, the earth based main frame/tilt table, the controls for the two robotic arms, and accurate autocad drawings of ASPOD. This final report contains the reports written by the students who worked on the ASPOD project this year.

# Acknowledgments

At this time I wish to thank Vicki Johnson for all her help throughout the past year. She took the time to answer all my questions. My thanks are also extended to the staff at NASA/USRA, especially, Cissy Novak, Sue McCowen, and Kay Nute. I also wish to thank our mentor Dr. Kim Arron. Our thanks also goes out to Gordon D. Ingmire for his support and help. And last but not least, I wish to thank all the undergraduates who worked on this project. They all contributed a lot of time and effort and it is greatly appreciated.

# Abstract

This report is a documentation of the synthesis and analysis process involved in the actual fabrication of a heavy duty prototype tilt table. The mechanism itself is intended to provide two axes of motion for a solar array that will track the sun from any ground based location. The final product meets or exceeds all listed goals and specifications for the project. Background and purpose of the ASPOD project itself are presented as the context in which the design process occurred.

# Introduction

In recent years, man has become very conscience about recycling and cleaning up the planet. For the past 37 years, man has been in space. During that time, space debris has built up in the most used orbits around earth. There are over 7,000 pieces of space debris circling the earth, that is over 3,000,000 kg worth of debris. Space debris is defined as any piece of space material that is no longer in use. This includes spent booster rockets, old satellites, paint flecks, and any debris caused by the collision of other objects. Space debris comes in many shapes and sizes. The majority of space debris are pieces under 10 cm. ASPOD will not be concerned with this type of space debris, it will be concerned with trackable debris, any debris greater than 10 cm. ASPOD will collect the larger space debris before they become smaller debris that cannot be tracked.

Each ASPOD will collect 10,000 lb. of space debris. To collect the space debris, ASPOD will use two robotic arms to grab the debris and bring it into the focal point of the solar cutting array. Each mission for ASPOD will depend on where the debris being collected is located. Once the debris is collected, ASPOD has four options as to what to do with the debris. First, ASPOD could rendezvous with the space shuttle and have the shuttle bring the debris back to earth to be studied or recycled. Second, ASPOD could rendezvous with the space station and leave the debris there to be studied or recycled in space. The third option is to have ASPOD burn up during reentry. The last option is to have ASPOD splash down in the ocean and retrieved similar to the Mercury missions.

# ASPOD - BASE AND TILT TABLE

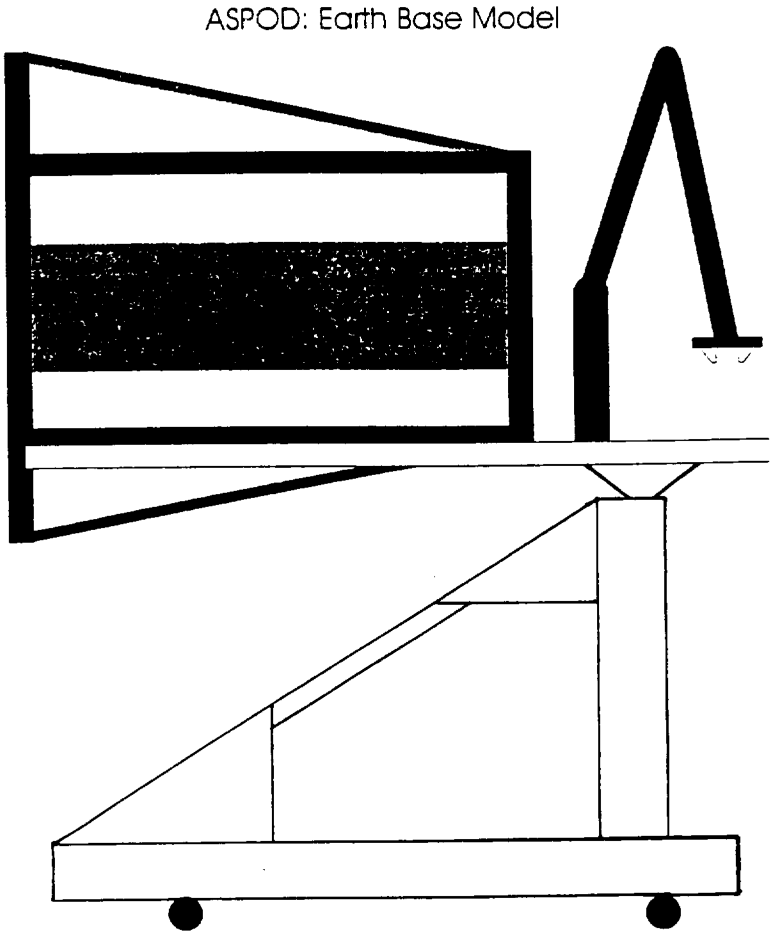
ASPOD: Earth Base Model

TERM DESIGN PROJECT

by
PAUL W. FOGARTY

AME 352
May 4, 1994

# Overview of the ASPOD Project

ASPOD (Autonomous Space Processor for Orbital Debris) is an ongoing project under the support of NASA/USRA with the general mission of perfecting a feasible means of clearing large size debris from earth's orbit. At the time of this assignment, the goal of the ASPOD lab was to provide a ground based version of such a device with three primary capabilities: (1) to track and follow the sun, providing a stable operating surface for processing of materials; (2) to use a solar array (i.e. mirrors and lenses) as a cutting tool to take advantage of the sun's freely available energy; (3) to demonstrate use of two or more robotic arms capable of seizing, holding and manipulating a variety of space debris (i.e. expended boosters, old satellites). The first of these capabilities is addressed by the design and model presented in this report.

# Tables And Graphs Employed

**Dynamics of Machines (DOM) Data:**

Table A - Range of angles used to calculate motion and force relations for all pins and links.

Tables B and C - Proof of no need for dynamic analysis based on angular velocities and accelerations near zero.

Tables D, E and F - Iterations to find range of crank input angles based on known table geometry.

Figures A, B and C - Angular relations of links based on input angle of crank.

Figures D and E - Proof of negligible nature of dynamic forces on mechanism.

Figure F - Mechanical advantage of linkage based on input angle. (Some room for improvement at lower values of theta 2).

Figure G - Velocity ratio for linkage.

Figure H - Representative table velocity based on velocity at instant center 3,4 at 100 times maximum omega.

Figure I - Range of motion for linkage.

**Spreadsheet Data:**

Table 1 - Range of link angles related to table top angle.

Tables 2, 3 - Constants used in calculations.

Table 4 - Forces in all links and pivots and transmission angle of screw.

Table 5 - Torque and power calculations for motor requirement.

Figure 1 - Table top orientation versus crank input angle.

Figure 2 - Coupler tension versus tabletop orientation. (Same as Resultant at C).

Figure 3 - Resultant forces at joints A and D.

Figure 4 - Forces on screw versus screw length (for possible considerations of buckling).

Figure 5 - Screw axial force versus table top angle (to identify ideal operating range).

Figure 6 - Torque in screw versus table position.

Figure 7 - Base power requirements to turn screw versus table position.

**Other Figures:**

Figures I, II and III - Three-way view of ASPOD.

Figure IV - First synthesis method for linkage.

Figure Zero - Primary Reference and Specifications

# Introduction

Goal: To design a tilting and rotating table mechanism with the ability to track the sun and support a heavy load over a full range of positions.

**Specifications:**

1) Table must be able to tilt 90 degrees from a vertical to a horizontal position.
2) Table must be able to rotate 360 degrees about a pivotal point normal to the table surface.
3) Entire structure must be stable and rigid in any position allowed by its motion.
4) Tilt and rotary motion must be fast enough to track the sun without falling behind.
5) Entire assembly should be self-contained.
6) Where possible, weight should be reduced and space consolidated.
7) Aesthetic considerations for presentation purposes should be made where not interfering with other constraints.
8) Minimize cost. Preliminary budget: $500.00.

## Task Outline:

It is the specific task of the design presented here to create a tilt table assembly that is strong, rigid, stable and capable of providing controlled motion with two degrees of freedom. One degree of freedom is provided by a rotating table top assembly capable of 360 degrees of motion. The second degree of freedom is in a 90 degree table tilt as measured from a 0 degree vertical table surface. Additional extras of the design include a substantial reduction in weight from the previous model, on board locations for all control and power sources; easier transportation and breakdown of ASPOD into two self-contained parts and substantial improvements in the structures rigidity and stability.

It is a key feature of the device that it was designed as a ground based model that tracked the sun. As a result of this, there has been no need or desire for any moving parts of the structure to acquire velocities requiring a dynamic analysis in the classic sense. As an indication of the truth of this conclusion, a direct measure of maximum table tip velocity with both motors running at peak 90 volt capacity results in a speed of more or less 0.0 in/s. When one considers the masses of the parts it becomes self evident that a point by point static analysis is of far more value. In addition, calculations of jerk do not enter into the picture due to the nature of the motor control programming. This arrangement relies on direct feedback from a photo sensing solar tracker which, by use of operational amplifiers, modulates motor power input along a continuous scale. In other words, as the tracker goes out of alignment --a slow process at approximately 15 minutes of arc per minute--the power to the proper motor increases or decreases accordingly from 0 to 90 volt input.

At the time this project was begun, an existing mechanism for tilt and rotation was already in place. Due to the serious flaws in this model, it was concluded that either modification or complete replacement was in order. A list of problems with this model as well as a set of preliminary redesigns is attached at the end of this report. During the design process all teams on the overall project were consulted with a view toward heading off possible unforeseen conflicts (e.g. effect of new design on robot arms' range of motion). It was concluded based on a review of the options presented that complete redesign provided the most attractive alternative. The first level of design addressing the tilt mechanism was based on numerous cardboard models where the relative link lengths and positions were first approximated and then later perfected. Toward the end of actual prototype synthesis many last minute decisions were made based on material availability and time constraints for project completion. It was left for final analysis to check the results of these modifications.

## Design Description

The final design consists of a modified "A" frame base with two vertical uprights supporting the primary pivot bar for the table top. The uprights are in turn supported by brackets, 1/4 inch triangular plates and two stabilizing bars that also serve as frame support for a control equipment housing. At all stages of table tilt and rotation there is ample clearance between the table and base.

The tilt mechanism itself consists of a standard four bar linkage arranged as follows (See detailed sketch or actual mechanisms). The crank consists of two 1/4 inch plates of aluminum pivoting at both ends on bicycle hubs. In between the two hubs about 3 1/2 inches from the coupler link lies a pivoting 3/4 inch nut through which all power is transmitted. The coupler consists of a simple bar of 1 inch aluminum box tubing with solid aluminum clamps at both ends mounting onto bicycle hubs. The rocker is itself continuous through a variety of mechanisms with the tilt table itself. At one end it consists of two triangular parallel plates of 1/6 inch aluminum riding on a bicycle hub. At the other end, it consists of a 20 lb. steel bar pivoting on 2 inch industrial bearings cases where the bulk of the table in eight is supported.

The driving source for the tilt table comes from a single motor and reduction gearbox mounted between the two primary uprights of the base frame. It should be pointed out that, since the output shaft is perpendicular to the pivoting axis no additional bending moments should arise.

The motor has a power output rating of 1/8 hp and the gear reducer is at 525:1. Attached to the motor, via an aluminum sleeve and tap screws, is a nineteen inch drill steel driving screw of 3/4 inch diameter with eight turns to the inch.

## Preliminary to Analysis:

Due to the fact that an end product was being worked with by the time of this write up, all measures taken for the final analysis process were taken directly from the tilt table itself. Measures were taken three times using rulers, a level and protractors with the data averaged. Based on the near exact reproduction of values for each set of measurements, length accuracies of 0.05 inches were expected. Measures were obtained with the table in full horizontal position.

## Kinematic Analysis:

Using varying input angles for theta 2 in the Fourbar program, theta 4 was checked until the known value for theta 4 (34.507 degrees, where table is in full upright position) was obtained. See the primary figure to see how these angles were first approximated graphically. Once the minimum value for theta 2 was obtained with respect to the ground link, the maximum value was obtained by the same process. For this calculation, theta 4 (table horizontal) was established at

124.507 degrees.

An initial position analysis using steps of 5 degrees was made giving a full range of positions from theta 2 minimum to a 2 maximum. Plots of static forces for all links over the given range were not obtainable from the DOM program requiring separate programming. However, printouts of data from DOM were possible over the full range for angles, theta, angular velocity, omega, and angular acceleration, alpha. Examination of this data should be sufficient to justify the prediction that a dynamic analysis of the mechanism was unnecessary.

The following spreadsheet and graphs are designed to show the forces operating in all components of the mechanism during regular full range operation of the tilt table. The data as presented suggest some possible areas for design improvement. Given position data for the fourbar equivalent mechanism from DOM, measures of center of mass location for the table and the tabletop angle it was possible to calculate forces in all links and joints. Starting with the ground rocker link, D, and the displacement angle between the ground link and true vertical (i.e. gravitation vector) moments about this point were used to calculate tension in the coupler. Since the coupler was a continuous piece, forces in the coupler were then used to calculate moments about the ground-crank link and resulting screw forces. The final step in force balance calculations was to determine all forces and reactions in terms of the input from the screw. This last step in turn made it possible for all motions in the fourbar equivalent linkage and table to be graphically interpreted in terms of motor/screw input.

AMPAD 22-141 50 SHEETS
22-142 100 SHEETS
22-144 200 SHEETS

# Tilt-Table Design Front view Figure I

[illegible] Base [illegible] [illegible] [illegible] lbm

with [illegible] [illegible] [illegible] lbm

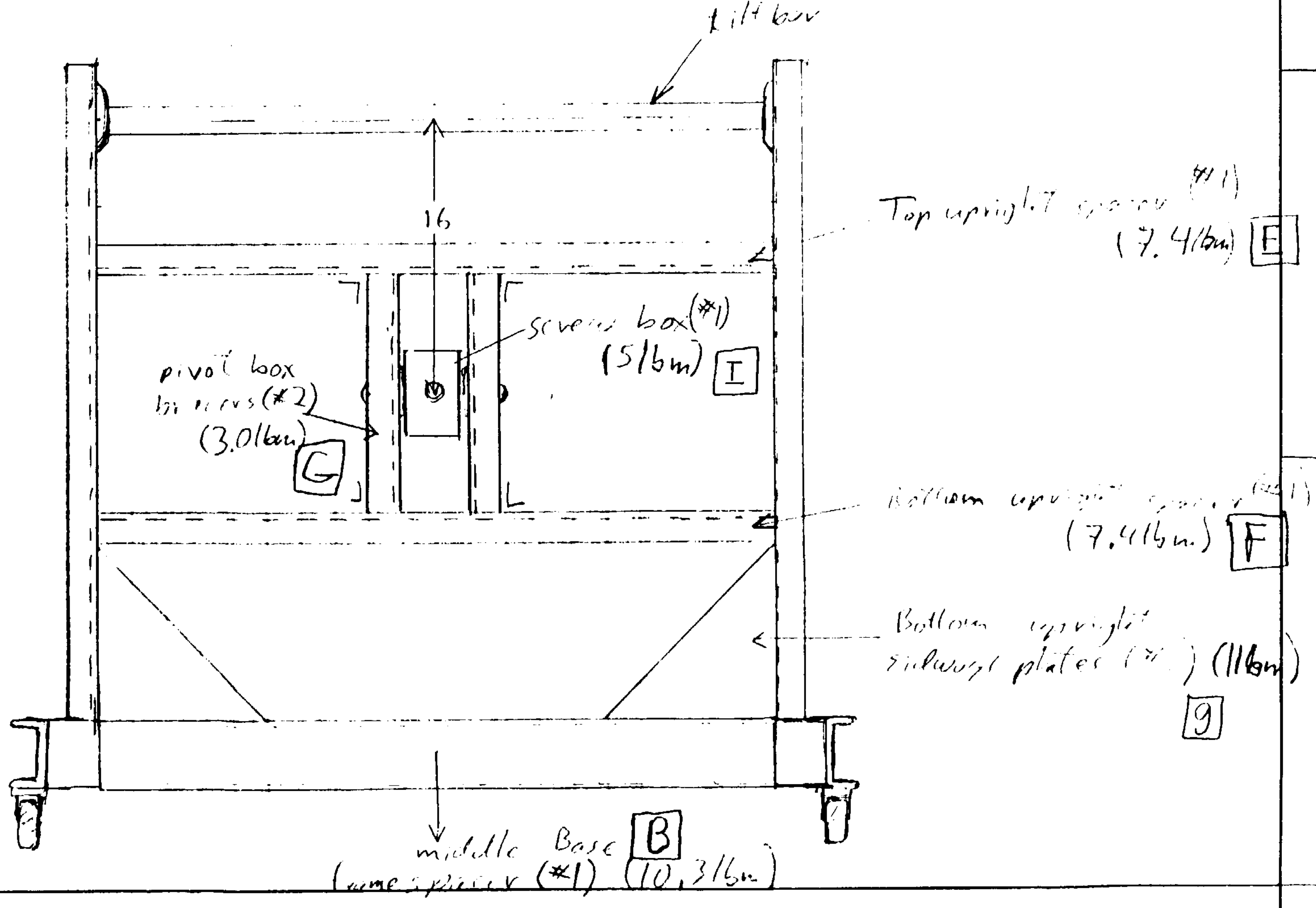
tilt bar
16
Top upright spacer (#1)
(7.4lbm) E
screw box (#1)
(5lbm) I
pivot box braces (#2)
(3.0lbm) G
Bottom upright spacer (#1)
(7.4lbm) F
Bottom upright sideways plates (#2) (11lbm)
g
middle Base B
(same spacer (#1)) (10.3lbm)

ORIGINAL PAGE IS OF POOR QUALITY

# Tilt-table Design Topview Figure II

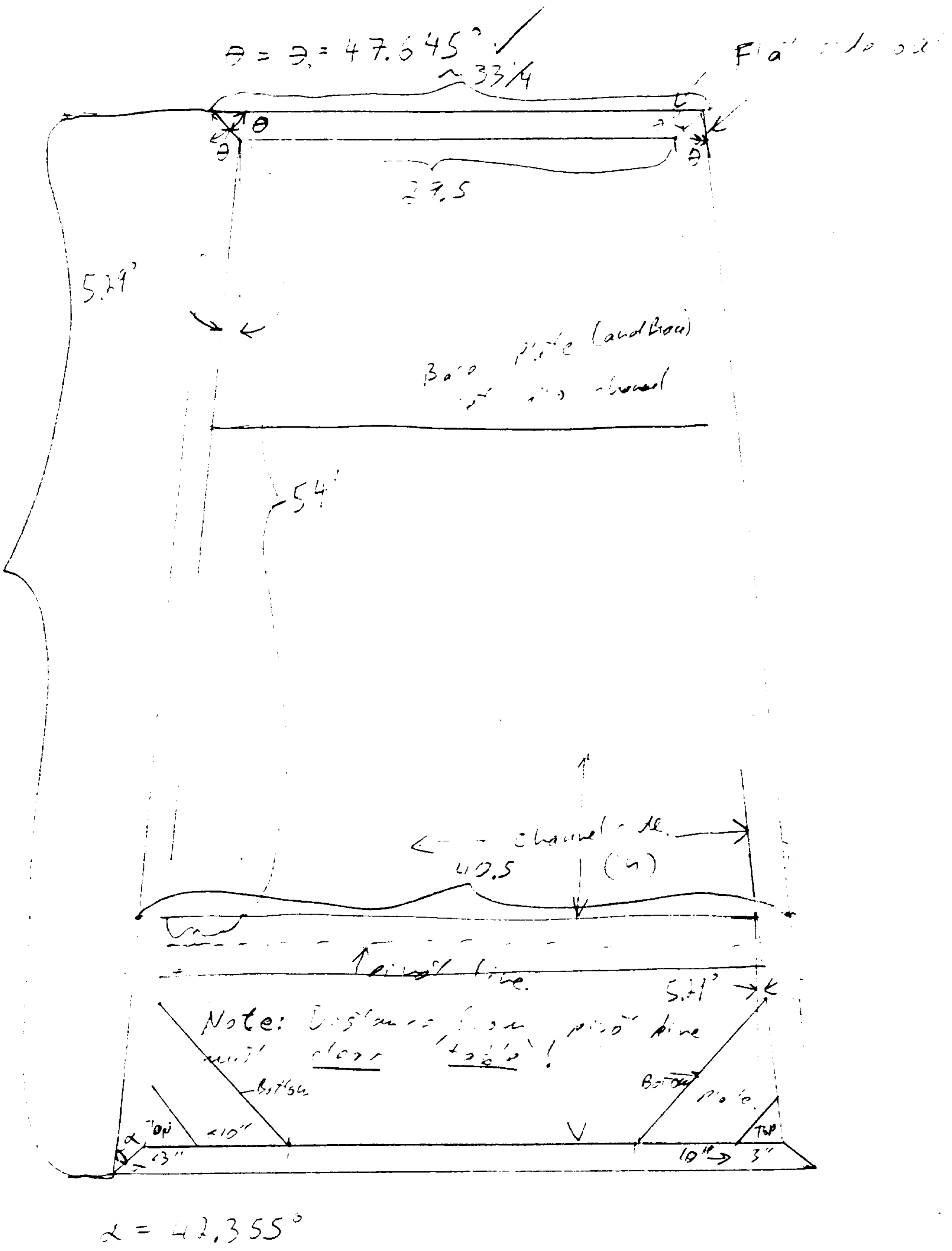
θ = θ₁ = 47.645° ✓
~33 1/4
Fla[illegible]
θ
θ
θ
27.5
5.29'
Base Plate (and Base)
[illegible] channel
54'
74"
channel [illegible]
(4)
40.5
Pivot line.
5.41'
Note: Distance from pivot line until clear table!
Bottom
Bottom
Plate.
Top
<10"
<3"
10"
3"
Top
α
α = 42.355°

ORIGINAL PAGE IS
OF POOR QUALITY

# Tilt-Table Design Side view Figure III

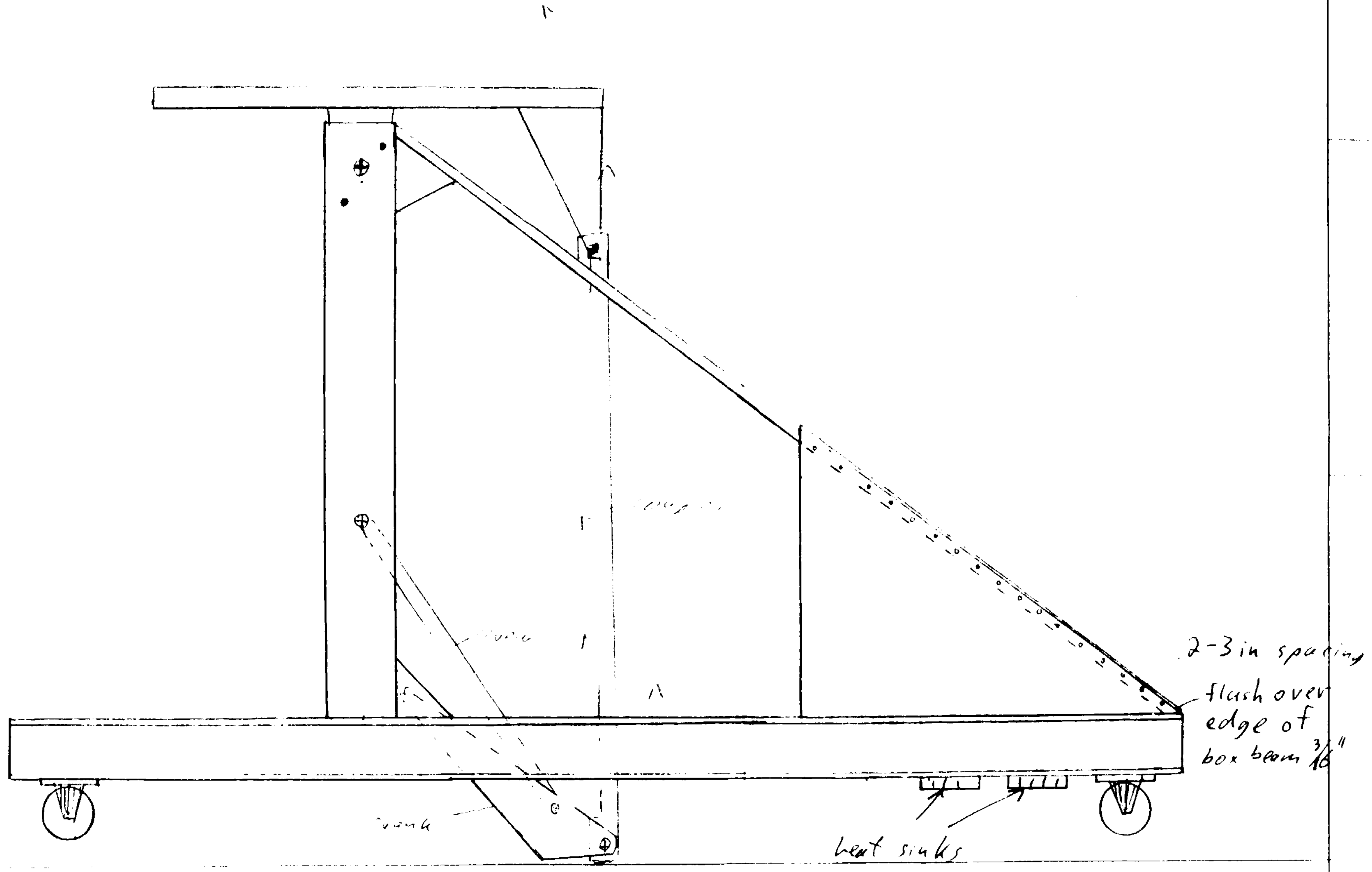
2-3 in spacing
flush over edge of box beam 3/16"
heat sinks
crank

ORIGINAL PAGE IS
OF POOR QUALITY

# Second stage synthesis method.

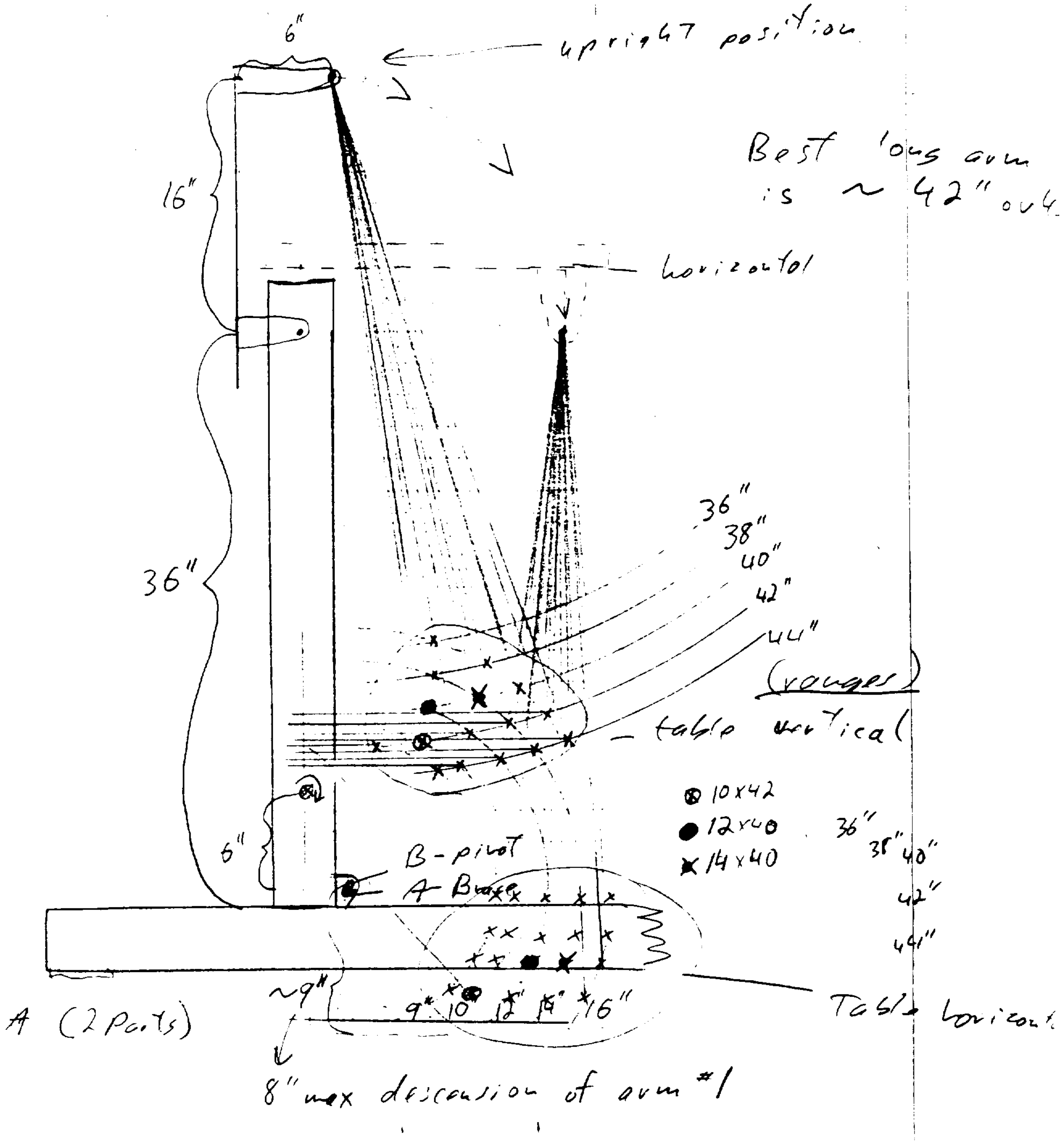
6"
upright position
Best long arm is ~ 42" out
16"
horizontal
36"
36"
38"
40"
42"
44"
(ranges)
table vertical
⊗ 10x42
● 12x40
✕ 14x40
36" 38" 40" 42" 44"
6"
B-pivot
A-Base
Table horizontal
~9"
9" 10" 12" 14" 16"
A (2 Parts)
8" max descension of arm #1

using 12" and 40" arms
screw length will vary from:
9" to 17"

maximum screw length ~ 16"
minimum 4"

ORIGINAL PAGE IS
OF POOR QUALITY

Figure IV Range of Motion Synthesis Process

FOURBAR 5.1 Angle or Link 2 Degrees

Paul W. Fogarty
Design # 1
04-30-1994
12:41

L1 = 31.15 Inches
L2 = 16.5
L3 = 31.25
L4 = 18.58

Cognate # 1
Grashof = Y
OPEN

Cplrpt = 0
@ 0 deg

w2 = .002 Rad/Sec
10.37 to 136 Deg
by 5 Deg

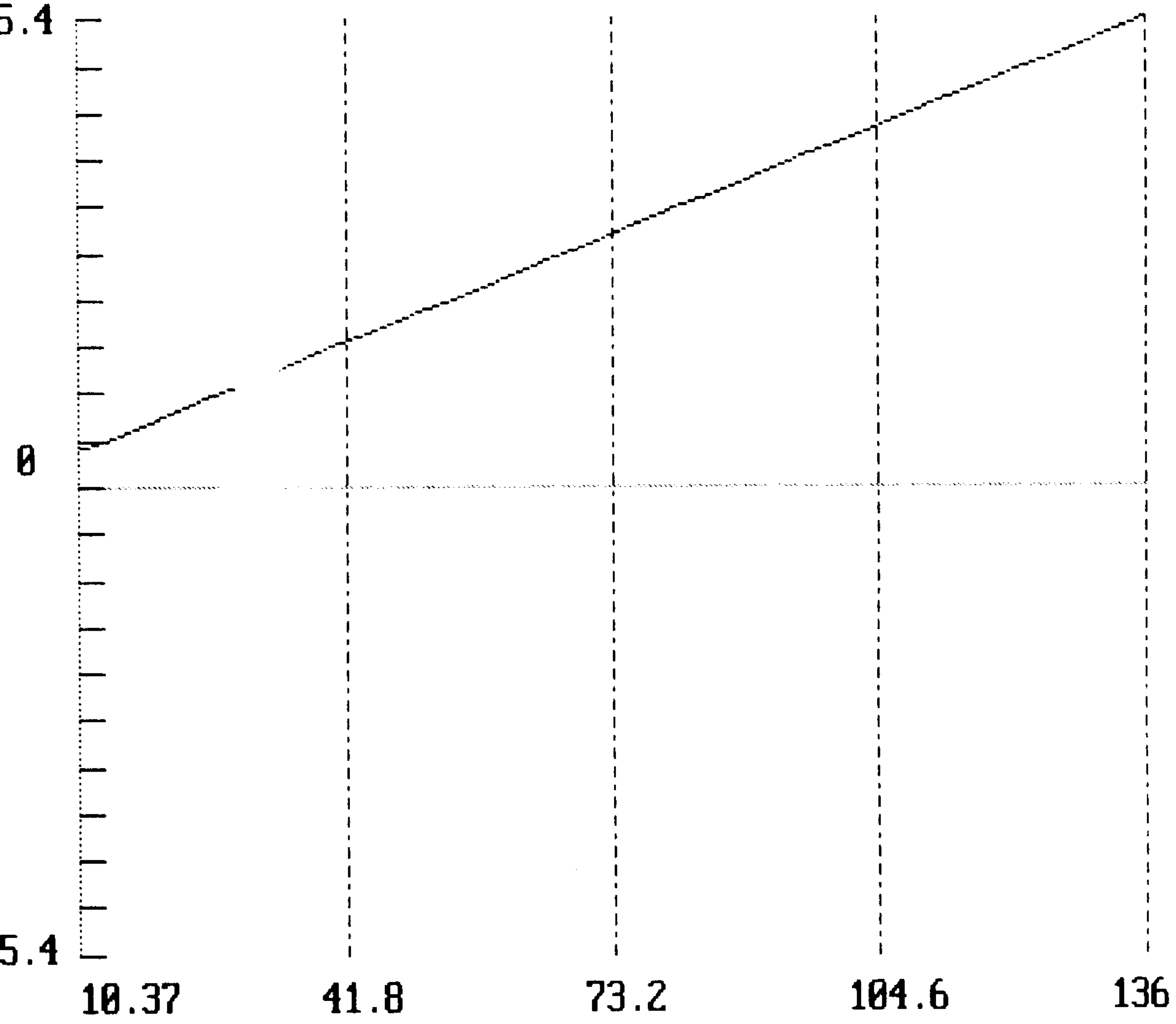

Figure # *A* Title *Range of $\theta_2$ Based on Constant $\omega_2$ Input*

```
FOURBAR 5.1           Angle  for Link   3           Degrees           FOURBAR

Paul W. Fogarty                                                        Paul W.
Design #  1                                                            Design
04-30-1994                                                             04-30-1
12:49                                                                  12:52

L1 =  31.15 Inches                                                     L1 =  3
L2 =  16.5                                                             L2 =  1
L3 =  31.25                                                            L3 =  3
L4 =  18.58                                                            L4 =  18

Cognate # 1                                                            Cognate
Grashof = Y                                                            Grashof
OPEN                                                                   OPEN

Cplrpt =  0                                                            Cplrpt =
@  0 deg                                                               @  0 deg

w2 =  .002 Rad/Sec                                                     w2 =  .0
10.37 to 136 Deg                                                       10.37 to
by 5 Deg                                                               by 5 Deg
```

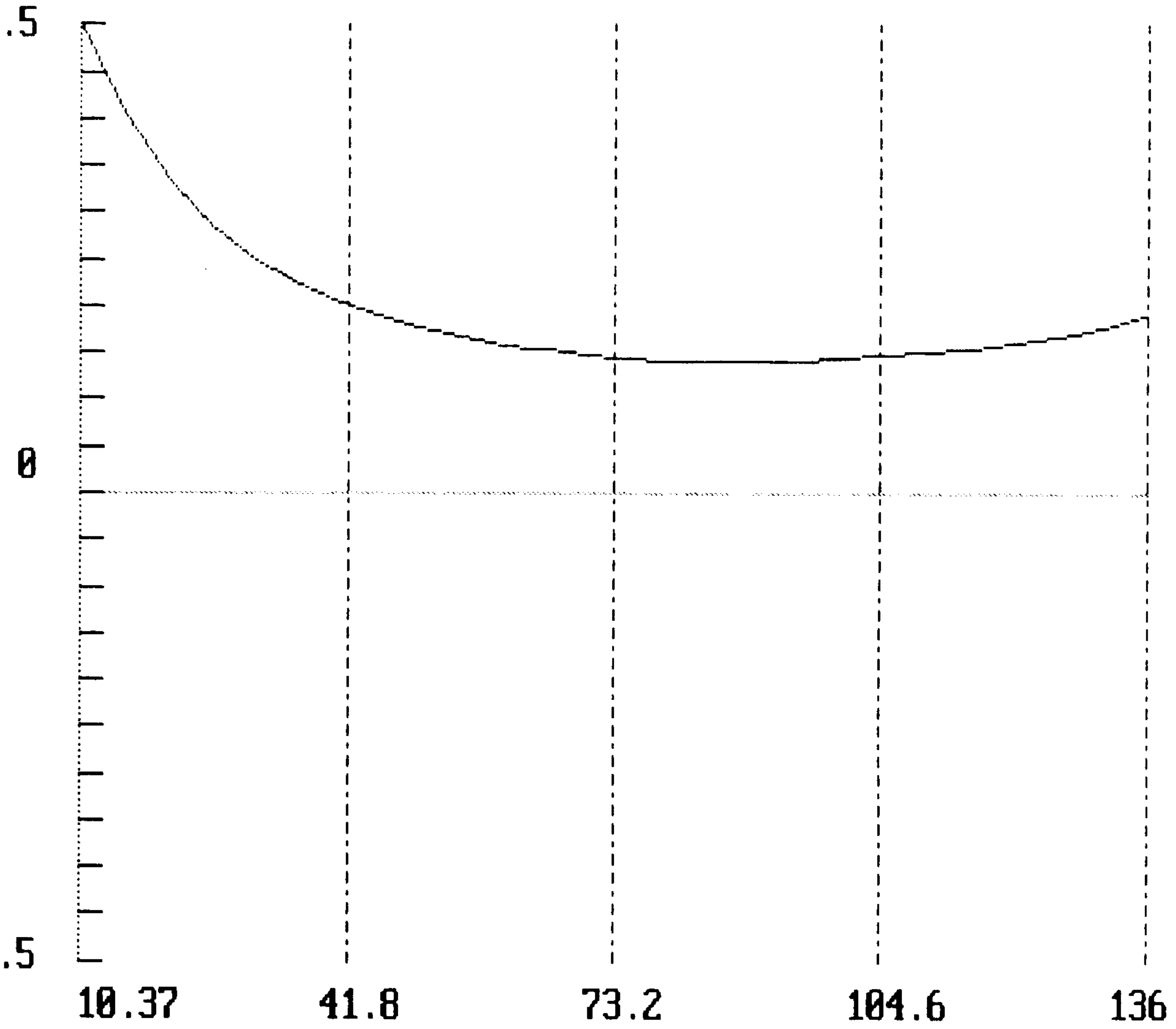

Figure # 6 Title Range of $\Theta_3$ Based on Constant $\omega_2$ Input Figure #

```
FOURBAR 5.1             Angle  for Link   4              Degrees

Paul W. Fogarty 129.3
Design #  1
04-30-1994
12:52

L1 =  31.15 Inches
L2 =  16.5
L3 =  31.25
L4 =  18.58
                    0
Cognate # 1
Grashof = Y
OPEN

Cplrpt =  0
@  0 deg

w2 =  .002 Rad/Sec
10.37 to 136 Deg
by 5 Deg       - 129.3
```

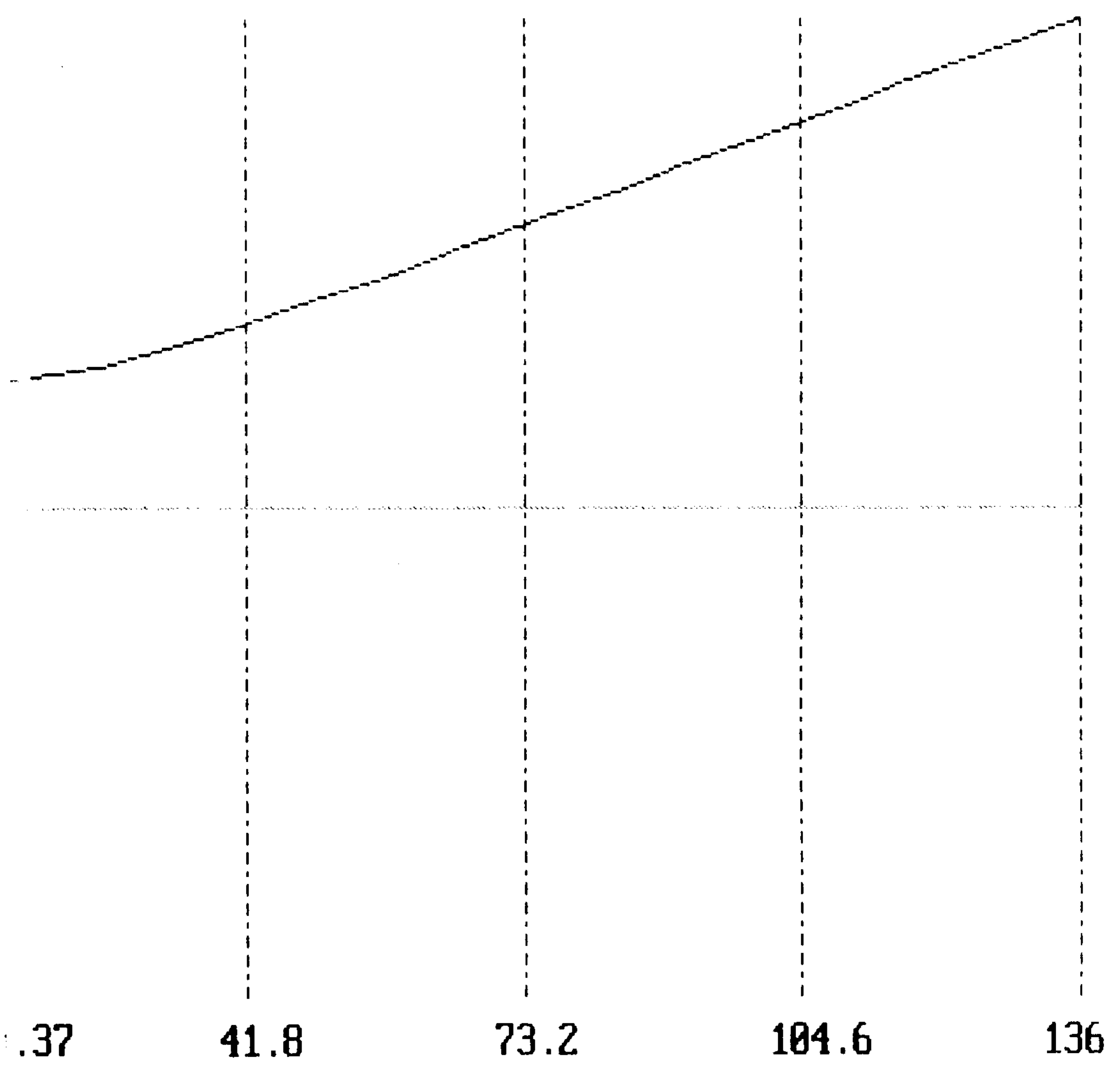

```
F

P
D
0
1

L
L
L
L

C
G
O

C
@

w
1
b
```

Figure # C     Title  Range of $\Theta_4$ based on Constant $\omega_2$ Input     F

```
FOURBAR 5.1            Omega  for Link  4            Radians/Sec

Paul W. Fogarty 0
Design #  1
04-30-1994
12:56

L1 =  31.15 Inches
L2 =  16.5
L3 =  31.25
L4 =  18.58

Cognate # 1
Grashof = Y
OPEN

Cplrpt =  0
@  0 deg

w2 =  .002 Rad/Sec
10.37 to 136 Deg
by 5 Deg       - 0
```

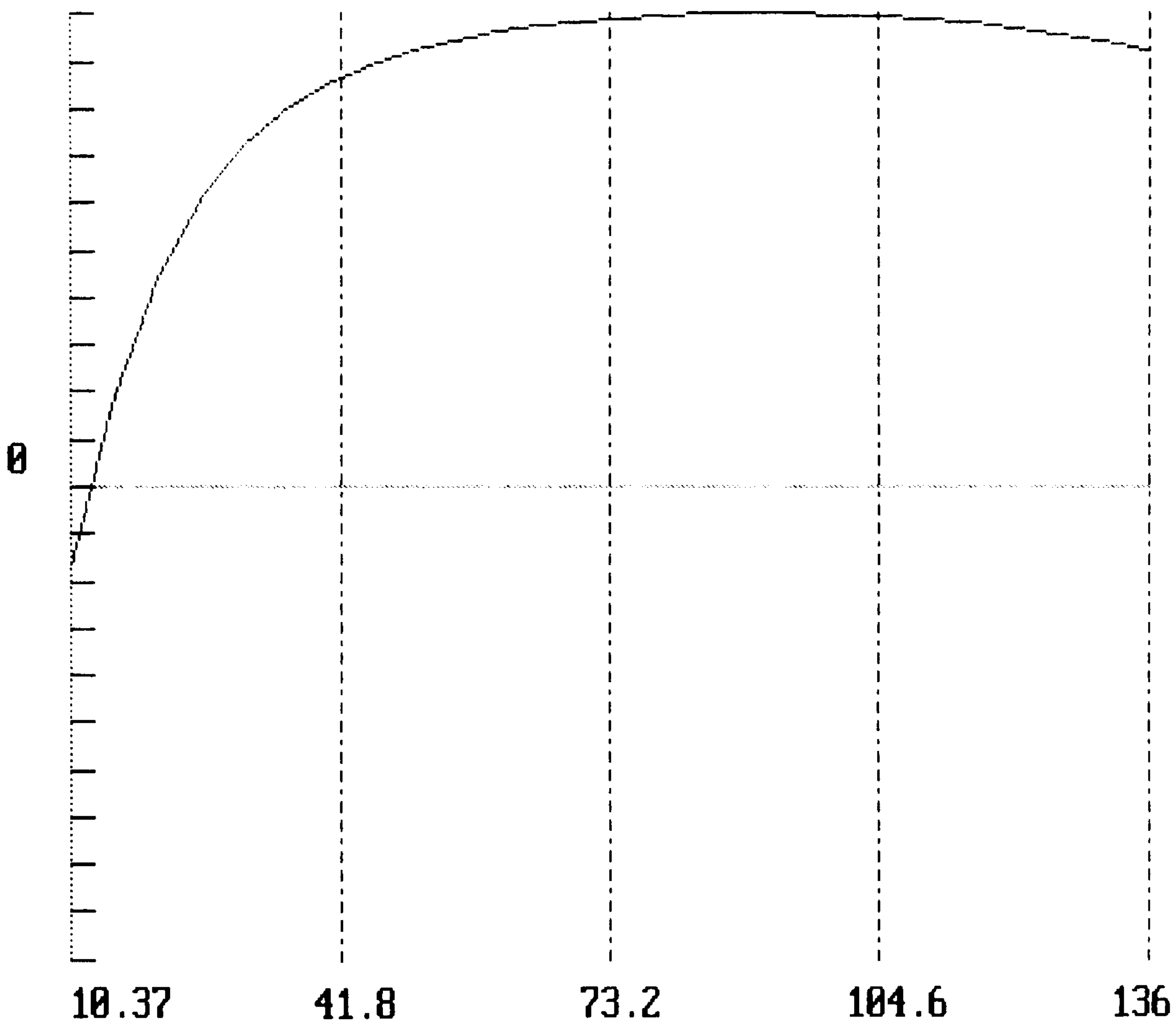

Figure # D    Title Range of $\omega_4$ Based on Constant $\omega_2$ Input

FOURBAR 5.1 Alpha for Link 4 Radians/Sec^2

Paul W. Fogarty 0
Design # 1
04-30-1994
12:59

L1 = 31.15 Inch
L2 = 16.5
L3 = 31.25
L4 = 18.58

Cognate # 1
Grashof = Y
OPEN

Cplrpt = 0
@ 0 deg

w2 = .002 Rad/Se
10.37 to 136 Deg
by 5 Deg -

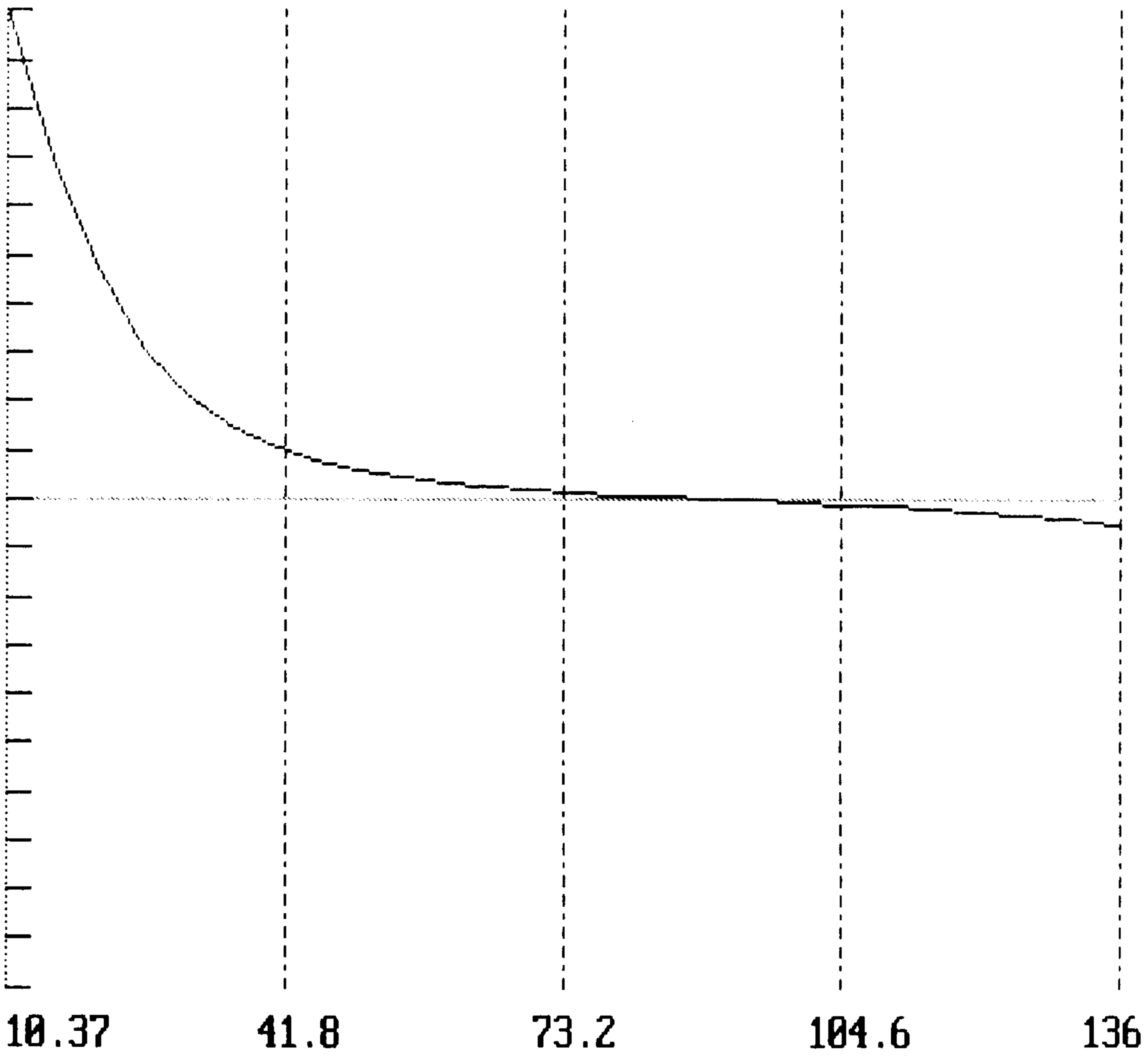

Figure # E tle Range of $\alpha_4$ Based on Constant $\omega_2$ input

FOURBAR 5.1 Mechanical Advantage Dimensionless

Paul W. Fogarty 7
Design # 2
04-30-1994
13:25

L1 = 31.15 Inches
L2 = 16.5
L3 = 31.25
L4 = 18.58

Cognate # 1
Grashof = Y
OPEN

Cplrpt = 31.25
@ 0 deg

w2 = .1 Rad/Sec
10.37 to 136 Deg
by 5 Deg - 7

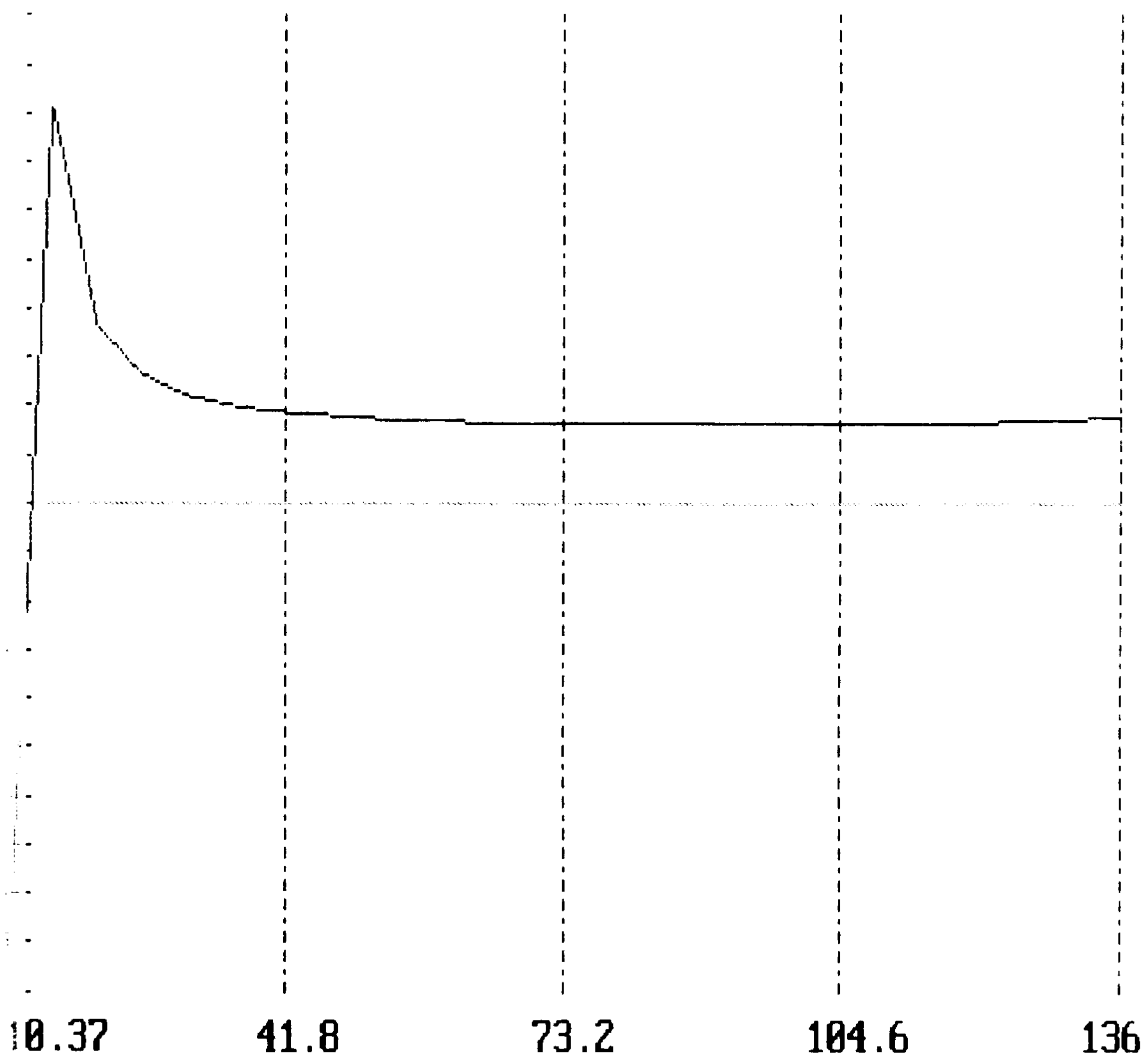

Figure # F Ti Mechanical Advantage Based on Constant $\omega_2$ Input

```
FOURBAR 5.1            Velocity Ratio            Dimensionless

Paul W. Fogarty .9
Design #  1
04-30-1994
13:03

L1 =  31.15 Inches
L2 =  16.5
L3 =  31.25
L4 =  18.58

Cognate # 1
Grashof = Y
OPEN

Cplrpt =  0
@  0 deg
```

≅ 2 in/min tip spd / $I_{23}$

```
w2 =  .002 Rad/Sec
10.37 to 136 Deg
by 5 Deg      - .9
```

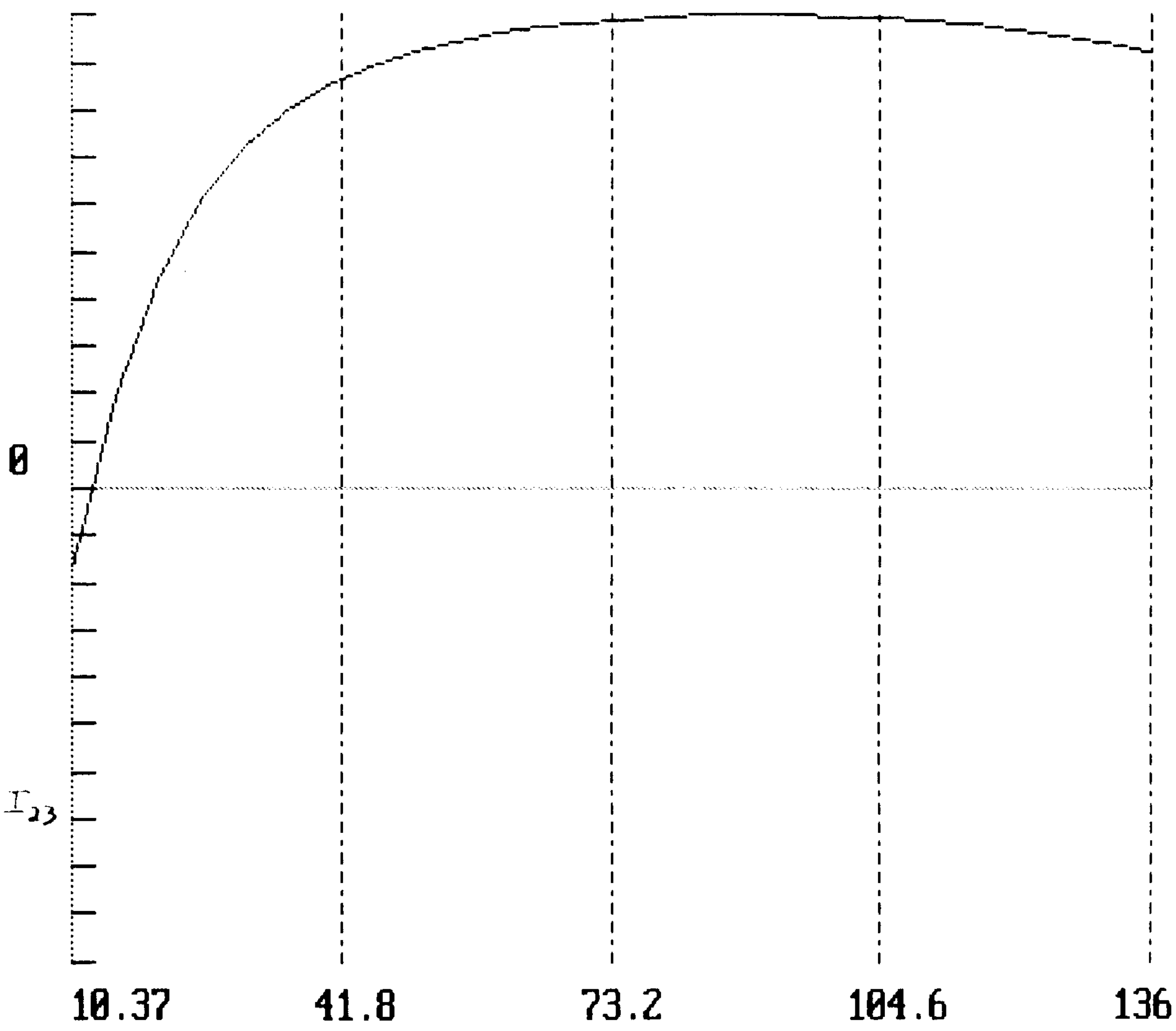

Figure # G     Title Velocity Ratio Based on Constant $\omega_2$ Input

FOURBAR 5.1 Velocity of I 3,4 Inches/Sec

Theta2 = 135

Paul W. Fogarty
Design # 2
04-30-1994
13:15

L1 = 31.15 Inches
L2 = 16.5
L3 = 31.25
L4 = 18.58

Cognate # 1
Grashof = Y
OPEN

Cplrpt = 31.25
@ 0 deg

= 77 in/min tip speed ~

w2 = .1 Rad/Sec
10.37 to 136 Deg
by 5 Deg

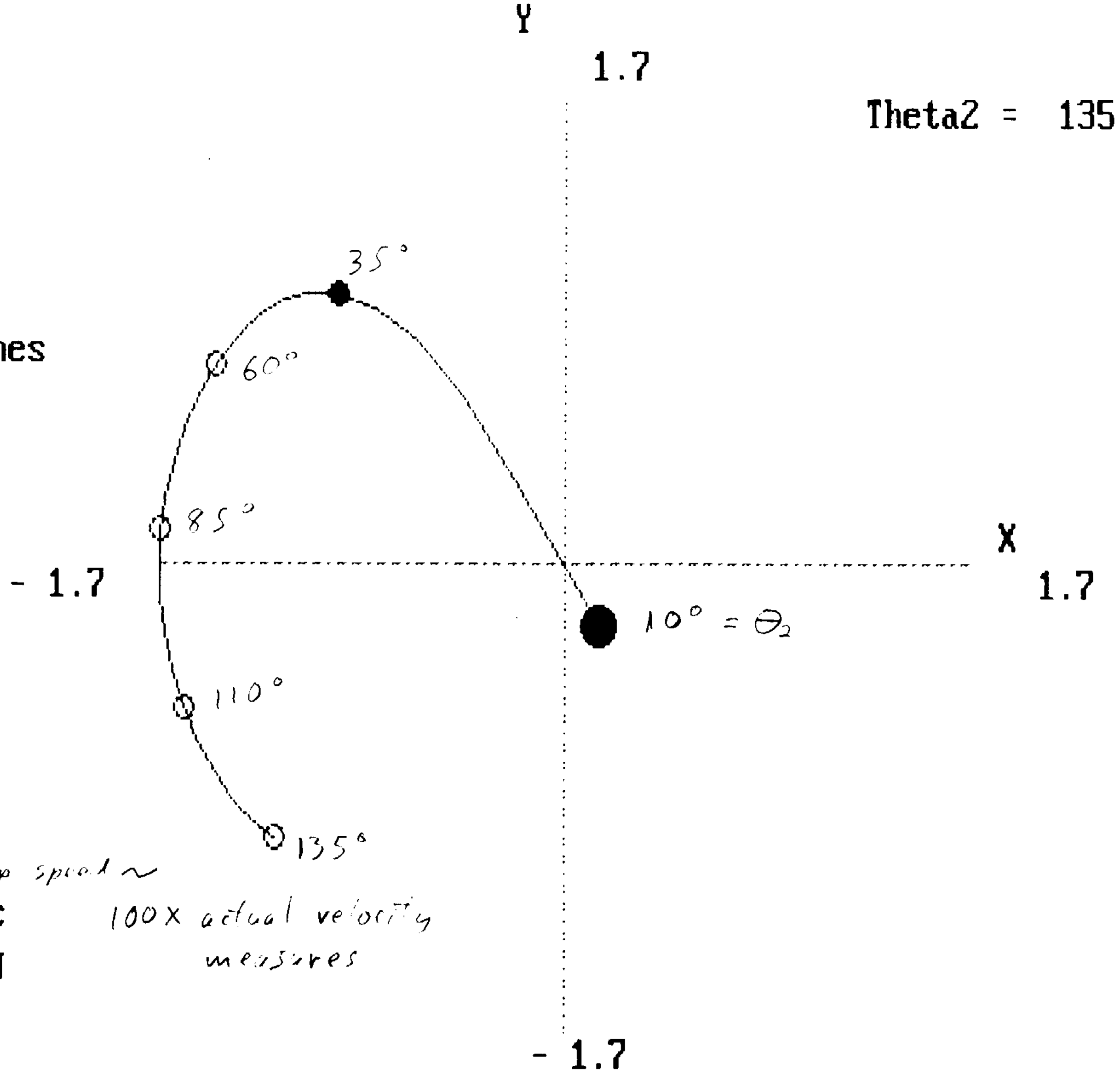

100 X actual velocity measures

Figure # H Title Representative table Velocity X 100 (Given Constant $\omega_2$)

```
FOURBAR 5.1       ASPOD1

Theta2 =  140

Paul W. Fogarty
Design #  2
04-30-1994
13:32

L1 =  31.15 Inches
L2 =  16.5
L3 =  31.25
L4 =  18.58

Cognate # 1
Grashof  = Y
OPEN

Cplrpt =  31.25
@  0 deg

w2 =  .1 Rad/Sec
10.37 to 136 Deg
by 10 Deg
```

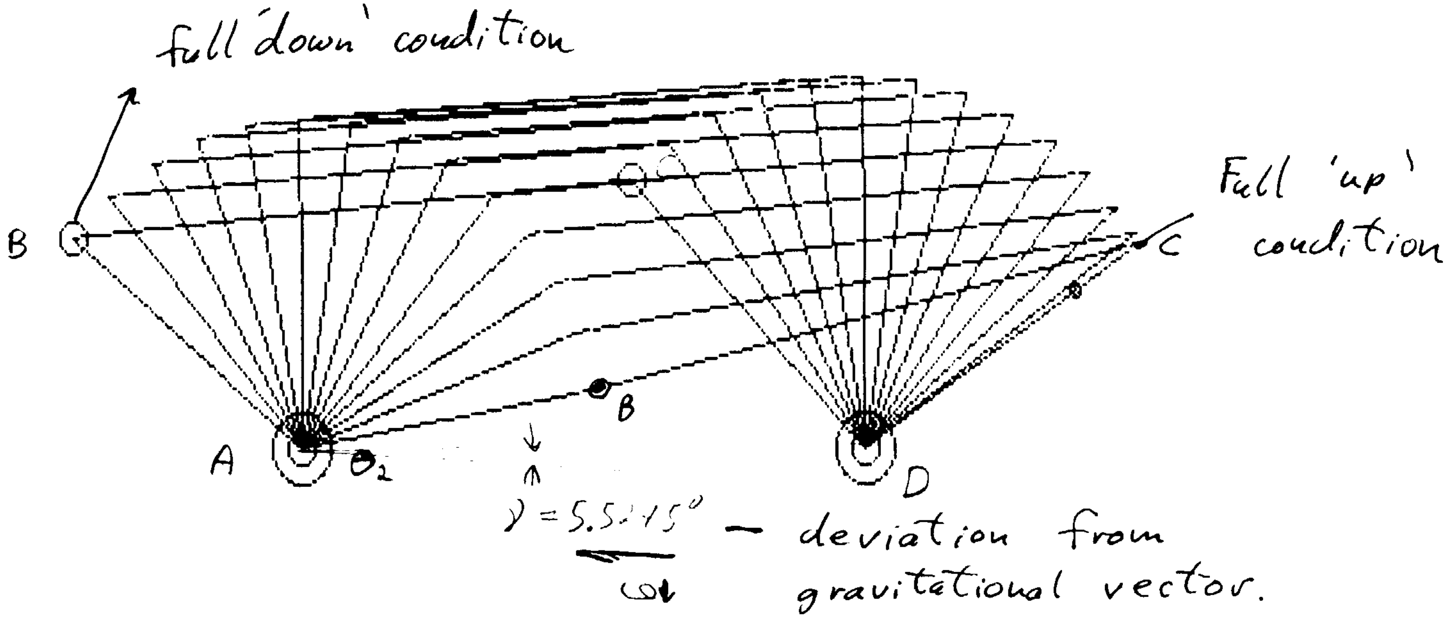
full 'down' condition
B
A
$\theta_2$
B
D
C
Full 'up' condition
$\gamma = 5.5415°$ — deviation from gravitational vector.
ω

Figure # I   Title Animation of Fourbar Linkage by 10° Increments

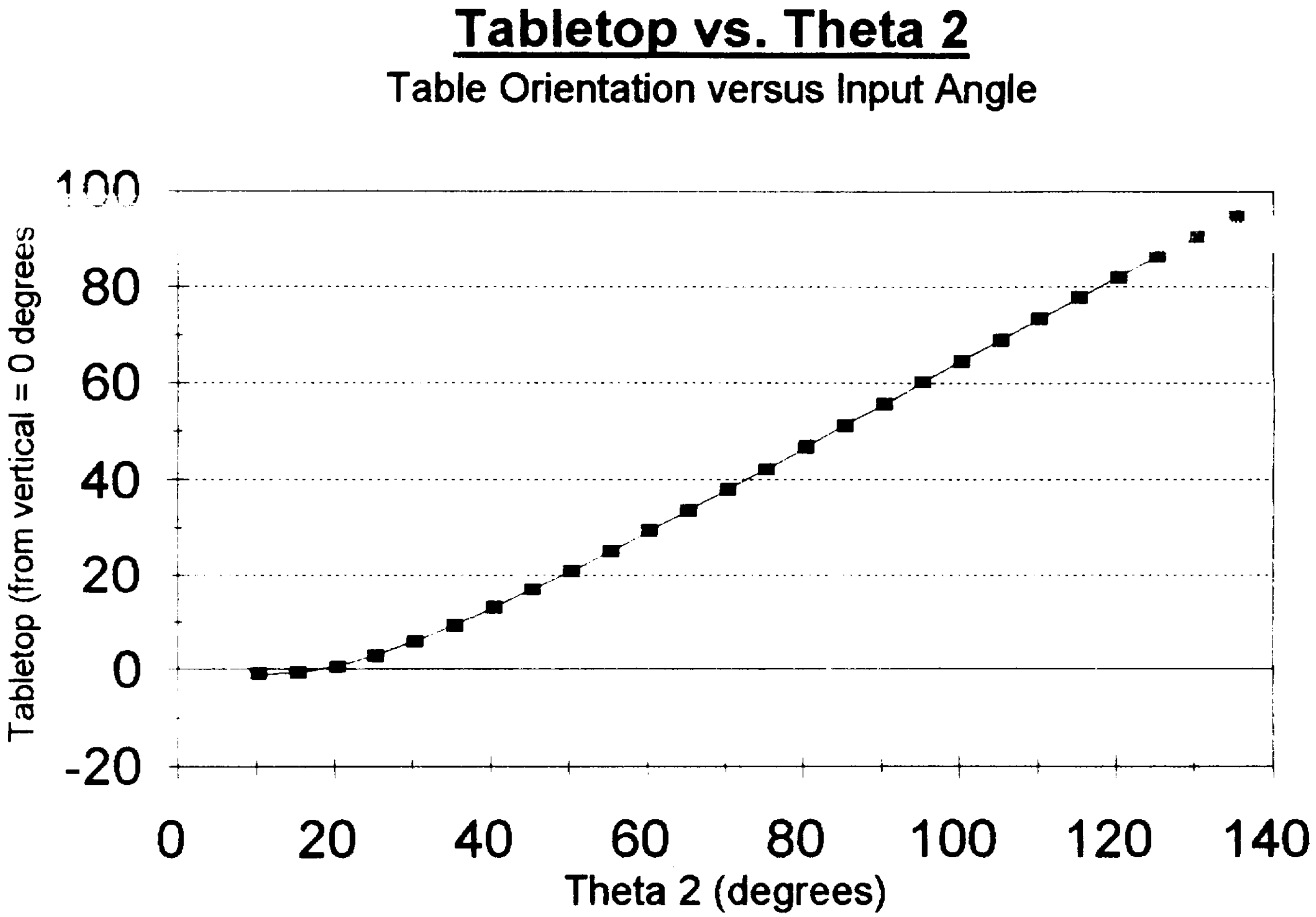
Tabletop vs. Theta 2
Table Orientation versus Input Angle
100
80
60
40
20
0
-20
Tabletop (from vertical = 0 degrees
0
20
40
60
80
100
120
140
Theta 2 (degrees)

Figure 1

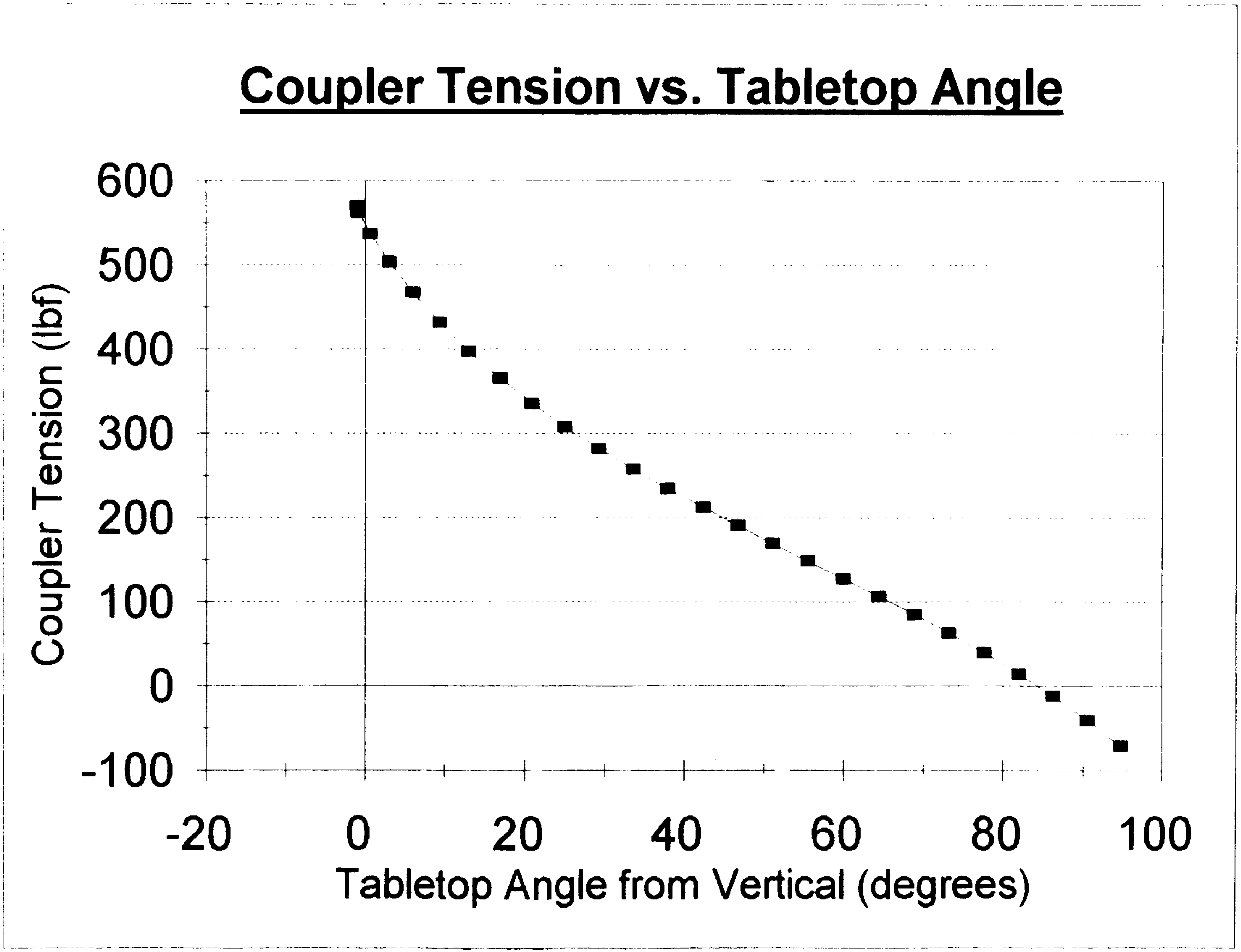
Coupler Tension vs. Tabletop Angle
Coupler Tension (lbf)
600
500
400
300
200
100
0
-100
-20
0
20
40
60
80
100
Tabletop Angle from Vertical (degrees)

Figure II

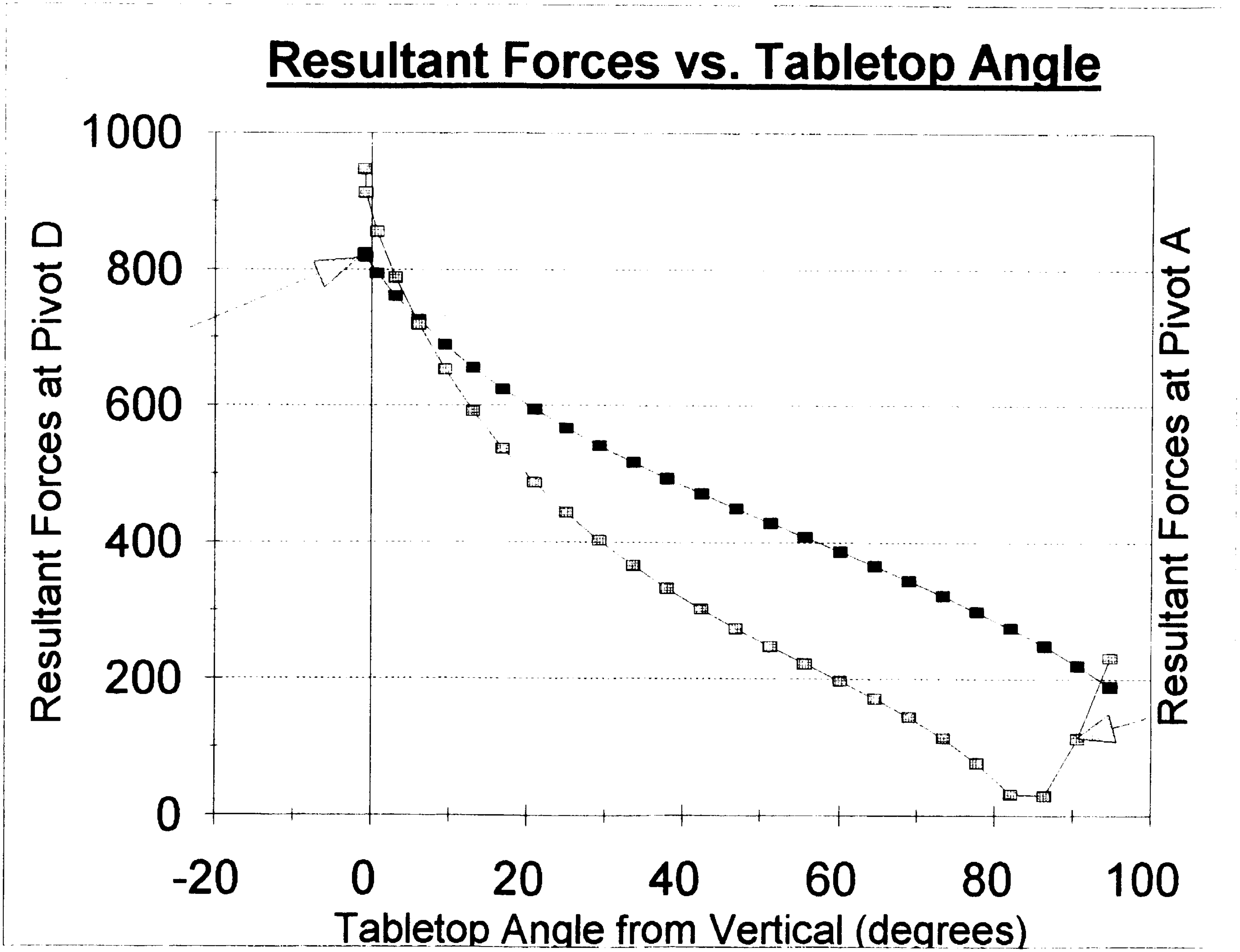
Resultant Forces vs. Tabletop Angle
Resultant Forces at Pivot D
Resultant Forces at Pivot A
1000
800
600
400
200
0
-20
0
20
40
60
80
100
Tabletop Angle from Vertical (degrees)

Figure 3

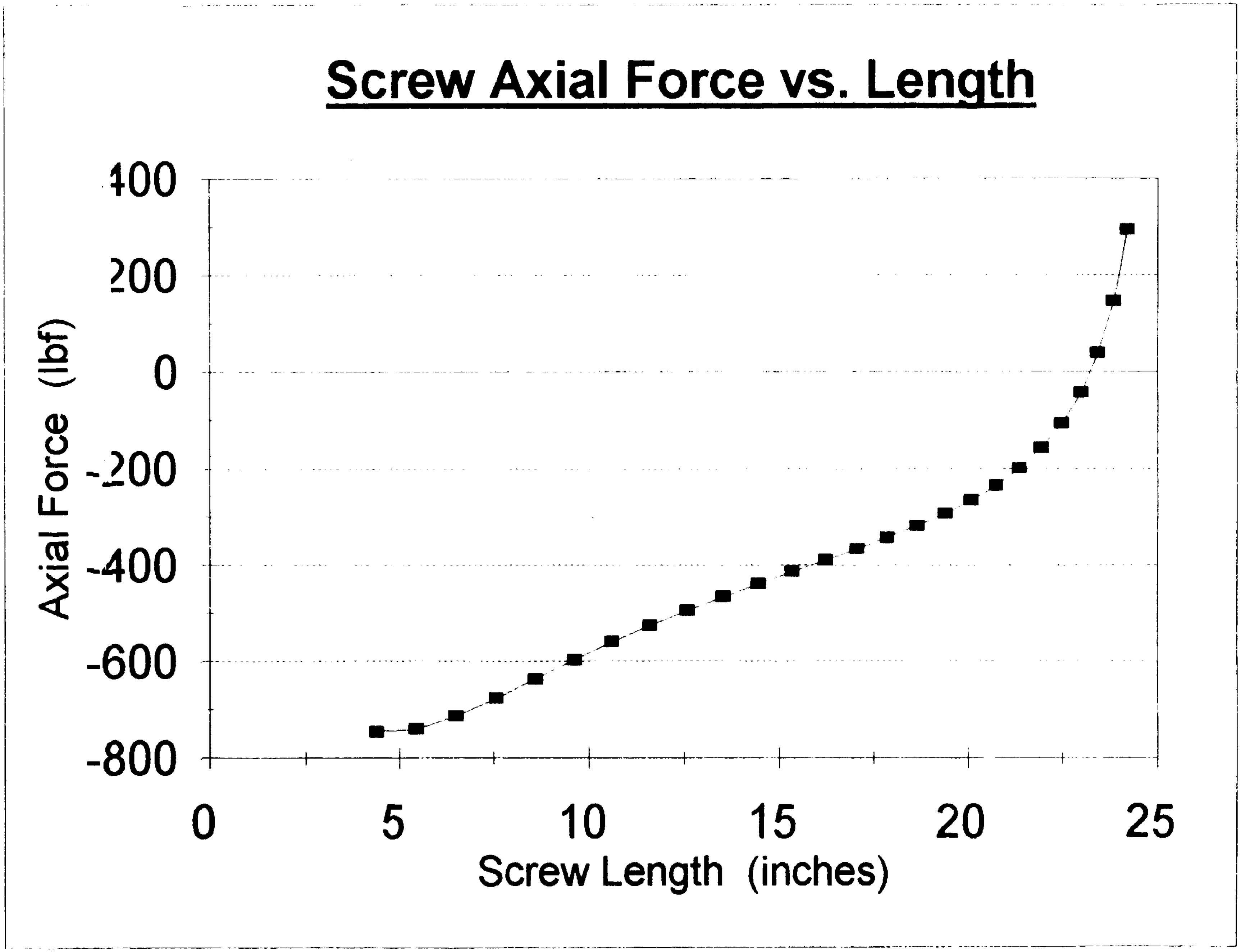
Screw Axial Force vs. Length
400
200
0
-200
-400
-600
-800
Axial Force (lbf)
0
5
10
15
20
25
Screw Length (inches)

Figure 4

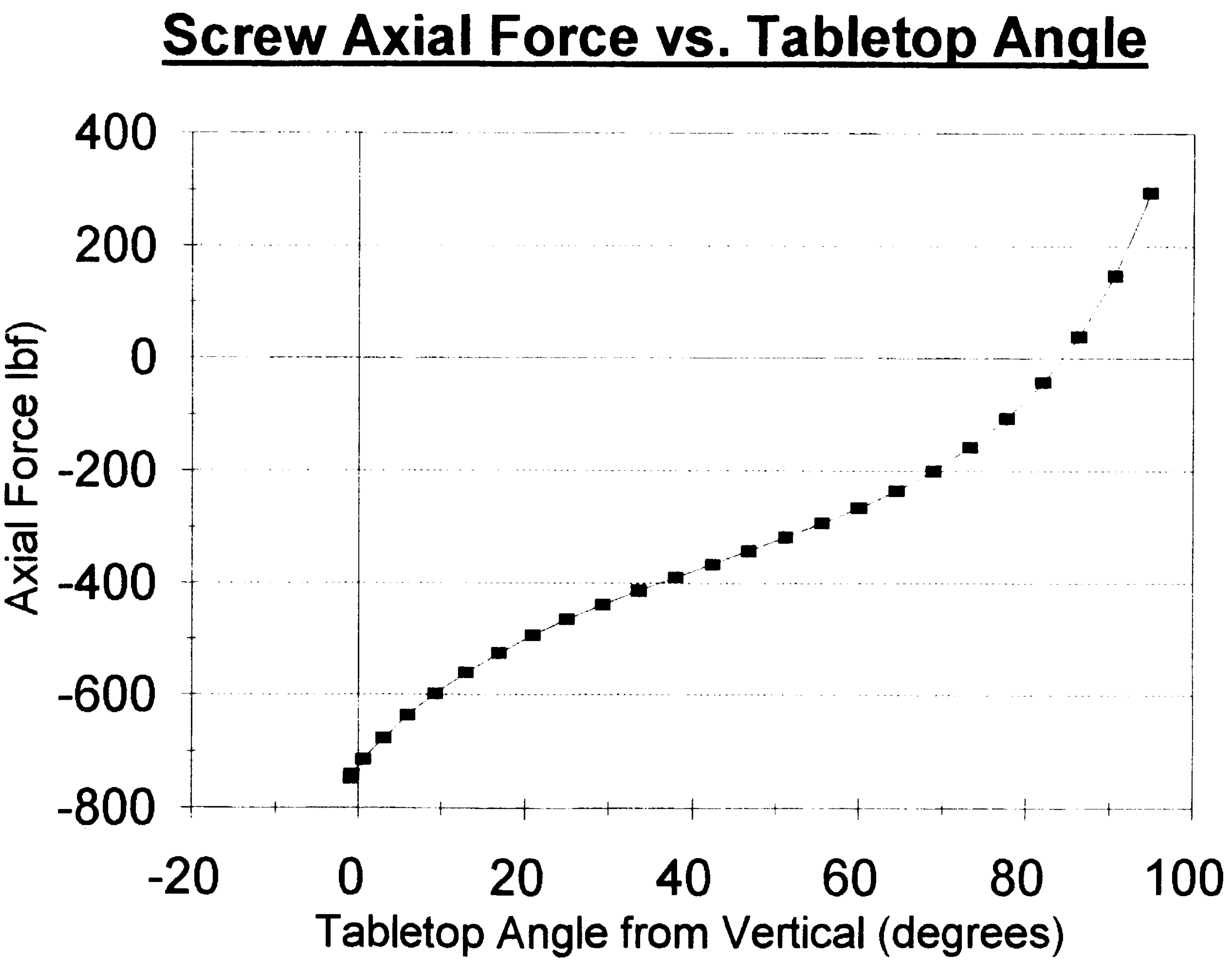
Screw Axial Force vs. Tabletop Angle

Figure 5

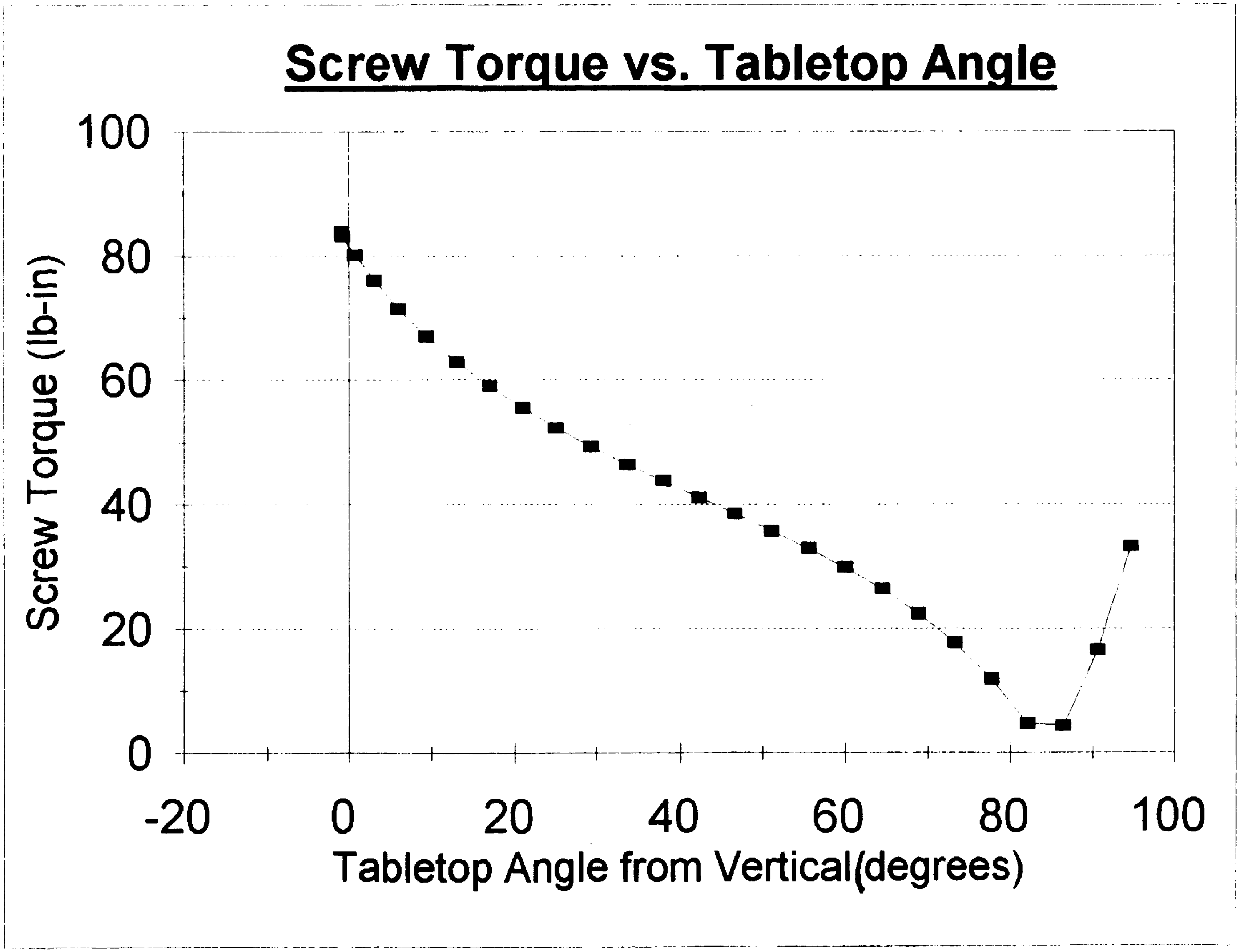
Screw Torque vs. Tabletop Angle
Screw Torque (lb-in)
100
80
60
40
20
0
-20
0
20
40
60
80
100
Tabletop Angle from Vertical(degrees)

Figure 6

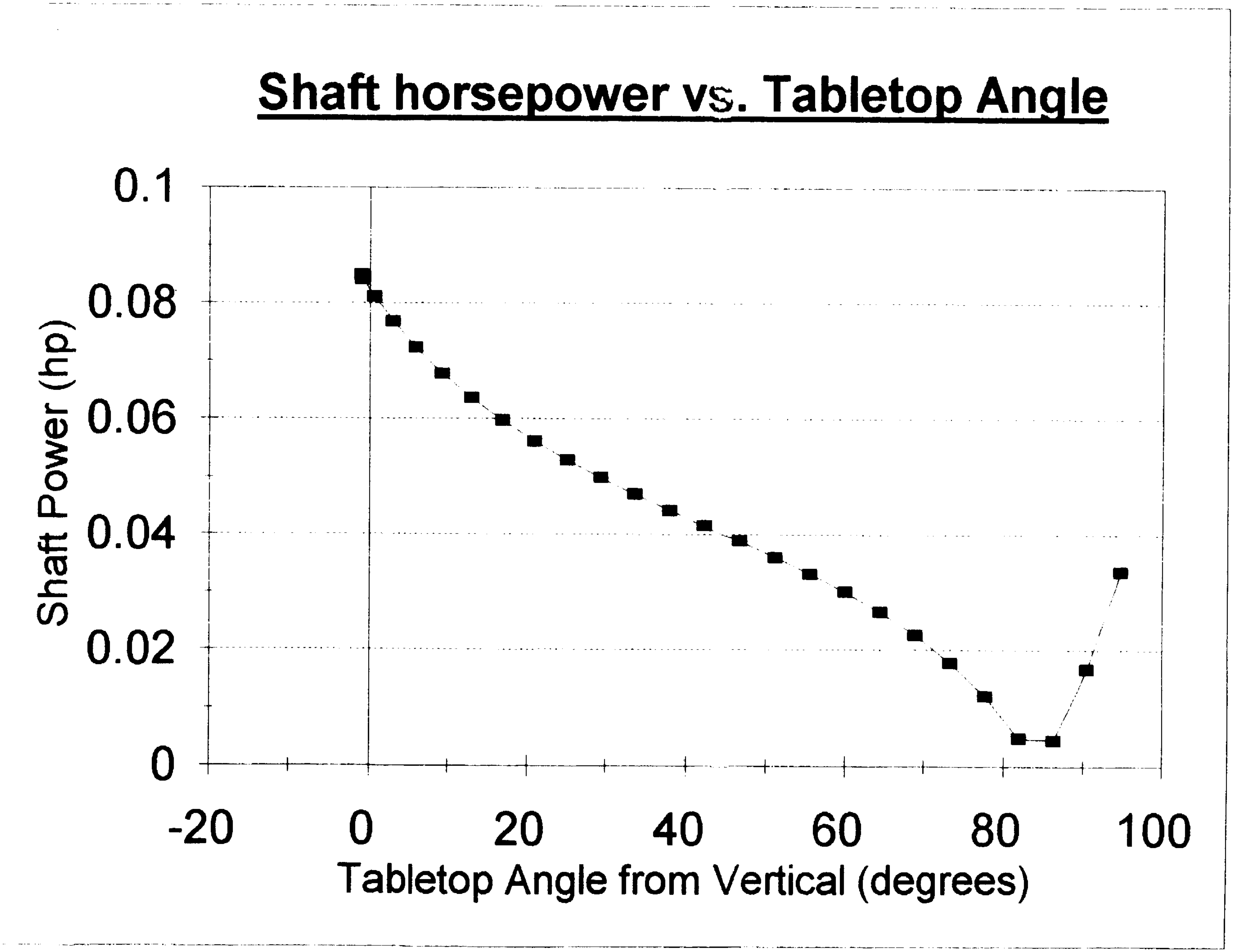
Shaft horsepower vs. Tabletop Angle
Shaft Power (hp)
0.1
0.08
0.06
0.04
0.02
0
-20
0
20
40
60
80
100
Tabletop Angle from Vertical (degrees)

Figure 7

## Results and Discussion:

Based upon analysis of forces in all components as a function of table position it is evident that the tilt motor has sufficient power to move the fully loaded table even in full vertical position. Forces acting on all parts with the possible exception of bearings in the bicycle hubs are well within the material strength limits for these components. When dealing with substantial masses that must be manipulated in a tight space, it appears inevitable that large stresses must be borne somewhere. With this in mind, it appears that the design, while capable of some improvements is a good starting point for such a task.

Possible room for improvement in the overall design might come from a study of large optical telescopes which work under the same fundamental constraints as for this project. A large mass must be continuously repositioned to track a particular object in the heavens. It is a common practice in such design to work in a polar coordinate system. One vector is defined by a plane normal to a fixed reference axis (i.e. the North star) and tracking occurs at a predetermined angular displacement from this axis and then rotates about the axis at a constant rate. Other room for improvement lies in testing iterations of the present design with shifts in key link lengths and pivot positions.

## Conclusion:

It is concluded that the final design as presented meets all specifications outlined in the task description. Moreover, the final design provides numerous benefits over the previous model in areas of weight reduction, rigidity, storage space and general aesthetics. Final improvements to the design would most likely be in the areas of (1) increasing crank length and screw angle to improve transmission angles and (2) continued reduction of weight for all components.

**References:**

Design of Machinery, Robert L. Norton, Worchester Polytechnic Institute, McGrawHill, Inc. (1992).

Vector Mechanics for Engineers, Beer and Johnston, McGrawHill, 5th Ed. (1988).

ASPOD Project Report, 1992. (Report of Previous Project).

Engineering Design and Graphics, James H. Earle, Addison Wesley, 7th Ed. (1992).

CRC Handbook of Chemistry and Physics, David R Lide (Editor), CRC Press, 72nd Ed. (1991-1992).

# Apendix

Old table flaws

General notes and figures on ASPOD design

Numerical computer outputs

Spreadsheet program for 'Quatro Pro' diskette

Reveal codes for program

# Tilt-table Design #3

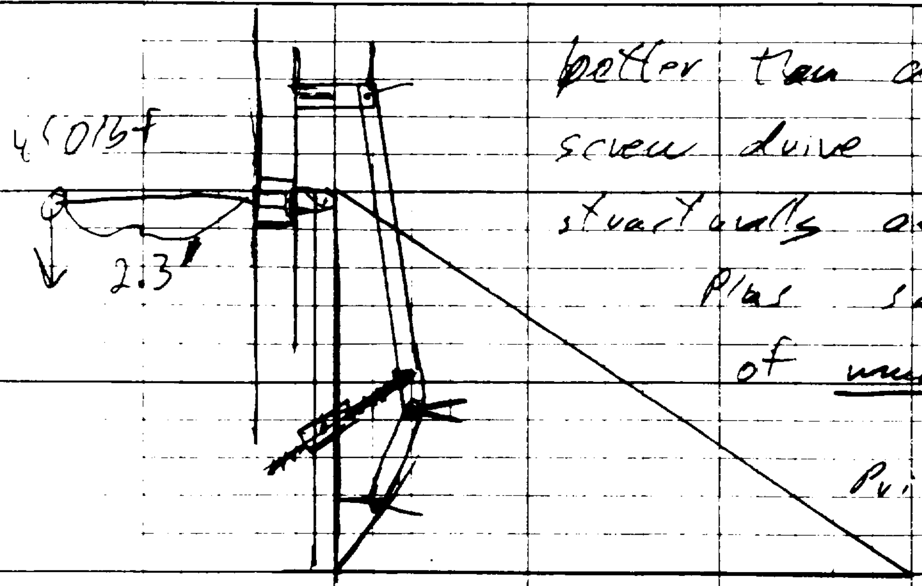

better than direct screw drive both structurally and aesthetically Plus saves on price of much longer screw

Primary design is the same but more sturdy

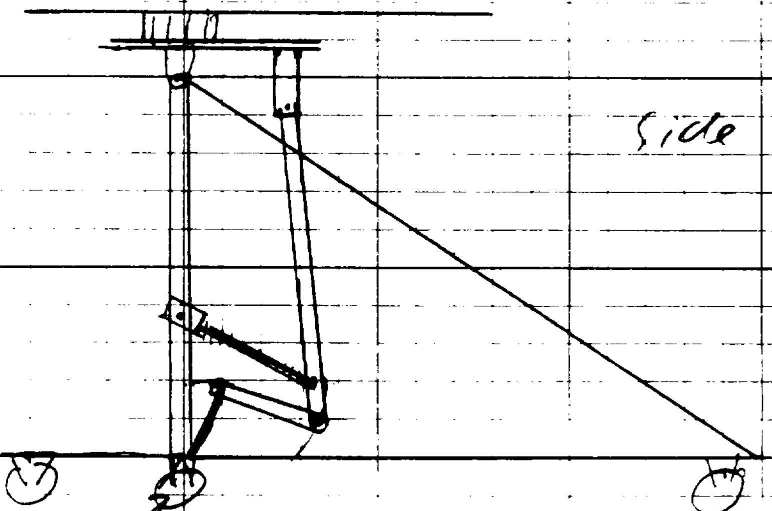

Side view

Weight? (50lbf?)

1/4" plates and hea rectange Tubing

extra wheel under middle of cross beam

front

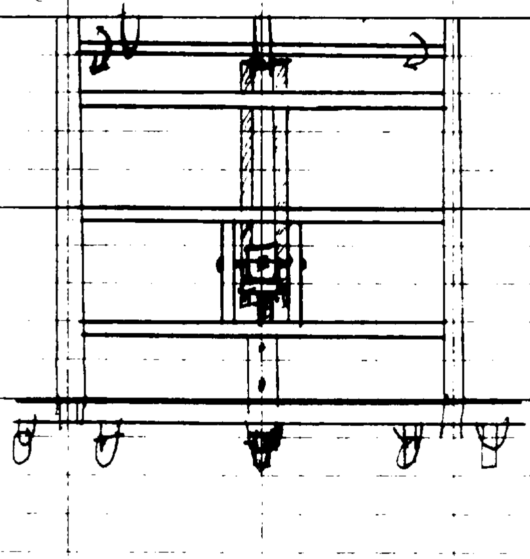

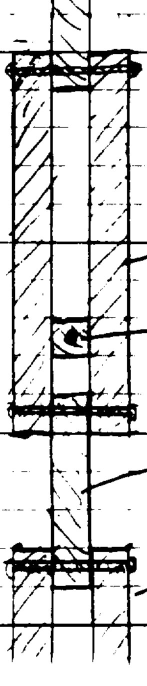
Table arm
upper arm
screw pivot
lower arm
base

# Preliminary Tilt Table design #2

Much stronger for the weight.

distance from screw box pivot to table pivot is same as distance from table screw pivot to table pivot.

$0° < \theta < 120°$

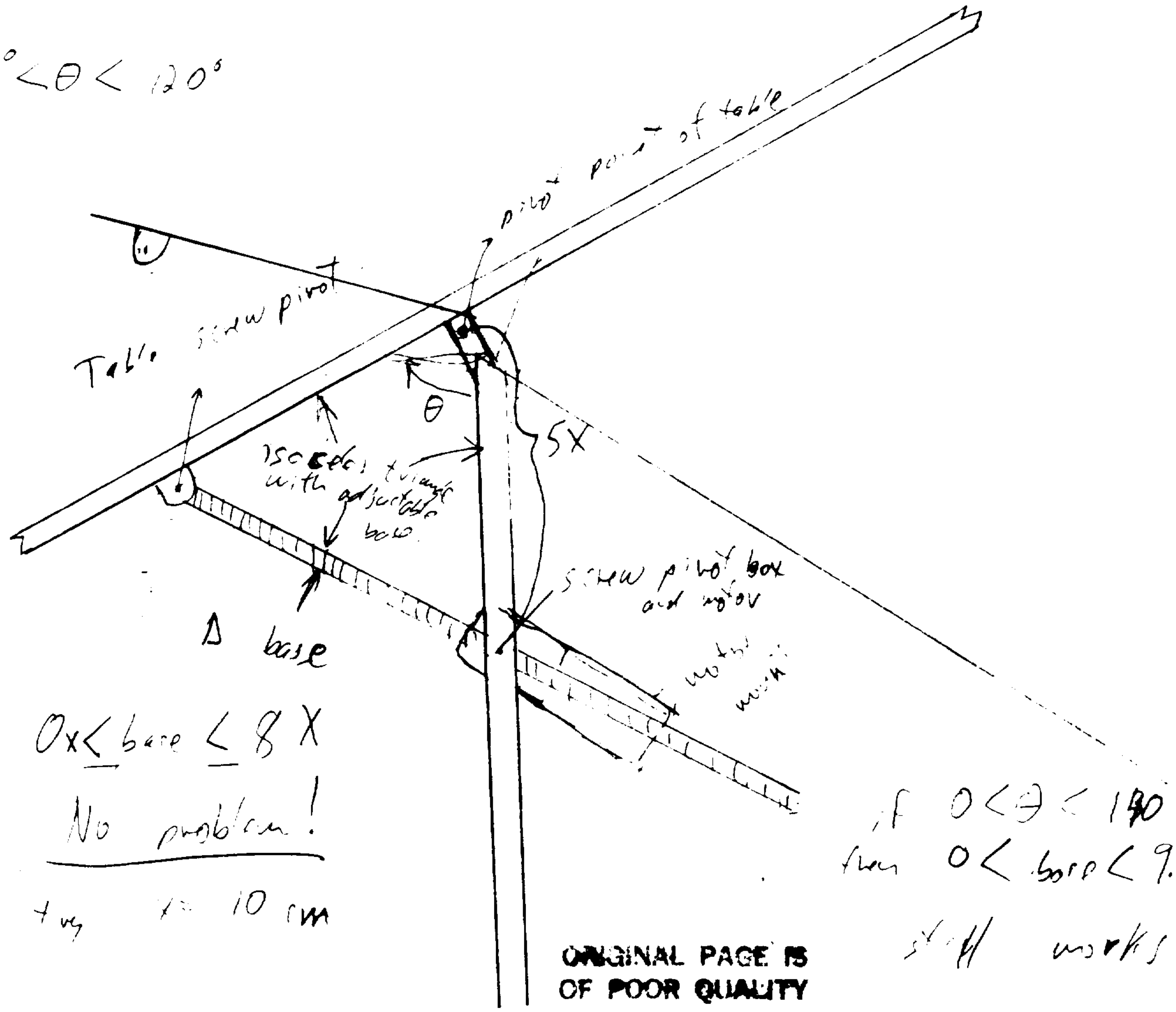
pivot point of table
Table screw pivot
$\theta$
5X
Isosceles triangle with adjustable base
screw pivot box and motor
motor mount
Δ base

$0x \leq$ base $\leq 8X$

No problem!

try x = 10 cm

if $0 < \theta < 140$
then $0 <$ base $< 9.4X$
still works

ORIGINAL PAGE IS
OF POOR QUALITY

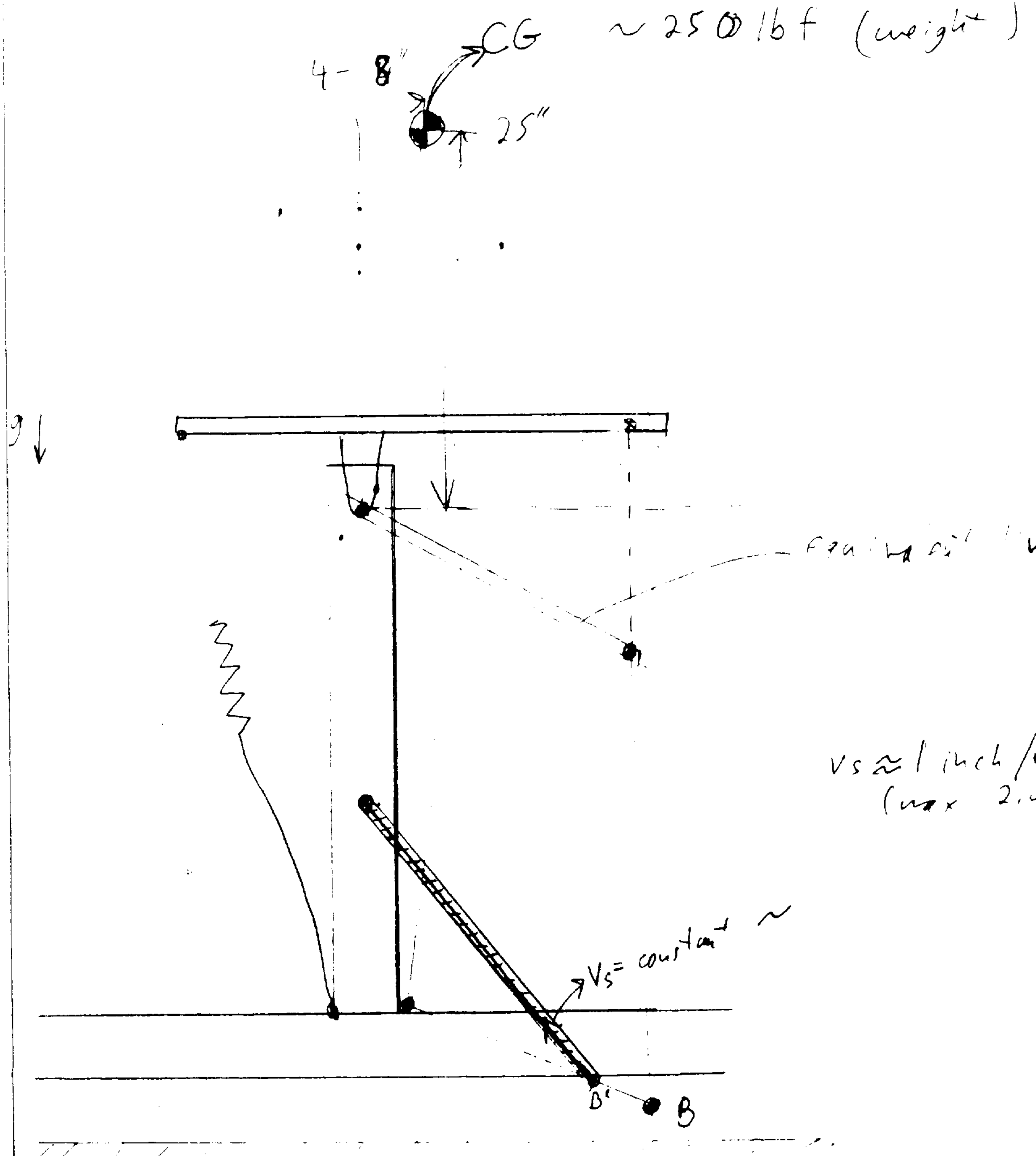
CG ~ 250 lbf (weight)
4 - 8"
25"
g
equivalent link
$V_s$ = constant ~
B'
B

$V_s \approx 1$ inch/minute
(max 2 inch/min)

ORIGINAL PAGE IS
OF POOR QUALITY

D. Fogarty. Addition to Boro Design # 10-1-93

X

Solution to insufficient 'Moment arm' for screw creating excessive compressive forces on screw/motor when Table is in full upright position

Presents Structure

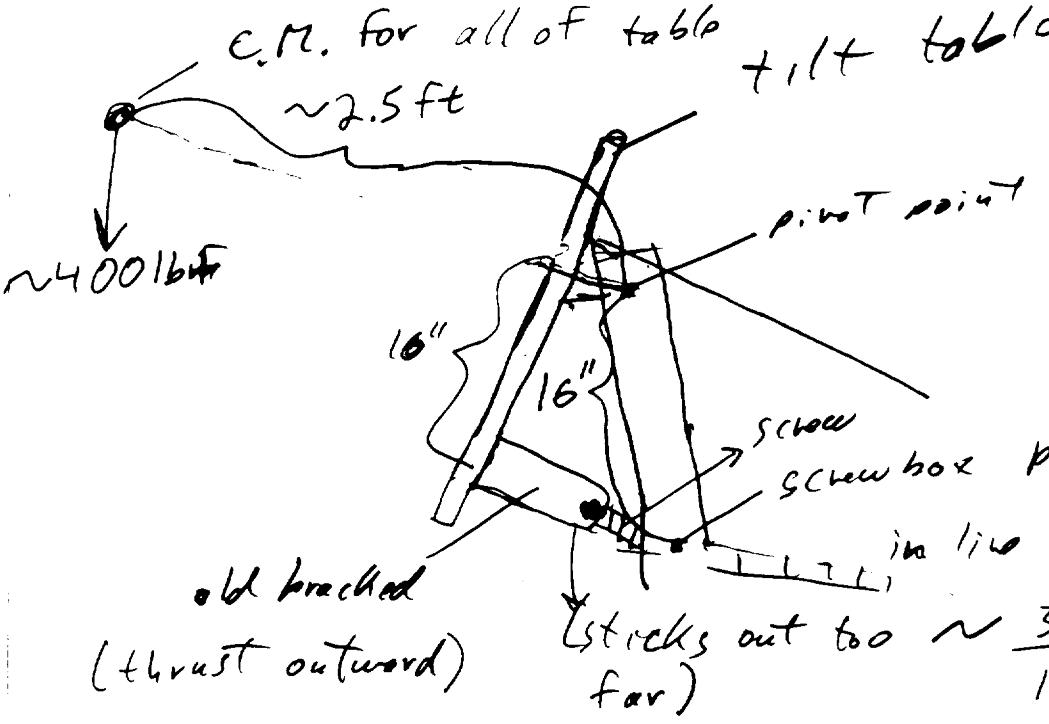
C.M. for all of table
~2.5ft
tilt table
~400lbf
pivot point
16"
16"
screw
screwbox pivot
old bracket
(thrust outward)
(sticks out too far)

in line force is ~ $\frac{30"}{16"}$ × CM for

~ 750 lbf

---

If bracket is re-designed to throw momen arm an extra 6" lower.
Still no parts interference but less compression is experienced

New design

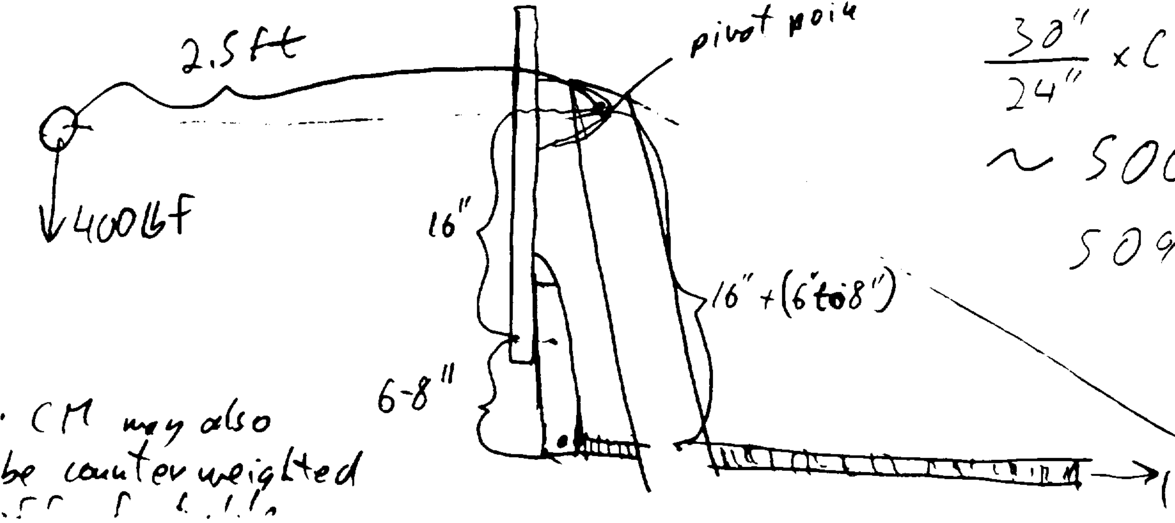
2.5ft
400lbf
pivot point
16"
6-8"
16"+(6"to8")
(move clo

$\frac{30"}{24"}$ × CM

~ 500 lbf v

50% improvem

Note: CM may also be counterweighted
[illegible]

AMPAD 22-141 50 SHEETS
22-142 100 SHEETS
22-144 200 SHEETS

(Side View)

Base Design #2

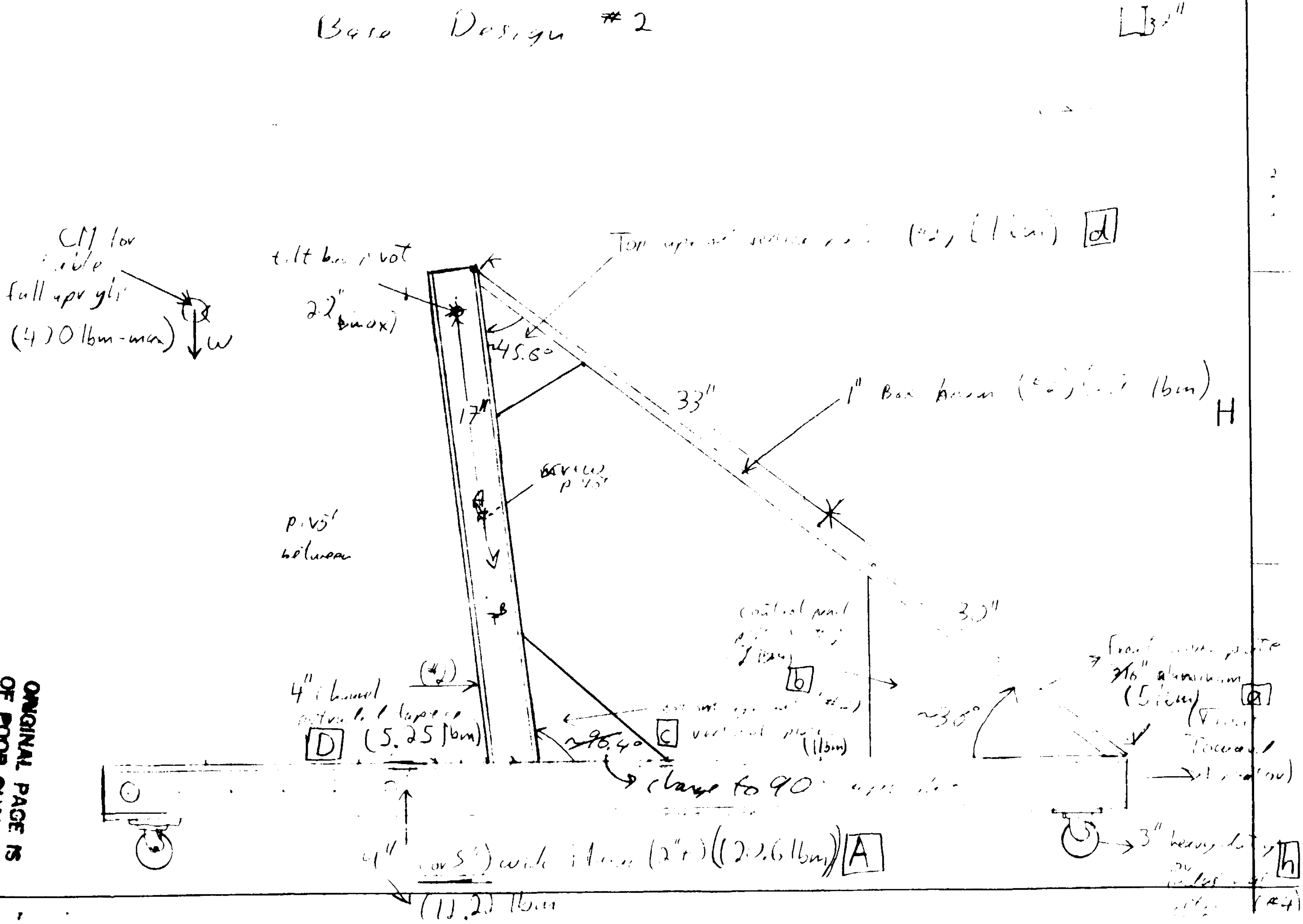
3"
CM for table full upright (420 lbm-max)
W
tilt bar pivot
22" (max)
Top [illegible] (2), (1 lbm) d
45.6°
33"
1" Box beam (2) [illegible] lbm) H
17"
pivot
pivot between
30"
control panel [illegible] 1 lbm) b
c vertical plate (1 lbm)
~96.4°
change to 90° [illegible]
~30°
front [illegible] plate 3/16" aluminum (5 lbm) a
4" channel [illegible] (5.25 lbm) D
(2)
4" (or 5") wide channel (2"+) ((22.6 lbm)) A
(11.2) lbm
3" heavy duty [illegible] h
(×4)

ORIGINAL PAGE IS OF POOR QUALITY

D. Fogarty   A[illegible]   [illegible]   2-19-93

Base design #1

[illegible] the maximum amount of existing materials — [illegible] used)   (not to scale)

☐ — [illegible]

The brace for these pivots must be the same distance from the table bottom (else isosceles form not maintained).

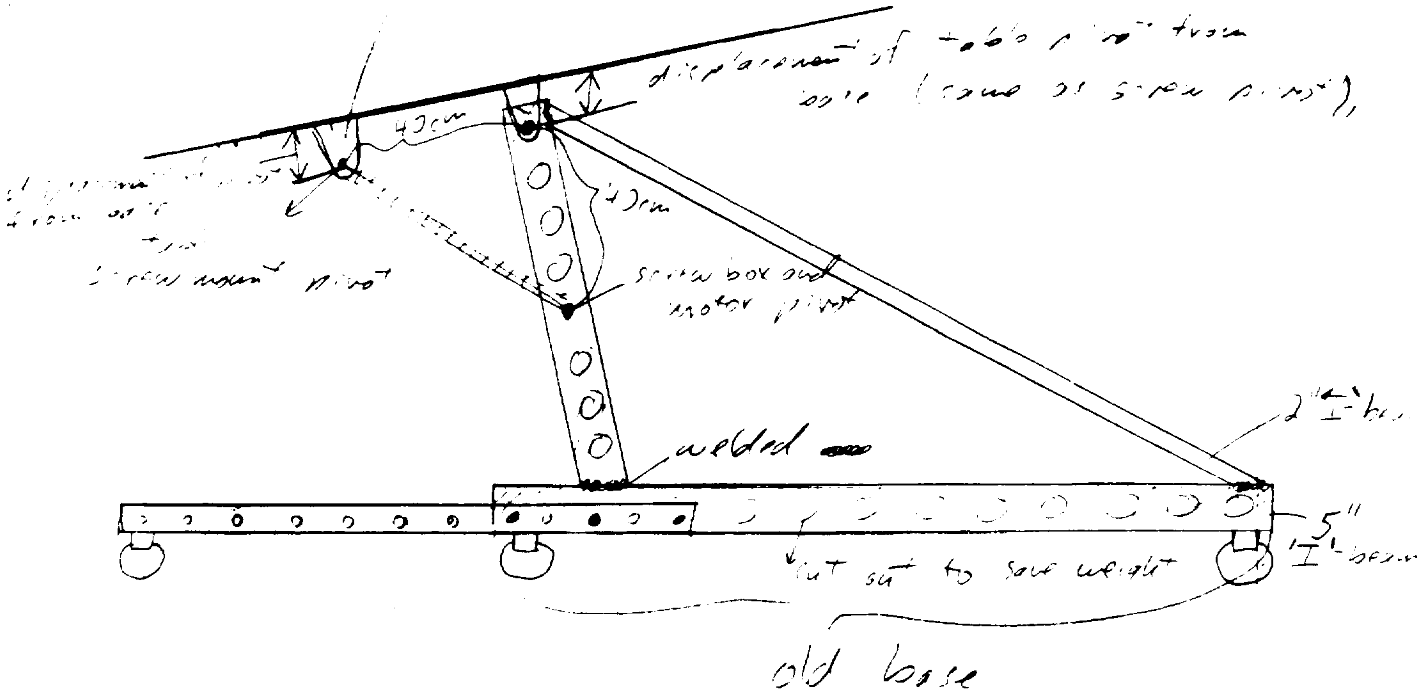

40cm
40cm
displacement of table pivot from axle (same as screw pivot),
displacement of [illegible] from axle [illegible] screw mount pivot
screw box and motor pivot
welded
2" I-beam
5" I-beam
cut out to save weight
old base

ORIGINAL PAGE IS OF POOR QUALITY

9LD Table

ASPD - Pr[illegible] T[illegible] [illegible]

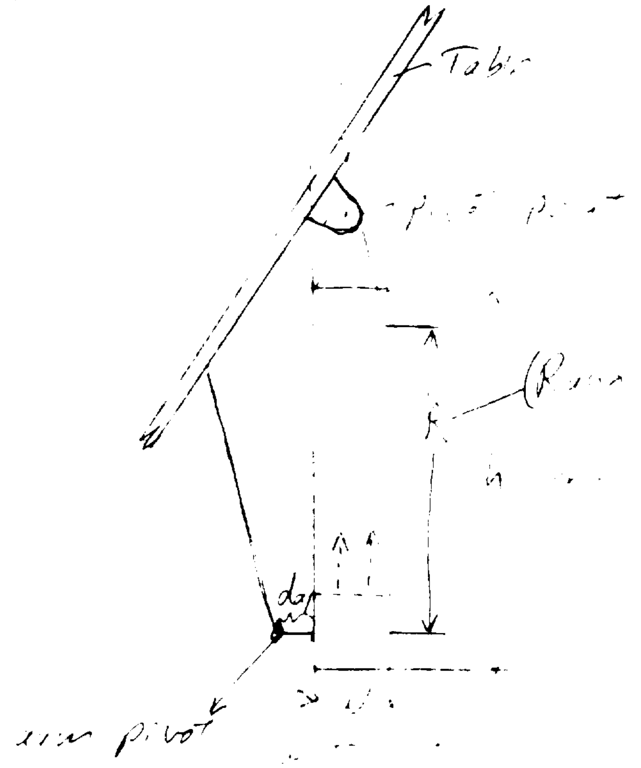
Table
upper pivot
$d_{ap}$
R
h
arm pivot
W

(R [illegible] screw operation for arm pivot

h [illegible])

working values: (approximate)

$d_{ap} \sim 3$ cm

$R \sim 35$ cm

$h \sim 45$ cm

$W \sim 8$ cm

Problem analysis: When table is at full upright (a common condition for D wagon in the summer) (not yet possible with present design

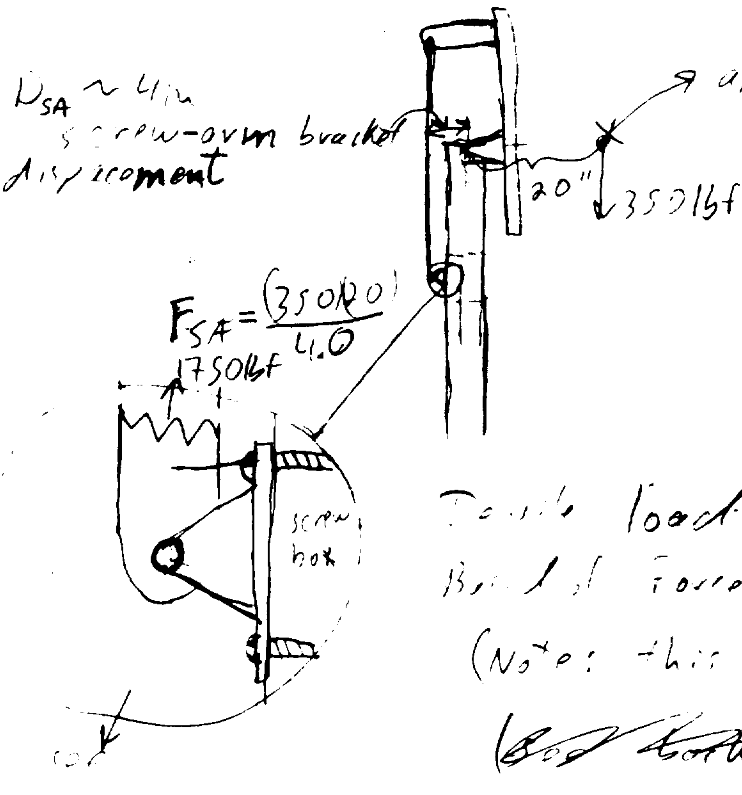
$D_{SA} \sim 4$in
screw-arm bracket displacement
20"
350 lbf
$F_{SA} = \frac{(350)(20)}{4.0}$
1750 lbf
screw box

approximat center of mass

max Weight = 350 lbf

displacement arm ~ 20 in

$D_{cm} = 20$ in

$W_{cm} = 350$ lbf

$D_{SA} = 4$ in

Results load of screw arm pivots and in shear

Bending Force of ~ 1750 lbf (est.)

(Note: this is static force no jerk)

ORIGINAL PAGE IS OF POOR QUALITY

10.5 ~

227 $\frac{63}{}$

found sun signal [illegible] beep

tatatatata! Clarso!!

Sound! Yes!

bells and whistle

all longer!

"A" frame [illegible]

[illegible] constraints

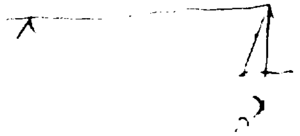

d = displacement of center of mass forward + 1 foot = 3 ft

tp = length of tilt-table pivot ~3 ft

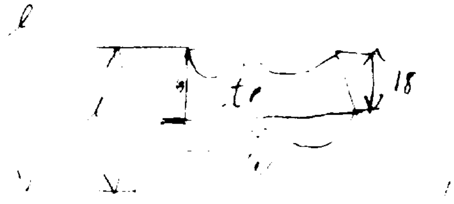

18 [illegible] area

[illegible] max [illegible]

length = $t_p + 18'' \frac{\sin\theta}{\cos\theta}$ maximize the total length, $l$ = minimize

45

colours silver or bronze and black with key parts in colour ie - arms logo tracker controls

add LEDs [illegible] project

Modified "A" frame

→ Place cover over front with [illegible]

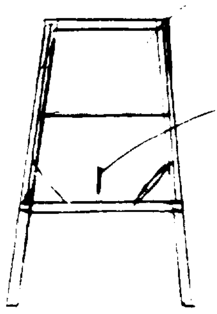
motor groups fully accessible

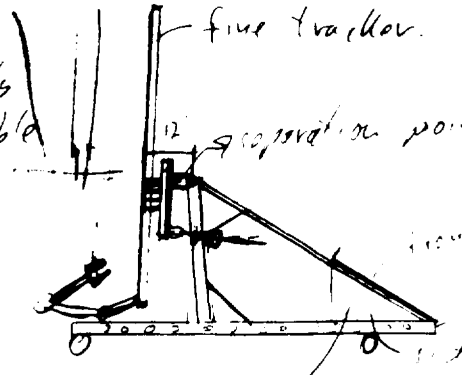
fine tracker
12
separation point

and [illegible]

[illegible]

[illegible]

(controls could also be input through here) - bright colors

and room

ORIGINAL PAGE IS OF POOR QUALITY

~~Thumbnail estimates~~

Key stress calculations 6061-0 assumed

Worst stress point should be at base of uprights

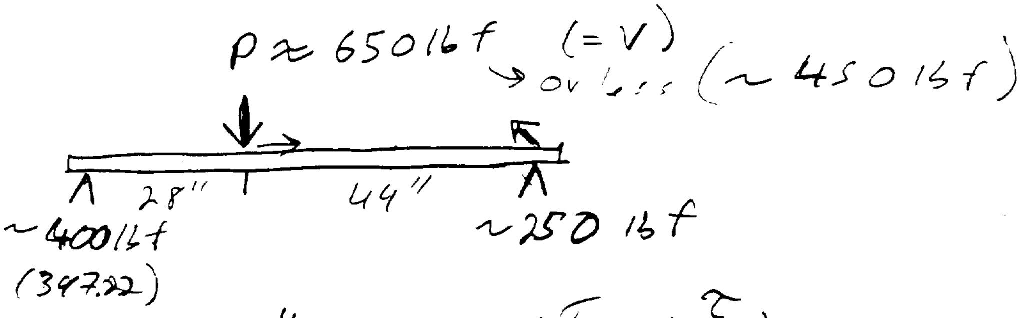

$P \approx 650\,lbf$ (= V)
→ or less (~450 lbf)
28"
44"
~400 lbf
(347.22)
~250 lbf

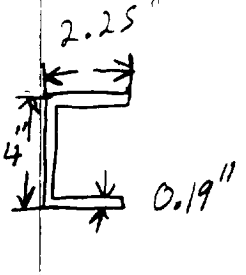

$I = 3.8565\ in^4$

$E = 1.00 \times 10^7\ psi$

$y = 2\,in$ (max)

$Q = 1.629\ in^3$

$b = \overset{\sigma}{(2\,in)}\ \overset{\tau}{(.19)}$

$V = P = 650\,lbf$

$$\tau = \frac{VQ}{Ib} = \frac{(650\,lbf)(1.629\,in^3)}{(3.8565\,in^4)(.19\,in)} = 1450\,psi$$

$\tau_{Allow} = 12{,}000$ (ultimate

$\tau_{safety} =$

$$\sigma = \frac{My}{I} = (12000)(2\,in) = 6223\,psi$$

$\sigma_{Allow} = (8000\,psi)$ (yield)

$$\sigma\ \text{safety factor} = \frac{\sigma_{Allow}}{\sigma} \overset{=(1.285)}{\doteq} 1.3\ (-1.4)$$

(safety factor can be increased by moving wheels inward (2.0)

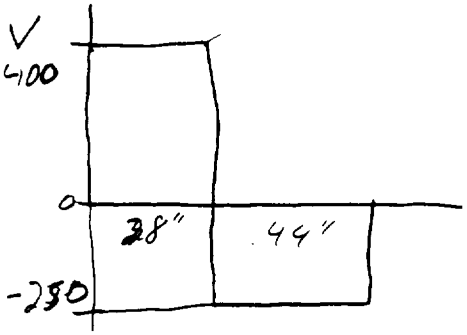

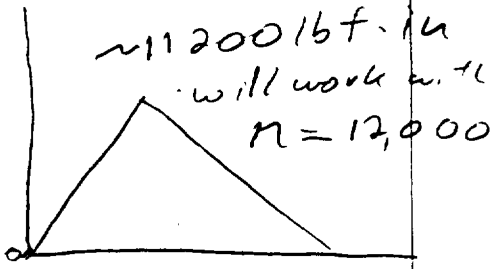

ORIGINAL PAGE IS
OF POOR QUALITY

**General Design Flaws in Old Table:**

1) Table locks in full vertical position and cannot return easily from any angle beyond 30 degrees from vertical.

2) Controls are external to frame and are poorly attached.

3) Base is an "H" frame with insufficient rigidity despite use of six inch "I" beam throughout mechanism.

4) Base is too short, making structure prone to instability.

5) Base is too heavy at 350 lbs. minus the tilt assembly.

6) Screw box mechanism is prone to severe bending moments which are only alleviated through use of teflon pads and 5 inch channel beam to restrain the box.

7) Entire frame assembly is composed of 6 inch "I" beam of substantial mass held together by 2 inch "L" brackets at the ends. There are no triangles to hold the base rigid.

8) Key load bearing components are poorly placed and insufficient in size (i.e. screw box pivot arm is mounted with 3/16 inch woodscrews).

9) Overall appearance is clunky and unelegant.

Brace Between arm

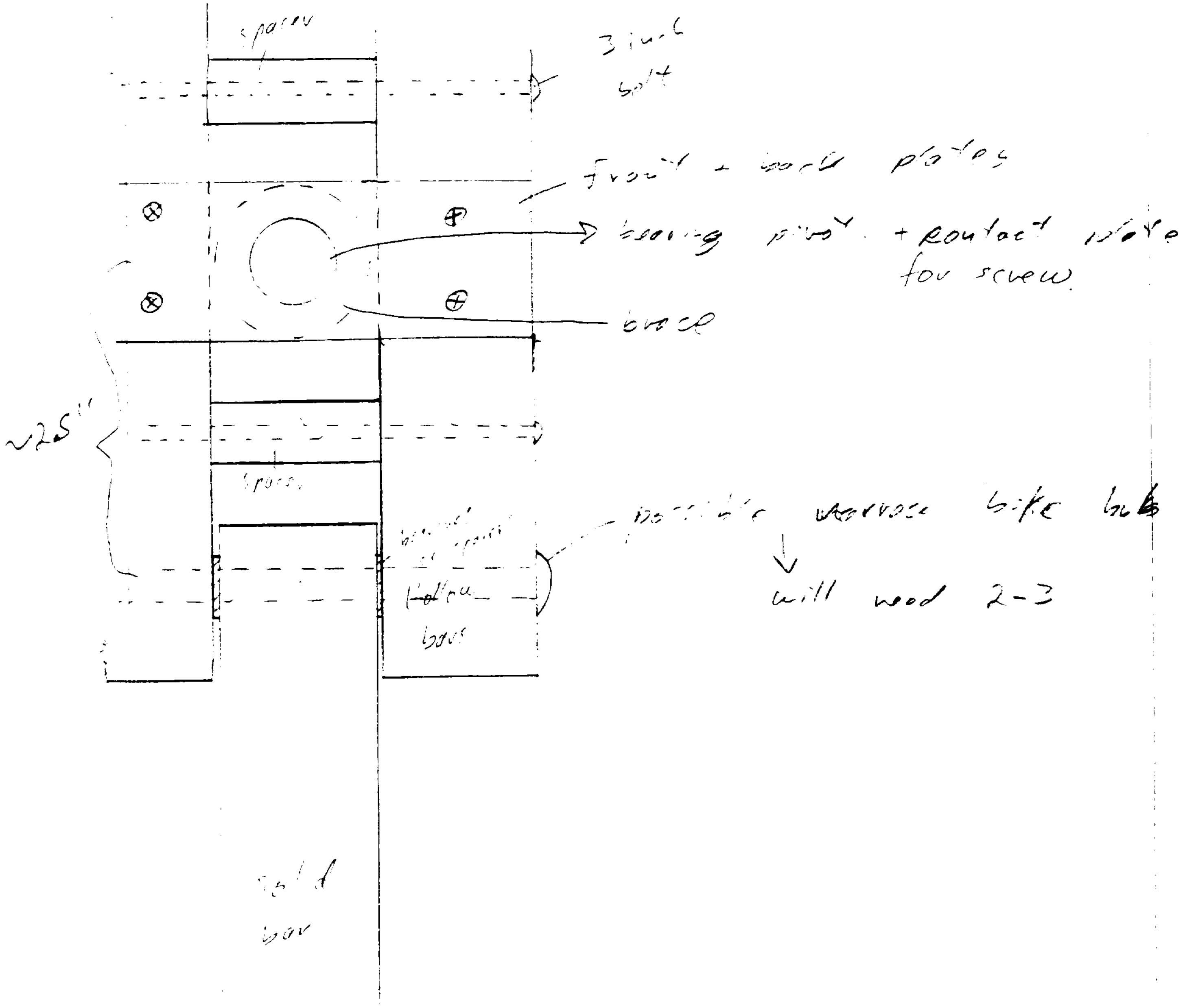
spacer
3 inch bolt
front + back plates
bearing pivot + contact plate for screw
brace
~25"
spacer
bonded at spacer
hollow bars
possible narrow bike hub
will need 2-3
solid bar

ORIGINAL PAGE IS OF POOR QUALITY

FOURBAR 5.1    Paul W Fogarty    Design # 1    04-30-1994 at 08:35

Angle - Degrees

| Trans. Angle | Link 2 | Link 3 | Link 4 |
|---|---|---|---|
| 20.089 | 10.370 | 13.544 | 33.633 |
| 22.786 | 15.370 | 10.977 | 33.762 |
| 26.070 | 20.370 | 9.151 | 35.221 |
| 29.744 | 25.370 | 7.832 | 37.576 |
| 33.680 | 30.370 | 6.858 | 40.538 |
| 37.793 | 35.370 | 6.123 | 43.916 |
| 42.028 | 40.370 | 5.559 | 47.587 |
| 46.348 | 45.370 | 5.120 | 51.468 |
| 50.728 | 50.370 | 4.776 | 55.503 |
| 55.150 | 55.370 | 4.504 | 59.654 |
| 59.600 | 60.370 | 4.291 | 63.891 |
| 64.068 | 65.370 | 4.125 | 68.193 |
| 68.546 | 70.370 | 3.999 | 72.545 |
| 73.025 | 75.370 | 3.908 | 76.933 |
| 77.499 | 80.370 | 3.848 | 81.347 |
| 81.962 | 85.370 | 3.815 | 85.778 |
| 86.408 | 90.370 | 3.809 | 90.218 |
| 89.170 | 95.370 | 3.829 | 94.659 |
| 84.780 | 100.370 | 3.875 | 99.096 |
| 80.429 | 105.370 | 3.948 | 103.519 |
| 76.127 | 110.370 | 4.049 | 107.922 |
| 71.884 | 115.370 | 4.181 | 112.297 |
| 67.715 | 120.370 | 4.348 | 116.633 |
| 63.636 | 125.370 | 4.555 | 120.919 |
| 59.666 | 130.370 | 4.808 | 125.142 |
| 55.831 | 135.370 | 5.115 | 129.285 |

Table = **A**    Title *Full Range of Angles 4-Bar Linkage*

```
FOURBAR 5.1    Paul W Fogarty   Design #  1   04-30-1994  at  08:37

                         Omega -  Radians/Sec

          Crank Angle          Link  2          Link  3          Link  4

               10.370            0.002           -0.001           -0.000
               15.370            0.002           -0.001            0.000
               20.370            0.002           -0.001            0.001
               25.370            0.002           -0.000            0.001
               30.370            0.002           -0.000            0.001
               35.370            0.002           -0.000            0.001
               40.370            0.002           -0.000            0.002
               45.370            0.002           -0.000            0.002
               50.370            0.002           -0.000            0.002
               55.370            0.002           -0.000            0.002
               60.370            0.002           -0.000            0.002
               65.370            0.002           -0.000            0.002
               70.370            0.002           -0.000            0.002
               75.370            0.002           -0.000            0.002
               80.370            0.002           -0.000            0.002
               85.370            0.002           -0.000            0.002
               90.370            0.002            0.000            0.002
               95.370            0.002            0.000            0.002
              100.370            0.002            0.000            0.002
              105.370            0.002            0.000            0.002
              110.370            0.002            0.000            0.002
              115.370            0.002            0.000            0.002
              120.370            0.002            0.000            0.002
              125.370            0.002            0.000            0.002
              130.370            0.002            0.000            0.002
              135.370            0.002            0.000            0.002
```

Table # B Title Link Angular Velocities (beyond maximum)

```
FOURBAR 5.1     Paul W Fogarty   Design # 1   04-30-1994  at  08:41

                     Alpha -  Radians/Sec^2

        Crank Angle           Link  2          Link  3          Link  4

             10.370            0.000            0.000            0.000
             15.370            0.000            0.000            0.000
             20.370            0.000            0.000            0.000
             25.370            0.000            0.000            0.000
             30.370            0.000            0.000            0.000
             35.370            0.000            0.000            0.000
             40.370            0.000            0.000            0.000
             45.370            0.000            0.000            0.000
             50.370            0.000            0.000            0.000
             55.370            0.000            0.000            0.000
             60.370            0.000            0.000            0.000
             65.370            0.000            0.000            0.000
             70.370            0.000            0.000            0.000
             75.370            0.000            0.000            0.000
             80.370            0.000            0.000            0.000
             85.370            0.000            0.000            0.000
             90.370            0.000            0.000            0.000
             95.370            0.000            0.000           -0.000
            100.370            0.000            0.000           -0.000
            105.370            0.000            0.000           -0.000
            110.370            0.000            0.000           -0.000
            115.370            0.000            0.000           -0.000
            120.370            0.000            0.000           -0.000
            125.370            0.000            0.000           -0.000
            130.370            0.000            0.000           -0.000
            135.370            0.000            0.000           -0.000
```

Table # C   Title Link Angular Acceleration ($\omega_2$ = constant)

```
FOURBAR 5.1    Paul W Fogarty   Design #  1   04-30-1994  at  17:57

                     Angle -  Degrees

         Trans. Angle          Link  2         Link  3         Link  4

             60.262            129.610          4.766          124.505
```

Table # D Title Determination of $\theta_2$ based on $\theta_4$ (maximum angle input at crank)

```
FOURBAR 5.1    Paul W Fogarty   Design #  1   04-30-1994  at  17:57

                     Angle -  Degrees

         Trans. Angle          Link  2         Link  3         Link  4

             24.700             18.370          9.809           34.509
```

Table # E Title Determination of $\theta_2$ based on $\theta_4$ (minimum angle at input crank)

```
FOURBAR 5.1    Paul W Fogarty   Design #  1   04-30-1994  at  17:59

                     Angle -  Degrees

         Trans. Angle          Link  2         Link  3         Link  4

             59.270             60.000          4.305           63.575
```

Table # F Title Determination of $\theta_2$ based on $\theta_4$ (mid-range angles at input crank)

```
FOURBAR 5.1    Paul W Fogarty   Design #  1   04-30-1994  at  17:59

                     Angle -  Degrees

         Trans. Angle          Link  2         Link  3         Link  4

             85.103            100.000          3.871           98.768
```

# STATIC STRESS ANALYSIS FOR ASPOD TILT-TABLE MECHANISM

*(Full Range of Motion from Vertical - 0 degrees- to Horizontal)*

**Raw Angular Data (all corrections by Theta 1 - 84.4725 degrees)**

Table 1

| Theta 2<br>degrees | Theta 3<br>degrees | Thete 4<br>degrees | Theta CM<br>degrees | Tabletop<br>degrees |
|---|---|---|---|---|
| 10.37 | 13.54 | 33.63 | 85.37 | -0.89 |
| 15.37 | 10.98 | 33.76 | 85.24 | -0.77 |
| 20.37 | 9.15 | 35.22 | 83.78 | 0.69 |
| 25.37 | 7.83 | 37.58 | 81.42 | 3.05 |
| 30.37 | 6.86 | 40.54 | 78.46 | 6.01 |
| 35.37 | 6.12 | 43.92 | 75.08 | 9.39 |
| 40.37 | 5.56 | 47.59 | 71.41 | 13.06 |
| 45.37 | 5.12 | 51.47 | 67.53 | 16.94 |
| 50.37 | 4.78 | 55.50 | 63.50 | 20.98 |
| 55.37 | 4.50 | 59.65 | 59.35 | 25.13 |
| 60.37 | 4.29 | 63.89 | 55.11 | 29.36 |
| 65.37 | 4.13 | 68.19 | 50.81 | 33.67 |
| 70.37 | 4.00 | 72.55 | 46.46 | 38.02 |
| 75.37 | 3.91 | 76.93 | 42.07 | 42.41 |
| 80.37 | 3.85 | 81.35 | 37.65 | 46.82 |
| 85.37 | 3.82 | 85.78 | 33.22 | 51.25 |
| 90.37 | 3.81 | 90.22 | 28.78 | 55.69 |
| 95.37 | 3.83 | 94.66 | 24.34 | 60.13 |
| 100.37 | 3.88 | 99.10 | 19.90 | 64.57 |
| 105.37 | 3.95 | 103.52 | 15.48 | 68.99 |
| 110.37 | 4.05 | 107.92 | 11.08 | 73.39 |
| 115.37 | 4.18 | 112.30 | 6.70 | 77.77 |
| 120.37 | 4.35 | 116.63 | 2.37 | 82.11 |
| 125.37 | 4.56 | 120.92 | -1.92 | 86.39 |
| 130.37 | 4.81 | 125.14 | -6.14 | 90.61 |
| 135.37 | 5.12 | 129.29 | -10.28 | 94.76 |

Table 2

**CONSTANTS USED:**

| | | |
|---|---|---|
| Mcm = | 260 | lbm |
| Rcm = | 22 | inches |
| AB = | 16.25 | inches |
| BC = | 31.25 | inches |
| CD = | 18.576 | inches |
| DA = | 31.145 | inches |
| FA = | 13.31 | inches |
| EA = | 12.13 | inches |
| Screw = | 24.25 | inches |

Table 3

**Constants not used:**
(Arbitrary masses)

| | | |
|---|---|---|
| Screw = | 4 | lbm |
| link AB= | 11 | lbm |
| linkBC= | 5 | lbm |
| motor= | 5 | lbm |

(In the following calculations all links are regarded as essentially massless. This approximation is essentially true when one considers the substancial difference between the mass concentrated at the idealized center of mass for the tabletop vs the relatively small link masses. It should further be noted that the mass of the rocker, by far the heaviest link is not disregarded in these calculations)

**A) Moments About Pivot "D" ( CW = +) = ZERO:**

Mom D = Mcm*g*Rcm*SIN(Theta CM) - CD*SIN(Theta 4)*T*COS(Theta 3) = 0

(This equation may then be solved for T, the tension/compression in the coupler, BC.)

**B) Resultant Force Acting at "D" ResD = SUM Fx X SUM Fy:**

(Vector addition is the rule)

**C) Moments About Pivot "A" (CW = +) = ZERO:**

(Used in solution of force, P, acting in screw and at pivot E)

(determintion of screw angle, EFA, relative to AB is needed)

**D) Length of Screw, EF, Used in Calculations of Buckling and Angle, EFA:**

EF = FA^2 + EA^2 - 2(FA)(EA)COSINE(Theta 2 + 8.815degrees)

**E) Determination of Angle EFA:**

(Law of Sines applied)

**F) Force, P, acting in screw EF ( - => compressive):**

P = -(T*cos(Theta 3)*AB)/sin(EFA)*FA

**G) Resultant of Forces Acting at Pivot A:**

Table 4

## Forces in All Relevant Links and Pivots

| T in BC Force (lbf) | Res D Force (lbf) | EF Length (inches) | EFA Angle (degrees | P screw Force (lbf) | Res A Force (lbf) |
|---|---|---|---|---|---|
| 569.98 | 825.00 | 4.40 | 65.06 | -746.11 | 946.99 |
| 562.45 | 819.19 | 5.45 | 65.69 | -739.71 | 913.19 |
| 537.61 | 795.38 | 6.51 | 65.31 | -713.24 | 856.27 |
| 504.00 | 762.40 | 7.56 | 64.33 | -676.35 | 788.74 |
| 467.54 | 726.34 | 8.60 | 62.98 | -636.15 | 719.60 |
| 431.45 | 690.52 | 9.63 | 61.39 | -596.60 | 653.69 |
| 397.18 | 656.45 | 10.64 | 59.62 | -559.45 | 592.97 |
| 365.21 | 624.61 | 11.63 | 57.73 | -525.25 | 537.90 |
| [illegible] | [illegible] | [illegible] | [illegible] | [illegible] | [illegible] |
| 307.90 | 567.47 | 13.55 | 53.68 | -465.13 | 443.51 |
| 282.06 | 541.69 | 14.48 | 51.56 | -438.43 | 403.12 |
| 257.71 | 517.37 | 15.37 | 49.40 | -413.33 | 366.51 |
| 234.54 | 494.24 | 16.24 | 47.20 | -389.32 | 333.14 |
| 212.29 | 472.01 | 17.08 | 44.97 | -365.88 | 302.52 |
| 190.70 | 450.45 | 17.88 | 42.71 | -342.45 | 274.15 |
| 169.54 | 429.31 | 18.65 | 40.44 | -318.41 | 247.54 |
| 148.59 | 408.38 | 19.39 | 38.15 | -293.05 | 222.07 |
| 127.62 | 387.43 | 20.09 | 35.84 | -265.52 | 197.06 |
| 106.41 | 366.24 | 20.75 | 33.52 | -234.72 | 171.56 |
| 84.73 | 344.58 | 21.37 | 31.19 | -199.29 | 144.34 |
| 62.34 | 322.21 | 21.95 | 28.85 | -157.35 | 113.68 |
| 38.95 | 298.86 | 22.49 | 26.50 | -106.29 | 77.11 |
| 14.27 | 274.23 | 22.98 | 24.15 | -42.46 | 31.14 |
| -12.06 | 247.98 | 23.44 | 21.78 | 39.54 | 29.48 |
| -40.43 | 219.74 | 23.85 | 19.42 | 147.95 | 112.77 |
| -71.31 | 189.08 | 24.21 | 17.05 | 295.79 | 231.49 |

(Given the calculated data on length of the screw for any given instant of position we may now work backwards with screw length as a linear function of position – i.e. constant velocity. This is a suficiently accurate representation of the actual screw-crank mechanism. Since the screw pitch and motor rotational speed are determined from the prototype itself, measures of torque on the motor and gear reducer are simplified)

Calculations of required motor power are based on the following assumptions:

1) Since no bending moments are applied to the screw the total torque required to turn the screw are a function of the axial force on the screw, the coefficient of kinetic friction between steel and brass (the materials of the screw and nut respectively) and the mean radius of the screw.

2) Power = Force x Velocity or Torque / time.

Uk = kinetic coefficient of friction = 0.3 max

Rs = Mean radius of screw = 0.375 inches

Screw velocity = RPM x 2PiRs = 2.5 in/sec max (Note this is the th

Table 5

| Torque In-lbf | Power In-lb/sec | Power hp |
|---|---|---|
| 83.94 | 559.58 | 0.0848 |
| 83.22 | 554.78 | 0.0841 |
| 80.24 | 534.93 | 0.081 |
| 76.09 | 507.26 | 0.0769 |
| 71.57 | 477.11 | 0.0723 |
| 67.12 | 447.45 | 0.0678 |
| 62.94 | 419.59 | 0.0636 |
| 59.09 | 393.94 | 0.0597 |
| 55.57 | 370.44 | 0.0561 |
| 52.33 | 348.85 | 0.0529 |
| 49.32 | 328.82 | 0.0498 |
| 46.50 | 310.00 | 0.047 |
| 43.80 | 291.99 | 0.0442 |
| 41.16 | 274.41 | 0.0416 |
| 38.53 | 256.84 | 0.0389 |
| 35.82 | 238.81 | 0.0362 |
| 32.97 | 219.79 | 0.0333 |
| 29.87 | 199.14 | 0.0302 |
| 26.41 | 176.04 | 0.0267 |
| 22.42 | 149.47 | 0.0226 |
| 17.70 | 118.01 | 0.0179 |
| 11.96 | 79.72 | 0.0121 |
| 4.78 | 31.85 | 0.0048 |
| 4.45 | 29.66 | 0.0045 |
| 16.64 | 110.96 | 0.0168 |
| 33.28 | 221.84 | 0.0336 |

(Note all these figures are substantial overestimates for required power)

# ASPOD

# RIMARY TILT-TA[illegible]

# ESIGN AND SPECIFIC[illegible]NS

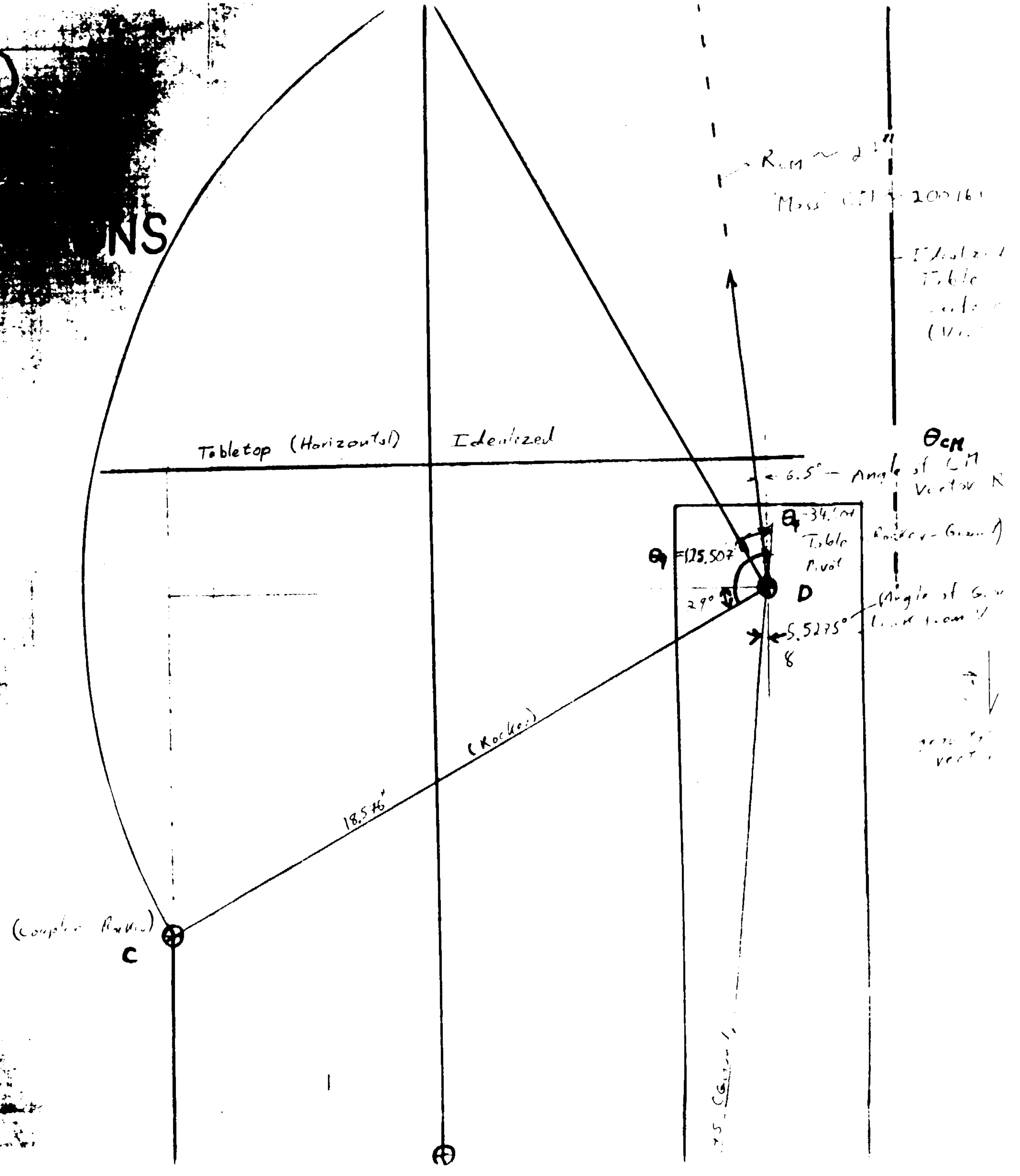

Rcm ~ 21"
Mass (CM) 200 lbs
Idealized Table
(V
Tabletop (Horizontal) Idealized
θCM
6.5° — Angle of CM Vector
θ₄ -34.°
Table Pivot
Rocker-Ground)
θ₃ =125.507°
29°
D
5.5275°
δ
Angle of Gr
(Rocker-Ground)
(Rocker)
18.5"
(Coupler Radius)
C

ORIGINAL PAGE IS
OF POOR QUALITY

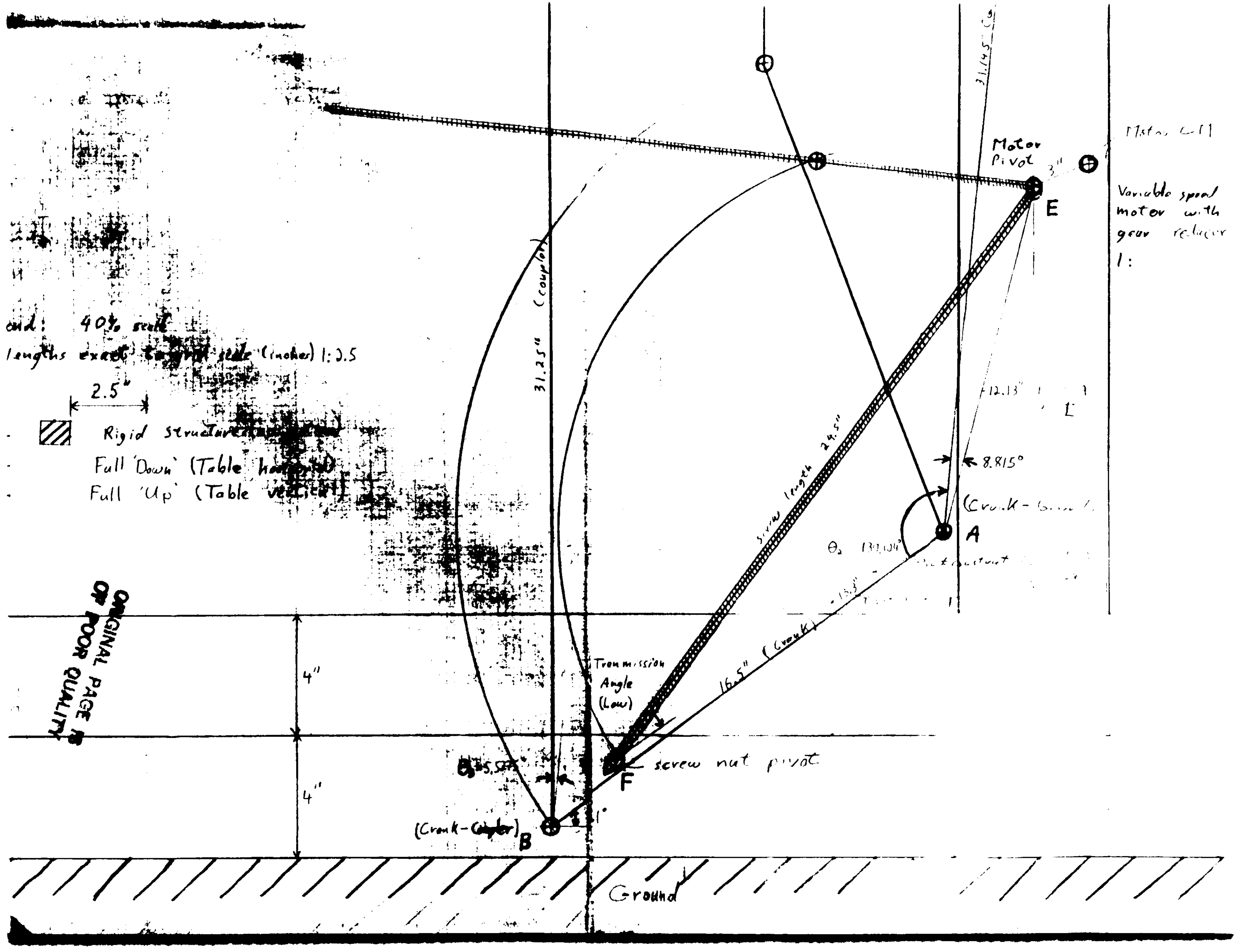

…nd: 40% scale
lengths except … scale (inches) 1:2.5
2.5"
▨ Rigid structure
Full 'Down' (Table horizontal)
Full 'Up' (Table vertical)
31.25" (coupler)
31.145" C
Motor Pivot
3"
Motor C…
Variable speed motor with gear reducer 1:
E
12.13"
L
8.815°
(Crank-Grou…
A
$\theta_2$ 130.04°
…t…ustrut
13.3"
screw length 24.5"
16.5" (Crank)
Transmission Angle (Low)
screw nut pivot
F
$\theta_3$ 5.5°
1°
(Crank-Coupler) B
4"
4"
Ground

ORIGINAL PAGE IS OF POOR QUALITY

# ASPOD SOLAR CUTTING ARRAY DESIGN PROJECT

SPONSORED BY

THE UNIVERSITIES SPACE RESEARCH ASSOCIATION
and
THE NATIONAL AERONAUTICS AND SPACE ADMINISTRATION

ADVISOR

Dr. Daniel J. Winarski

DESIGN GROUP LEADER

Jack W. Rust

DESIGN GROUP

MATHEW MULLER
THOMAS A. MARTUCCI III
DANIEL WILLIAMS

ORIGINAL PAGE IS
OF POOR QUALITY

# Table of Contents

GROUP RESPONSIBILITIES.................................................... 1
INTRODUCTION.................................................... 2
DESIGNING FOR THE SPACE ENVIRONMENT.................................................... 6
MOUNTING OF LENSES AND MIRRORS.................................................... 13
CHOSEN BRACKET DESIGN.................................................... 19
CUTTING ARRAY PERFORMANCE & HEAT TRANSFER MODEL....... 23
APPENDIX.................................................... 37
FINANCIAL SUMMARY.................................................... 45
REFERENCES.................................................... 46

# GROUP RESPONSIBILITIES

| | | |
|---|---|---|
| Jack Rust | Introduction and<br>Designing for the space environment.<br>(pages 2-12) | 11 |
| Thomas Martucci III | Mounting of lenses and mirrors.<br>(pages 13-18) | 6 |
| Dan Williams | Chosen bracket design.<br>(pages 19-22) | 4 |
| Matthew Muller | Cutting array performance and<br>Heat transfer model.<br>(pages 23-35) | 13 |

# INTRODUCTION:

For the past three years, engineers at the University of Arizona in association with the Universities Space Research Association and NASA have been attempting to address the problem of man made orbital debris. Since the inception of space flight over thirty years ago, such debris has continued to accumulate in earth orbit to the point where it now poses a serious navigational hazard to both manned and unmanned spacecraft. This problem has taken on new urgency in light of a recent near miss incident involving the space shuttle Atlantis and a derelict Soviet booster rocket.

Under the leadership of Dr. Kumar Ramohalli, U. of A. engineering students have developed a prototype orbital spacecraft called ASPOD (Automated Space Processor for Orbital Debris). ASPOD is designed to systematically gather and process large pieces of unwanted debris and store it for future disposal. Principle features of the spacecraft include two mechanical manipulator arms to capture and position debris for processing, and a solar powered cutting array to reduce large debris into manageable pieces. The cutting array assembly consists of four silver plated mirrors and five fresnel lenses mounted on a frame made of graphite/epoxy tubing. The mirrors reflect radiation from the sun, channeling it into the fresnel lenses. The lenses in turn focus this energy on a small point in space. The mechanical arms can then maneuver a large piece of debris through this point where the intensely focused beam of solar radiation will dismember it.

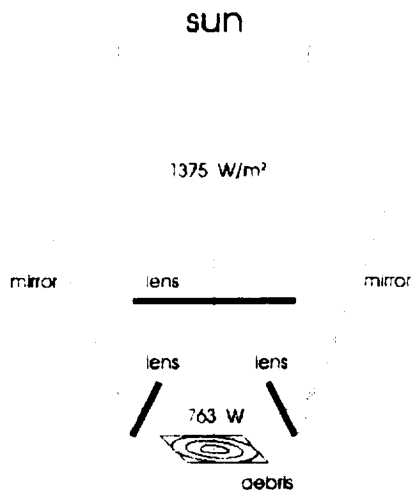
sun
1375 W/m²
mirror
lens
mirror
lens
lens
763 W
debris

Figure 1

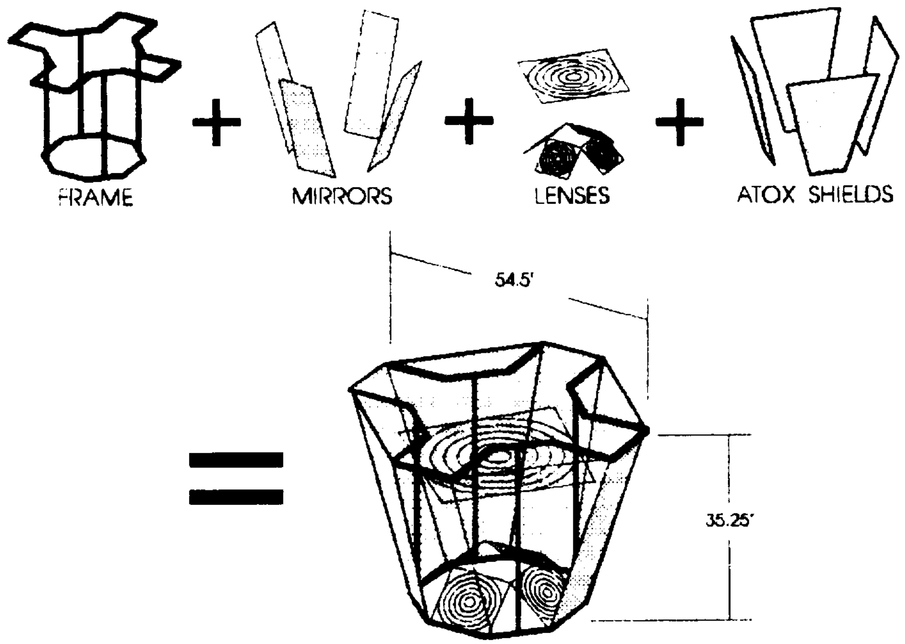
FRAME
MIRRORS
LENSES
ATOX SHIELDS
54.5'
35.25'

CUTTING ARRAY COMPONENTS

Figure 2

Previous design iterations of the cutting torch utilized a heavy kevlar and aluminum frame. The design emphasis being to make the frame so stiff and inflexible that the optics could not be misaligned under any circumstances. Although the prototype performed adequately in ground testing, its excessive weight made it impractical for space flight. Thus a lightweight graphite/epoxy frame was constructed to replace it.

The current undergraduate design team lead by Jack Rust was charged with the task of "designing and fabricating mounting pads to physically affix the array and an alignment jig to ensure the ideal focal point" In addition, the team has been asked to study the problems associated with launch, insertion, and operation of the cutting torch in the harsh environment of low earth orbit. Based on these and other studies, the design team would implement changes as necessary to improve the performance of the cutting torch in all aspects.

weight ≠ mass

Limitations and constraints as delineated by the client appear to be somewhat flexible. The entire assembly should be able to fit within a cube measuring ~~four~~ six feet by ~~four~~ six feet and should weigh no more than 70 lbm; criteria fulfilled by the previous design. In addition, the cutting torch must operate effectively when aligned with the sun to a tolerance of ±1° of arc. This being the current limitation of the solar tracking apparatus. Having invested substantial time and money into the development of the new lightweight graphite/epoxy frame, the client naturally wishes to incorporate it into the new design. Initial research has revealed that the frame, though lightweight, tends to exhibit considerable deflections when loaded. Therefore, if the frame is used it must me modified or complimented such that the mirrors and lenses will be positioned accurately enough to work properly during ground tests. In addition, the sensitive nature of the composite matrix precludes drilling or machining the frame in any way. To do so would substantially weaken the frame components. Therefore, use of conventional metal fasteners will be avoided when mounting optical components to the frame.

With regard to cutting performance, client specifications are not narrowly defined. It is expected that the new design will be able to outperform the previous model which was able to cut through .005" aluminum sheet.

Based on initial investigation and study, the design team has established its own target specifications for weight and performance. We believe it is possible to design a cutting array weighing no more than 30 lbm that can cut through .015" stainless steel sheet metal. Clearly, this would be an extraordinary improvement on the previous design and would more than adequately satisfy the requirements which our client has thus far promulgated.

# DESIGNING FOR THE SPACE ENVIRONMENT

Although the solar powered cutting array for the ASPOD prototype is to be tested and proven only on the ground, the ultimate goal is a design that will function properly in the harsh environment of space. To this end, the cutting array will incorporate design features which account for the effects of extraterrestrial radiation and monatomic oxygen corrosion. Both phenomena are quite prevalent in the Low Earth Orbit (LEO) environment and both have the potential to seriously affect design performance.

## ENVIRONMENTAL RADIATION

Orbital radiation originates from three primary sources; the sun, the earth's radiation belt, and cosmic sources outside the solar system. The intensity of the radiation flux exhibited in LEO varies as a function of satellite altitude and solar activity. Aside from the obvious physiological hazards radiation poses to astronaut crews, it also creates serious material problems in unmanned spacecraft. Mechanical properties of many materials have been known to degrade following prolonged exposure to radiation. Radiation data for a number of materials are given below.

| Radiation Damage Thresholds for Certain Classes of Materials | |
|---|---|
| Electronic Components | $10^1 - 10^3$ rad |
| Polymeric Materials | $10^7 - 10^9$ rad |
| Lubricants, Hydraulic Fluid | $10^5 - 10^7$ rad |
| Ceramic, Glasses | $10^6 - 10^8$ rad |
| Structural Metals, Alloys | $10^9 - 10^{11}$ rad |

Table 1

Throughout the course of the ASPOD program, Dr. Ramoholli and others have expressed a keen interest in using graphite/epoxy composite materials whenever possible in the construction of the spacecraft.

Although it possesses an exceptional strength to weight ratio, little is known about the behavior of this material following prolonged exposure to extraterrestrial radiation. At what cumulative exposure level does the composite's material strength begin to degrade? Will the performance of the solar cutting array be adversely affected by prolonged radiation exposure?

In order to answer these and other questions, a number of composite tensile test specimens have been fabricated by this design team and tested at The University of Arizona Physical Metallurgy Laboratory. Five of these specimens were irradiated at The University of Arizona Nuclear Engineering Radiography Laboratory. A diagram of the apparatus used to simulate an extraterrestrial gamma radiation environment is shown.

RADIATION EXPOSURE APPARATUS

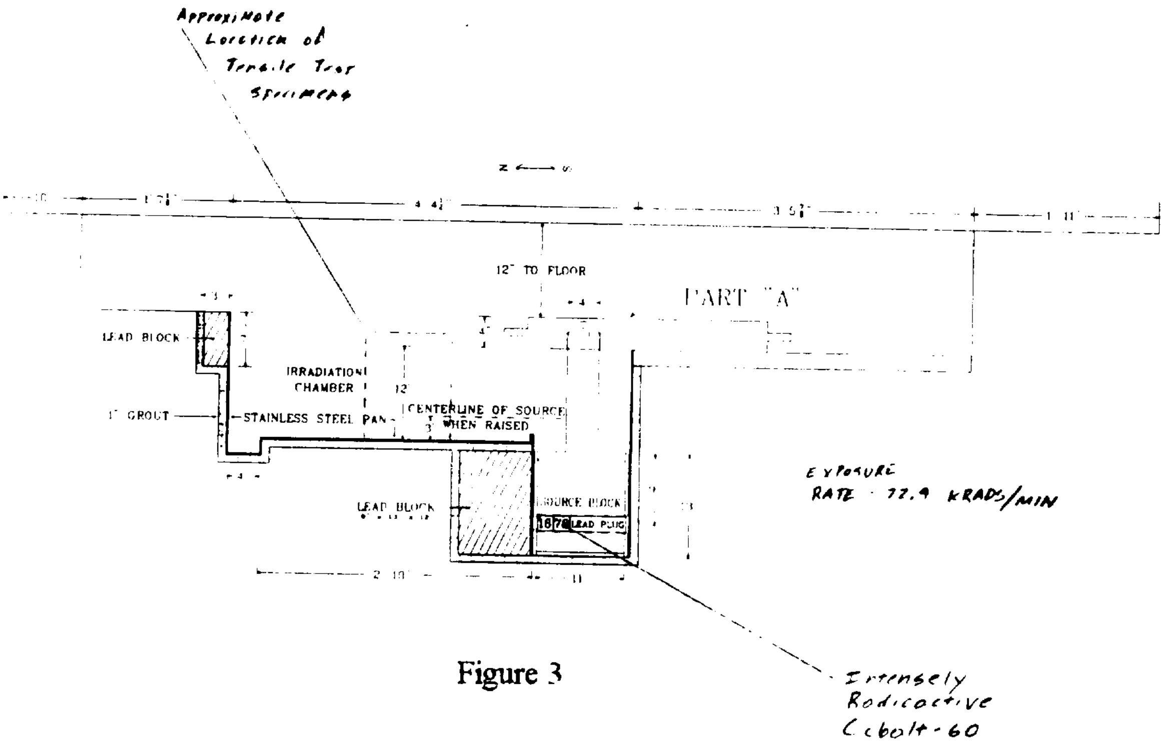
12" TO FLOOR
PART "A"
LEAD BLOCK
IRRADIATION CHAMBER
1" GROUT
STAINLESS STEEL PAN
CENTERLINE OF SOURCE WHEN RAISED
LEAD BLOCK
SOURCE BLOCK
1878
LEAD PLUG

Approximate Location of Tensile Test Specimens

EXPOSURE RATE · 72.9 KRADS/MIN

Intensely Radioactive Cobalt-60

Figure 3

ORIGINAL PAGE IS OF POOR QUALITY

When the source block is lifted, the tensile test specimens are exposed to an intensely radioactive cobalt 60 point source. Each specimen is exposed at a rate of approximately 73,000 rads per minute. The exceptionally high exposure rate allows one to simulate several years of space exposure over the course of a few hours.

In this manner, five composite tensile test specimens were subjected to varying degrees of exposure then tested to destruction. The ultimate tensile strengths of these specimens is shown below.

| Radiation Exposure | Ultimate Stress ($lbf/in^2$) |
|---|---|
| Non Radiated | 87,093 to 108,415 |
| $10^7$ Rad | 94,228 |
| $5 \times 10^7$ Rad | 85,031 |
| $10^8$ Rad | 87,634 |
| $5 \times 10^8$ Rad | 100,686 |
| $10^9$ Rad | 117,497 |

Table 2

Although the radiation exposure was increased by orders of magnitude with each succeeding specimen, the change in ultimate tensile strength was relatively small. It would take hundreds of years in space before the composite material could accumulate as much exposure as it did in this test. Thus, these results would seem to indicate that the performance of the cutting array will not be adversely affected by extraterrestrial radiation.

## MONATOMIC OXYGEN CORROSION

By far the most severe environmental factor affecting the design, monatomic oxygen corrosion has proven to be very destructive to orbiting satellites in the past. It has often resulted in the premature failure of satellite components particularly solar panels incorporating silver and/or graphite/epoxy parts.

As with extraterrestrial radiation, the intensity of ATOX corrosion would appear to be a function of solar activity as well as altitude. Corrosion data for some materials is listed below.

| Thickness loss per year of different solar array materials at 400 km altitude under minimum and maximum solar activity conditions | | |
|---|---|---|
| Material | Thickness Loss | |
| | Maximum | Minimum |
| Silver interconnector | 16.09 | 194 |
| Kapton (Rigid) | 4.6 | 55.4 |
| Epoxy | 4.81 | 58.06 |

Table 3

Silver coatings similar to that used on the ASPOD mirrors are particularly vulnerable to the affects of ATOX corrosion. The nominal thickness of mirror film to be used on this project is less than seventy microns. Under normal orbital conditions, the surface would be completely destroyed in less than six months without some form of adequate protection.

In order to solve this problem from an engineering standpoint, it is necessary to gain some understanding of how the mechanism of ATOX corrosion works. At the fringes of the atmosphere oxygen gas is ionized by high energy radiation primarily from the sun. The resulting negative ions oxidize quite readily with all manner of materials. In the ASPOD mirrors, ATOX would infiltrate through defects in the coating which protects the silver surface. Once beneath the coating, ATOX corrodes all of the silver in the immediate vicinity of the defect. Thus, the severity of the corrosion occurring over time is directly dependent on the degree to which the protective coating has been punctured by high energy particles, micro meteoroids, or other abrasions. When ATOX ions impact the surface of the mirrors at high relative velocities, corrosion problems are greatly exacerbated.

High energy ions striking the mirrors deliver sufficient kinetic energy to punctuate and erode the mirrors protective coating. In addition, ions which strike at large angles of incidence with the surface infiltrate horizontally into the silver material. This has the effect of undercutting the protective surface and depriving it of structural support. Over time, the protective surface material flakes off exposing the silver beneath.

With continued exposure to high relative velocity particle erosion in an ATOX environment the mirror material will degrade much more rapidly than it would if shielded from high velocity impacts. The annual decrease in material thickness of any substance exposed to ATOX corrosion is expressed by the following equations:

$$\phi_{AO} = N_d\, V_s \cos\theta$$

Eqn #1 ?

Where:

$\phi_{AO}$ = ATOX flux in atoms / cm$^2$ sec
$N_d$ = ATOX density
$V_s$ = Spacecraft Velocity
$\theta$ = Angle of Incidence
$t = 365 * 86{,}400 * \phi_{AO} * R_e$
$t$ = Annual Thickness Loss
$R_e$ = ATOX reaction coefficient

Separate Equation

One can use the above equations to calculate the orbital lifetime of an unprotected 70 micron silvered mirror. Bearing in mind that ASPOD will be required to change orbit and altitude frequently and consulting the graph of altitude vs. ATOX flux shown below, one may reasonably assume a mean flux of $10^{14}$ atoms / cm$^2$ sec.

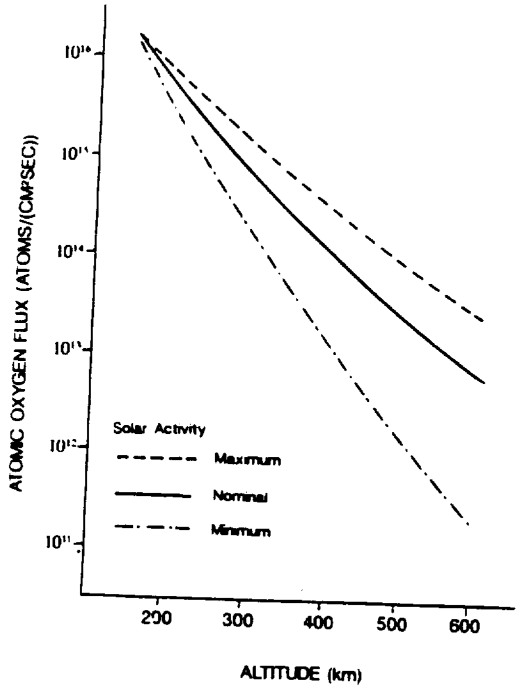

'OMIC OXYGEN FLUX DEPENDENCE UPON ALTITUDE

Figure 4

Assuming a reactivity coefficient of $10.5 \times 10^{-24}$ cm$^3$ / atom for silver, calculations indicate that the mirror would be eaten at the rate of 330 microns per year. Thus, without adequate protection the mirror would be completely destroyed within three months. The mirror lifetime will of course vary depending upon ATOX flux variations. The flux in turn is dependent upon both the eleven year solar cycle and relative velocity of the ATOX particles.

If the mirrors could be shielded from high velocity particles, the flux could be considerably attenuated and the lifetime of the mirrors increased. This is the primary reasoning behind the shrouded ASPOD design pictured in Figure 2.

Although the mirrors will still be exposed to a substantial ATOX flux, the flux component in the direction of motion ($V_s$ ) can be cut considerably. Thereby extending the life of the mirrors.

When the torch is not in use, ASPOD will simply maneuver the assembly such that the top and bottom openings are ninety degrees away from the direction of satellite motion. Although not the most sophisticated method for protecting the mirrors, it is both simple and inexpensive. In addition, it will help to lend much needed structural support. Ideally, the shroud and mirror panels would be fabricated from the same lightweight graphite/epoxy materials used in the frame. This project will likely use polyethylene panels unless a more inexpensive means can be found to fabricate large sheets of composite. Although heavier than composite materials, polyethylene will adequately serve the requirements of a ground based demonstration array.

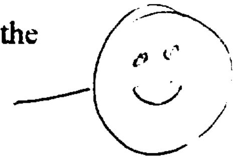

# MOUNTING OF LENSES AND MIRRORS

The original configuration of the ASPOD solar cutting array has been retained as shown Figure 2. However, the new design will incorporate a considerably larger central fresnel lens. It measures four square feet whereas the previous design used a one square foot lens which enabled it to cut .005 in. aluminum sheet metal with some difficulty. The new lens can cut similar metal instantaneously and makes short work of steel or brass specimens of much greater thickness. Performance data about this lens gathered from experimental techniques and computer simulation is discussed in detail later in the this report. In addition to a larger lens, the new design also incorporates panels which enclose the entire array about the central axis. Figure 2 shows the array partially enclosed allowing a view of the internal mirror and lens arrangement. Ideally, the panels would be fabricated out of graphite/epoxy which exhibits an excellent strength-to-weight ratio. The ground prototype will likely incorporate PVC panels which are easier to fabricate and several times cheaper. The enclosure will provide protection against monatomic oxygen corrosion in addition to providing much needed structural support. The new design will also incorporate lighter mirrors than the 52 lbm (total mirror weight) of the previous design. The new mirrors make use of 3M brand SS-95 High Performance Silver Reflective Film commonly known as "Silverlux" which exhibits slightly better reflective properties than the old aluminum mirror. The film is coated with an adhesive backing and will be mounted on a PVC substrate material identical to the enclosure panels.

In order to "physically affix the array" and "ensure the ideal focal point" as requested by our sponsor in their proposal, the new design will incorporate adjustable mounting brackets for all of the lenses. To arrive at this design, a number of questions needed to be addressed. Among them,

1)In which direction and to what extent should they be movable?

2) What degree of precision will be required in the adjustment?

3) What material exhibits the best combination of strength, weight, machinability, corrosion and radiation resistance and low cost?

The cutting array is designed to support the weight of all optical components and maintain them in proper position to function effectively when fully assembled and standing relatively still on a test table or mounted to the spacecraft. Nevertheless, misalignment of optical components due to mechanical shock, transporting of the array, repeated assembly and disassembly and general wear and tear are inevitable. Therefore, the new design must provide for manual adjustment of the lenses so that all of the energy can be directed into the smallest possible focal zone as shown in Figure 1. Each of the mirrors are to be fastened to the frame at four points and are not likely to be so severely misaligned as to require manual adjustment. Therefore, they will be fixed and the lenses will be adjusted to accommodate them if necessary.

## MANEUVERABILITY OF LENSES AND MIRROR

### LARGE FRESNEL LENS ;

The large central lens projects the largest and hottest focal zone centered directly beneath the array. The most logical approach would be to adjust the focus of the central lens first then adjust the four surrounding small lenses so that they can contribute their energy to the same point on the cutting surface. To do this, the central lens must exhibit linear freedom of motion along the vertical axis of the array. See figure below.

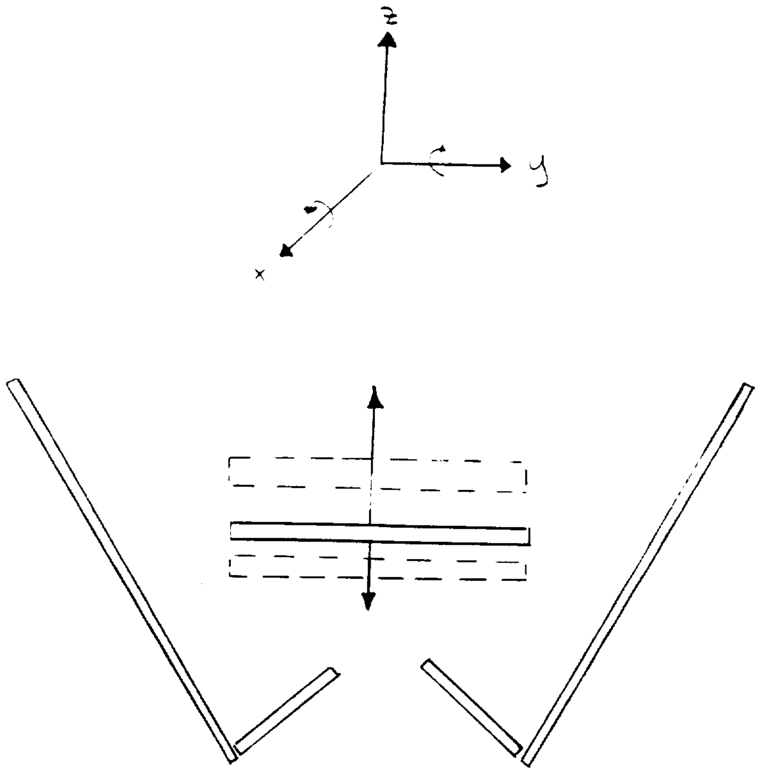

LIMITED ROTATION IN $(\ni_X, \bullet)$ & $(\ni_Y, \bullet)$ DIRECTIONS

Figure 5

There can be limited rotation in the $(\theta_X, \bullet)$ and $(\theta_Y, \bullet)$ directions.

## SMALL LENSES

Similarly, each of the small surrounding lenses will need to translate along the plane of its corresponding mirror. In addition, each should be capable of rotary motion about the base axis as pictured in Figure 6.

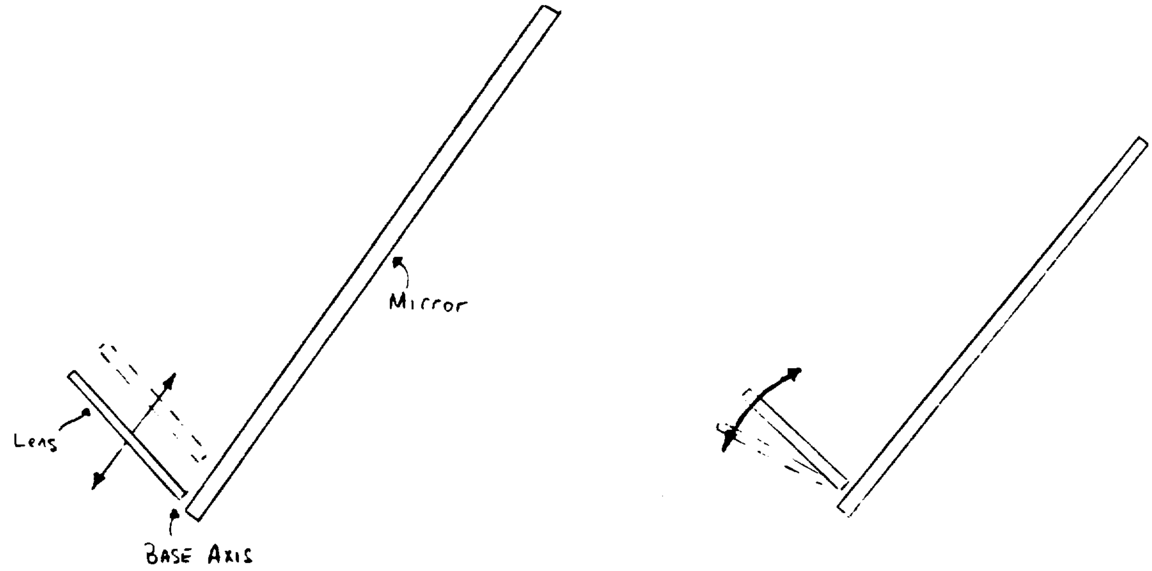

Figure 6

## MIRRORS :

The precision and extent of mirror movement required depends on the extent to which shock or movement of the array may misalign the mirrors and the extent to which that would affect the performance of the cutting array. Experimental results detailed in the heat transfer and performance section of this report show that a fresnel lens can still maintain very high focal zone temperatures even when misaligned by several degrees. Thus a rigid mount for the mirrors will be sufficient.

A tabular summary of component maneuverability is shown below.

| fresnel lens size | motion | DOF | amount |
|---|---|---|---|
| LARGE | induced translation | 1 | ± 2 in. |
|  | limited rotation | 2 | approximately 5° |
| SMALL | induced translation | 1 | ± 2 in. |
|  | rotation | 1 | 20° |

Table 4

## DEGREE OF PRECISION

### LARGE LENS

For the large central lens, a 2 in. linear range of motion should be more than adequate to adjust the lens focus under normal circumstances. The focusing mechanism should provide for both coarse and fine adjustment. The coarse adjustment should allow focusing of the mirror along its axis of motion down to the within an inch of the desired location. The fine adjustment will make use of fine threaded lead screws allowing focusing down to the nearest sixteen thousandths of an inch.

### SMALL LENSES

The surrounding small lenses will have similar linear focusing requirements. In addition, mounting brackets for the small lenses should allow for radial positioning across a range of twenty degrees down to the nearest degree. Based on the data gathered by experimentation with the fresnel lenses, positioning the mirrors anywhere within these ranges of motion should not seriously hamper their effectiveness.

## MATERIALS SELECTION

In selecting materials from which to fabricate the mounting brackets, a number of factors must be taken in to account. A combination of adequate strength and light weight is of paramount importance.

At the same time the design team must be able to produce the design in the AME production lab. The brackets must also be resistant to monatomic oxygen corrosion and radiation effects. Aluminum fulfills all of these requirements in addition to being inexpensive.

# CHOSEN BRACKET DESIGN

Adhering to the aforementioned design criteria, we have engineered the following brackets.

## LARGE FRESNEL LENS

Below is a three dimensional drawing of our chosen design. For a detailed description consult blueprint number two.

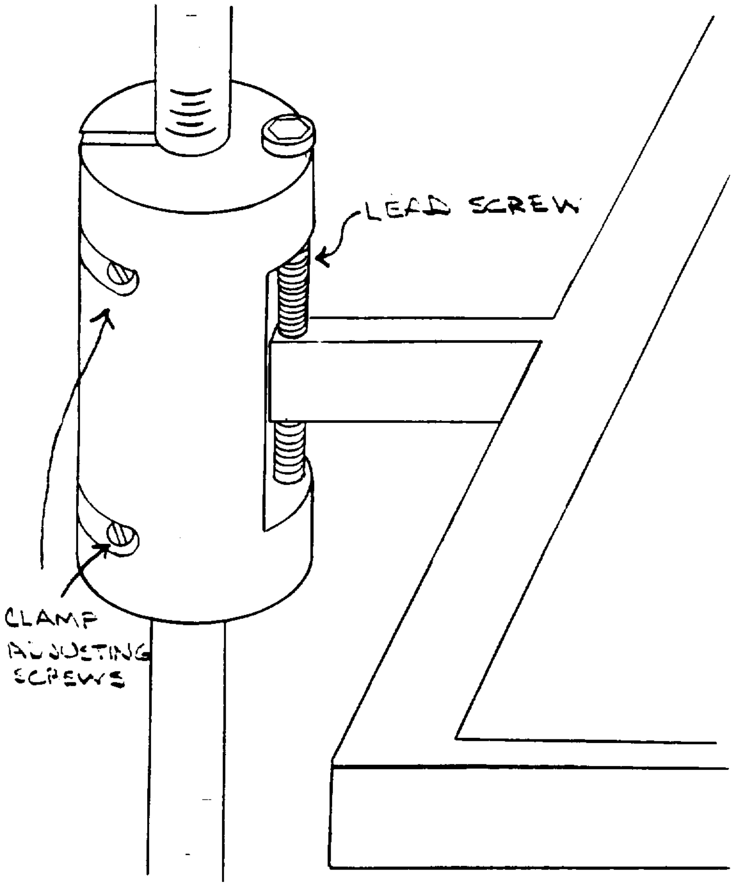
LEAD SCREW
CLAMP ADJUSTING SCREWS

Figure 7

The large fresnel lens is supported by four adjustable brackets, each of which is attached to a vertical member of the composite frame. To position the large fresnel lens, the clamp adjusting screws are loosened allowing the bracket to slide freely along the vertical frame member. The bracket can then be moved to within roughly one inch of the desired position. This independent freedom of motion for each bracket allows us to compensate for any misalignment of the large fresnel lens. In this manner, the trade-off between ultra-tight tolerances (fixed optics) verses loose tolerances (adjustable optics) is addressed. Tolerances are not as easily controlled as adjustable optics. Refer to blueprint number two for detailed technical specifications.

SMALL LENS BRACKET

Below is a three dimensional view of our chosen bracket design.

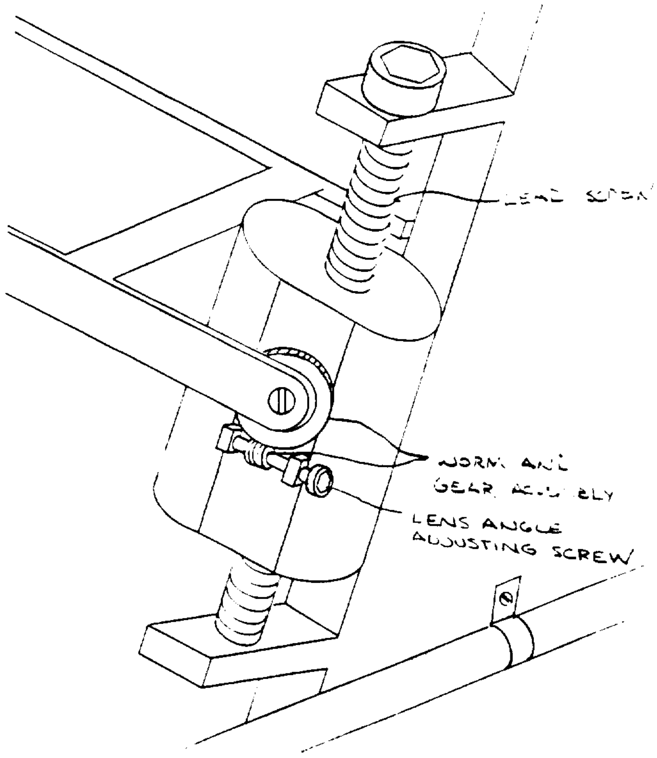

Figure 8

This bracket allows two directions of motion as required. The translational motion along the plane of the mirror is controlled by the large lead screw which can be turned by hand or with an Allen wrench. This design will give a two inch range of motion. The angle of the lens will be controlled by a worm and worm gear assembly. Control is achieved by turning the adjusting screw. The worm gear concept was chosen since it allows for positive control in both directions.

## DEGREE OF PRECISION

### LARGE FRESNEL LENS BRACKET

The lead screw which controls the fine adjustment will have sixteen threads per inch. For a quarter inch turn a 0.015 in. travel of the large fresnel lens will result. This meets the adjustability precision criteria.

### SMALL FRESNEL LENS BRACKET

The small lens bracket will have the same translational precision as the large lens bracket. The worm gear assembly provides for a large angle of adjustment far beyond the twenty degree range of rotation required. One quarter turn of the lens angle adjusting screw results in approximately one degree rotation of the small lens which satisfies the precision adjustability requirement for rotation.

## TOLERANCES

A tolerance of 0.010 in. will be assumed in machining these brackets. This will facilitate manufacturing while at the same time fulfilling the design requirements.

## MATERIAL SELECTION

Material selection was based upon a number of considerations. These included cost, machinability, corrosion resistance, availability, durability, thermal considerations, and weight. Aluminum best satisfies these criteria in the following ways:

- It is lightweight which is beneficial in maneuvering the assembly
- It is inexpensive and available in all required shapes and sizes
- Machinability characteristics are desirable (turns, mills, and cuts easily)

# CUTTING ARRAY PERFORMANCE & HEAT TRANSFER MODEL

The total power output of the solar cutting device can be calculated. This output is a function of the surface area and transmissivity of the lenses, the efficiency of the mirrors, and the insolation coefficient $G_{SC}$. The coefficient $G_{SC}$ is a constant which represents the amount of solar radiation hitting an extra-terrestrial surface normal to the suns rays. The calculations in the appendix yield a solar cutting power of 763 Watts.

A heat transfer program was designed to provide cutting estimates for various materials under the focal region of the proposed solar cutting torch. The source code for the program is located in appendix. The heat transfer model was designed for rapid estimates of the cutting limits applied to various materials for two geometries. The following assumptions were made in the creation of the heat transfer model.

- The focal region of the lens cutting system produces 763 Watts evenly distributed about a radius of 2.0 centimeters.
- All materials absorb 49.3% of the energy provided at the focal region.
- Materials experience both radiation and conductive heat transfer.
- Materials do not experience convective heat transfer because of the vacuum environment of space.
- The materials do not experience chemical reactions, such as burning, because of the limited atmosphere.
- The model uses finite differences with Euler explicit forward differentiation to simulate the heat transfer.

The equations for the heat transfer analysis start with the conservation of energy.

$$Q_{stored} = Q_{in} - Q_{out}$$

Next we turn to the basic heat transfer equations.

$$Q_{conduction} = Q_c = kA\left(\frac{dT}{dx}\right)$$

$$Q_{radiation} = Q_r = \sigma A T^4$$

$$Q_{stored} = Q_s = mc\left(\frac{dT}{dt}\right)$$

$$Q_{spc} = \text{solar energy input}$$

When combined with the energy equations the following relationship is produced.

$$Q_{in} = (Q_c)_{in}$$

$$Qout = (Q_c + Q_r)_{out}$$

$$mc\left(\frac{dT}{dt}\right) = k(A_c)_{in}\left(\frac{dT}{dx}\right) - k(A_c)_{out}\left(\frac{dT}{dx}\right) - \sigma A_r T^4$$

The heat transfer model uses finite differences to represent the differential terms of the energy balance equation. This finite differences model is applied to two geometric shapes. the rectangular bar and the plate. Both geometries will simplify to a one-dimensional heat transfer problem. The bar is broken down into a series of small blocks. The block elements are placed end to end. The solar heat input is directed at the center block and the heat flows outward from the center block. Because the flow is symmetrical to the left and to the right of the heat source, the analysis is simplified by only looking at half of the bar.

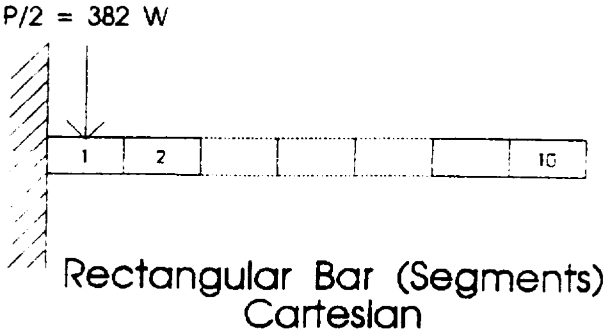

Figure 9

This new configuration experiences only half of the solar heat input and the heat flow proceeds from the source element to the end element in a one-dimensional flow. The differential length (dx) or (dL) of each element is constant and is strategically chosen so as to correspond to the size of the solar input region. The actual distance (dL) used in the program is equal to half of the diameter of the focal region. The first element of the model is then the only element to experience the direct heat input of Qspot.

The conduction area (Ac) between all blocks and the radiation area (Ar) are defined by the following equations.

$$A_c = w \cdot h$$

$$A_r = w \cdot dL$$

The mass of any given block is then defined.

$$m = A_r \cdot h$$

The plate geometry differs slightly from the bar geometry. Instead of block elements the plate uses concentric rings.

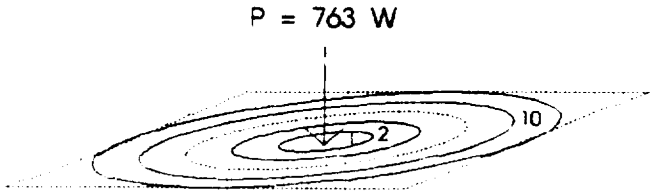

Plate (Concentric Rings)
Radial

Figure 10

The distance dR is used instead of dL. The conduction area and the radiation area are different for each ring element.

$$A_c(i) = 2\pi(i \cdot dR) \cdot h$$

$$\begin{aligned} A_r(i) &= \pi\left[(i \cdot dR)^2 - ((i-1) \cdot dR)^2\right] \\ &= \pi \cdot dR^2\left[(i)^2 - (i^2 - 2i + 1)\right] \\ &= \pi \cdot dR^2 \cdot (2i - 1) \end{aligned}$$

The conduction area (Ac) for an element *i* is defined as the area of the outer edge of the ring element. This is the conduction area for the exit surface of the element.

The solar input (Qspot) is applied to the first ring element which is actually a disc. The plate geometry behaves in the same manner as the bar geometry in all other aspects.

The following is a table of the heat transfer coefficients for the various materials used in the program.

| Material | Density "rho" (kg/m^3) | Thermal Conductivity "k" (W/m·K) | Heat Capacity "c" (J/kg·K) | Melting Temperature "Tmelt" (K) |
|---|---|---|---|---|
| Aluminum (pure) | 2707 | 204 | 896 | 660+273 |
| Brass (70%Cu,30%Zn) | 8522 | 111 | 385 | 1083+273 Cu |
| Carbon Steel (1.0% C) | 7800 | 43 | 473 | 1537+273 |
| Copper (pure) | 8954 | 386 | 383 | 1083+273 |
| Iron (pure) | 7897 | 73 | 452 | 1537+273 |
| Lead (pure) | 11373 | 35 | 130 | 327+273 |
| Silver (pure) | 10524 | 419 | 234 | 961+273 |
| Titanium | 4507 | Not Available | 523 | 1670+273 |

Table 5

Now we take a close look at the program itself. *Quick Basic* was used for the model because it was easily accessible. The complete program is listed in the appendix. On the following page is a flow chart to explain the desired functionality of the program.

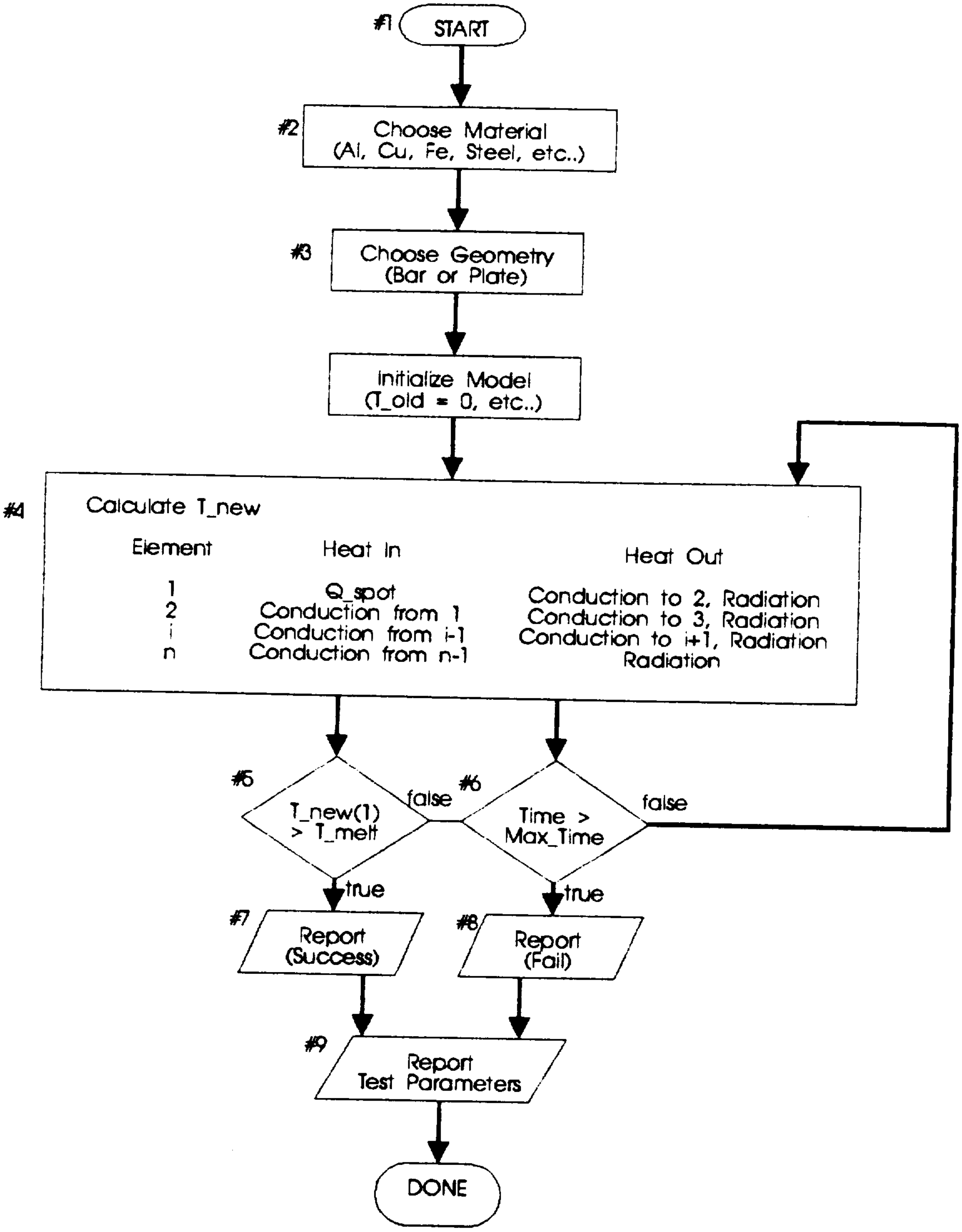#1
START
#2
Choose Material
(Al, Cu, Fe, Steel, etc..)
#3
Choose Geometry
(Bar or Plate)
Initialize Model
(T_old = 0, etc..)
#4
Calculate T_new
Element
Heat In
Heat Out
1
Q_spot
Conduction to 2, Radiation
2
Conduction from 1
Conduction to 3, Radiation
i
Conduction from i-1
Conduction to i+1, Radiation
n
Conduction from n-1
Radiation
#5
T_new(1) > T_melt
false
#6
Time > Max_Time
false
true
true
#7
Report (Success)
#8
Report (Fail)
#9
Report Test Parameters
DONE

Figure 11

Block #1 is the starting block of the program. This corresponds to lines 10 through 70 of the program. The following constants are defined.

- Number of differential elements, nEnd
- Maximum number of time steps, TheEnd
- Distance between differential bar elements, dL [meters]
- Distance between differential ring elements, dR [meters]
- Pi ($\pi$), pi
- Stefan-Boltzman constant ($\sigma$), S [$W/m^2 \cdot K^4$]
- Elapsed time, Time [sec]
- Time step, dt [sec]

The following element properties are dimensioned.

- Next temperature of an element, Tnew(i) [K]
- Last temperature of an element, Told(i) [K]
- Conduction area out of an element, Ac(i) [$m^2$]
- Radiation surface area of the top of an element, Ar(i) [$m^2$]
- Conductive heat transfer out of an element, Qc(i) [W]
- Radiative heat transfer out of top surface of an element, Qr(i) [W]

The starting temperature is initialized.

- Last temperature of all elements is set to zero degrees Kelvin, Told(i) = 0

This corresponds to lines 0 through 99 of the program.

In block #2 the user chooses the desired material to test. This process selects the following material constants.

- Melting Temperature, Tmelt
- Thermal Conductivity, k
- Heat Capacity, c
- Density, rho

Block #2 corresponds to line 100 through 299 of the program.

In block #3 the user defines the geometry of the material. The following decisions are made.

- Bar or Plate Geometry
- Thickness of Specimen, h [mm]
- Width of Bar (bar geometry only), w [mm]

From this information the following is calculated.

- Thickness of Specimen, h [m]
- Width of Bar (bar geometry only), w [m]
- Conduction Cross-sectional Area of each element, Ac(i) [m^2]
- Radiation Surface Area of each element, Ar(i) [m^2]
- Solar heat gain from the lens system, Qspot [W]
- Finite distance between elements, dx [m]

The solar heat gain is calculated assuming the material will absorb 50% of the radiation applied to it. This corresponds to lines 300 through 399 of the program.

The next few lines of the program (400 through 499) correspond to anything on the block diagram. Two things occur in this portion of the code.

- A report header is printed
- Some constants are combined into one value

Block #4 is the main loop of the program. This block of code calculates and updates the new temperatures for all of the finite elements according to the following schedule. Remember that Qc(i) refers to the heat flux out of the element *i* to the element *i-1*.

| Element | Heat In | Heat Out |
|---|---|---|
| 1 | Qspot | Qc(1) + 2*Qr(1) |
| 2 | Qc(1) | Qc(2) + 2*Qr(2) |
| i | Qc(i-1) | Qc(i) + 2*Qr(i) |
| nEnd | Qc(nEnd-1) | 2*Qr(nEnd) |

The radiation heat flux is doubled because it occurs out of both the top and the bottom of each element. All heat transfer terms are calculated from the temperature readings at the last time step. The values for Told are only updated after all the Tnew values have been calculated. The program also checks for abnormal heat transfer. If the temperature of any element (i) at any instance is greater than the temperature of the previous element (i-1) then the program makes a note of the abnormal heat flow which will be reported at the end of the simulation. Block #4 corresponds to lines 500 through 799 of the program.

Block #5 tests to see if the material has melted. If so, the program proceeds to block #7 which reports the melting results. This refers to line 770 and lines 900 to 999.

Block #6 test to see if the simulation is out of time. If not, the program loops back block #4. If so, the program proceeds to block #8 which reports the failure to melt. This refers to line 780 and lines 800 to 899.

Block #9 reports the test information. This includes the following.

- Material properties
- Simulation geometry
- Any noted abnormalities

This block refers to lines 1000 to 1130 of the code.

The Heat transfer model needed to be calibrated. To do this we compared it to the experimental results obtained from melting the steel strips. The value for absorptivity was adjusted until the computer model reaches its closest match to the experimentation. The calibration resulted in the best value for absorptivity of the material. This value is used for all of the materials in the simulation because it is the only value available. Here are the results from this experiment with the calibrated computer model.

| Experimental Results<br>Steel Strip (width = 13 mm) | | | |
|---|---|---|---|
| Thickness (in) | Model Melting Time (sec) | Experimental Melting Time (sec) | Error |
| 0.005 | 0.9 | 4.7 | |
| 0.006 | 1.2 | 4.8 | |
| 0.007 | 1.5 | 3.6 | |
| 0.008 | 1.8 | 11.7 | |
| 0.009 | 2.3 | 7.7 | |
| 0.010 | 3.2 | 9.3 | |
| 0.011 | 4.4 | 8.0 | |
| 0.012 | 5.8 | 12 | |
| 0.013 | 7.4 | 24 | |
| 0.014 | 9.5 | 18.6 | |
| 0.015 | 12.5 | 17.4 | |
| 0.016 | 18.5 | 21.4 | |
| 0.017 | 43.3 | 23.4 | |
| 0.018 | ---- | 16.2 | |
| 0.019 | ---- | ---- | |
| 0.020 | ---- | ---- | |

Table 6

The computer results behave in an exponential manner and the experimental results behave in a somewhat linear manner. Both however have reasonable consistency for the maximum thickness that can be cut. There are several reasons that contribute to the difference in behavior.

- Oxidization - The metal oxide has a different melting temperature than the metal itself.
- Blackening - The material blackens when it oxidizes and therefore changes the absorptivity.
- Coefficients - The thermodynamic constants used in the model are actually a function of temperature.
- Convection - The model does not account for convective heat transfer in the metal whereas the experiment definitely was affected by convection.
- Human Error - Many of the experimental results have a bias error due to the lag from positioning the strip in the focal zone.

The shaded values are bad data points and were thrown out of the correlation analysis. Using *QuattroPro*, a regression analysis was performed on the experimental and theoretical melting times. This analysis resulted in an 83% correlation, 100% meaning perfect correlation and 0% meaning no correlation. Below is a graphical representation of theoretical versus experimental melting times.

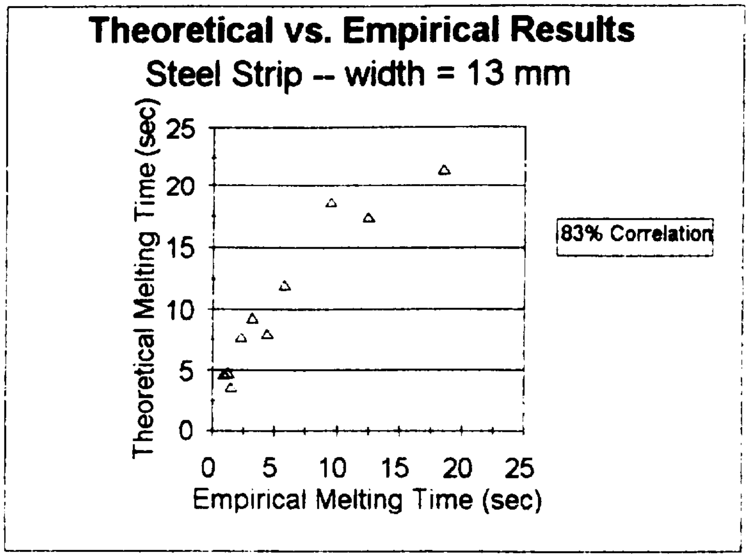

Figure 12

The heat transfer computer model yielded the following results for maximum thickness of materials that can be cut within 10 seconds.

| Maximum Material Thickness<br>(Cutting Time = 10 sec) | | |
|---|---|---|
| Material | Thickness (mm) | |
| | Bar Geometry<br>(width = 15 mm) | Plate Geometry |
| Aluminum | 1.75 | 0.55 |
| Brass | 1.15 | 0.45 |
| Carbon Steel | 0.04 | 0.04 |
| Copper | 0.60 | 0.15 |
| Iron | 0.04 | 0.04 |
| Lead | 7.55 | 4.00 |
| Silver | 0.85 | 0.20 |
| Titanium | Not Available | Not Available |

Table 7

In conclusion the model and the experimentation are both useful in obtaining a general idea for the melting capacity of the lens configuration. More experimentation will result in a better fit for the model. This and other model improvements will produce more precise limits to the melting ability of the solar cutting array. This computer model may later be adapted for on-line use with the ASPOD vessel to calculate feed rates for metal cutting.

# APPENDIX

## POWER OUTPUT DERIVATION

Values used in determining the expected power output of the fresnel lens cutting system.

- Extra-Terrestrial Insolation, $G_{SC} = 1353\ W/m^2$

Central Lens

- Transmissivity, $\alpha_{ctr} = 82\%$
- Area, $A_{ctr} = 4\ ft^2 = 4/(3.2808^2) = .372\ m^2$

Auxiliary Lenses

- Transmissivity, $\alpha_{aux} = 82\%$
- Area, $A_{aux} = 1\ ft^2 = 0.093\ m^2$

Mirrors

- Efficiency, n = 82%

$Power_{out} = Power_{ctr} + 4 * Power_{aux}$

$P_{ctr} = G_{sc} * A_{ctr} * \alpha_{ctr}$

$= 1375 * .372 * 0.82 = 419\ W$

$P_{sml} = G_{sc} * A_{sml} * Trans * Refl$

$= 1375 * .093 * 0.82 * 0.82 = 86\ W$

$Power_{out} = (419) = 4 * (86) = 763\ W$

## COMPUTER MODEL PROGRAM CODE

```
REM Init Programming Constants
10 nEnd = 10: TheEnd = 100000: dL = .01: dR = .01
20 DIM Tnew(1 TO nEnd), Told(1 TO nEnd), Ac(1 TO nEnd), Ar(1 TO nEnd)
30 DIM Qc(1 TO nEnd), Qr(1 TO nEnd)
40 pi = 3.141592654#: S = .00000005997#    'S = Stefan-Boltzmann Constant
50 FOR i = 1 TO nEnd
60 Told(i) = 0 'SET INITIAL TEMP = 0
70 NEXT i
80 time = 0
90 dt = .1


REM Choose Material
100 PRINT "          MELTING PROGRAM"
110 PRINT "Finite Difference Heat Transfer Analysis"
120 PRINT "         Using Euler Explicit"
130 PRINT
140 PRINT "Select Material for testing"
150 PRINT "    1. Aluminum"
155 PRINT "    2. Brass (70% Cu, 30% Zn)"
160 PRINT "    3. Carbon Steel (1.0% C)"
165 PRINT "    4. Copper"
170 PRINT "    5. Iron"
175 PRINT "    6. Lead"
180 PRINT "    7. Silver"
```

```
185 PRINT "     8. Titanium"
190 PRINT "     9. <custom>"
200 INPUT Material
210 SELECT CASE Material
        CASE IS = 1           'Aluminum
            k = 202: c = 896: rho = 2707: Tmelt = 948
            Mater$ = "Aluminum"
        CASE IS = 2           'Brass
            k = 111: c = 385: rho = 8522: Tmelt = 1083 + 273'Tmelt Cu
            Mater$ = "Brass (70% Cu, 30% Zn)"
        CASE IS = 3           'Carbon Steel
            k = 43: c = 473: rho = 7800: Tmelt = 1537 + 273
            Mater$ = "Carbon Steel (1.0% C)"
        CASE IS = 4           'Copper
            k = 386: c = 383: rho = 8954: Tmelt = 1083 + 273
            Mater$ = "Copper(pure)"
        CASE IS = 5           'Iron
            k = 73: c = 452: rho = 7897: Tmelt = 1537 + 273
            Mater$ = "Iron"
        CASE IS = 6           'Lead
            k = 35: c = 130: rho = 11373: Tmelt = 327 + 273
            Mater$ = "Lead"
        CASE IS = 7           'Silver
            k = 419: c = 234: rho = 10524: Tmelt = 961 + 273
            Mater$ = "Silver"
REM     CASE IS = 8           'Titanium
REM         k = xxx: c = 523: rho = 4507: Tmelt = 1670 + 273
REM         Mater$ = "Titanium"
    CASE ELSE           '<custom>
        PRINT "Enter the thermal conductivity (W/m·K)";
        INPUT k
        PRINT "Enter the heat capacity (J/kg·K)";
        INPUT c
        PRINT "Enter the density (kg/m^3)";
        INPUT rho
        PRINT "Enter the melting temperature (K)";
        INPUT Tmelt
        Mater$ = "Custom Material"
    END SELECT


REM Choose Geometry
300 PRINT "Select test geometry"
310 PRINT "     1. Rectangular Bar"
320 PRINT "     2. Plate"
330 INPUT Geometry
340 SELECT CASE Geometry
    CASE IS = 1     'Rectangular Bar
        PRINT "Enter bar thickness (mm)"
        INPUT h
        h = h / 1000
        PRINT "Enter bar width (mm)"
        INPUT w
        w = w / 1000
```

```
            FOR i = 1 TO nEnd
            Ac(i) = w * h          'Conductive Area Out
            Ar(i) = w * dL      'Radiative Area Surfaces
            NEXT i
            Qspot = .493 * 763 / 2        '49.3% ABSORPTION. 1/2 Left & 1/2 Right
            Geom$ = "Rectangular Bar"
            dx = dL
        CASE ELSE      'Plate
            PRINT "Enter plate thickness (mm)"
            INPUT h
            h = h / 1000
            FOR i = 1 TO nEnd
            Ac(i) = 2 * pi * (i * dR) * h
            REM    Ar(i) = π·[(i·dR)² - (dR(i - 1))²]
            REM    Ar(i) = π·dR²·[(i²) - (i²-2i+1)]
            REM    Ar(i) = π·dR²·(2i-1)
            Ar(i) = pi * (dR ^ 2) * ((2 * i) - 1)
            NEXT i
            Qspot = .493 * 763            '49.3% ABSORPTION.
            Geom$ = "Plate"
            dx = dR
       END SELECT

470 Abnormal = 0
480 PRINT "   Time   T1   T2   T3   T4   T5   T6   T7"
490 dtOVERcRHOh = dt / (c * rho * h)
```

```
REM Main Loop

500 FOR j = 1 TO TheEnd
510 time = CINT((time + dt) * (1 / dt)) * dt

520 FOR i = 1 TO nEnd

REM Calculate Qconduction
550 IF i <> nEnd THEN
560 Qc(i) = k * Ac(i) * (Told(i) - Told(i + 1)) / dx
570 ELSE
580 Qc(i) = 0
590 END IF

REM Calculate Qr
600 Qr(i) = S * Ar(i) * Told(i) ^ 4


REM Calculate Tnew
650 IF i = 1 THEN
660 Tnew(i) = Told(i) + (dtOVERcRHOh / Ar(i)) * (Qspot - Qc(i) - 2 * Qr(i))
670 ELSE
680 Tnew(i) = Told(i) + (dtOVERcRHOh / Ar(i)) * (Qc(i - 1) - Qc(i) - 2 * Qr(i))
685 IF Tnew(i) > Tnew(i - 1) THEN Abnormal = 1
690 END IF

REM Examine Tnew
```

```
700 Told(i) = Tnew(i)
710 NEXT i

740 PRINT USING " ####.##"; time;
750 PRINT USING " ####.#"; Tnew(1); Tnew(2); Tnew(3); Tnew(4); Tnew(5); Tnew(6); Tnew(7)
770 IF Tnew(1) >= Tmelt GOTO 900
780 NEXT j

REM Report No Melt
800 PRINT
810 PRINT "MATERIAL DID NOT MELT IN TIME ALLOWED"
820 GOTO 1000

REM Report Tmelt
900 PRINT
910 PRINT "MATERIAL MELTED AT "; Tnew(1); " KELVIN";
915 PRINT " IN "; time; "SECONDS"
920 GOTO 1000

REM Report Test Parameters
1000 PRINT
1010 PRINT Mater$; " - "; Geom$
1020 PRINT "thickness = "; h * 1000; " mm"
1029 IF Geometry = 1 THEN
1030 PRINT "width="; w * 1000; " mm"
1031 END IF
```

```
1040 PRINT "thermal conductivity ="; k; "W/m·K"
1050 PRINT "heat capacity ="; c; " J/kg·K"
1060 PRINT "density ="; rho; " kg/m^3"
1070 PRINT "melting temperature ="; Tmelt; " K"

1100 IF Abnormal <> 0 THEN
1110 PRINT "The system behaved abnormally."
1120 PRINT "Use a smaller time step (dt)."
1130 END IF

1500 INPUT "Run another sample(y/n)"; YESorNO$
1510 IF UCASE$(YESorNO$) = "N" THEN END
1520 CLS
1600 GOTO 50
```

# ASPOD Cutting Array Redesign Project
# Financial Summary
# December, 1993

| ITEM | QUANTITY | UNIT COST | SUBTOTAL |
|---|---|---|---|
| | | | |
| PROTOTYPE: | | | |
| | | | |
| 3/4" PVC TEE | 8 | 0.12 | 0.96 |
| 3/4" PVC 45 deg ELBOW | 16 | 0.26 | 4.16 |
| 3/4" PVC 90 deg ELBOW | 8 | 0.10 | 0.80 |
| 3/4" SCH 40 PVC PIPE | 40 (feet) | 0.102 | 4.08 |
| 1,1/4" X 2,1/4" HAND RAIL #240 | 1 | 1.38 | 1.38 |
| 3/8" X 1,3/8" RE STOP #866 WP | 1 | 0.51 | 0.51 |
| 1/4" X 3/4" FLAT SCREEN MLD #142 | 1 | 0.25 | 0.25 |
| 1,3/8" FULL ROUND #232 FIR | 1 | 0.89 | 0.89 |
| 1/2" X 9" CARRIAGE BOLT | 1 | 1.45 | 1.45 |
| 1/4" X 2" LAG SCREW | 1 | 0.10 | 0.10 |
| 1/4" X 5" CARRIAGE BOLT | 1 | 0.18 | 0.18 |
| 3/8" X 48" WOOD DOWEL | 1 | 0.49 | 0.18 |
| 3/8" X 40" NOM BULLNOSE PB SHELVING | 3 | 0.59 | 1.77 |
| 34,1/2" X 21" MULTI-ELEMENT FRESNEL | 1 | 89.00 | 89.00 |
| | | | |
| TEST EQUIPMENT: | | | |
| | | | |
| 20 LB TENSION SCALE | 1 | 4.00 | 4.00 |
| | | | |
| FINAL PROTOTYPE (PROJECTED): | | | |
| | | | |
| LARGE LEAD SCREWS | 4 | 5.00 | 20.00 |
| SMALL LEAD SCREWS | 4 | 3.75 | 15.00 |
| 3" DIA. ALUMINUM STOCK | 5 (feet) | 6.00 | 30.00 |
| 1/8" ALUMINUM STOCK (frames) | 10 (feet) | 1.20 | 12.00 |
| WORM GEAR ASSY. | 4 | 50.00 | 200.00 |
| 4' X 1' PVC PANELS | 4 | 2.00 | 8.00 |
| 4' X 3' PVC PANELS | 4 | 4.00 | 16.00 |
| | | | |
| | | TOTAL COST: | $411.02 |

# REFERENCES

1. Duffie, John A. and Beckman, William A. Solar Engineering of Thermal Processes: 2nd Edition. New York: John Wiley & Sons, 1991.
2. Gere, J. M. and Timoshenko, S. P. Mechanics of Materials: 3rd Edition. Boston: PWS-KENT Publishing Company, 1990.
3. Haffner, James W. Radiation and Shielding in Space. New York: Academic Press, 1967.
4. Halliday, David and Resnick, Robert Fundamentals of Physics: 3rd Edition. New York: John Wiley & Sons, 1988.
5. Holman, J. P. Heat Transfer: 5th Edition. New York: McGraw-Hill, 1981.
6. Srinivasan, V. and Banks, B. A. Materials Degradation in Low Earth Orbit. Warrendale, PA: The Minerals, Metals, and Materials Society, 1990.

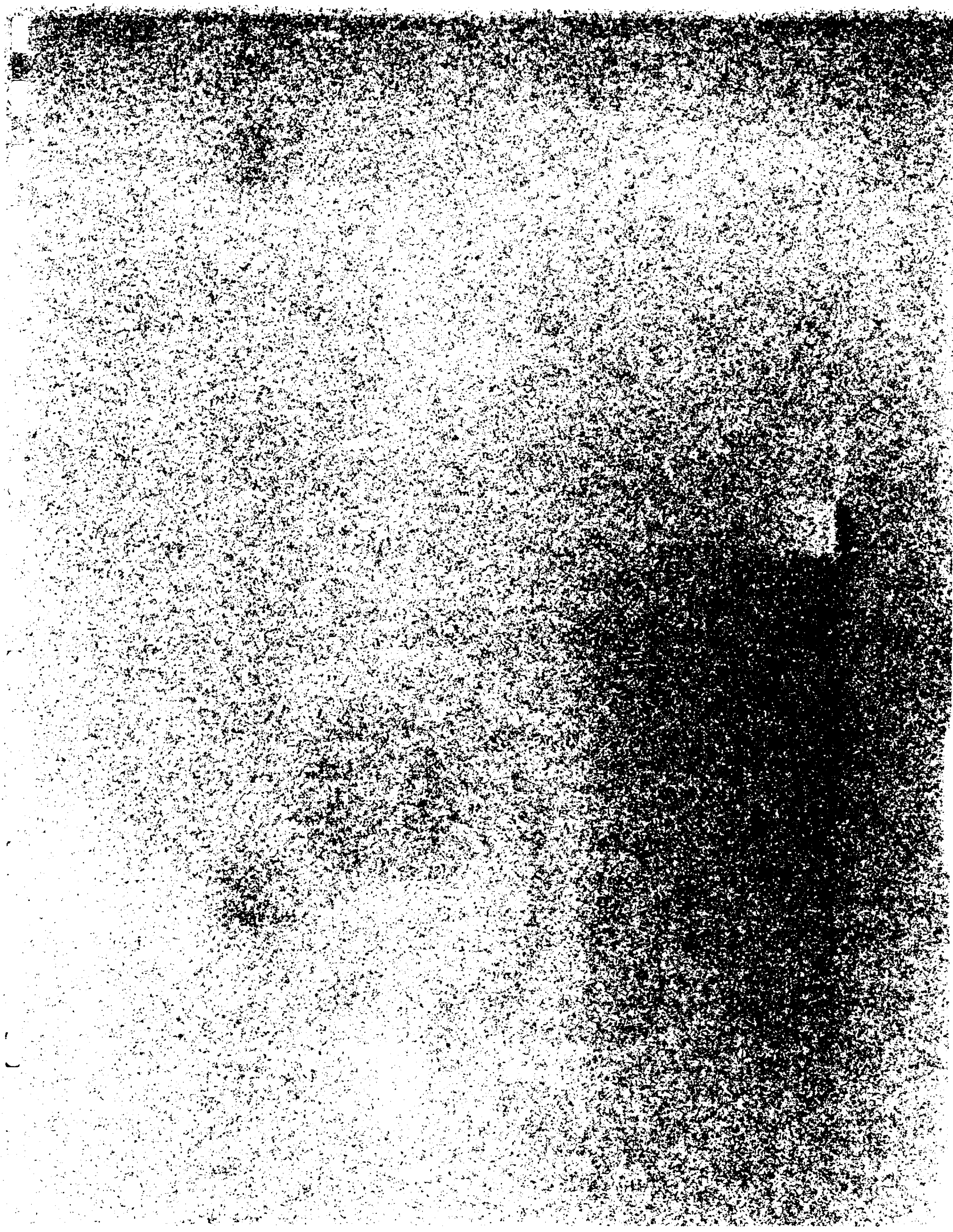

# Table of Contents

GROUP RESPONSIBILITIES .......... 2
INTRODUCTION .......... 3
DESIGNING FOR THE SPACE ENVIRONMENT .......... 7
MOUNTING OF LENSES AND MIRRORS .......... 14
CHOSEN BRACKET DESIGN .......... 20
CUTTING ARRAY PERFORMANCE AND HEAT TRANSFER MODEL .......... 26
APPENDIX .......... 40
FINANCIAL SUMMARY .......... 48
REFERENCES .......... 49

# GROUP RESPONSIBILITIES

| | |
|---|---|
| Jack Rust | Introduction and<br>Designing for the space environment.<br>(pages 3-11) |
| Thomas Martucci III | Mounting of lenses and mirrors.<br>(pages 14-19) |
| Dan Williams | Chesen bracket design.<br>(pages 20-25) |
| Matthew Muller | Cutting array performance and<br>Heat transfer model.<br>(pages 26-39) |

## INTRODUCTION:

For the past three years, engineers at the University of Arizona in association with the Universities Space Research Association and NASA have been attempting to address the problem of man made orbital debris. Since the inception of space flight over thirty years ago, such debris has continued to accumulate in earth orbit to the point where it now poses a serious navigational hazard to both manned and unmanned spacecraft. This problem has taken on new urgency in light of a recent near miss incident involving the space shuttle Atlantis and a derelict Soviet booster rocket.

Under the leadership of Dr. Kumar Ramohalli, U. of A. engineering students have developed a prototype orbital spacecraft called ASPOD (Autonomous Space Processor for Orbital Debris). ASPOD is designed to systematically gather and process large pieces of unwanted debris and store it for future disposal. Principle features of the spacecraft include two mechanical manipulator arms to capture and position debris for processing, and a solar powered cutting array to reduce large debris into manageable pieces. The cutting array assembly consists of four silver plated mirrors and five fresnel lenses mounted on a frame made of graphite/epoxy tubing. The mirrors reflect radiation from the sun, channeling it into the fresnel lenses. The lenses in turn focus this energy on a small point in space. The mechanical arms can then maneuver a large piece of debris through this point where the intensely focused beam of solar radiation will dismember it.

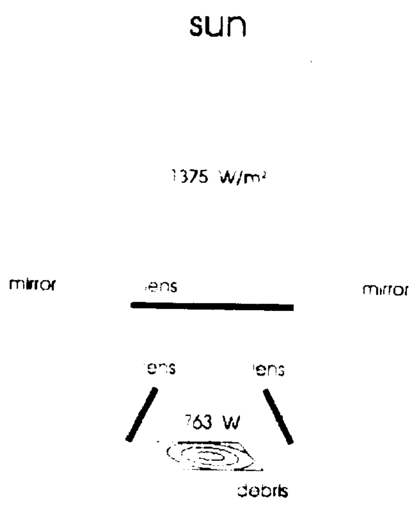
sun
1375 W/m$^2$
mirror
lens
mirror
lens
lens
763 W
debris

Figure 1

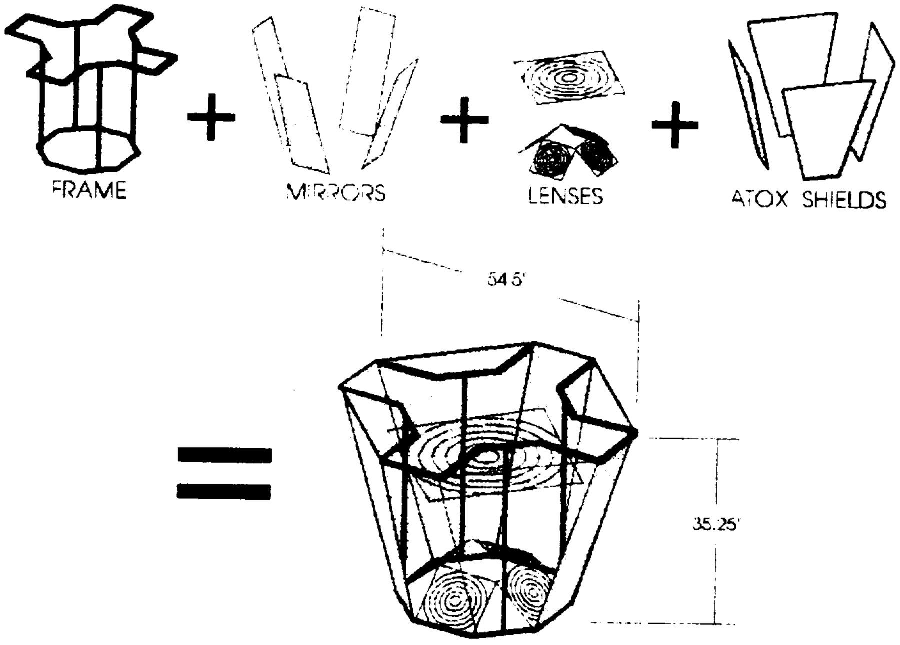
FRAME
MIRRORS
LENSES
ATOX SHIELDS
54.5'
35.25'

CUTTING ARRAY COMPONENTS

Figure 2

Previous design iterations of the cutting torch utilized a heavy kevlar and aluminum frame. The design emphasis being to make the frame so stiff and inflexible that the optics could not be misaligned under any circumstances. Although the prototype performed adequately in ground testing, its excessive weight made it impractical for space flight. Thus a lightweight graphite/epoxy frame was constructed to replace it.

The current undergraduate design team lead by Jack Rust was charged with the task of "designing and fabricating mounting pads to physically affix the array and an alignment jig to ensure the ideal focal point" In addition, the team was asked to study the problems associated with operation of the cutting torch in the harsh environment of low earth orbit. Based on these and other studies, the design team implemented changes as necessary to improve the performance of the cutting torch in all aspects.

Limitations and constraints as delineated by Dr. Ramohalli were somewhat flexible. The entire assembly was to fit within a cube measuring six feet by six feet and weigh no more than 70 lbm; criteria fulfilled by the previous design. In addition, the cutting torch must operate effectively when aligned with the sun to a tolerance of $\pm 1^\circ$ of arc. This being the current limitation of the solar tracking apparatus. Having invested substantial time and money into the development of the new lightweight graphite/epoxy frame, Dr. Ramohalli naturally wished to incorporate it into the new design. Initial research revealed that the frame, though lightweight, tended to exhibit considerable deflections when loaded. Therefore,it had to be complimented such that the mirrors and lenses could be positioned accurately enough to work properly during ground tests. In addition, the sensitive nature of the composite matrix precluded drilling or machining the frame in any way. To do so would have substantially weakened the frame components. Therefore, use of conventional metal fasteners was avoided when mounting optical components to the frame.

With regard to cutting performance, specifications were not narrowly defined. It was expected that the new design should be able to outperform the previous model which was able to cut through .005" aluminum sheet.

Based on initial investigation and study, the design team established its own target specifications for weight and performance. As a result, we have successfully designed a cutting array weighing less than 40 lbm that can cut through .015" stainless steel sheet metal. Clearly, this is an extraordinary improvement on the previous design and more than adequately satisfies the requirements which Dr. Ramohalli has thus far promulgated.

# Designing for the Space Environment

## INTRODUCTION

Although the solar powered cutting array for the ASPOD prototype is to be tested and proven only on the ground, the ultimate goal is a design that will function properly in the harsh environment of space. To this end, the orbital cutting array should incorporate design features which account for the effects of extraterrestrial radiation and monatomic oxygen corrosion. Both phenomena are quite prevalent in the Low Earth Orbit (LEO) environment and both have the potential to seriously affect design performance.

## ENVIRONMENTAL RADIATION

Orbital radiation originates from three primary sources; the sun, the earth's radiation belt, and cosmic sources outside the solar system. The intensity of the radiation flux exhibited in LEO varies as a function of satellite altitude and solar activity. Aside from the obvious physiological hazards radiation poses to astronaut crews, it also creates serious material problems in unmanned spacecraft. Mechanical properties of many materials have been known to degrade following prolonged exposure to radiation. Radiation data for a number of materials provided in reference 3 are restated below.

| Radiation Damage Thresholds for Certain Classes of Materials | |
|---|---|
| Electronic Components | $10^1 - 10^3$ rad |
| Polymeric Materials | $10^7 - 10^9$ rad |
| Lubricants, Hydraulic Fluid | $10^5 - 10^7$ rad |
| Ceramic, Glasses | $10^6 - 10^8$ rad |
| Structural Metals, Alloys | $10^9 - 10^{11}$ rad |

Table 1

Throughout the course of the ASPOD program, Dr. Ramoholli and others have expressed a keen interest in using graphite/epoxy composite materials whenever possible in the construction of the spacecraft.

Although it possesses an exceptional strength to weight ratio, little is known about the behavior of this material following prolonged exposure to extraterrestrial radiation. At what cumulative exposure level does the composite's material strength begin to degrade? Will the performance of the solar cutting array be adversely affected by prolonged radiation exposure?

In order to answer these and other questions, a number of composite tensile test specimens have been fabricated by this design team and tested at The University of Arizona Physical Metallurgy Laboratory. Five of these specimens were irradiated at The University of Arizona Nuclear Engineering Radiography Laboratory. A diagram of the apparatus used to simulate an extraterrestrial gamma radiation environment is shown.

RADIATION EXPOSURE APPARATUS

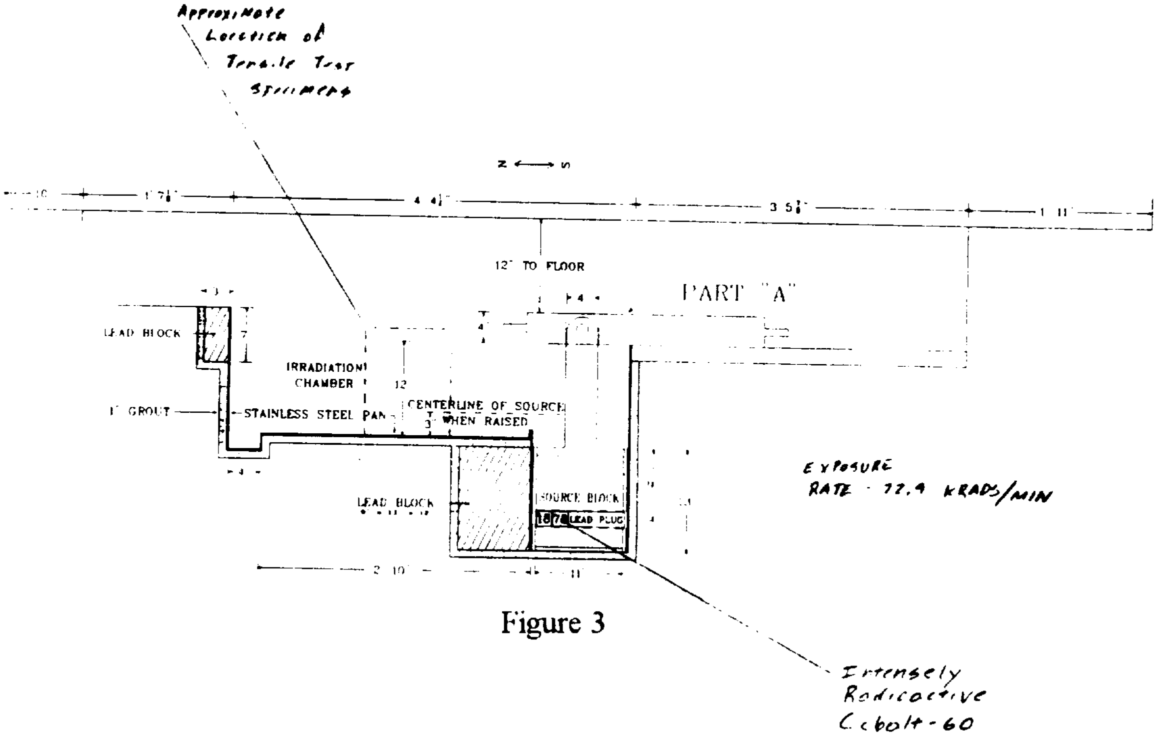
Approximate Location of Tensile Test Specimens
N ⟷ S
10
1' 7½"
4' 4½"
3' 5⅛"
1' 11"
12" TO FLOOR
PART "A"
4
3
7
LEAD BLOCK
IRRADIATION CHAMBER
12
1" GROUT
STAINLESS STEEL PAN
CENTERLINE OF SOURCE WHEN RAISED
3
4
LEAD BLOCK
SOURCE BLOCK
18
7
LEAD PLUG
2' 10"
11"
Exposure Rate - 77.4 krads/min
Intensely Radioactive Cobalt-60

Figure 3

When the source block is lifted, the tensile test specimens are exposed to an intensely radioactive cobalt 60 point source. Each specimen is exposed at a rate of approximately 73,000 rads per minute. The exceptionally high exposure rate allows one to simulate several years of space exposure over the course of a few hours.

In this manner, five composite tensile test specimens were subjected to varying degrees of exposure then tested to destruction. The ultimate tensile strengths of these specimens is shown below.

| **Radiation Exposure** | **Ultimate Stress ($lbf/in^2$)** |
|---|---|
| Non Radiated | 87,093 to 108,415 |
| $10^7$ Rad | 94,228 |
| $5 \times 10^7$ Rad | 85,031 |
| $10^8$ Rad | 87,634 |
| $5 \times 10^8$ Rad | 100,686 |
| $10^9$ Rad | 117,497 |

Table 2

Although the radiation exposure was increased by orders of magnitude with each succeeding specimen, the change in ultimate tensile strength was relatively small. It would take hundreds of years in space before the composite material could accumulate as much exposure as it did in this test. Thus, these results would seem to indicate that the performance of the cutting array will not be adversely affected by extraterrestrial radiation.

## MONATOMIC OXYGEN CORROSION

By far the most severe environmental factor affecting the design, monatomic oxygen corrosion has proven to be very destructive to orbiting satellites in the past. It has often resulted in the premature failure of satellite components particularly solar panels incorporating silver and/or graphite/epoxy parts.

As with extraterrestrial radiation, the intensity of ATOX corrosion would appear to be a function of solar activity as well as altitude. Corrosion data for some materials given in reference 6 is listed below.

| Thickness loss per year of different solar array materials at 400 km altitude under minimum and maximum solar activity conditions | | |
|---|---|---|
| Material | Thickness Loss | |
| | Maximum | Minimum |
| Silver interconnector | 16.09 | 194 |
| Kapton (Rigid) | 4.6 | 55.4 |
| Epoxy | 4.81 | 58.06 |

Table 3

Silver coatings similar to that used on the ASPOD mirrors are particularly vulnerable to the affects of ATOX corrosion. The nominal thickness of mirror film to be used on this project is less than seventy microns. Under normal orbital conditions, the surface would be completely destroyed in less than six months without some form of adequate protection.

In order to solve this problem from an engineering standpoint, it is necessary to gain some understanding of how the mechanism of ATOX corrosion works. At the fringes of the atmosphere oxygen gas is ionized by high energy radiation primarily from the sun. The resulting negative ions oxidize quite readily with all manner of materials. In the ASPOD mirrors, ATOX would infiltrate through defects in the coating which protects the silver surface. Once beneath the coating, ATOX corrodes all of the silver in the immediate vicinity of the defect. Thus, the severity of the corrosion occurring over time is directly dependent on the degree to which the protective coating has been punctured by high energy particles, micro meteoroids, or other abrasions. When ATOX ions impact the surface of the mirrors at high relative velocities, corrosion problems are greatly exacerbated.

High energy ions striking the mirrors deliver sufficient kinetic energy to punctuate and erode the mirrors protective coating. In addition, ions which strike at large angles of incidence with the surface infiltrate horizontally into the silver material. This has the effect of undercutting the protective surface and depriving it of structural support. Over time, the protective surface material flakes off exposing the silver beneath.

With continued exposure to high relative velocity particle erosion in an ATOX environment the mirror material will degrade much more rapidly than it would if shielded from high velocity impacts. The annual decrease in material thickness of any substance exposed to ATOX corrosion is expressed by the following equations:

$$\phi_{\mathrm{AO}} = N_d \; V_s \cos\theta$$

Where:

$\phi_{AO}$ = ATOX flux in atoms / cm$^2$ sec

$N_d$ = ATOX density

$V_s$ = Spacecraft Velocity

$\theta$ = Angle of Incidence

$t = 365 * 86{,}400 * \phi_{AO} * R_e$

$t =$ Annual Thickness Loss

$R_e =$ ATOX reaction coefficient

One can use the previous equations to calculate the orbital lifetime of an unprotected 70 micron silvered mirror. Bearing in mind that ASPOD will be required to change orbit and altitude frequently and consulting the graph of altitude vs. ATOX flux shown below, one may reasonably assume a mean flux of $10^{14}$ atoms / cm$^2$ sec.

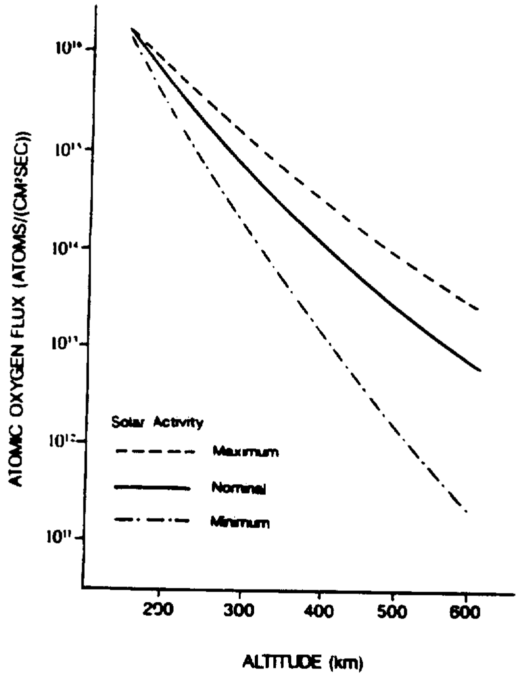

ATOMIC OXYGEN FLUX DEPENDENCE UPON ALTITUDE

Figure 4

Assuming a reactivity coefficient of $10.5 \times 10^{-24}$ cm$^3$ / atom for silver, calculations indicate that the mirror would be eaten at the rate of 330 microns per year. Thus, without adequate protection the mirror would be completely destroyed within three months. The mirror lifetime will of course vary depending upon ATOX flux variations. The flux in turn is dependent upon both the eleven year solar cycle and relative velocity of the ATOX particles.

If the mirrors could be shielded from high velocity particles, the flux could be considerably attenuated and the lifetime of the mirrors increased. This is the primary reasoning behind the shrouded ASPOD design pictured in Figure 2.

Although the mirrors will still be exposed to a substantial ATOX flux, the flux component in the direction of motion ($V_s$ ) can be cut considerably. Thereby extending the life of the mirrors.

When the torch is not in use, ASPOD will simply maneuver the assembly such that the top and bottom openings are ninety degrees away from the direction of satellite motion. Although not the most sophisticated method for protecting the mirrors, it is both simple and inexpensive. In addition, it will help to lend much needed structural support. Ideally, the shroud and mirror panels would be fabricated from the same lightweight graphite epoxy materials used in the frame. This project uses acrylic mirror panels. Although heavier than composite materials, acrylic adequately fulfills the requirements of a ground based demonstration array.

# MOUNTING OF LENSES AND MIRRORS

The original configuration of the ASPOD solar cutting array has been retained as shown Figure 2. However, the new design  incorporates a considerably larger central fresnel lens. It measures four square feet whereas the previous design used a one square foot lens which enabled it to cut .005 in. aluminum sheet metal with some difficulty. The new lens can cut similar metal instantaneously and makes short work of steel or brass specimens of much greater thickness. Performance data about this lens gathered from experimental techniques and computer simulation is discussed in detail later in this report. In addition to a larger lens, the new design also can incorporates panels which enclose the entire array about the central axis. Figure 2 shows the array partially enclosed allowing a view of the internal mirror and lens arrangement. Ideally, the panels would be fabricated out of graphite/epoxy which exhibits an excellent strength-to-weight ratio. The ground prototype may incorporate PVC panels which are easy to fabricate and several times cheaper or it can be operated with no panels at all. In space, enclosure will provide protection against monatomic oxygen corrosion in addition to providing additional structural support. The new design will also incorporate lighter mirrors than the 52 lbm (total mirror weight) of the previous design. The new mirrors panels are made of 1/8" silver coated acrylic; half as thick as the old ones. In addition, the new panels incorporate alluminum channel beams bolted to the back for reinforcement instead of the old bulky mirror frames with a considerable savings in weight.

In order to "physically affix the array" and "ensure the ideal focal point" as requested by our sponsor in their proposal, the new design will incorporate adjustable mounting brackets for all of the lenses. To arrive at this design, a number of questions needed to be addressed. Among them,

1)In which direction and to what extent should they be movable?

2) What degree of precision will be required in the adjustment?

3) What material exhibits the best combination of strength, weight, machinability, corrosion and radiation resistance and low cost?

The cutting array is designed to support the weight of all optical components and maintain them in proper position to function effectively when fully assembled and standing relatively still on a test table or mounted to the spacecraft. Nevertheless, misalignment of optical components due to mechanical shock, transporting of the array, repeated assembly and disassembly and general wear and tear are inevitable. Therefore, the new design must provide for manual adjustment of the lenses so that all of the energy can be directed into the smallest possible focal zone as shown in Figure 1. Each of the mirrors are to be fastened to the frame at four points and are not likely to be so severely misaligned as to require manual adjustment. Therefore, they will be fixed and the lenses will be adjusted to accommodate them if necessary.

## MANEUVERABILITY OF LENSES AND MIRROR

### LARGE FRESNEL LENS :

The large central lens projects the largest and hottest focal zone centered directly beneath the array. The most logical approach would be to adjust the focus of the central lens first then adjust the four surrounding small lenses so that they can contribute their energy to the same point on the cutting surface. To do this, the central lens must exhibit linear freedom of motion along the vertical axis of the array. See figure below.

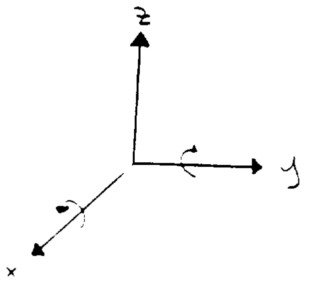

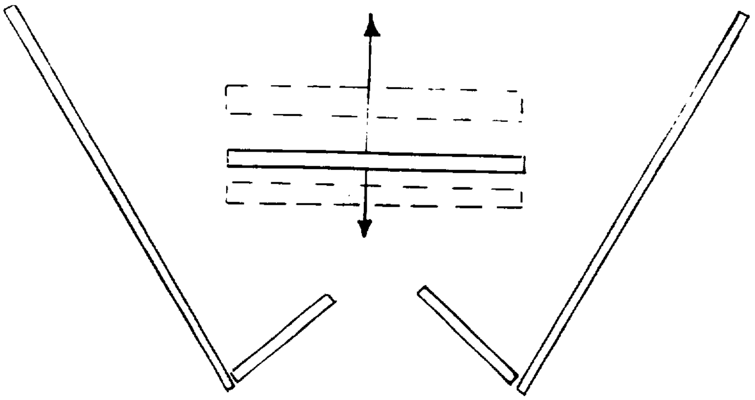

Figure 5

There can be limited rotation in the $(\theta, X)$ and $(\theta, Y)$ directions.

## SMALL LENSES

Each lens should be capable of rotary motion about the base axis of it's corresponding mirror as pictured in Figure 6.

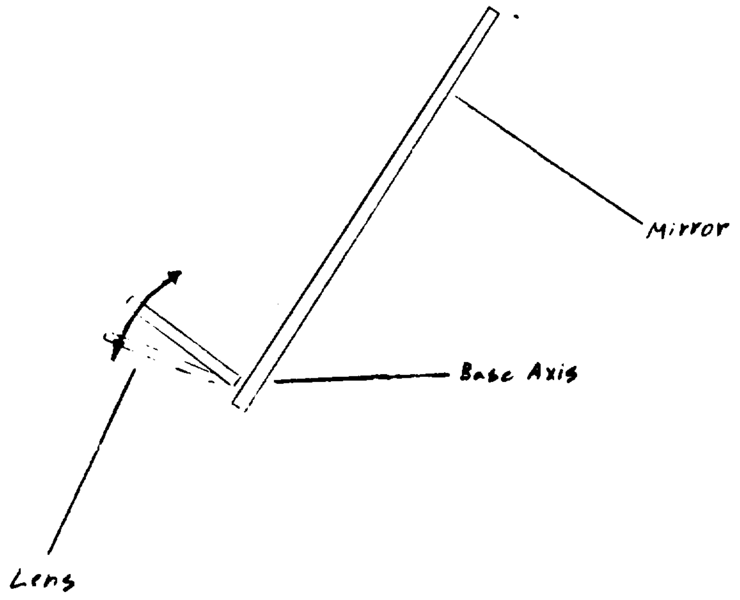
Mirror
Base Axis
Lens

Figure 6

## MIRRORS :

The precision and extent of mirror movement required depends on the extent to which shock or movement of the array may misalign the mirrors and the extent to which that would affect the performance of the cutting array. Experimental results detailed in the heat transfer and performance section of this report show that a fresnel lens can still maintain very high focal zone temperatures even when misaligned by several degrees. Thus a rigid mount for the mirrors will be sufficient.

A tabular summary of component maneuverability is shown below.

| fresnel lens size | motion | DOF | amount |
|---|---|---|---|
| LARGE | induced translation | 1 | ± 2 in. |
|  | limited rotation | 2 | approximately 5° |
| SMALL | rotation | 1 | 20° |

Table 4

## DEGREE OF PRECISION

## LARGE LENS

For the large central lens, a 2 in. linear range of motion should be more than adequate to adjust the lens focus under normal circumstances. The focusing mechanism provides for both coarse and fine adjustment. The coarse adjustment allows focusing of the mirror along its axis of motion down to the within an inch of the desired location. The fine adjustment makes use of fine threaded lead screws allowing focusing down to the nearest sixteen thousandths of an inch.

## SMALL LENSES

Mounting brackets for the small lenses should allow for radial positioning across a range of twenty degrees down to the nearest degree. Based on the data gathered by experimentation with the fresnel lenses, positioning the mirrors anywhere within this range of motion should not seriously hamper their effectiveness.

## MATERIALS SELECTION

In selecting materials from which to fabricate the mounting brackets, a number of factors must be taken in to account. A combination of adequate strength and light weight is of paramount importance.

At the same time the design team must be able to produce the design in the AME production lab. The brackets must also be resistant to monatomic oxygen corrosion and radiation effects. Aluminum fulfills all of these requirements in addition to being inexpensive.

# CHOSEN BRACKET DESIGN

## LARGE FRESNEL LENS

Below is a three dimensional drawing of our chosen design. For a detailed description consult blueprint number two.

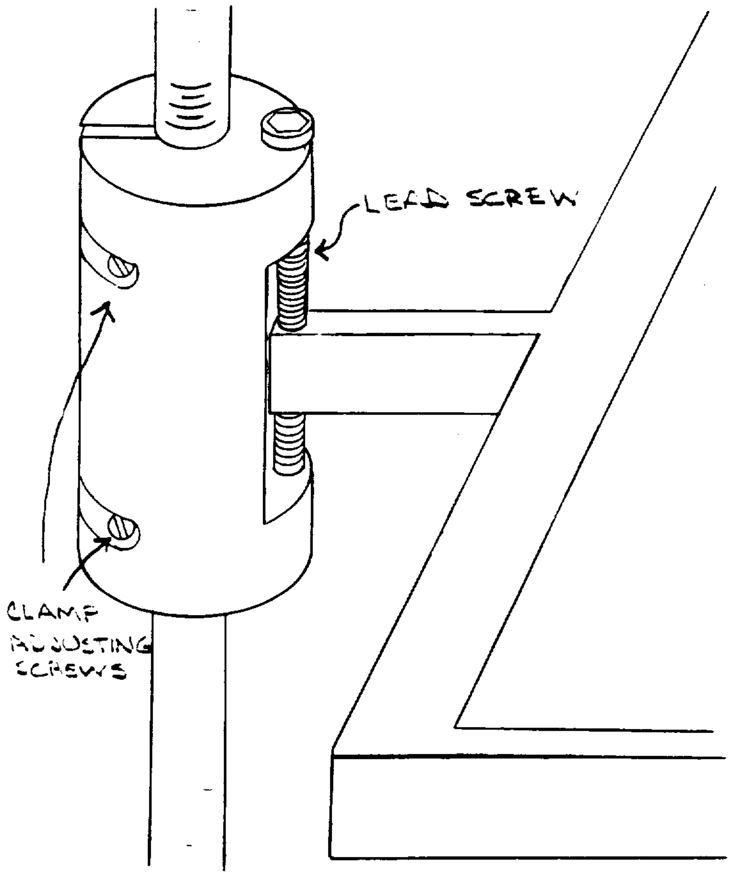
LEAD SCREW
CLAMP ADJUSTING SCREWS

Figure 7

The large fresnel lens is supported by four adjustable brackets, each of which is attached to a vertical member of the composite frame.

To position the large fresnel lens, the clamp adjusting screws are loosened allowing the bracket to slide freely along the vertical frame member. The bracket can then be moved to within roughly one inch of the desired position. This independent freedom of motion for each bracket allows us to compensate for any misalignment of the large fresnel lens. In this manner, the trade-off between ultra-tight tolerances (fixed optics) verses loose tolerances (adjustable optics) is addressed. Tolerances are not as easily controlled as adjustable optics. Refer to blueprint number two for detailed technical specifications.

The large lens adjustable bracket design has been successfully implemented in exact accordance with the specifications layed out in blueprint #2. Initial testing of the cutting array as a whole and the bracket in particular has demonstrated that the system can be quickly and easily adjusted.

Originally, the large fresnel lens was to be completely enclosed and supported by a rectangular frame. Since the large fresnel lens is itself quite stiff, all the extra support seemed unnecessary. The subsequent redesign shown below uses four plastic sandwich clamps to support the lens on each side. This fulfills the same rigidity requirements at considerable savings in weight, material, and cost.

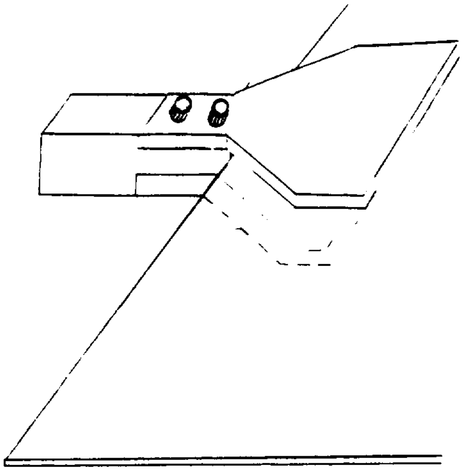

Figure 8

## SMALL LENS BRACKET

Below is a three dimensional view of our previously chosen bracket design.

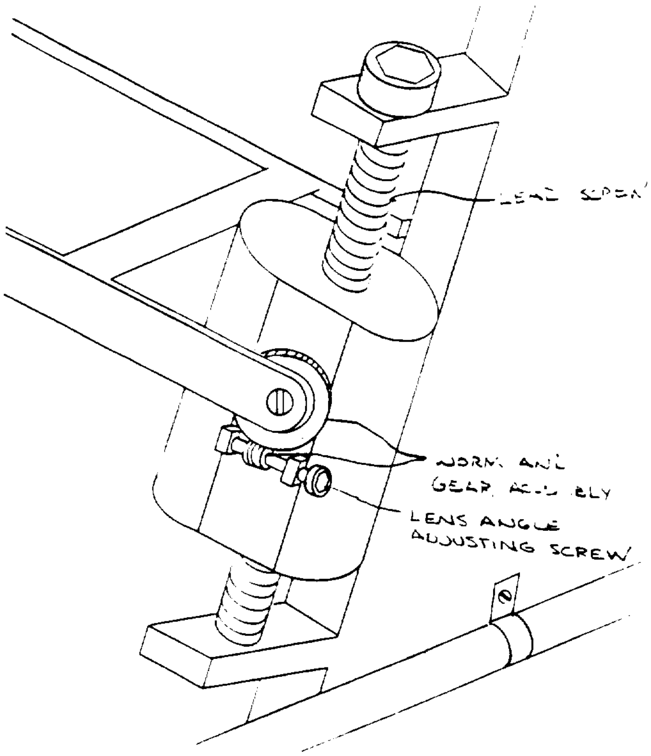
LEAD SCREW
WORM AND
GEAR ASSEMBLY
LENS ANGLE
ADJUSTING SCREW

Figure 9

This design was eliminated after further development revealed that lateral motion of the small lens along the mirror was redundant and ultimately unnecessary since the large mirror can be adjusted to achieve the same effect. Furthermore, the tilt table could not accomodate the worm gear mechanism required for the operation of each small fresnel lens. Below is a diagram of the alternative design which was ultimately installed on the cutting array.

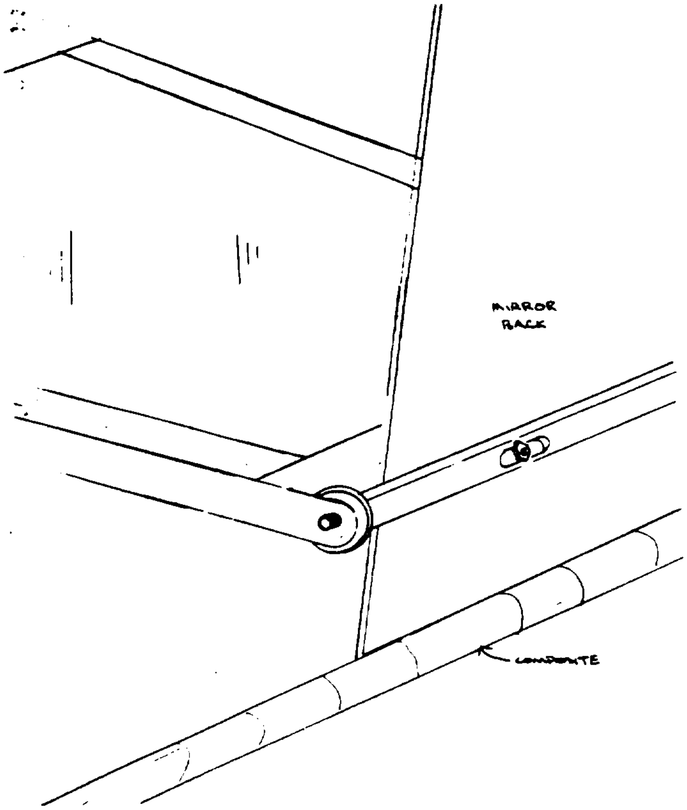

Figure 10

The alternative design is much less bulky and easily accomodated by the tilt table. In addition, it is both easier to fabricate and assemble and simpler to operate. To adjust the angle of the lens, one can simply loosen the allen head screws on either side, move the lens to the desired position, and tighten the screws once again.

## DEGREE OF PRECISION

### LARGE FRESNEL LENS BRACKET

The lead screw which controls the fine adjustment has sixteen threads per inch. For a quarter inch turn a 0.015 in. travel of the large fresnel lens will result. This meets the adjustability precision criteria.

### SMALL FRESNEL LENS BRACKET

The small lens bracket neither requires nor posesses as precise a position control mechanism as the large lens. However, subsequent testing of the cutting array has proven this mechanism to be more than adequate to the task.

## TOLERANCES

A tolerance of 0.010 in. was exceeded in machining these brackets. More precise tollerances were employed between the large lens bracket and the composite frame.

## MATERIAL SELECTION

Material selection was based upon a number of considerations. These included cost, machinability, corrosion resistance, availability, durability, thermal considerations, and weight. Aluminum best satisfies these criteria in the following ways:

- It is lightweight which is beneficial in maneuvering the assembly
- It is inexpensive and available in all required shapes and sizes
- Machinability characteristics are desirable (turns, mills, and cuts easily)

# CUTTING ARRAY PERFORMANCE & HEAT TRASFER MODEL

The total power output of the solar cutting device can be calculated. This output is a function of the surface area and transmissivity of the lenses, the efficiency of the mirrors, and the insolation coefficient $G_{SC}$. The coefficient $G_{SC}$ is a constant which represents the amount of solar radiation hitting an extra-terrestrial surface normal to the suns rays. The calculations in the appendix yield a solar cutting power of 763 Watts.

A heat transfer program was designed to provide cutting estimates for various materials under the focal region of the proposed solar cutting torch. The source code for the program is located in appendix. The heat transfer model was designed for rapid estimates of the cutting limits applied to various materials for two geometries. The following assumptions were made in the creation of the heat transfer model.

- The focal region of the lens cutting system produces 763 Watts evenly distributed about a radius of 2.0 centimeters.
- All materials absorb 49.3% of the energy provided at the focal region.
- Materials experience both radiation and conductive heat transfer.
- Materials do not experience convective heat transfer because of the vacuum environment of space.
- The materials do not experience chemical reactions, such as burning, because of the limited atmosphere.
- The model uses finite differences with Euler explicit forward differentiation to simulate the heat transfer.

The equations for the heat transfer analysis start with the conservation of energy.

$$Q_{stored} = Q_{in} - Q_{out}$$

Next we turn to the basic heat transfer equations.

$$Q_{conduction} = Q_c = kA\left(\frac{dT}{dx}\right)$$

$$Q_{radiation} = Q_r = \sigma A T^4$$

$$Q_{stored} = Q_s = mc\left(\frac{dT}{dt}\right)$$

$$Q_{spot} = \text{solar energy input}$$

When combined with the energy equations the following relationship is produced.

$$Q_{in} = (Q_c)_{in}$$

$$Qout = (Q_c + Q_r)_{out}$$

$$mc\left(\frac{dT}{dt}\right) = k(A_c)_{in}\left(\frac{dT}{dx}\right) - k(A_c)_{out}\left(\frac{dT}{dx}\right) - \sigma A_r T^4$$

The heat transfer model uses finite differences to represent the differential terms of the energy balance equation. This finite differences model is applied to two geometric shapes, the rectangular bar and the plate. Both geometries will simplify to a one-dimensional heat transfer problem. The bar is broken down into a series of small blocks. The block elements are placed end to end. The solar heat input is directed at the center block and the heat flows outward from the center block. Because the flow is symmetrical to the left and to the right of the heat source, the analysis is simplified by only looking at half of the bar.

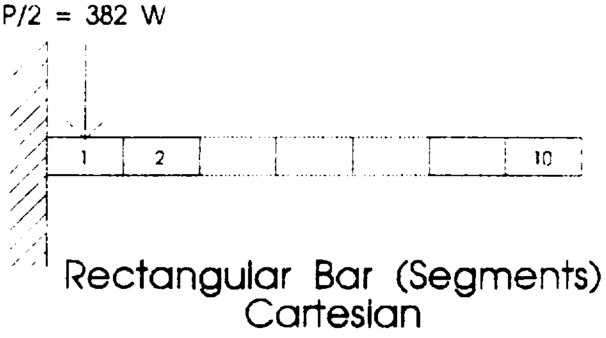

Figure 11

This new configuration experiences only half of the solar heat input and the heat flow proceeds from the source element to the end element in a one-dimensional flow. The differential length (dx) or (dL) of each element is constant and is strategically chosen so as to correspond to the size of the solar input region. The actual distance (dL) used in the program is equal to half of the diameter of the focal region. The first element of the model is then the only element to experience the direct heat input of Qspot.

The conduction area (Ac) between all blocks and the radiation area (Ar) are defined by the following equations.

$$A_c = w \cdot h$$
$$A_r = w \cdot dL$$

The mass of any given block is then defined.

$$m = A_r \cdot h$$

The plate geometry differs slightly from the bar geometry. Instead of block elements the plate uses concentric rings.

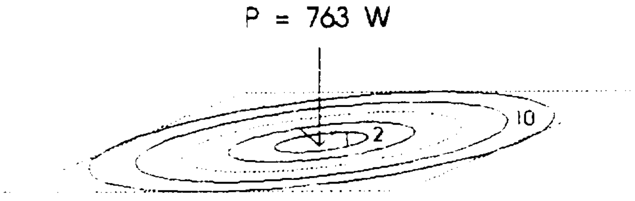

Plate (Concentric Rings)
Radial

Figure 12

The distance dR is used instead of dL. The conduction area and the radiation area are different for each ring element.

$$A_c(i) = 2\pi(i \cdot dR) \cdot h$$

$$\begin{aligned} A_r(i) &= \pi\left[(i \cdot dR)^2 - ((i-1) \cdot dR)^2\right] \\ &= \pi \cdot dR^2\left[(i)^2 - (i^2 - 2i + 1)\right] \\ &= \pi \cdot dR^2 \cdot (2i - 1) \end{aligned}$$

The conduction area (Ac) for an element $i$ is defined as the area of the outer edge of the ring element. This is the conduction area for the exit surface of the element.

The solar input (Qspot) is applied to the first ring element which is actually a disc. The plate geometry behaves in the same manner as the bar geometry in all other aspects.

The following is a table of the heat transfer coefficients for the various materials used in the program.

| Material | Density "rho" (kg/m^3) | Thermal Conductivity "k" (W/m·K) | Heat Capacity "c" (J/kg·K) | Melting Temperature "Tmelt" (K) |
|---|---|---|---|---|
| Aluminum (pure) | 2707 | 204 | 896 | 660+273 |
| Brass (70%Cu,30%Zn) | 8522 | 111 | 385 | 420+273 Zn |
| Carbon Steel (1.0% C) | 7800 | 43 | 473 | 1537+273 |
| Copper (pure) | 8954 | 386 | 383 | 1083+273 |
| Iron (pure) | 7897 | 73 | 452 | 1537+273 |
| Lead (pure) | 11373 | 35 | 130 | 327+273 |
| Silver (pure) | 10524 | 419 | 234 | 961+273 |
| Titanium | 4507 | Not Available | 523 | 1670+273 |

Table 5

Now we take a close look at the program itself. *Quick Basic* was used for the model because it was easily accessible. The complete program is listed in the appendix. On the following page is a flow chart to explain the desired functionality of the program.

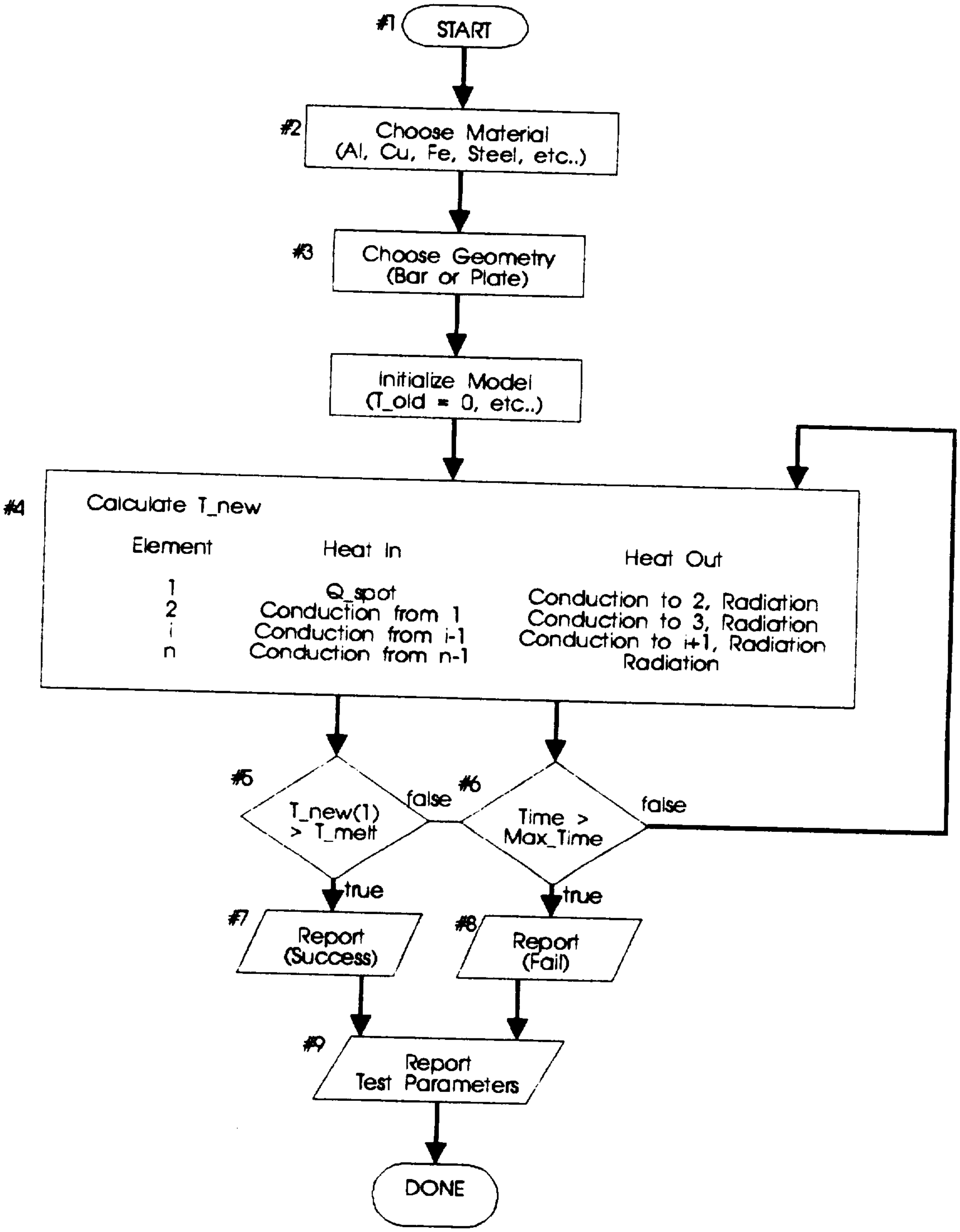
#1 START
#2 Choose Material (Al, Cu, Fe, Steel, etc..)
#3 Choose Geometry (Bar or Plate)
Initialize Model (T_old = 0, etc..)
#4 Calculate T_new
Element
Heat In
Heat Out
1
Q_spot
Conduction to 2, Radiation
2
Conduction from 1
Conduction to 3, Radiation
i
Conduction from i-1
Conduction to i+1, Radiation
n
Conduction from n-1
Radiation
#5 T_new(1) > T_melt
false
#6 Time > Max_Time
false
true
true
#7 Report (Success)
#8 Report (Fail)
#9 Report Test Parameters
DONE

Figure 13

Block #1 is the starting block of the program. This corresponds to lines 10 through 70 of the program. The following constants are defined.

- Number of differential elements, nEnd
- Maximum number of time steps, TheEnd
- Distance between differential bar elements, dL [meters]
- Distance between differential ring elements, dR [meters]
- Pi ($\pi$), pi
- Stefan-Boltzman constant ($\sigma$), S [$W / m^2 \cdot K^4$]
- Elapsed time, Time [sec]
- Time step, dt [sec]

The following element properties are dimensioned.

- Next temperature of an element, Tnew(i) [K]
- Last temperature of an element, Told(i) [K]
- Conduction area out of an element, Ac(i) [$m^2$]
- Radiation surface area of the top of an element, Ar(i) [$m^2$]
- Conductive heat transfer out of an element, Qc(i) [W]
- Radiative heat transfer out of top surface of an element, Qr(i) [W]

The starting temperature is initialized.

- Last temperature of all elements is set to zero degrees Kelvin. Told(i) = 0

This corresponds to lines 0 through 99 of the program.

In block #2 the user chooses the desired material to test. This process selects the following material constants.

- Melting Temperature, Tmelt
- Thermal Conductivity, k
- Heat Capacity, c
- Density, rho

Block #2 corresponds to line 100 through 299 of the program.

In block #3 the user defines the geometry of the material. The following decisions are made.

- Bar or Plate Geometry
- Thickness of Specimen, h [mm]
- Width of Bar (bar geometry only), w [mm]

From this information the following is calculated.

- Thickness of Specimen, h [m]
- Width of Bar (bar geometry only), w [m]
- Conduction Cross-sectional Area of each element, Ac(i) [m^2]
- Radiation Surface Area of each element, Ar(i) [m^2]
- Solar heat gain from the lens system, Qspot [W]
- Finite distance between elements, dx [m]

The solar heat gain is calculated assuming the material will absorb 50% of the radiation applied to it. This corresponds to lines 300 through 399 of the program.

The next few lines of the program (400 through 499) correspond to anything on the block diagram. Two things occur in this portion of the code.

- A report header is printed
- Some constants are combined into one value

Block #4 is the main loop of the program. This block of code calculates and updates the new temperatures for all of the finite elements according to the following schedule. Remember that Qc(i) refers to the heat flux out of the element *i* to the element *i+1*.

| Element | Heat In | Heat Out |
|---|---|---|
| 1 | Qspot | Qc(1) + 2*Qr(1) |
| 2 | Qc(1) | Qc(2) + 2*Qr(2) |
| i | Qc(i-1) | Qc(i) + 2*Qr(i) |
| nEnd | Qc(nEnd-1) | 2*Qr(nEnd) |

The radiation heat flux is doubled because it occurs out of both the top and the bottom of each element. All heat transfer terms are calculated from the temperature readings at the last time step. The values for Told are only updated after all the Tnew values have been calculated. The program also checks for abnormal heat transfer. If the temperature of any element (i) at any instance is greater than the temperature of the previous element (i-1) then the program makes a note of the abnormal heat flow which will be reported at the end of the simulation. Block #4 corresponds to lines 500 through 799 of the program.

Block #5 tests to see if the material has melted. If so, the program proceeds to block #7 which reports the melting results. This refers to line 770 and lines 900 to 999.

Block #6 test to see if the simulation is out of time. If not, the program loops back block #4. If so, the program proceeds to block #8 which reports the failure to melt. This refers to line 780 and lines 800 to 899.

Block #9 reports the test information. This includes the following.

- Material properties
- Simulation geometry
- Any noted abnormalities

This block refers to lines 1000 to 1130 of the code.

The heat transfer model needed to be calibrated. To do this we compared it to the experimental results obtained from melting the steel strips. The value for absorbtivity was adjusted until the computer model reaches its closest match to the experimentation. The calibration resulted in the best value for absorbtivity of the material. This value is used for all of the materials in the simulation because it is the only value available. Here are the results from this experiment with the calibrated computer model.

Experimental Results

Steel Strip (width = 13 mm)

| Thickness (in) | Model Melting Time (sec) | Experimental Melting Time (sec) |
|---|---|---|
| 0.005 | 0.9 | 4.7 |
| 0.006 | 1.2 | 4.8 |
| 0.007 | 1.5 | 3.6 |
| 0.008 | 1.8 | 11.7 |
| 0.009 | 2.3 | 7.7 |
| 0.010 | 3.2 | 9.3 |
| 0.011 | 4.4 | 8.0 |
| 0.012 | 5.8 | 12 |
| 0.013 | 7.4 | 24 |
| 0.014 | 9.5 | 18.6 |

| | | |
|---|---|---|
| 0.015 | 12.5 | 17.4 |
| 0.016 | 18.5 | 21.4 |
| 0.017 | 43.3 | 23.4 |
| 0.018 | ---- | 16.2 |
| 0.019 | ---- | ---- |
| 0.020 | ---- | ---- |

Table 6

The computer results behave in an exponential manner and the experimental results behave in a somewhat linear manner. Both however have reasonable consistency for the maximum thickness that can be cut. There are several reasons that contribute to the difference in behavior.

- Oxidization - The metal oxide has a different melting temperature than the metal itself.
- Blackening - The material blackens when it oxidizes and therefore changes the absorbtivity.
- Coefficients - The thermodynamic constants used in the model are actually a function of temperature.
- Convection - The model does not account for convective heat transfer in the metal whereas the experiment definitely was affected by convection.
- Human Error - Many of the experimental results have a bias error due to the lag from positioning the strip in the focal zone.

The shaded values are bad data points and were thrown out of the correlation analysis. Using *QuattroPro*, a regression analysis was performed on the experimental and theoretical melting times. This analysis resulted in an 83% correlation, 100% meaning perfect correlation and 0% meaning no correlation. Below is a graphical representation of theoretical versus experimental melting times.

ORIGINAL PAGE IS
OF POOR QUALITY

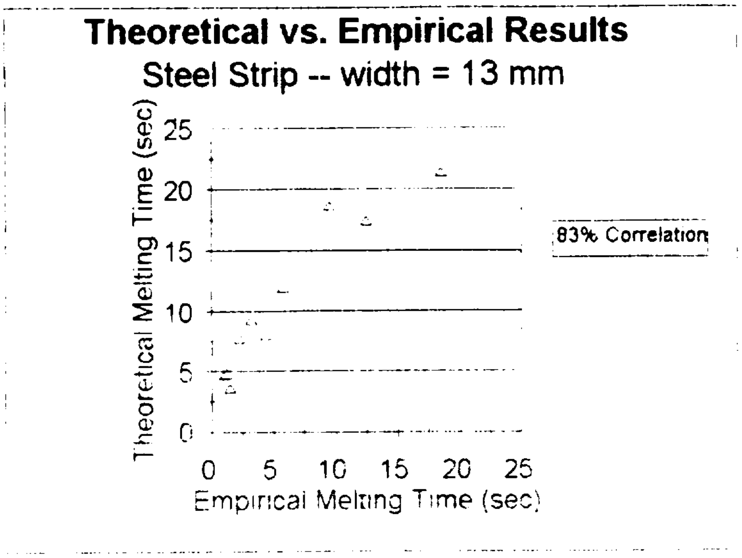

Figure 14

The heat transfer computer model yielded the following results for maximum thickness of materials that can be cut within 10 seconds.

Maximum Material Thickness

(Cutting Time = 10 sec)

| Material | Thickness (mm) | |
|---|---|---|
| | Bar Geometry (width = 15 mm) | Plate Geometry |
| Aluminum | 1.75 | 0.55 |
| Brass | 1.15 | 0.45 |
| Carbon Steel | 0.04 | 0.04 |
| Copper | 0.60 | 0.15 |
| Iron | 0.04 | 0.04 |
| Lead | 7.55 | 4.00 |
| Silver | 0.85 | 0.20 |
| Titanium | Not Available | Not Available |

ORIGINAL PAGE IS
OF POOR QUALITY

In conclusion the model and the experimentation are both useful in obtaining a general idea for the melting capacity of the lens configuration. More experimentation will result in a better fit for the model. This and other model improvements will produce more precise limits to the melting ability of the solar cutting array. This computer model may later be adapted for on-line use with the ASPOD vessel to calculate feed rates for metal cutting.

ORIGINAL PAGE IS
OF POOR QUALITY

# APPENDIX

## POWER OUTPUT DERIVATION

Values used in determining the expected power output of the fresnel lens cutting system.

- Extra-Terrestrial Insolation. $G_{SC} = 1353$ W/m$^2$

Central Lens

- Transmissivity, $\alpha_{ctr} = 82\%$
- Area. $A_{ctr} = 4$ ft$^2$ $= 4\ (3.2808^2) = .372$ m$^2$

Auxiliary Lenses

- Transmissivity, $\alpha_{aux} = 82\%$
- Area. $A_{aux} = 1$ ft$^2$ $= 0.093$ m$^2$

Mirrors

- Efficiency. $n = 82\%$

$$\text{Power}_{out} = \text{Power}_{ctr} + 4 * \text{Power}_{aux}$$

$$P_{ctr} = G_{sc} * A_{ctr} * \alpha_{ctr}$$

$$= 1375 * .372 * 0.82 = 419 \text{ W}$$

$$P_{sml} = G_{sc} * A_{sml} * \text{Trans} * \text{Refl}$$

$$= 1375 * .093 * 0.82 * 0.82 = 86 \text{ W}$$

$$\text{Power}_{out} = (419) = 4 * (86) = 763 \text{ W}$$

ORIGINAL PAGE IS
OF POOR QUALITY

## COMPUTER MODEL PROGRAM CODE

```
REM Init Programming Constants
10 nEnd = 10: TheEnd = 100000: dL = .01: dR = .01
20 DIM Tnew(1 TO nEnd), Told(1 TO nEnd), Ac(1 TO nEnd), Ar(1 TO nEnd)
30 DIM Qc(1 TO nEnd), Qr(1 TO nEnd)
40 pi = 3.141592654#: S = .00000005997#    'S = Stefan-Boltzmann Constant
50 FOR i = 1 TO nEnd
60 Told(i) = 0 'SET INITIAL TEMP = 0
70 NEXT i
80 time = 0
90 dt = .1


REM Choose Material
100 PRINT "          MELTING PROGRAM"
110 PRINT "Finite Difference Heat Transfer Analysis"
120 PRINT "         Using Euler Explicit"
130 PRINT
140 PRINT "Select Material for testing"
150 PRINT "     1. Aluminum"
155 PRINT "     2. Brass (70% Cu, 30% Zn)"
160 PRINT "     3. Carbon Steel (1.0% C)"
165 PRINT "     4. Copper"
170 PRINT "     5. Iron"
175 PRINT "     6. Lead"
180 PRINT "     7. Silver"
```

ORIGINAL PAGE IS
OF POOR QUALITY

```
185 PRINT "     8. Titanium"
190 PRINT "     9. <custom>"
200 INPUT Material
210 SELECT CASE Material
        CASE IS = 1             'Aluminum
                k = 202: c = 896: rho = 2707: Tmelt = 948
                Mater$ = "Aluminum"
        CASE IS = 2             'Brass
                k = 111: c = 385: rho = 8522: Tmelt = 1083 + 273'Tmelt Cu
                Mater$ = "Brass (70% Cu, 30% Zn)"
        CASE IS = 3             'Carbon Steel
                k = 43: c = 473: rho = 7800: Tmelt = 1537 + 273
                Mater$ = "Carbon Steel (1.0% C)"
        CASE IS = 4             'Copper
                k = 386: c = 383: rho = 8954: Tmelt = 1083 + 273
                Mater$ = "Copper(pure)"
        CASE IS = 5             'Iron
                k = 73: c = 452: rho = 7897: Tmelt = 1537 + 273
                Mater$ = "Iron"
        CASE IS = 6             'Lead
                k = 35: c = 130: rho = 11373: Tmelt = 327 + 273
                Mater$ = "Lead"
        CASE IS = 7             'Silver
                k = 419: c = 234: rho = 10524: Tmelt = 961 + 273
                Mater$ = "Silver"
REM     CASE IS = 8             'Titanium
REM             k = xxx: c = 523: rho = 4507: Tmelt = 1670 + 273
```

ORIGINAL PAGE IS
OF POOR QUALITY

```
REM          Mater$ = "Titanium"
    CASE ELSE          '<custom>
        PRINT "Enter the thermal conductivity (W/m·K)";
        INPUT k
        PRINT "Enter the heat capacity (J/kg·K)";
        INPUT c
        PRINT "Enter the density (kg/m^3)";
        INPUT rho
        PRINT "Enter the melting temperature (K)";
        INPUT Tmelt
        Mater$ = "Custom Material"
    END SELECT


REM Choose Geometry
300 PRINT "Select test geometry"
310 PRINT "     1. Rectangular Bar"
320 PRINT "     2. Plate"
330 INPUT Geometry
340 SELECT CASE Geometry
    CASE IS = 1     'Rectangular Bar
        PRINT "Enter bar thickness (mm)"
        INPUT h
        h = h / 1000
        PRINT "Enter bar width (mm)"
        INPUT w
        w = w / 1000
```

ORIGINAL PAGE IS
OF POOR QUALITY

```
          FOR i = 1 TO nEnd
          Ac(i) = w * h          'Conductive Area Out
          Ar(i) = w * dL         'Radiative Area Surfaces
          NEXT i
          Qspot = .493 * 763 / 2          '49.3% ABSORPTION. 1/2 Left & 1/2 Right
          Geom$ = "Rectangular Bar"
          dx = dL
     CASE ELSE      'Plate
          PRINT "Enter plate thickness (mm)"
          INPUT h
          h = h / 1000
          FOR i = 1 TO nEnd
          Ac(i) = 2 * pi * (i * dR) * h
          REM     Ar(i) = π·[(i·dR)² - (dR(i - 1))²]
          REM     Ar(i) = π·dR²·[(i²) - (i²-2i+1)]
          REM     Ar(i) = π·dR²·(2i-1)
          Ar(i) = pi * (dR ^ 2) * ((2 * i) - 1)
          NEXT i
          Qspot = .493 * 763             '49.3% ABSORPTION.
          Geom$ = "Plate"
          dx = dR
     END SELECT

470 Abnormal = 0
480 PRINT "    Time    T1    T2    T3    T4    T5    T6    T7"
490 dtOVERcRHOh = dt / (c * rho * h)
```

ORIGINAL PAGE IS OF POOR QUALITY

```
REM Main Loop

500 FOR j = 1 TO TheEnd
510 time = CINT((time - dt) * (1 / dt)) * dt

520 FOR i = 1 TO nEnd

REM Calculate Qconduction
550 IF i < nEnd THEN
560 Qc(i) = k * Ac(i) * (Told(i) - Told(i - 1)) / dx
570 ELSE
580 Qc(i) = 0
590 END IF

REM Calculate Qr
600 Qr(i) = S * Ar(i) * Told(i) ^ 4


REM Calculate Tnew
650 IF i = 1 THEN
660 Tnew(i) = Told(i) + (dtOVERcRHOh / Ar(i)) * (Qspot - Qc(i) - 2 * Qr(i))
670 ELSE
680 Tnew(i) = Told(i) + (dtOVERcRHOh / Ar(i)) * (Qc(i - 1) - Qc(i) - 2 * Qr(i))
685 IF Tnew(i) > Tnew(i - 1) THEN Abnormal = 1
690 END IF

REM Examine Tnew
```

ORIGINAL PAGE IS
OF POOR QUALITY

```
700 Told(i) = Tnew(i)
710 NEXT i

740 PRINT USING " ####.##": time;
750 PRINT USING " ####.#": Tnew(1): Tnew(2): Tnew(3): Tnew(4): Tnew(5):
Tnew(6): Tnew(7)
770 IF Tnew(1) >= Tmelt GOTO 900
780 NEXT j

REM Report No Melt
800 PRINT
810 PRINT "MATERIAL DID NOT MELT IN TIME ALLOWED"
820 GOTO 1000

REM Report Tmelt
900 PRINT
910 PRINT "MATERIAL MELTED AT ": Tnew(1): " KELVIN":
915 PRINT " IN ": time. "SECONDS"
920 GOTO 1000

REM Report Test Parameters
1000 PRINT
1010 PRINT Mater$: " - ": Geom$
1020 PRINT "thickness = "; h * 1000: " mm"
1029 IF Geometry = 1 THEN
1030 PRINT "width=": w * 1000: " mm"
1031 END IF
```

ORIGINAL PAGE IS
OF POOR QUALITY

```
1040 PRINT "thermal conductivity ="; k; "W/m·K"

1050 PRINT "heat capacity ="; c; " J/kg·K"

1060 PRINT "density ="; rho; " kg/m^3"

1070 PRINT "melting temperature ="; Tmelt; " K"


1100 IF Abnormal <> 0 THEN

1110 PRINT "The system behaved abnormally."

1120 PRINT "Use a smaller time step (dt)."

1130 END IF


1500 INPUT "Run another sample(y/n)"; YESorNO$

1510 IF UCASE$(YESorNO$) = "N" THEN END

1520 CLS

1600 GOTO 50
```

ORIGINAL PAGE IS
OF POOR QUALITY

# ASPOD Cutting Array Redesign Project
## Financial Summary
May, 1994

| ITEM | QUANTITY | UNIT COST | SUB TOTAL |
|---|---|---|---|
| PROTOTYPE: | | | |
| 3/4" PVC TEE | 8 | 0.12 | 0.96 |
| 3/4" PVC 45 deg ELBOW | 16 | 0.26 | 4.16 |
| 3/4" PVC 90 deg ELBOW | 8 | 0.10 | 0.80 |
| 3/4" SCH 40 PVC PIPE | 40 (feet) | 0.102 | 4.08 |
| 1 1/4" X 2 1/4" HAND RAIL #240 | 1 | 1.38 | 1.38 |
| 3/8" X 1 3/8" RE STOP #866 WP | 1 | 0.51 | 0.51 |
| 1/4" X 3/4" FLAT SCREEN MLD #142 | 1 | 0.25 | 0.25 |
| 1 3/8" FULL ROUND #232 FIR | 1 | 0.89 | 0.89 |
| 1/2" X 9" CARRIAGE BOLT | 1 | 1.45 | 1.45 |
| 1/4" X 2" LAG SCREW | 1 | 0.10 | 0.10 |
| 1/4" X 5" CARRIAGE BOLT | 1 | 0.18 | 0.18 |
| 3/8" X 48" WOOD DOWEL | 1 | 0.49 | 0.49 |
| 3/8" X 40" NOM BULLNOSE PB SHELVING | 3 | 0.59 | 1.77 |
| 34 1/2" X 21" MULTI-ELEMENT FRESNEL | 1 | 89.00 | 89.00 |
| TEST EQUIPMENT: | | | |
| 20 LB TENSION SCALE | 1 | 4.00 | 4.00 |
| FINAL PROTOTYPE (PROJECTED): | | | |
| 1" ALLUMINUM BAR STOCK | 4(feet) | 5.00 | 20.00 |
| MISCELLANEOUS FASTENERS | | | 15.00 |
| 1" HOSE CLAMPS | 16 | 1.55/2 | 13.27 |
| 1/2" ALLUMINUM BAR STOCK | 5 (feet) | | 10.11 |
| ALLUMINUM CHANNEL STOCK | 24(feet) | 6.29/12" section | 26.92 |
| NAT UHMW 3.5"x48" | 1 | 6.00 | 6.00 |
| 1"x1"x1/8" ANGLE ALLUM STOCK | 8(feet) | | 6.50 |
| 1/8" ACRYLIC SILVER MIRRORS | 4 | | 100.00 |
| | | TOTAL COST: | $307.82 |

ORIGINAL PAGE IS OF POOR QUALITY

# REFERENCES

1. Duffie, John A. and Beckman, William A. *Solar Engineering of Thermal Processes 2nd Edition*. New York: John Wiley & Sons, 1991.
2. Gere, J. M. and Timoshenko, S. P. *Mechanics of Materials: 3rd Edition*. Boston: PWSKENT Publishing Company, 1990.
3. Haffner, James W. *Radiation and Shielding in Space*. New York: Academic Press, 1967.
4. Halliday, David and Resnick, Robert *Fundamentals of Physics: 3rd Edition*. New York: John Wiley & Sons, 1988.
5. Holman, J. P. Heat Transfer: 5th Edition. New York: McGraw-Hill, 1981.
6. Srinivasan, V. and Banks, B. A. *Materials Degradation in Low Earth Orbit* Warrendale, PA: The Minerals, Metals, and Materials Society, 1990.

ORIGINAL PAGE IS
OF POOR QUALITY

The control system for the Autonomous Space Processor of Orbital Debris (ASPOD) consists of the control card, the hardware interface, and the software necessary to manipulate the robotic arm. This report will focus on the controller card and the software used for the ASPOD.

The controller card is the main processor of the control system. The Omnitech Robotics MC-3000 card is a personal computer compatible application board designed to use three Hewlett Packard HCTL-1100 motion controller integrated chips. The MC-3000 yields three axes of motion control. Two MC-3000 boards are necessary to control all six axes designed for one robotic arm. Each axis of motion control provided by the MC-3000 is closed loop control and has two position control modes and two velocity control modes.

The mode used to operate the robotic arm for the ASPOD is the trapazoidal profile control mode. This mode controls the velocity and acceleration of the actuators while providing point-to-point position moves. In this mode, the controller moves at constant acceleration as specified by the command input until the maximum velocity is reached or until the half of the motor's position move is completed. Then it either moves at constant maximum velocity until the deceleration point, or it immediately slows at constant deceleration to a stop at the command position, respectively. After the motor is decelerated, the card checks for the programmed position and adjusts to the programmed value. The trapazoidal mode appears to be the ideal for robotic applications because it offers reasonable velocity and acceleration regulation with positioning control. Thus, this mode was chosen to best suit the ASPOD's specifications.

For practical application, the robotic arms of the ASPOD must be manipulated in two ways. The arms must respond to both manual and preprogrammed control. Manual control will be needed for initial contact with the space debris, or for other applications requiring

PRECEDING PAGE BLANK NOT FILMED

human judgement. The arms will also perform several repeated tasks usually too tedious for the operator, so preprogrammed instruction must also be provided for the robotic arms.

Programming the MC-3000 to control the arms with a repetitious set of instructions can be achieved by using a command interpreter. This interpreter, called MCBasic, is included among the software provided by Omnitech Robotics. The MCBasic interpreter uses a series of functions and motion control commands particular to the MC-3000 combined with a BASIC programming language interpreter. This allows for testing of the MC-3000 operation and for development of user program applications. MCBasic is a DOS based program similar to the BASIC interpreter included with many personal computers. MCBasic's functions and commands are given in source code on the distribution software. The code, labeled EXER.C, contains the syntax used by the interpreter to control the MC-3000's motions. The BASIC language commands that come with MCBasic are standard ANSI Basic compliant BASIC.

An interactive program is also provided with the MC-3000 software called EXER. This is the executable form of EXER.C that can immediately perform a command desired by the user. For longer programs, an ASCII text editor, such as the Edit command used in DOS, can be used. By using a text editor, preprogramming of the MC-3000 is accomplished thus fulfilling one of ASPOD's motion control requirements.

Manual control is achieved through a Windows 3.1 based point and click menu of motion commands. This method provides a graphical user interface to allow simple operation of the MC-3000 motion control libraries. The program provided by Omnitech Robotics, called the Motion Control Center, is a menu driven application that allows selection of the MC-3000 commands with a mouse. Figure 1 shows the Motion Control Center environment. The commands for the Motion Control Center are the same functions and commands used in the MCBasic environment.

The MCBasic motion control commands are given in the following tables. The source code EXER.C is given in the appendix as supplemental description of the motion control commands.

Table 1 Control Modes

| Command Name | Function |
|---|---|
| sel_mode | Enter Control mode selection loop |
| trap_mode | Enter Trapazoidal profile mode |
| prop_mode | Enter Proportional Velocity mode |
| pos_mode | Enter Position Control mode |
| int_mode | Enter Integral Velocity mode |
| init | Enter Initialization/Idle mode |

Table 2 Position Commands

| | |
|---|---|
| set_cmd_pos N | Set command position to N<br>(-8388608 <= N <= 8388607) [q.counts] |
| get_cmd_pos | Display command position. [q.counts] |
| set_final pos N | Set final position to N, for trap_mode<br>(-8388608 <= N <= 8388607) [q.counts] |
| get_final_pos | Display final position [q.counts] |
| get_act_pos | Display actual position [q.counts] |
| clr_act_pos | Clear actual position to zero [q.counts] |

Table 3 Velocity Commands

| | |
|---|---|
| set_max_vel N | Set maximum velocity to N<br>(0 <= N <= 127) [q.counts/time] |
| get_max_vel | Display maximum velocity<br>[q.counts/sample time] |
| set_prop_vel N | Set proportional velocity to N<br>(-2048 <= N <= 2048) [q.counts/time] |
| get_prop_vel | Display proportional velocity<br>[q.counts/sample time] |
| set_int_vel N | Set integral velocity to N<br>(-127 <= N <= 127) [q.counts/time] |
| get_int_vel | Display integral velocity<br>[q.counts/sample time] |
| get_act_vel | Display actual velocity<br>[q.counts/sample time] |

Table 4 Acceleration Commands

| | |
|---|---|
| set_accel N | Set acceleration to N<br>(0 <= N <= 65535)<br>[q.counts/(sample time^2)*256] |
| get_accel | Display acceleration |

Table 5 Compensation Filter Commands

| | |
|---|---|
| set_gain N | Set compensation gain<br>(0 <= N <= 225) |
| get_gain | Display compensation gain |
| set_pole N | Set compensation pole<br>(0 <= N <= 255) |
| get_pole | Display compensation pole |

| | |
|---|---|
| set_zero N | Set compensation zero (0 <= N <= 255) |
| get_zero | Display compensation zero |
| set_timer N | Set sample timer to N (0 <= N <= 255) |

Table 6 Motor Output Commands

| | |
|---|---|
| set_dac N | Set DAC output register value (0 <= N <= 255) |
| get_dac | Display DAC output register value |
| set_pwm N | Set PWM register output value (-100 <= N <= 100) |
| get_pwm | Display PWM register value |
| set_bipolar | Set bipolar DAC output mode |
| set_unipolar | Set unipolar DAC output mode |
| set_sign_rev N | Set PWM sign reversal on or off (N=1 for on, N=0 for off) |

Table 7 Commutator Commands

| | |
|---|---|
| align | Align commutator via encoder |
| open_loop_comm | Open loop communication |
| closed_loop_comm | Closed loop communication |
| set_ring N | Set commutator ring register to N (0 <= N <= 127) [q.counts/torque cycle] |
| get_ring | Display commutator ring value |
| set_x N | Set commutator X register to N (0 <= N <= 127) |
| get_x | Display commutator X value |
| set_y N | Set commutator Y register to N |
| get_y | Display commutator Y register value (0 <= N <= 127) |
| set_offset N | Set commutator offset register to N (-127 <= N <= 127) |
| get_offset | Display commutator offset register |
| set_max_adv N | Set commutator maximum advance |
| set_vel_timer N | Set commutator velocity timer (0 <= N <= 127) |
| comm_count N | Set commutator units for q.counts or encoder. (N=0 for q.counts, N=1 for encoder) |
| num_phases N | Set number of phases to 3 or 4 (N=3 for 3 phase, N=4 for 4 phase) |

Table 8 Miscellaneous Commands

| | |
|---|---|
| reset | Soft reset of HCTL-1100 |
| set_status | Set status register to N (0 <= N <= 255) |
| get_status | Display status |
| clr_emerg_flags | Clear emergency flags |
| delay N | Time delay, in N multiples (0 <= N <= 2147483647) [milliseconds] |
| quit | Quit program, return to DOS |
| set_do N | Set digital output byte to N (0 <= N <= 15) |
| get_di | Display digital input byte |
| set_base N | Set MC-3000 base address variable |
| fine_home N | Flag indicating if index is used for |

| | |
|---|---|
| | homing. (N=1 if index used, N=0 otherwise) |
| home | Home axis, uses D10, and Index |
| regin N | Register input from HCTL-1100 reg. N (0 <= N <= 60; restricted to user registers) |
| regout N M | Register output to HCTL-1100 reg. N, value M. (0 <= N <= 60; restricted to user registers)<br>(0 <= M <= 255) |

MCBasic can load and run example programs to test the operation of the MC-3000. These files are included in the distribution disk provided by Omnitech Robotics. In tables 9 and 10, two of the sample programs will be examined to illustrate the method of programming the MC-3000 using the ASCII text editor. The code on the left is the instruction the command interpreter translates. To the right is a note about the code.

Table 9 TRAP.CMD Trapazoidal Control

| | |
|---|---|
| set_base 768 | This is the first axis on the robotic arm. The number 768 is the port address assigned to that axis via the MC-3000 card. |
| set_gain 10 | Gain compensator is set to 10. |
| set_zero 240 | Zero compensator is set to 240. |
| set_pole 0 | Pole compensator is set to 0. |
| set_timer 40 | Timer set to 40. |
| clr_act_pos | Actual position cleared to avoid confusing the final position with the actual position. |
| set_max_vel 10 | Maximum velocity set to 10 q.counts/timer |
| set_accel 2 | Maximum acceleration set to 2 q.counts/(timer^2)*256. |
| sel_mode | Selection Mode loop is initiated. |
| set_final_pos 100000 | Motor will stop at 100,000 q.counts |
| trap_mode | Trapazoidal profile selected. Motion starts. |
| delay 3000 | A delay of instruction reading is given to the command interpreter so that the motor can finish its movements. |
| set_final_pos 0 | Tells motor return back to initial position. |
| set_accel 10 | Acceleration set for faster return. |
| trap_mode | Trapazoidal profile selected. Motion starts. |
| delay 3000 | Another delay so motor can finish movements. |
| quit | End of program. |

As it is shown, the program gives a demonstration of how the trapazoidal profile can be used to move the motor. In this example, the motor is given two different accelerations. For the first acceleration of 2 quadrature counts per time squared, the motor achieves maximum velocity before it completes half the required distance. At this point, the motor continues to operate at constant velocity until it reaches the next deceleration point. At this point, the motor slows until it comes to rest at the desired position. For the second acceleration of 10 quadrature counts per time squared, the motor reaches the midpoint position before completing maximum velocity. At this point, the motor immediately decelerates until the desired position is reached.

The next example is for a commutator. This example is for a three phase motor with eight electrical torque cycles per mechanical revolution. I assumes a commercial brushless amplifier which requires hall effect sensor inputs, so the commutator outputs need to have fifty percent duty cycle, with overlap 120 electrical degrees from phase to phase. It uses a 192 line encoder.

Table 10 Commutator Example

| | |
|---|---|
| num_phases 3 | Sets commutator for a three phase motor. |
| comm_count 0 | Sets the commutator for quadrature counts for all units being programmed instead of full encoder counts. |
| set_ring 96 | Sets ring counter to 96 quadrature counts. This value is found as follows:<br>192 line encoder * 4 = 768 q.counts/rev<br>768 q.counds/8 pole motor = 96 q.counts/pole<br>(96 q.counts/pole / 3 phases = 32 q.counts) |
| set_x 16 | X = time 1 phase active = 16 |
| set_y 16 | Y = time 2 phase active = 16 |
| set_offset -96 | Satisfies constraint equation:<br>80H <= 1.5(Ring) + offset +/- max advance <= 7FH<br>(-128D) (127D)<br>This is equal to "set_offset 0" meaning no offset is required. However the above constraint shows that "set_offset -96" meets the constraint equation, while "set_offset 0" does not. |
| set_max_adv 0 | No phase advance. |
| set_vel_timer 0 | No phase advance. |
| set_sign_rev 1 | PWM sign reversal set on. |
| set_gain 10 | (The rest of the example is a variation of the trapazoidal profile control example.) |
| set_zero 240 | |
| set_pole 0 | |
| set_timer 40 | |
| clr_act_pos | |
| set_max_vel 50 | |
| set_accel 2 | |
| set_final_pos 100000 | |
| trap_mode | |
| quit | |

The ASPOD needs both the programmed instruction and the manual control to manipulate the robotic arms. The command interpreter takes instructions from either control option and translates those commands to the MC-3000. The MC-3000 then controls each motor of the robotic arm. By using the commands shown in tables one through eight, a usable code can be obtained that results in the desired actions of the arm. Using the Windows 3.1 Motion Control Center also uses the command interpreter to perform the necessary functions needing in performing manual control. By experimenting and optimizing these different programming approaches, useful programs necessary to demonstrate the robotic arms have been created to suit ASPOD's purposes.

# PROPOSED REDESIGN FOR ASPOD'S SOLAR TRACKING DEVICE

By

David A. Rowney

For

Dr. Ramohalli
AME 499
Independent Study
Spring1994

# TABLE OF CONTENTS

INTRODUCTION ........ 1
PROJECT DESIGN CRITERIA ........ 1
PROBLEM DEFINITION ........ 2
THE PROPOSED SOLUTION ........ 2
SOLAR TRACKER DESIGNS ........ 3
  Spring 1993 Design ........ 3
    Solar Tracking Device ........ 4
    Control System ........ 5
  The Proposed Fall 1993 Design ........ 6
    The Solar Tracking Device ........ 6
    The Control System ........ 11
SOLAR TRACKING THEORY ........ 12
SOLAR TRACKING PARAMETERS ........ 15
  The Solar Spectrum ........ 16
  Solar Insolation ........ 17
  The Solar Wavelength Regions ........ 19
  Atmospheric Affects ........ 21
    Atmospheric Absorption ........ 21
    Cloud Effects ........ 27
  Terrestrial Effects ........ 34
    Terrestrial Objects ........ 34
    Plant Effects ........ 36
  Solar Cell Selection ........ 37
    Solar Cell Materials ........ 37
    Solar Cell Characteristics ........ 37
  The Final Selection Of Photo Cells ........ 44
    Infrared Diode Boxes And Hot Mirrors ........ 44
SOLAR TRACKER TESTING ........ 46
  The Test ........ 53
CONCLUSION ........ 54
  Items To Be Completed ........ 54
  Design Troubleshooting Hints ........ 56
ENDNOTES ........ 58
REFERENCES ........ 61
APPENDIX ........ 63

## INTRODUCTION

The need for controlling and removing space debris from Low Earth Orbit is the prominent concern for the ASPOD Program. ASPOD stands for Autonomous Space Processor for Orbital Debris. As one of the designers of the ASPOD Solar Tracking Table during 1992-1993 AME 412 Mechanical Engineering Design Class, my group succeeded in accomplishing all but one of its starting goals in the project. This goal was to have the solar tracking device track with ± 1 degree of the sun. In the final design of the school year though, this goal was not achieved. The group only succeeded in tracking within ± 5 degrees of the sun. As group leader for the project, I found this unacceptable and so have sought to clear up this loose end. This project seeks to accomplish the needed criteria of last year's project. This goal is stated within the lines of the problem definition.

## PROJECT DESIGN CRITERIA

The needs of the solar tracking table to accurately track the sun are a must if the ASPOD project is to work as a whole to demonstrate its concept. Therefore, the solar tracker must:

1. Be light, compact and easily movable.
2. Be easily mountable and work with the existing ASPOD structure.
3. Track within ± 1 degree of the sun.
4. Cost less than $500.

## PROBLEM DEFINITION

Design and build a solar tracking device that satisfies all design criteria and which can track the sun.

## THE PROPOSED SOLUTION

This research paper and its design proposes to correct the tracking problems of the previous design. In order to do this, there will be a redesign of the present tracking device and a slight re modification of the control circuits. A complete description of these designs will be demonstrated in the coming sections of this paper. Whenever possible, components of the old device will be used in the new in order to reduce costs.

This paper will seek to explore the theory behind solar tracking and the possible sources of error for a solar tracker. It will also describe and compare the proposed design with the previous design and propose a possible accuracy test for the device. Finally, it will cover the time table for completion. Final cost analysis will be given in the final paper when the project is completed.

# SOLAR TRACKER DESIGNS

## Spring 1993 Design

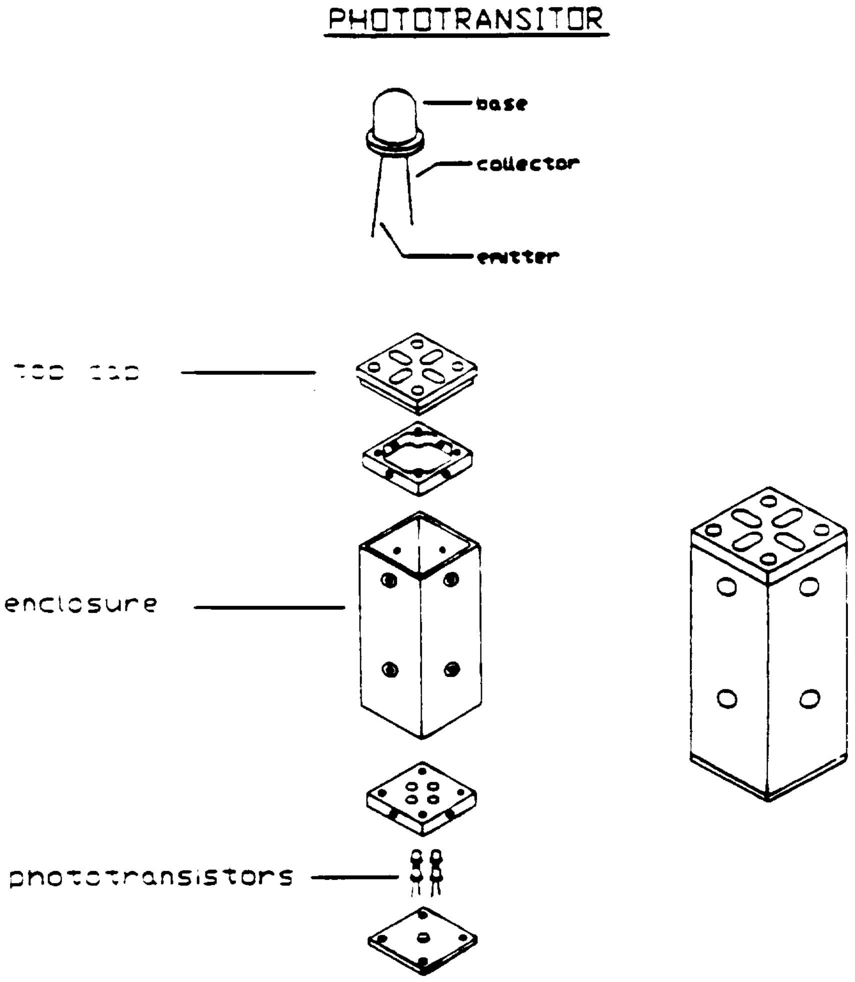
PHOTOTRANSITOR
base
collector
emitter
top cap
enclosure
phototransistors

FIGURE 3.0. Solar Tracking Device for Spring 1993.

## Solar Tracking Device

The design for the Spring 1993 solar tracking device consisted of a rectangular aluminum box of dimensions 4"x2"x2". As seen in Figure 3.0, this tracking device is made up of a top cap, an enclosure, a bottom plate and four phototransistors. The top cap covered the phototransistors and allowed sunlight through four holes situated above the phototransistors. They received the light and converted it to a current which was used to track by using the concepts of solar tracking theory.

The problem with this design is that the holes in the cap are too large and the overall enclosure length is too short. The enclosure needs to be longer to create a narrower cone of light to touch the phototransistors. This is one of the reasons for the ± 5 degree tracking ability. Other reasons may come from faulty controls. The following design seeks to overcome these faults.

## Control System

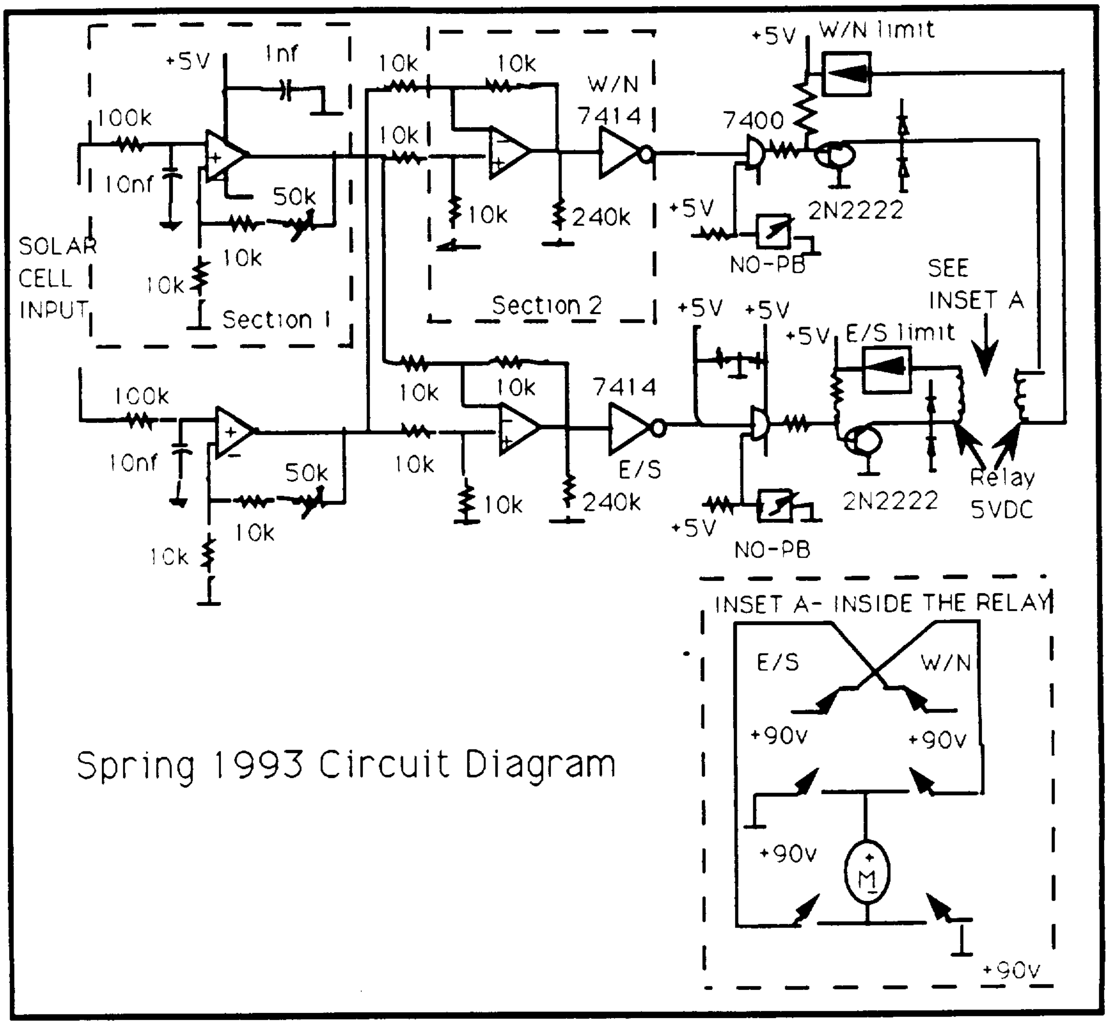
+5V
1nf
100k
10nf
50k
10k
10k
SOLAR CELL INPUT
Section 1
100k
10nf
50k
10k
10k
10k
10k
10k
10k
W/N
7414
10k
240k
Section 2
10k
10k
10k
10k
7414
E/S
10k
240k
+5V
W/N limit
7400
2N2222
+5V
NO-PB
SEE INSET A
+5V
+5V
+5V
E/S limit
2N2222
Relay 5VDC
+5V
NO-PB
INSET A- INSIDE THE RELAY
E/S
W/N
+90v
+90v
+90v
M
+90v
Spring 1993 Circuit Diagram

FIGURE 3.1. Spring 1993 Controls Circuit

The above figure shows the current design of the circuit for one of the axes. It is duplicated the same way for the other axis and its motor. As seen, it is composed of operational amplifiers, resistors, relays, two solar cells per axis and one motor. These give the feedback necessary to move the solar tracking table via the motors. The amplifiers increase the output of the solar cells and allow for the necessary input for the control box to turn on the motors. The present configuration allows for movement up and down in tilting and in rotation, right to left or left to right depending upon the input.

## The Proposed Fall 1993 Design

### The Solar Tracking Device

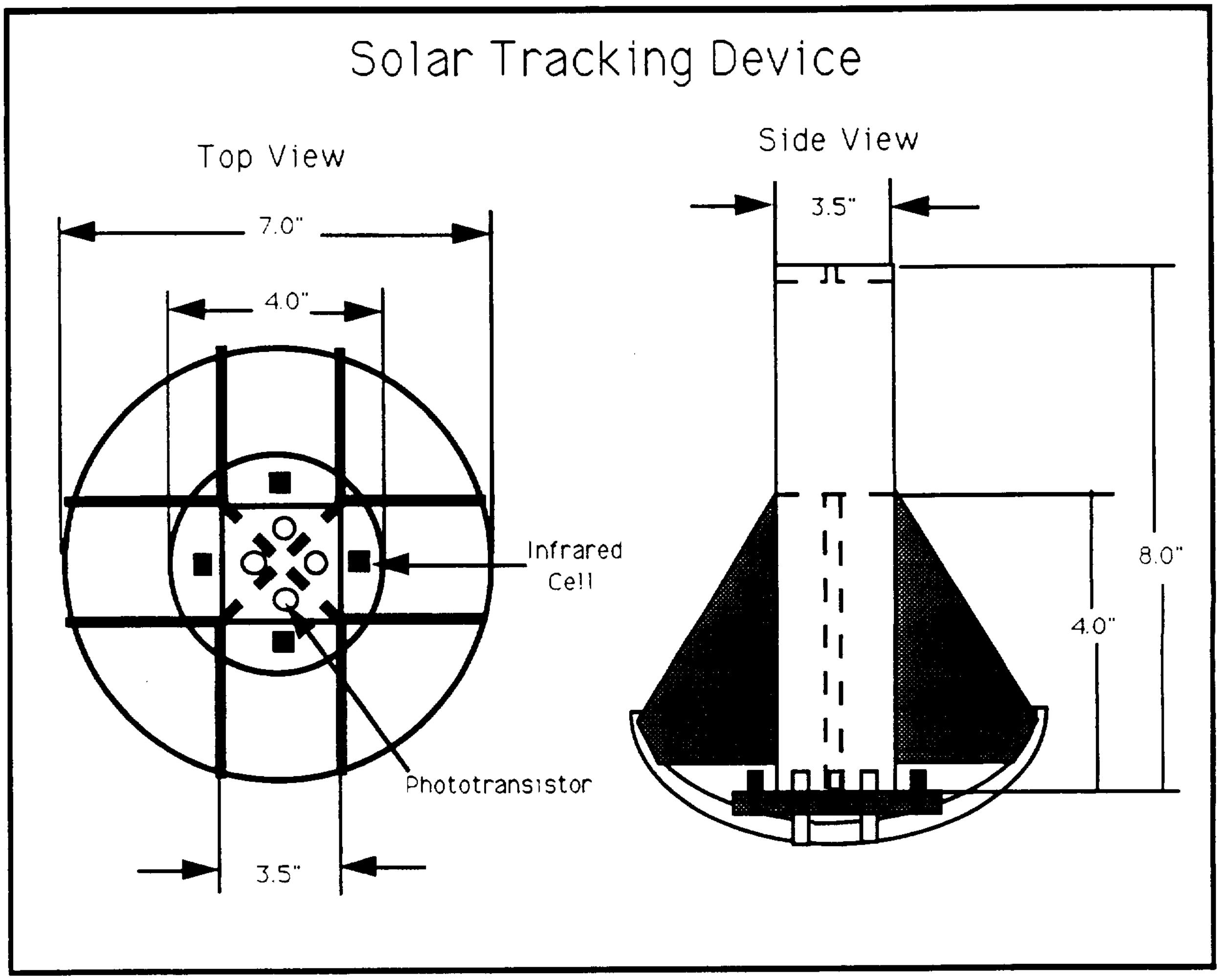
Solar Tracking Device
Top View
Side View
7.0"
4.0"
3.5"
Infrared Cell
Phototransistor
3.5"
8.0"
4.0"

FIGURE 3.3 Solar Tracking Device for Fall 1993

As seen in Figure 3.3, the Fall 1993 Design hardware consists of a tracking dish, a phototransistor tube, angled dividers, four phototransistors and four infrared cells. The entire structure inside and out will be painted black and will be made out of PVC plastic and aluminum. It will incorporate a two part tracking system, one primary and one secondary.

The Primary Tracking System

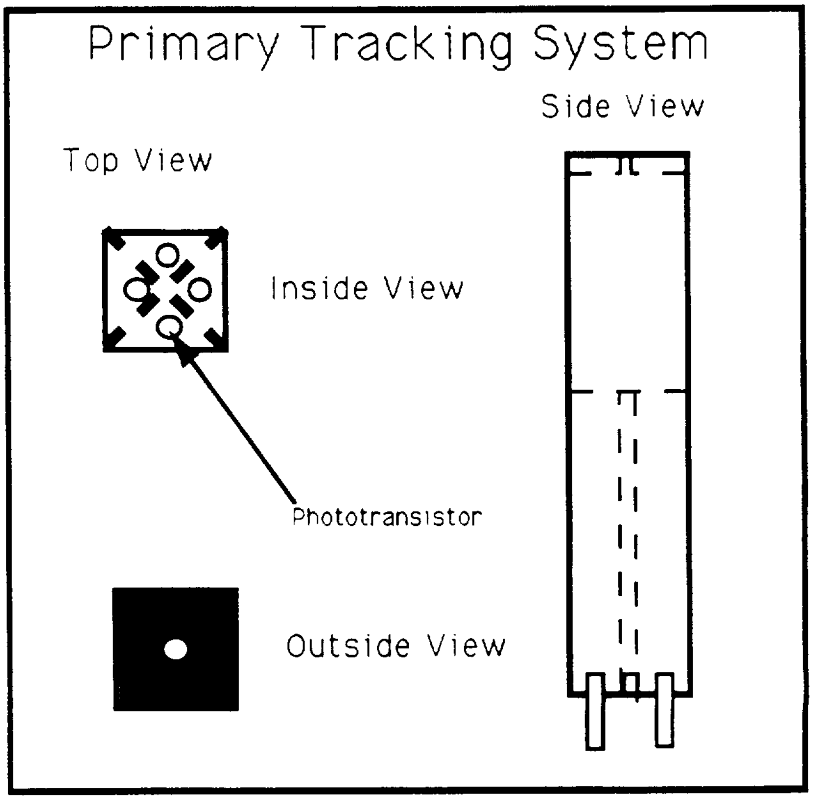
Primary Tracking System
Side View
Top View
Inside View
Phototransistor
Outside View

FIGURE 3.4. The Primary Tracking System

The primary tracking system consists of a phototransistor enclosure tube which holds the phototransistors equally spaced between smaller dividers. This tube will be 8" long and have a 3.5" diameter. A top cap will be mounted on top so that it snugly fits partially inside the tube. In the center of it, will be drilled a round hole less than 1/4 inch in diameter. Its exact size has not been determined as yet. The cone angles and distances will be calculated using geometric and trigonometric principles and will be determined before machining the device. The hole will cause a shaft or cone of light to illuminate the phototransistors. Depending upon the location of this cone the tracker will either stay straight or move left or right.

The primary system although accurate, can be confused because of its tight viewing window. Should the tracker lose the cone of light, it will become essentially blind. Therefore a secondary system will be used to overcome this problem.

### The Secondary Tracking System

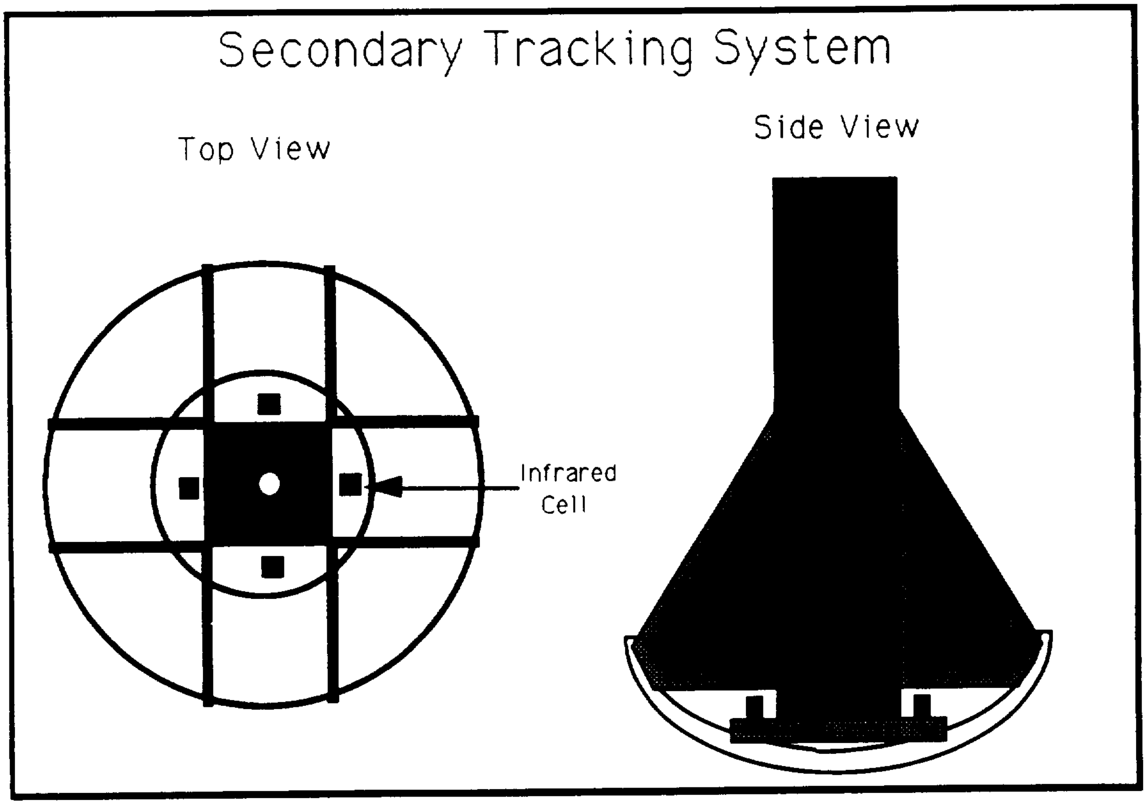

FIGURE 3.5 The Secondary Solar Tracking System

The secondary system as seen in Figure 3.5, consists of a tracking dish to minimize reflected light, four infrared cells and four sets of dividers that hold the tube in place and divide the four sections equally. It will be designed to minimize the confusion of the primary system. It can only be confused if a mirror or a glass surface is nearby to cause a reflection of sunlight. The infrared cells will be spaced equally and will turn on when the primary system fails or when the tracker needs to first align up. They will be designed to be sensitive to a unique solar infrared wavelength. Because of their angle of view as seen in Figure 3.6, they will roughly line up the tracker so that the primary system can take over and track. As soon as this happens, the secondary system will shut down.

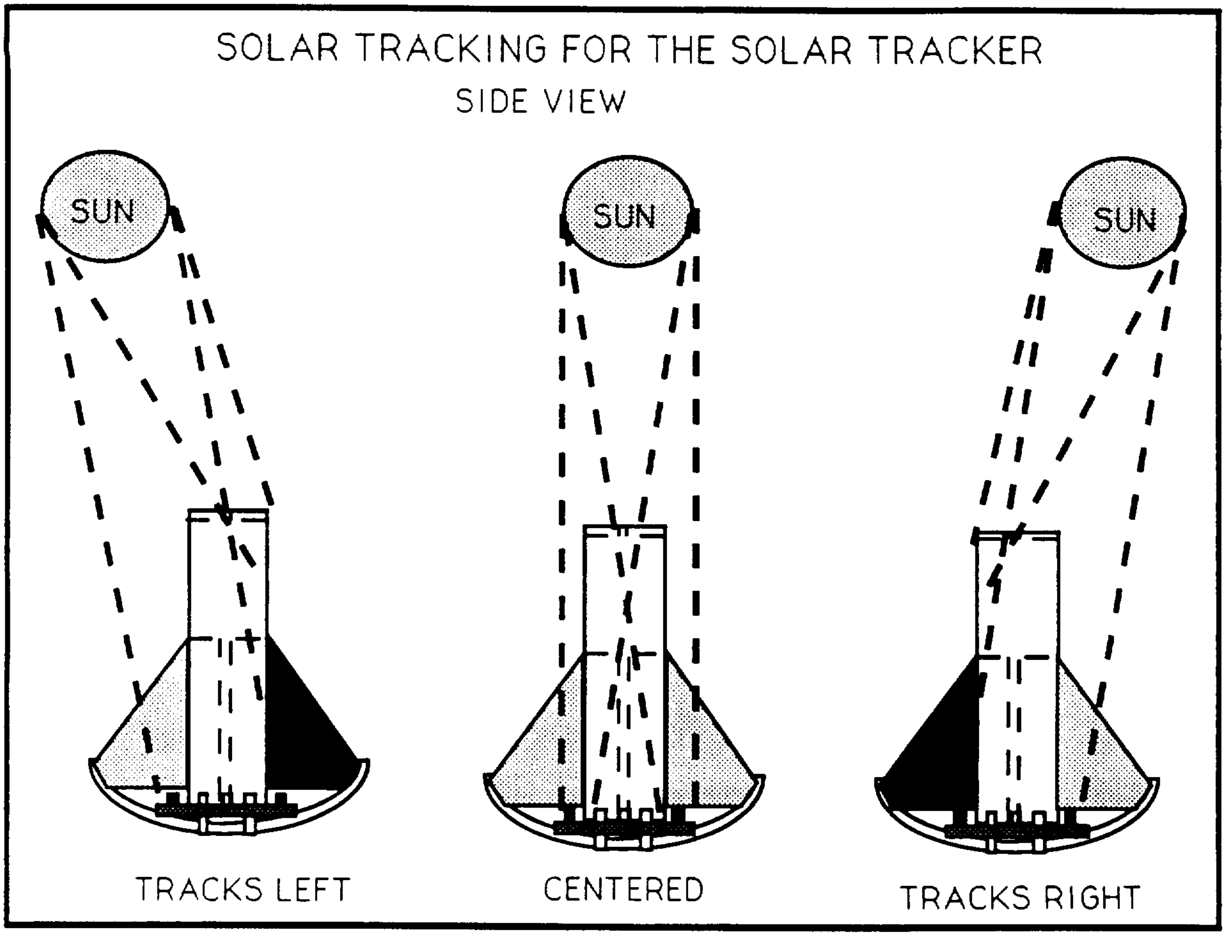
SOLAR TRACKING FOR THE SOLAR TRACKER
SIDE VIEW
SUN
SUN
SUN
TRACKS LEFT
CENTERED
TRACKS RIGHT

FIGURE 3.6. Tracking of the Solar Tracking Device

The tracking ability of this device is analogous to trying to aim within the ballpark and then once inside, focus on the scoreboard. In order to do this, the secondary system will overlap the primary system angle and due to its sensitivity to a certain solar wavelength, it will automatically go for the sun. The tracking ability of this device is illustrated in Figure 3.6. The choice and reasons for choosing this wavelength will be discussed following this section.

## The Control System

In order for the solar tracker to track, a control system must be used. The previous design has a control system already built. This one was shown in Figure 3.3 and has been discussed. This system will be slightly modified to work with the proposed design.

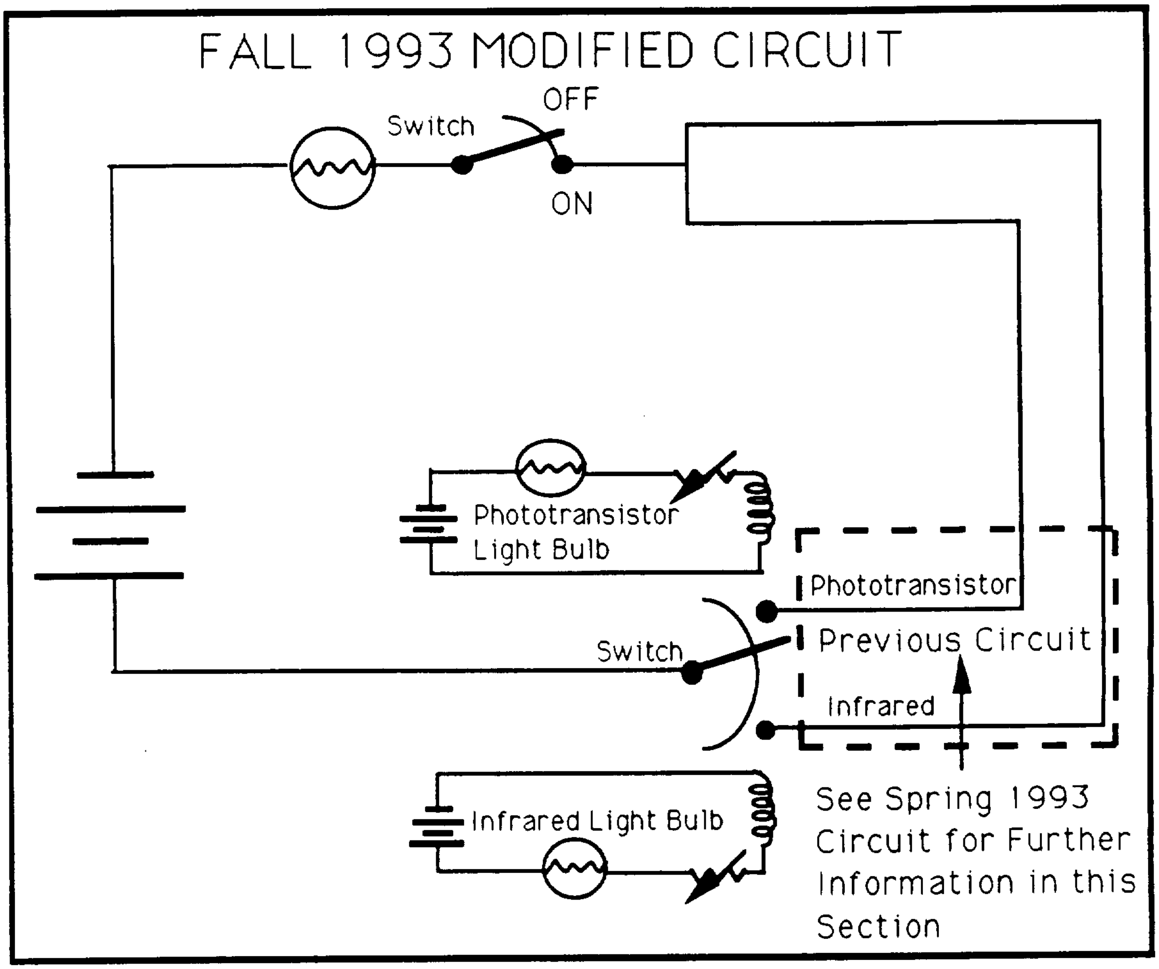
FALL 1993 MODIFIED CIRCUIT
OFF
Switch
ON
Phototransistor
Light Bulb
Phototransistor
Switch
Previous Circuit
Infrared
Infrared Light Bulb
See Spring 1993
Circuit for Further
Information in this
Section

FIGURE 3.7. Fall 1993 Controls System

As seen in Figure 3.7, the control system will receive the input from the primary and secondary systems and depending on how out of align the tracker is, it will switch to one of these systems. When both systems balance out, then the control circuit switches to the off position. This will be done using magnetic switches. In order to troubleshoot and determine which tracking system is on, a series of colored lights will be used. They will be induced to turn on by the current flow using an inductor that is near either the primary or secondary part of the circuit. These lights will be of two different colors, one for the primary and the other for the secondary.

## SOLAR TRACKING THEORY

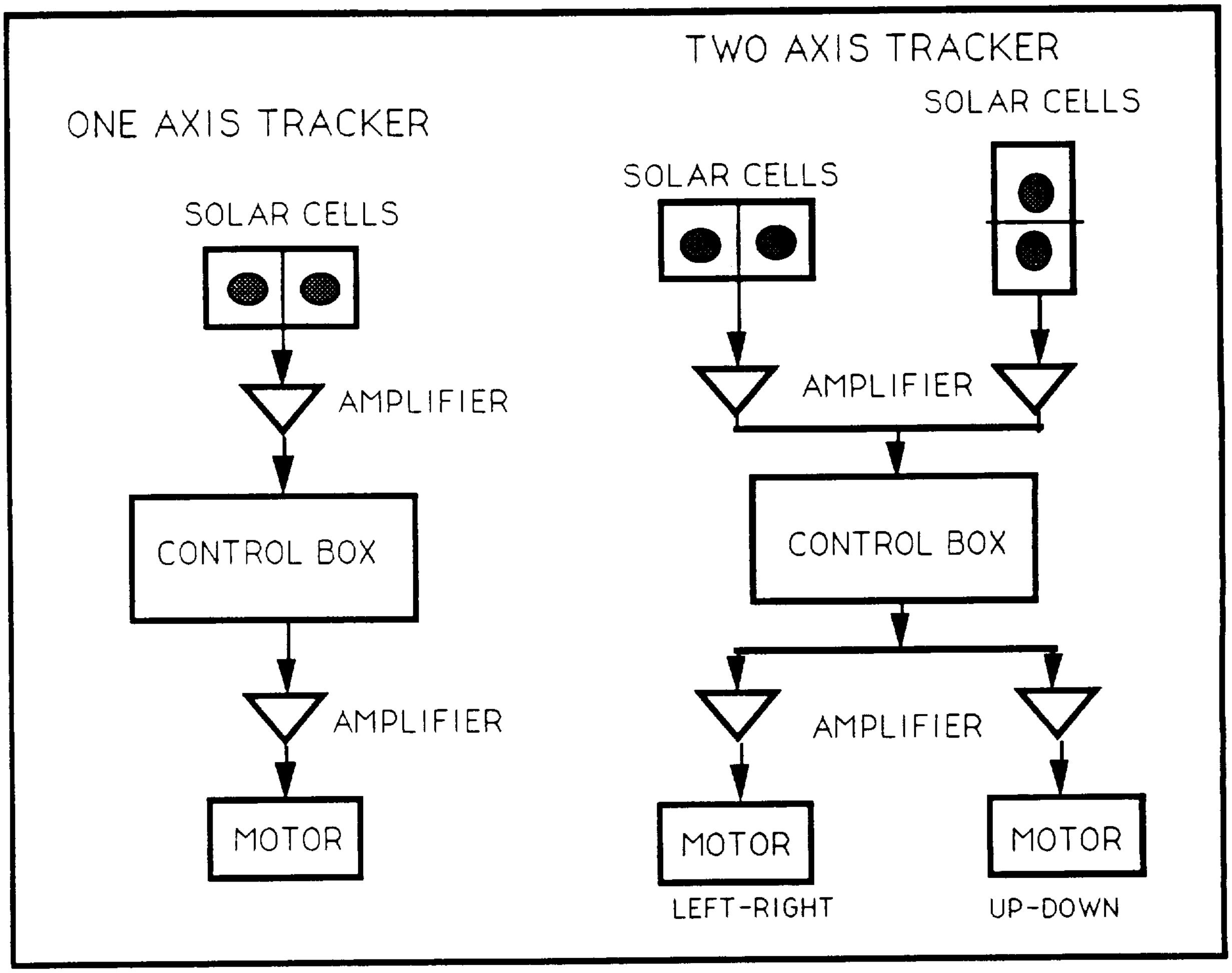
TWO AXIS TRACKER
ONE AXIS TRACKER
SOLAR CELLS
SOLAR CELLS
SOLAR CELLS
AMPLIFIER
AMPLIFIER
CONTROL BOX
CONTROL BOX
AMPLIFIER
AMPLIFIER
MOTOR
MOTOR
MOTOR
LEFT-RIGHT
UP-DOWN

FIGURE 4.0. Solar Cells and Axis Trackers

The basics of solar tracking are dependent upon sensors which can react to the sun's energy. The most basic and often used device is a solar cell. These cells collect the sun's energy and transform it into electrical energy. The electrons in the solar cells are induced to move when photons of light strike and excite them. This movement sets up a current of electrons which creates the electrical energy. By comparing the electrical potential between two cells, one can use this concept to track the sun. As Figure 4.0 shows, the imbalance between these two cells can be transmitted to a control device which then can turn on a motor. This motor then turns the tracking device or table until the balance is restored. This one degree of freedom tracker is the most basic tracker and this concept has been used for many years.

In contrast to a one axis tracker, a two axis tracker such as ASPOD's is more complex. ASPOD's system is illustrated below in Figure 4.1.

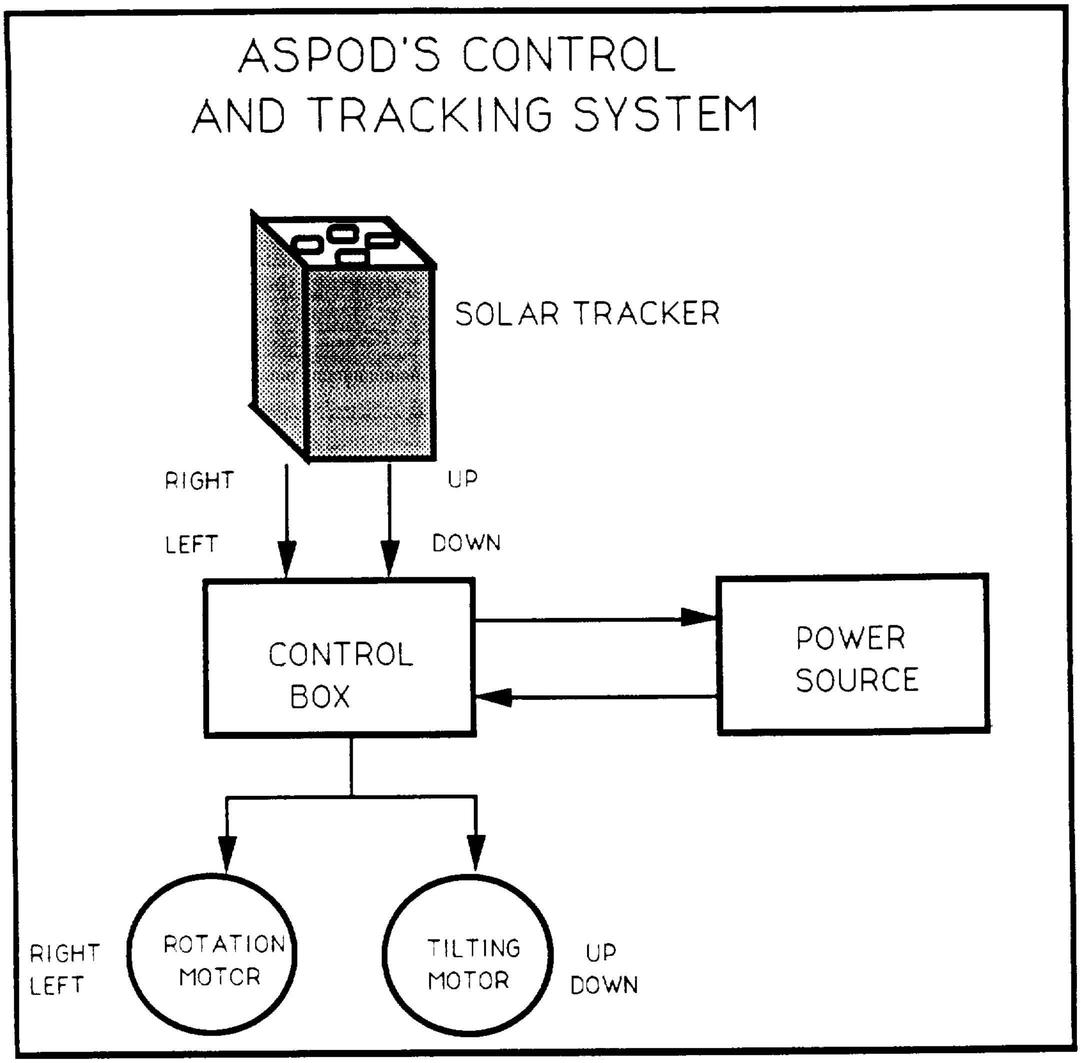
ASPOD'S CONTROL
AND TRACKING SYSTEM
SOLAR TRACKER
RIGHT
LEFT
UP
DOWN
CONTROL
BOX
POWER
SOURCE
RIGHT
LEFT
ROTATION
MOTOR
TILTING
MOTOR
UP
DOWN

FIGURE 4.1. ASPOD's Solar Tracking Controls System

In a two degree of freedom tracker though the concept is done in two directions and the control box must be able to handle this increased input. Complex control circuits are used in this tracker and it must now use two motors to correct any imbalances in the system. Approaches in the circuitry to correct these imbalances can be done in two ways. The first is through positive feedback which increases the error angle by moving the tracking axis move just slightly ahead of the target and then stopping. The second way is by negative feedback where the error angle is decreased by moving the tracking axis across the target, then slightly reversing or stopping the drive mechanism. At present, ASPOD's solar tracking table uses a two degree of freedom tracker and this report will seek to correct its problems.

## SOLAR TRACKING PARAMETERS

In order to design a solar tracking device, one must look at the factors that influence its tracking ability. There are many parameters that need to be investigated. These include solar radiation and insolation, the various regions of the Solar Spectrum, the affects of the atmosphere and terrestrial objects on the Solar Spectrum and finally the characteristics of the solar cells and circuitry that is used to track the sun. All of these are important parameters to a solar tracker and if not properly looked at, then errors in tracking can occur. Therefore, a proper review of these factors will be considered in this report.

## The Solar Spectrum

The sun is the lifeblood of the Earth's energy budget. Without it, Earth would be a lifeless mass of rock. The wavelengths of electromagnetic radiation or light are shown in Figure 5.0. To understand the sun and its radiation, scientists have likened it to a 6000 degree Kelvin blackbody. The radiation coming from this "blackbody" is the energy that keeps the Earth warm and us living.

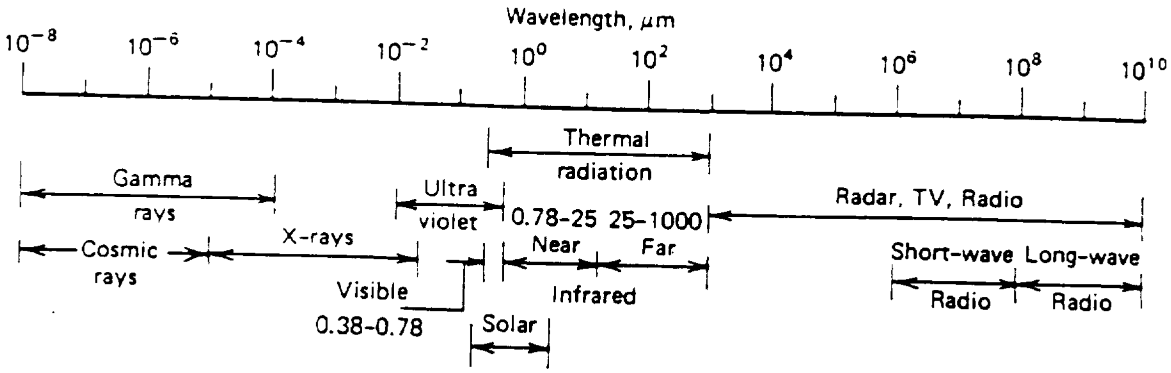
Wavelength, μm
10^-8
10^-6
10^-4
10^-2
10^0
10^2
10^4
10^6
10^8
10^10
Thermal radiation
Gamma rays
Ultra violet
0.78-25
25-1000
Radar, TV, Radio
Cosmic rays
X-rays
Near
Far
Short-wave Radio
Long-wave Radio
Visible
0.38-0.78
Infrared
Solar

FIGURE 5.0. The spectrum of electromagnetic radiation. For diagram reference, see Endnote 1.

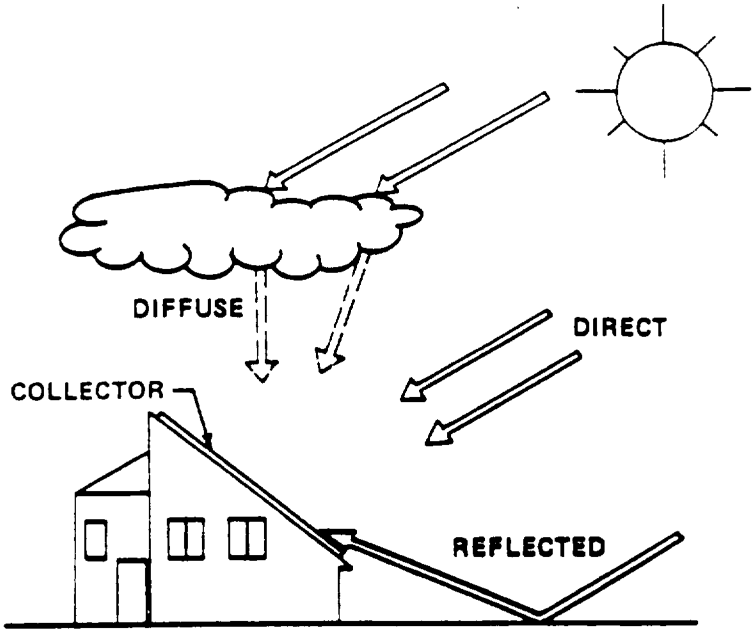
DIFFUSE
DIRECT
COLLECTOR
REFLECTED

FIGURE 5.2. Diffuse, direct and reflected light as seen from the ground. For picture reference, see Endnote 3.

In space all light is direct or beam light. In the atmosphere, the light becomes scattered or diffused. It is also reflected from clouds and other terrestrial sources. This illustrated in Figure 5.3.

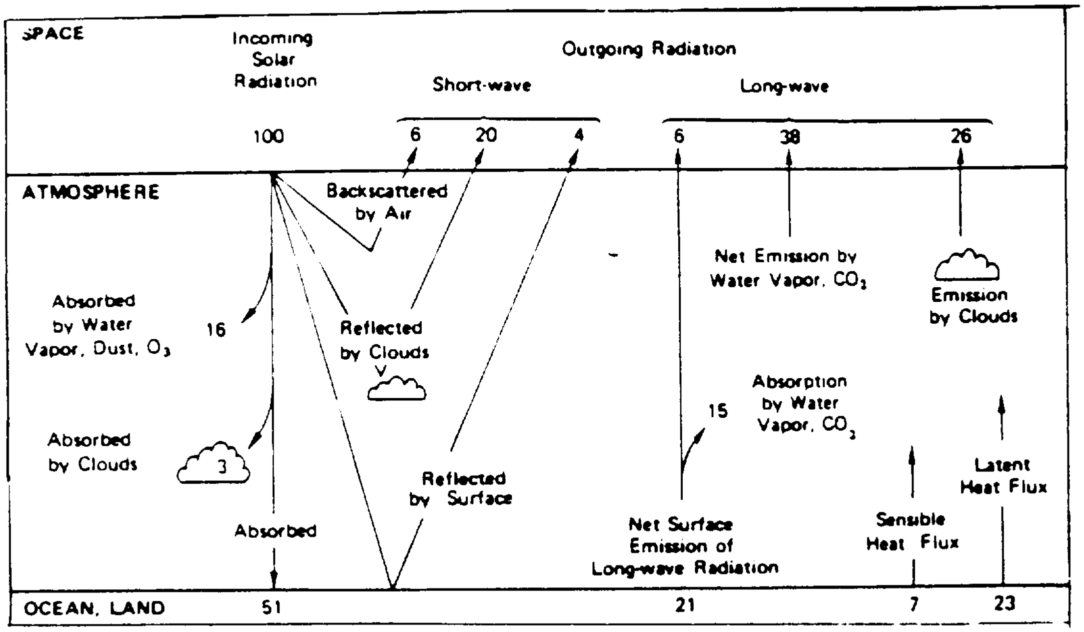
SPACE
Incoming Solar Radiation
Outgoing Radiation
Short-wave
Long-wave
100
6
20
4
6
38
26
ATMOSPHERE
Backscattered by Air
Net Emission by Water Vapor, CO₂
Emission by Clouds
Absorbed by Water Vapor, Dust, O₃
16
Reflected by Clouds
Absorption by Water Vapor, CO₂
15
Absorbed by Clouds
3
Reflected by Surface
Latent Heat Flux
Sensible Heat Flux
Absorbed
Net Surface Emission of Long-wave Radiation
OCEAN, LAND
51
21
7
23

FIGURE 5.3. Solar and Thermal radiation interaction in the Earth's Atmosphere. Numbers are percentages. For picture reference, see Endnote 4.

PRECEDING PAGE BLANK NOT FILMED

From experimental pyrometer data run during my solar engineering class, I found that in Tucson approximately 60-80% is beam normal light while the rest is diffuse or reflected. This is very dependent upon the time of day. At noon, the majority of light is direct while towards evening or in the early morning, it contains much more diffuse light because the light must travel through more of the atmosphere. In the atmosphere the light can be reflected, absorbed or transmitted and this can reduce the amount of direct light hitting the ground surface and any solar tracker. Beam light is the most important light for a tracker because this is the energy that the tracker converts in its solar cells. Diffuse or reflected light can confuse a solar tracker but beam light cannot because it comes directly from the source.

## The Solar Wavelength Regions

As stated previously, the sun emits radiation in the 0.2 to 3.0 micrometer range. Within this range, regions of light subdivide the Solar Spectrum. The primary regions the sun emits in are in the Ultraviolet (UV), Visible and Infrared (IR). For UV light, the wavelengths are from 0.2 to 0.4 micrometers. For Visible, this region extends from greater than 0.4 to 0.7 micrometers and is the peak of the sun's light. Infrared encompasses from 0.71 to 3.0 micrometers and beyond up to the microwave region. If a solar tracker were in space, all of these regions could be used but since ASPOD is presently ground based, we must endure atmospheric interference in some of these regions.

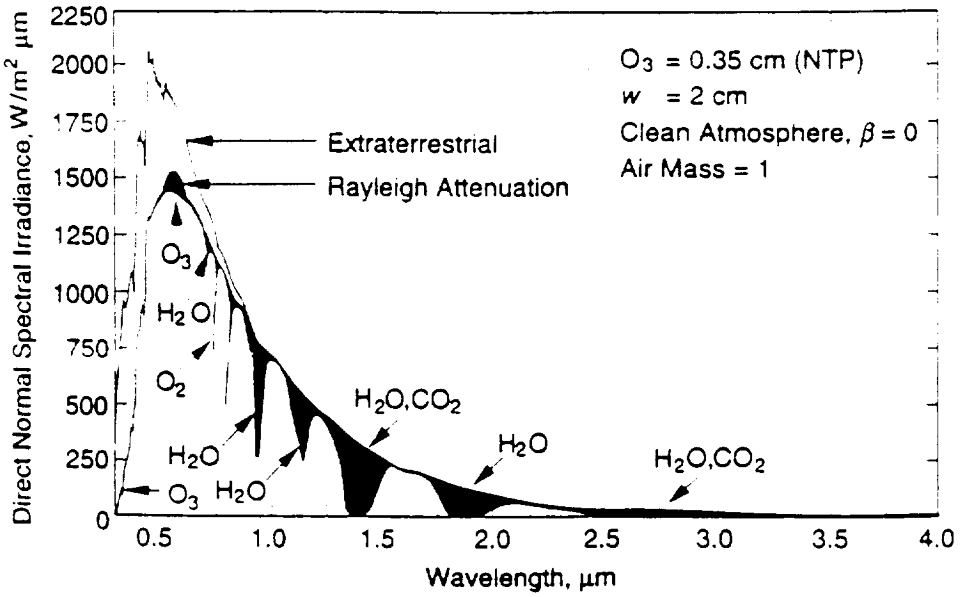

FIGURE 5.4. Atmospheric absorption and Rayleigh scattering affects on the solar spectrum. For diagram reference, see Endnote 5.

As Figure 5.4 shows, the solar spectrum in space (m=0) in this figure is compared to a blackbody at 6000 degrees Kelvin and to sea level radiation (m=1). By the time the sunlight reaches sea level, there has been a considerable decrease in various wavelengths of the solar spectrum. This limits their possible use in a ground-based solar tracker. These decreases show up in the UV, visible and IR regions.

## Atmospheric Affects

### Atmospheric Absorption

The reasons for the decreases in the UV, visible and IR regions are due to atmospheric absorption by various molecular and elemental gases. Tables 5.1a ,5.1b, 5.1c, 5.1d show the wavelengths that are absorbed and the types of gases that absorb them.

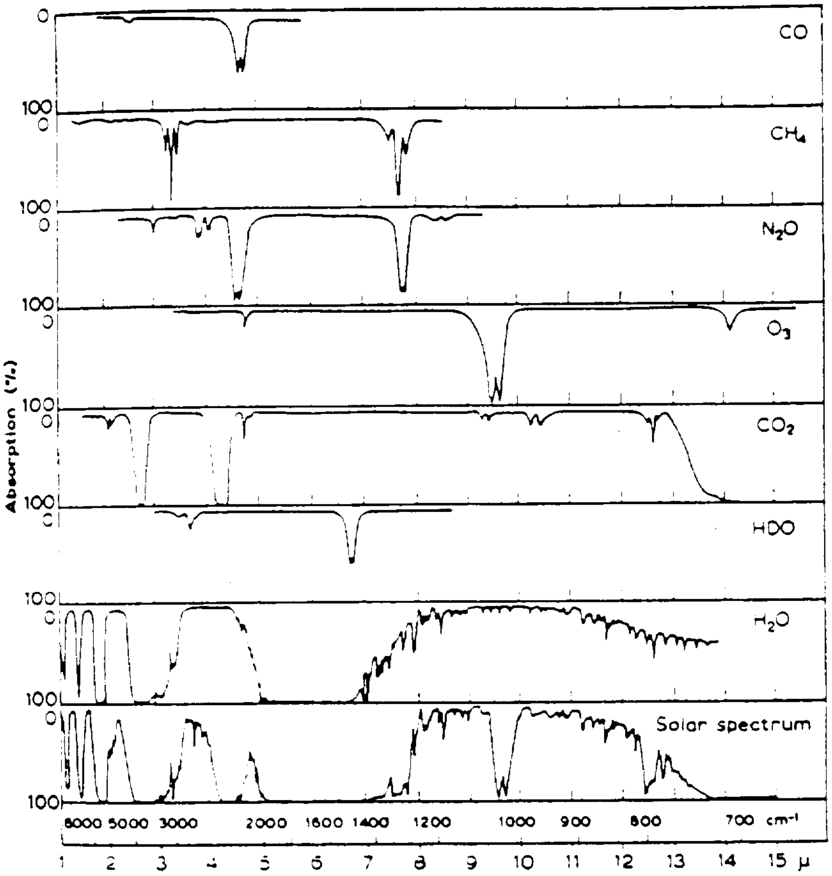

FIGURE 5.5. The near infrared light spectrum and the affects of absorption by various atmospheric gases. For diagram reference see endnote 6 in the Endnote section of this paper.

TABLE 5.1a

## ATMOSPHERIC ABSORPTION GASES AND THEIR ABSORPTION WAVELENGTHS

| REGIONS | SOLAR | OZONE | OXYGEN | WATER | CARBON DIOXIDE |
|---|---|---|---|---|---|
| | | Absorption | Absorption | Absorption | Absorption |
| | Wavelengths | Wavelengths | Wavelengths | Wavelengths | Wavelengths |
| | Micrometers | Micrometers | Micrometers | Micrometers | Micrometers |
| Ultraviolet | 0.20 | 0.20 | VARIES | | |
| Ultraviolet | 0.21 | 0.21 | FROM | | |
| Ultraviolet | 0.22 | 0.22 | 0.20 | | |
| Ultraviolet | 0.23 | 0.23 | TO | | |
| Ultraviolet | 0.24 | 0.24 | 0.30 | | |
| Ultraviolet | 0.25 | 0.25 | | | |
| Ultraviolet | 0.26 | 0.26 | | | |
| Ultraviolet | 0.27 | 0.27 | | | |
| Ultraviolet | 0.28 | 0.28 | | | |
| Ultraviolet | 0.29 | 0.29 | | | |
| Ultraviolet | 0.30 | 0.30 | | | |
| Ultraviolet | 0.31 | | | | |
| Ultraviolet | 0.32 | | | | |
| Ultraviolet | 0.33 | | | | |
| Ultraviolet | 0.34 | | | | |
| Ultraviolet | 0.35 | | | | |
| Ultraviolet | 0.36 | | | | |
| Ultraviolet | 0.37 | | | | |
| Ultraviolet | 0.38 | | | | |
| Ultraviolet | 0.39 | | | | |
| Visible | 0.40 | | | | |
| Visible | 0.41 | | | | |
| Visible | 0.42 | | | | |
| Visible | 0.43 | | | | |
| Visible | 0.44 | | | | |
| Visible | 0.45 | | | | |
| Visible | 0.46 | | | | |
| Visible | 0.47 | | | | |
| Visible | 0.48 | | | | |
| Visible | 0.49 | | | | |

*See endnotes 7 and 8 for references in the Endnote section of this report.

# TABLE 5.1B
# ATMOSPHERIC ABSORPTION GASES AND THEIR ABSORPTION WAVELENGTHS

| REGIONS | TERRESTRIAL | SOLAR | OZONE | OXYGEN | WATER | CARBON DIOXIDE |
|---|---|---|---|---|---|---|
| | | | Absorption | Absorption | Absorption | Absorption |
| | Wavelengths | Wavelengths | Wavelengths | Wavelengths | Wavelengths | Wavelengths |
| | Micrometers | Micrometers | Micrometers | Micrometers | Micrometers | Micrometers |
| Visible | | 0.50 | | | | |
| Visible | | 0.51 | | | | |
| Visible | | 0.52 | | | | |
| Visible | | 0.53 | | | | |
| Visible | | 0.54 | | | | |
| Visible | | 0.55 | | | | |
| Visible | | 0.56 | | | | |
| Visible | | 0.57 | | | | |
| Visible | | 0.58 | | | | |
| Visible | | 0.59 | | | | |
| Visible | | 0.60 | | | | |
| Visible | | 0.61 | | | | |
| Visible | | 0.62 | | | | |
| Visible | | 0.63 | | | | |
| Visible | | 0.64 | | | | |
| Visible | | 0.65 | | | | |
| Visible | | 0.66 | | | | |
| Visible | | 0.67 | | | | |
| Visible | | 0.68 | | | | |
| Visible | | 0.69 | 0.69 | 0.69 | | |
| Visible | | 0.70 | | | | |
| Infrared | | 0.71 | | | | |
| Infrared | | 0.72 | | | | |
| Infrared | | 0.73 | | | | |
| Infrared | | 0.74 | | | | |
| Infrared | | 0.75 | | | | |
| Infrared | | 0.76 | 0.76 | 0.76 | | |
| Infrared | | 0.77 | | | | |
| Infrared | | 0.78 | | | | |
| Infrared | | 0.79 | | | | |

*See endnotes 7 and 8 for references in the Endnote section of this report.

## TABLE 5.1C
## ATMOSPHERIC ABSORPTION GASES AND THEIR ABSORPTION WAVELENGTHS

| REGIONS | TERRESTRIAL | SOLAR | OZONE | OXYGEN | WATER | CARBON DIOXIDE |
|---|---|---|---|---|---|---|
| | | | Absorption | Absorption | Absorption | Absorption |
| | Wavelengths | Wavelengths | Wavelengths | Wavelengths | Wavelengths | Wavelengths |
| NEAR | Micrometers | Micrometers | Micrometers | Micrometers | Micrometers | Micrometers |
| Infrared | | 0.80 | | | 0.80 | |
| Infrared | | 0.87-0.89 | | | 0.87-0.89 | |
| Infrared | | 0.90 | | | 0.90 | |
| Infrared | | 0.91-0.99 | | | 0.91-0.99 | |
| Infrared | 1.00 | 1.00 | | | 1.016 | |
| Infrared | 1.07-1.10 | 1.07-1.10 | | | 1.07-1.10 | |
| Infrared | 1.10 | 1.10 | | | 1.10-1.20 | |
| Infrared | 1.20 | 1.20 | | | 1.25-1.30 | |
| Infrared | 1.30 | 1.30 | | | 1.34-1.39 | |
| Infrared | 1.40 | 1.40 | | | 1.40-1.50 | |
| Infrared | 1.50 | 1.50 | | | 1.50-1.54 | |
| Infrared | 1.60 | 1.60 | | | | 1.60 |
| Infrared | 1.70 | 1.70 | | | 1.69-1.79 | |
| Infrared | 1.80 | 1.80 | | | 1.87 | |
| Infrared | 1.90 | 1.90 | | | 1.90 | |
| Infrared | 2.00 | 2.00 | | | 1.91-1.99 | |
| Infrared | 2.10 | 2.10 | | | 2.00-2.08 | 2.00 |
| Infrared | 2.20 | 2.20 | | | 2.27-2.30 | |
| Infrared | 2.30 | 2.30 | | | 2.31-2.40 | |
| Infrared | 2.40 | 2.40 | | | 2.41-2.50 | |
| Infrared | 2.50 | 2.50 | | | 2.51-2.59 | |
| Infrared | 2.60 | 2.60 | | | 2.60-2.70 | |
| Infrared | 2.70 | 2.70 | | | 2.70 | |
| Infrared | 2.80 | 2.80 | | | 2.70-2.80 | 2.70 |
| Infrared | 2.90 | 2.90 | | | 2.90-2.99 | |
| Infrared | 3.00 | 3.00 | | | | |
| Infrared | 3.10 | | 3.14 | | | |
| Infrared | 3.20 | | | | 3.20 | |
| Infrared | 3.30 | | 3.30 | | 3.00-3.57 | |
| Infrared | 3.40 | | | | | |

*See endnotes 7 and 8 for references in the Endnote section of this report.

## TABLE 5.1D
## ATMOSPHERIC ABSORPTION GASES AND THEIR ABSORPTION WAVELENGTHS

| REGIONS | TERRESTRIAL | OZONE | OXYGEN | WATER | CARBON DIOXIDE |
|---|---|---|---|---|---|
| | | Absorption | Absorption | Absorption | Absorption |
| | Wavelengths | Wavelengths | Wavelengths | Wavelengths | Wavelengths |
| FAR | Micrometers | Micrometers | Micrometers | Micrometers | Micrometers |
| Infrared | 3.50 | | | | |
| Infrared | 3.60 | 3.60 | | | |
| Infrared | 3.70 | | | | |
| Infrared | 3.80 | | | | |
| Infrared | 3.90 | | | | |
| Infrared | 4.00 | | | | |
| Infrared | 4.10 | | | | |
| Infrared | 4.20 | | | | |
| Infrared | 4.30 | | | | 4.30 |
| Infrared | 4.40 | | | | |
| Infrared | 4.50 | | | | |
| Infrared | 4.60 | | | | |
| Infrared | 4.70 | 4.74 | | | |
| Infrared | 4.80 | | | 4.88-6.30 | 4.80 |
| Infrared | 4.90 | | | | |
| Infrared | 5.00 | | | | |
| Infrared | 5.10 | | | | |
| Infrared | 5.20 | | | | 5.20 |
| Infrared | 5.30 | | | | |
| Infrared | 5.40 | | | | |
| Infrared | 5.50 | 5.58 | | | |
| Infrared | 5.60 | | | | |
| Infrared | 5.70 | 5.79 | | | |
| Infrared | 5.80 | | | | |
| Infrared | 5.90 | | | | |
| Infrared | 6.00 | | | | |
| Infrared | 6.10 | | | | |
| Infrared | 6.20 | | | | |
| Infrared | 6.30 | | | 6.30 | |

*See endnotes 7 and 8 for references in the Endnote section of this report.

In the Ultraviolet, 0.2-0.4 micrometers, this region shows the most severe absorption. This is fortunate for life because these rays are harmful to life but for a ground based solar tracker, this region is unusable. The reasons for this are shown in Figure 5.1 and Table 5.1. As these wavelengths go through the upper atmosphere, Ozone interacts with UV and absorbs these wavelengths. Other gases such as Oxygen and Nitrogen gas and elemental Oxygen and Nitrogen also help to deplete this region. By the time the light reaches the lower atmosphere and the surface almost all of the UV has been absorbed by the atmosphere. This leaves little to track the sun by for a solar tracker.

In the next region, Visible Light, there is the least amount of absorption. As stated this region covers from 0.4 to 0.76 micrometers from blue to red light. In the atmosphere ozone and molecular oxygen absorb weakly at 0.69 and 0.76 micrometers. These are about the only wavelengths affected for this region. Consequently, this is the region that life has taken advantage of using. This is the area where our eyes are able to see in and plants use for photosynthesis. It is also a prime area to use for solar tracking.

In the last region, Infrared, this area is made up of two sub regions; Near IR or Solar IR from 0.8 to 3.0 micrometers and Far IR or Terrestrial IR from 4.0 to 50 micrometers. Near IR is solar in nature and can be quite useful for tracking the sun. This tracking area though does not extend past this band area for the sun does not emit in wavelengths greater than 3.0 micrometers. Consequently, Far IR is not part of the solar spectrum. It is radiation emitted into space by the Earth which acts like a 300 degree Kelvin blackbody. The Earth emits wavelengths in the IR from 1 to 15 micrometers.

Therefore the wavelengths of potential tracking use are in the 0.7 to 1.0 micrometers. The question is which one is best for the job? In order to answer this one must look again at the atmosphere. Although Near IR is solar in nature and FAR IR is terrestrial, they are both affected by the atmosphere. In the lower atmosphere below 50 kilometers, water and carbon dioxide absorb some of their wavelengths. Once absorbed, they transmit the energy back to earth as heat. It is in the lower atmosphere where water increasingly becomes a factor due to its nature of forming clouds. This factor will be investigated in the next section.

### Cloud Effects

In the lower atmosphere as stated previously and in Tables 5.1, clouds are a factor due to water absorbing certain wavelengths in the IR. During the researching of this report, further information was found which illustrated the absorption qualities of water in our atmosphere. In a paper by Stephen Cox entitled "Radiation Characteristics of Clouds in the Solar Spectrum", he researched the absorption and emission qualities of clouds upon the Solar Spectrum. His data is duplicated in Table 5.2. From this data, I have graphed curves to possibly show how clouds can affect a solar tracking device. As seen in Table 5.2, clouds in the 0.7 to 6.3 micrometer range tend to absorb increasingly in wavelengths of 0.95 micrometers and greater while shorter wavelengths are more scattered through the top, sides and bottom of the cloud. This is graphed and illustrated in Figures 5.5, 5.6, 5.7 and 5.8 where the viewing angles are graphed for 0 and 30 degrees from the zenith.

Figure 5.9 bar graphs the total break up of the light as it passes through a cloud.

TABLE 5.2
Cloud Affects Upon Wavelength Regions

| ZENITH ANGLE 0 DEGREES Wavelength Region (1E-6) Meters | Cloud Top % | Cloud Base % | Cloud Sides % | Cloud Absorption % |
|---|---|---|---|---|
| 0.70 | 50.80 | 32.30 | 16.90 | 0.00 |
| 0.76 | 50.90 | 32.40 | 16.70 | 0.00 |
| 0.95 | 51.70 | 28.30 | 15.80 | 4.20 |
| 1.15 | 49.10 | 25.80 | 15.00 | 10.10 |
| 1.40 | 36.50 | 15.60 | 11.60 | 36.30 |
| 1.80 | 26.70 | 8.70 | 8.80 | 55.80 |
| 2.80 | 0.40 | 0.00 | 0.16 | 99.40 |
| 3.30 | 0.40 | 0.00 | 0.17 | 99.40 |
| 6.30 | 0.60 | 0.00 | 0.22 | 99.20 |

|  | Cloud Top % | Cloud Base % | Cloud Sides % | Cloud Absorption % |
|---|---|---|---|---|
| Total Wavelengths % | 48.80 | 29.20 | 15.80 | 6.30 |

| ZENITH ANGLE 30 DEGREES Wavelength Region (1E-6) Meters | Cloud Top % | Cloud Base % | Cloud Sides % | Cloud Absorption % |
|---|---|---|---|---|
| 0.70 | 26.20 | 22.70 | 51.20 | 0.00 |
| 0.76 | 26.10 | 22.60 | 51.10 | 0.20 |
| 0.95 | 29.50 | 19.20 | 49.30 | 2.00 |
| 1.15 | 28.60 | 18.20 | 47.60 | 5.60 |
| 1.40 | 26.10 | 16.00 | 43.30 | 14.60 |
| 1.80 | 24.30 | 15.00 | 40.80 | 19.90 |
| 2.80 | 4.40 | 3.60 | 10.80 | 81.20 |
| 3.30 | 1.30 | 1.70 | 4.00 | 93.00 |
| 6.30 | 1.40 | 1.40 | 4.00 | 93.20 |

|  | Cloud Top % | Cloud Base % | Cloud Sides % | Cloud Absorption % |
|---|---|---|---|---|
| Total Wavelengths % | 26.60 | 21.00 | 49.70 | 2.70 |

*See Endnote 9 for cited documentary table information on Table 5.2 in the Endnotes section of this report.

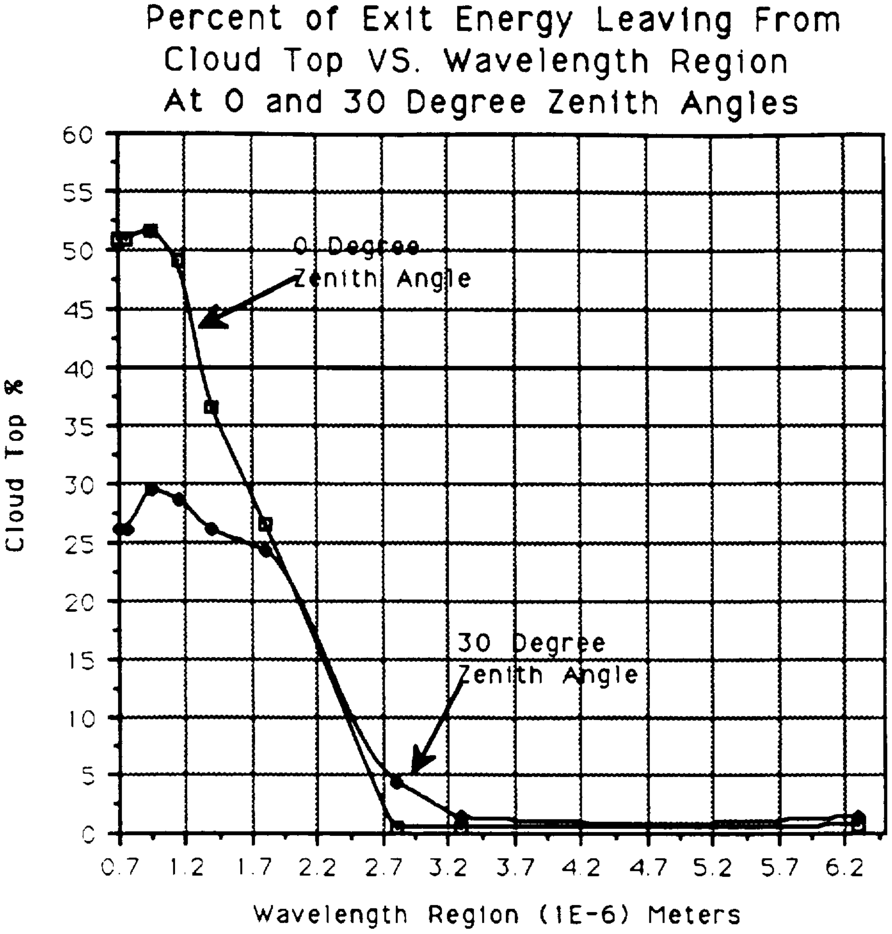

FIGURE 5.5. Light energy wavelengths exiting a cloud's top as compared to the zenith angle. Graph created from data in Table 5.2. Refer to endnote 9 in the Endnotes section of this report.

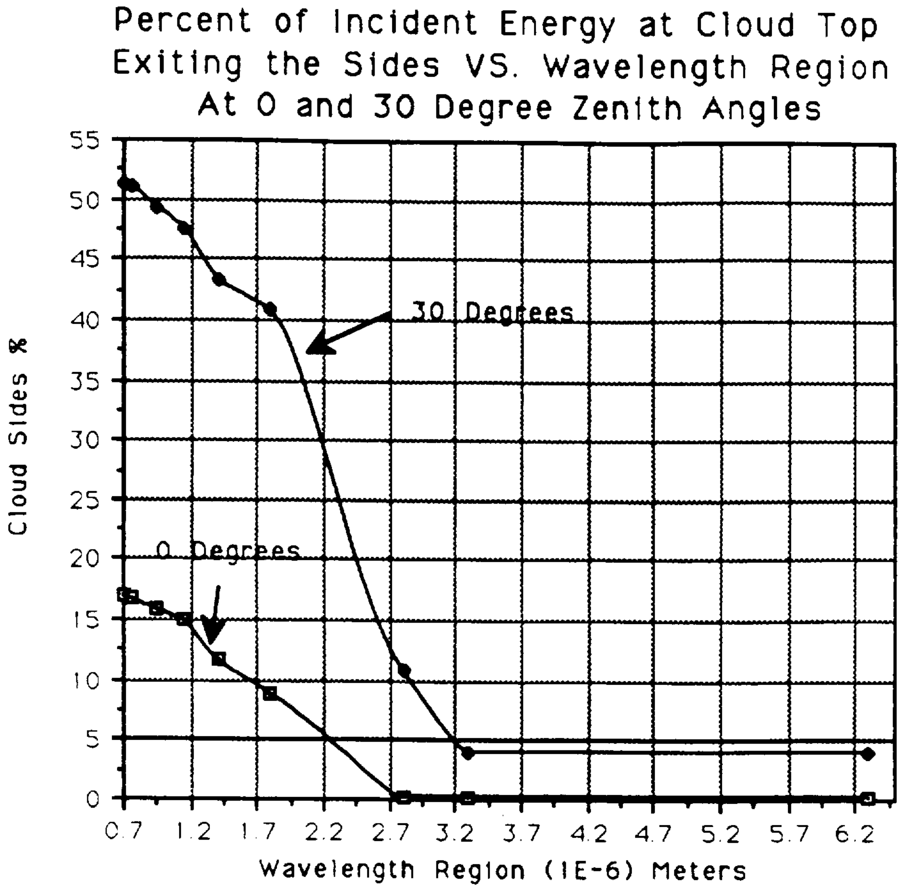

FIGURE 5.6. Light energy wavelengths exiting a cloud's sides as compared to the zenith angle. Graph created from data in Table 5.2. Refer to endnote 9 in the Endnotes section of this report.

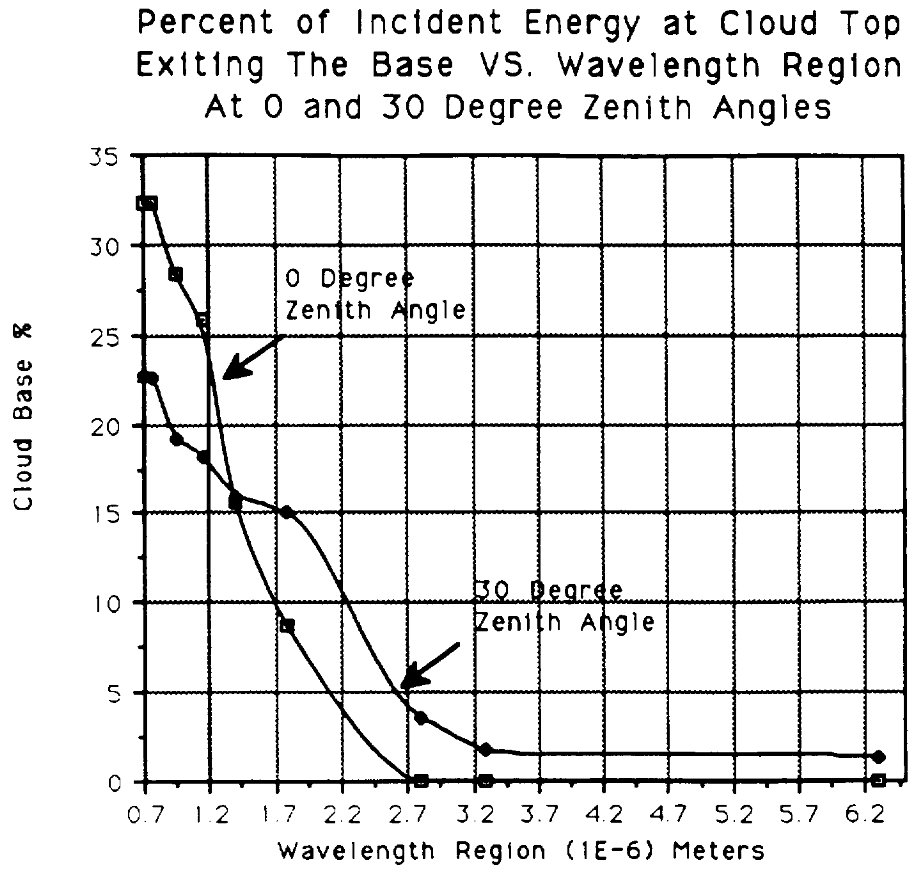

FIGURE 5.7. Light energy wavelengths exiting a cloud's base as compared to the zenith angle. Graph created from data in Table 5.2. Refer to endnote 9 in the Endnotes section of this report.

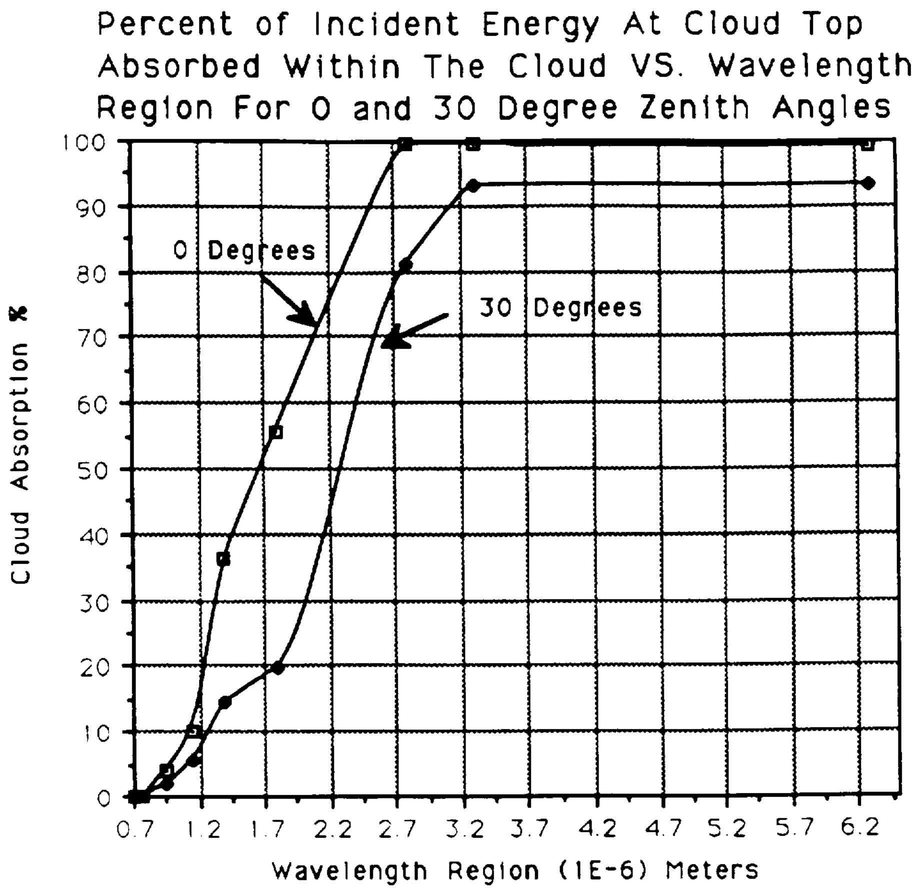

FIGURE 5.8. Cloud absorption of light wavelengths as compared to the zenith angle. Graph created from data in Table 5.2. Refer to endnote 9 in the Endnotes section of this report.

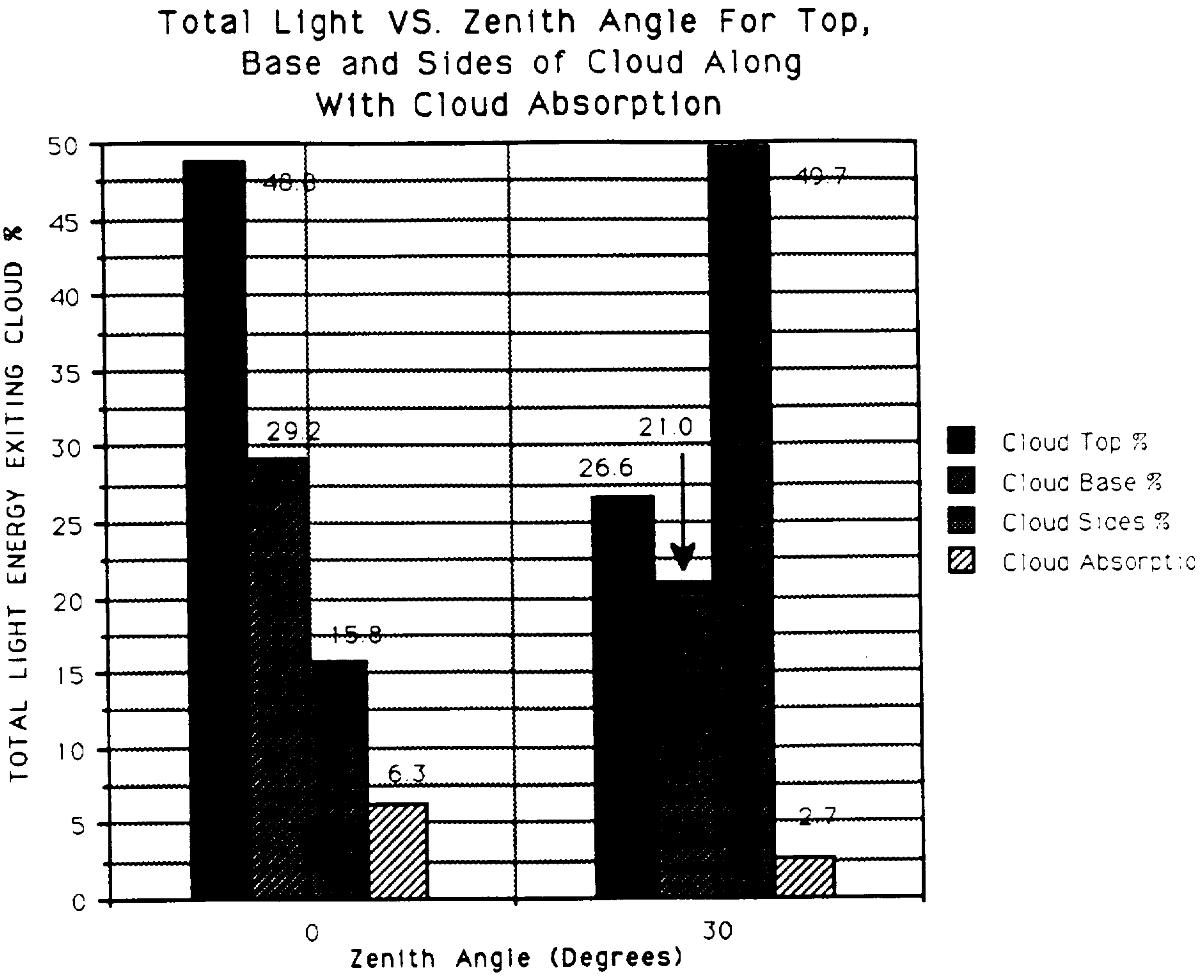

FIGURE 5.9. Total light energy exiting a cloud compared to the zenith angle. Graph created from data in Table 5.2. Refer to endnote 9 in the Endnotes section of this report.

What all these graphs and tables show are that Near IR is better for tracking the sun. They show that for a cloud's base, wavelengths between 0.7 and 2.7 micrometers can get through but are reduced by two-thirds their original strength. The light is scattered through the top and sides of the cloud as the zenith angle increases. They further demonstrate that a solar tracker using IR should have a design that encompasses a band between 0.7 to 0.9 micrometers if one wishes to avoid errors. Any long wavelengths longer than 1.0 micrometers tend to be increasingly absorbed by the clouds and therefore are not usable.

Potentially, this information is very useful. If, while using a solar tracker on mildly cloudy days, a small cumulus cloud should wander across the view, the tracker using these 0.7 to 0.9 micrometer bands could theoretically continue tracking. This is if it were sensitive enough to the partially reduced beam light getting through the bottom of the cloud. On very cloudy days though, this would not be the case for there would be too much reduction and scattering in the sunlight.

## Terrestrial Effects

### Terrestrial Objects

Once the light passes through any cloud layers, it then comes in contact with the ground. It is here where plants, buildings and Terrestrial IR become a factor in choosing solar tracking wavelengths. The Terrestrial IR comes from the ground and buildings which absorb the energy and re-emit it in the Far IR. This is demonstrated in Figure 5.11 where the atmosphere is shown to be opaque and allows the earth's heat to escape into space in the 8-12 micrometer bands.

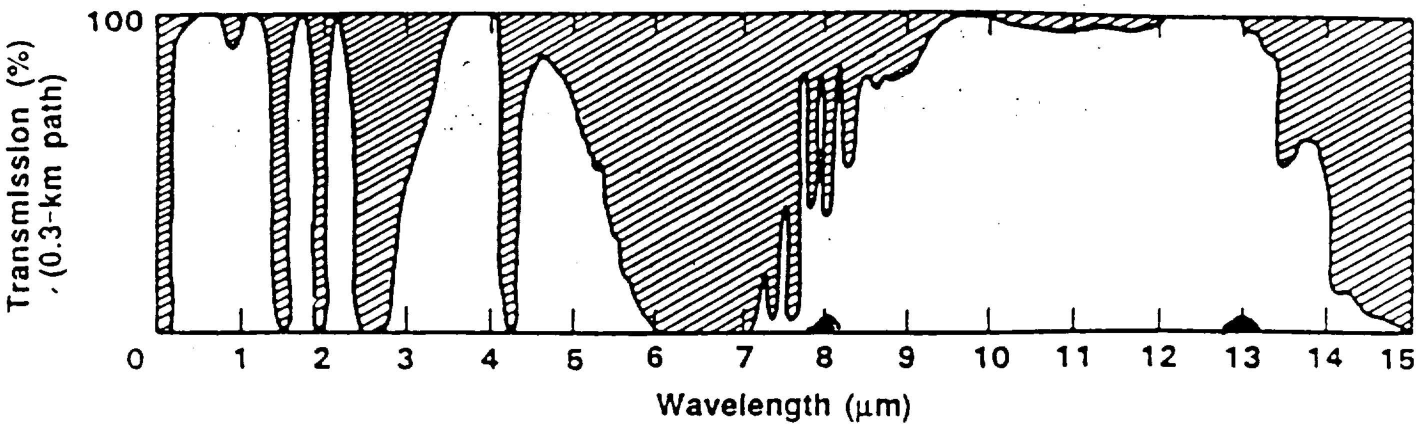

FIGURE 5.11. Optical transmission of the atmosphere showing the presence of transmission windows and strong absorption bands in the atmosphere. Refer to endnote 10 for reference information.

In addition to this, diffuse and reflected bands of light can combine to confuse a solar tracker. Diffuse light comes from the sky while reflected light comes from buildings, plants and other terrestrial sources.

## Plant Effects

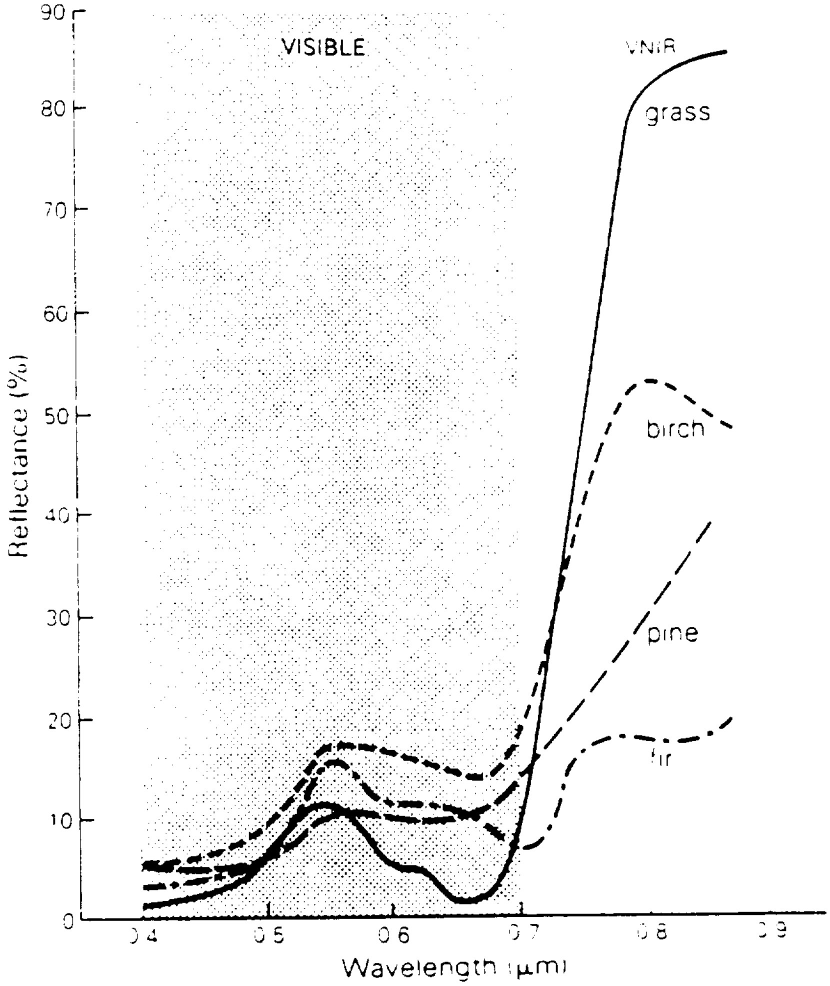

FIGURE 5.12. The reflectance of certain common plants at different wavelengths. For diagram reference, see Endnote 11.

Another area of contention for a solar tracker is the light absorbed and re-emitted by plants. As seen in Figure 5.12, plants such as grasses and trees tend to reflect wavelengths of 0.7 to 0.9 micrometers. Grass by far has the highest reflectance, peaking at 0.9 micrometers. For a tracker to use these wavelengths, it is advisable that it not be placed in a grassy area or near a lot of trees.

## Solar Cell Selection

### Solar Cell Materials

The last problem area is the use of materials that are sensitive to the Sun's Radiation and which can convert it for a tracker's use. These materials are used in the manufacturing of solar cells and are listed in Table 5.3.

TABLE 5.3

| | Solar Cell Materials | |
|---|---|---|
| Cadmium Sulphide | Cadmium Selenide | Cadmium Telluride |
| Gallium Aluminum Arsenide | Gallium Arsenide | Gallium Antimonide |
| Indium Phosphate | Indium Antimonide | |
| Silicon | Zinc Sulphide | |

*For reference information refer to endnote 12 in the Endnote section of this report.

Of these, the most commonly used and the cheapest is Silicon. Gallium Arsenide is also used but is more expensive. These two will be discussed and compared as to their characteristics within this report.

### Solar Cell Characteristics

The spectral response for a typical silicon cell is shown in Figure 5.13 . With an open circuit voltage of just under 600 millivolts, it is more sensitive towards the IR region peaking at about 0.87 micrometers. This is illustrated in Figure 5.14.

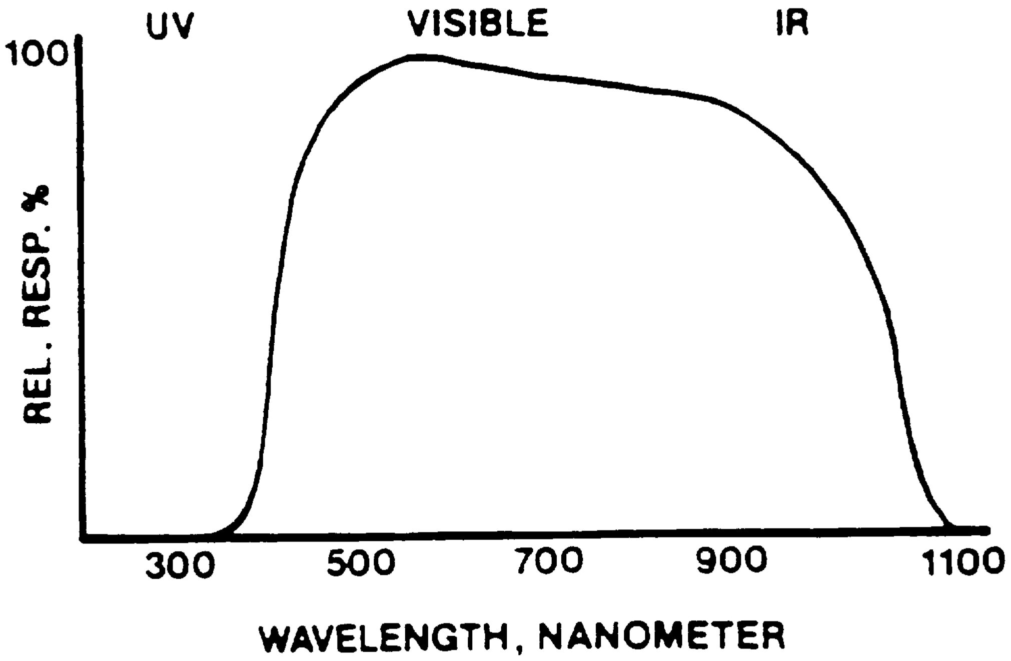

FIGURE 5.13. The spectral response curve for a typical solar cell. Refer to endnote 13 in the Endnotes section of this report.

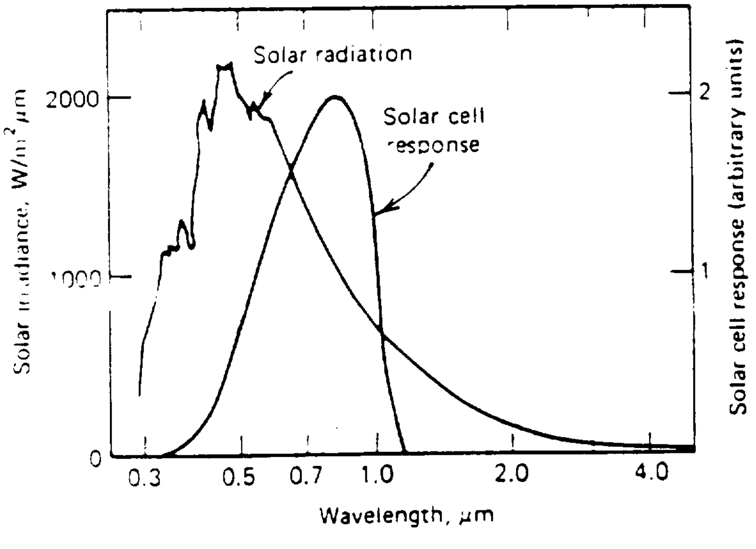

FIGURE 5.14 Spectral response curve for a silicon cell and the Solar Spectrum. Refer to endnote 14 in the Endnotes section.

tracker. In contrast, PT and PD cells do not have this problem and are more accurate. In addition, silicon PT cells are sensitive to a broad band of light from 0.4 to 1.1 micrometers. As seen in Figure 5.16 , this ranges from visible to near IR. It is for these reasons that this project has looked into using these cells in the proposed design.

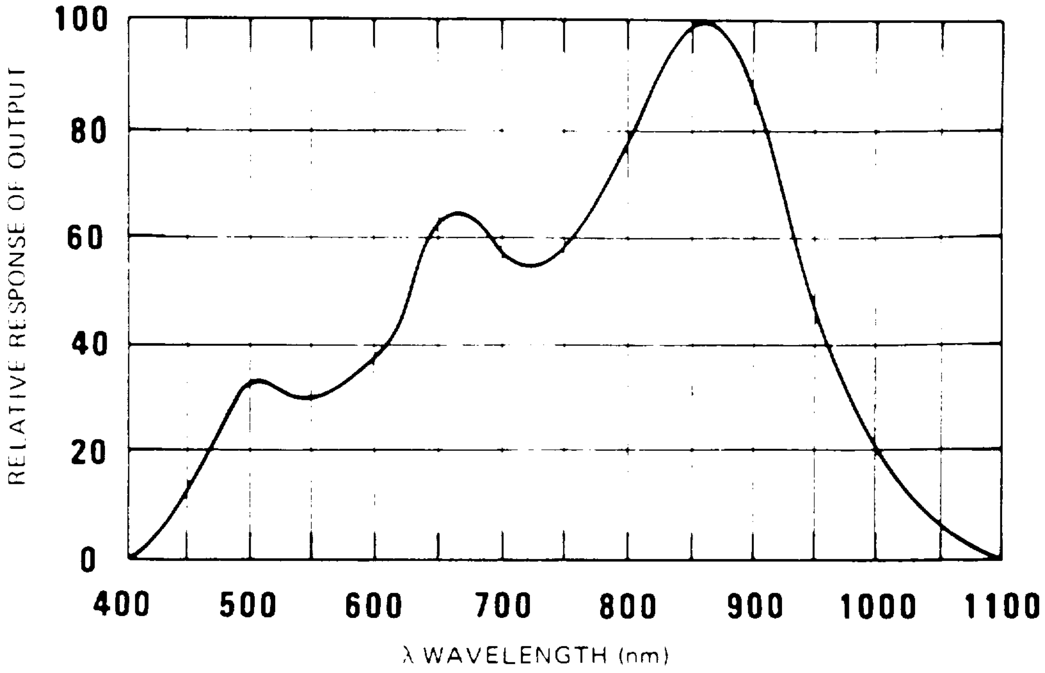

FIGURE 5.16. The spectral response for a NPN phototransistor with an overcoating applied for peak sensitivity at 880 nanometers. Refer to endnote 16 in the Endnotes section of this report.

PRECEDING PAGE BLANK NOT FILMED

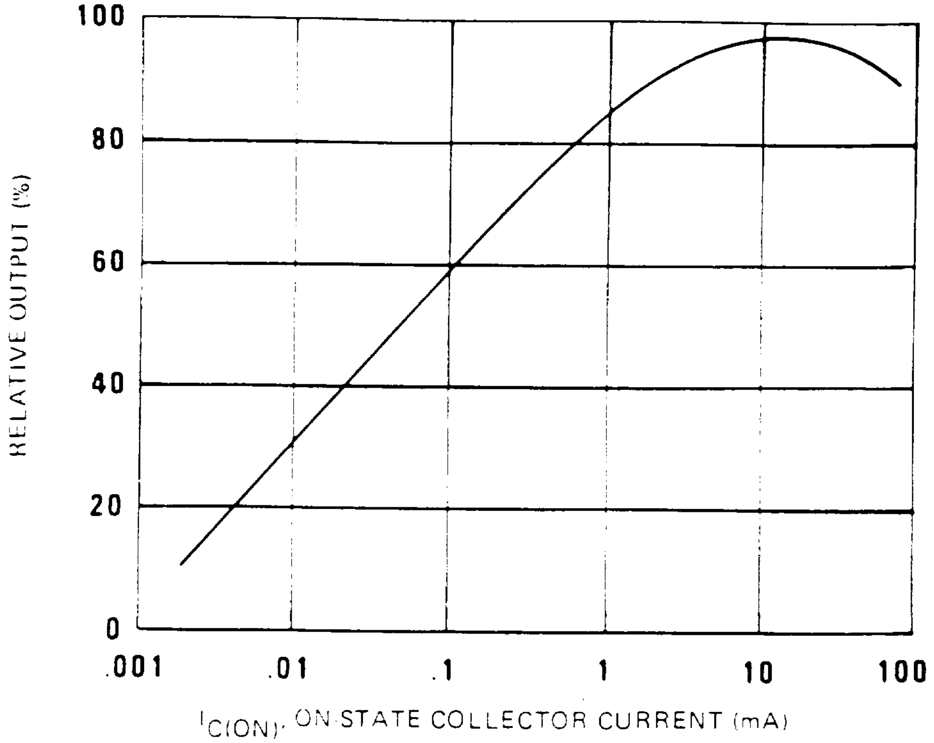

FIGURE 5.17. Relative output versus collector current for a phototransistor. Refer to endnote 17 in the Endnotes section of this report.

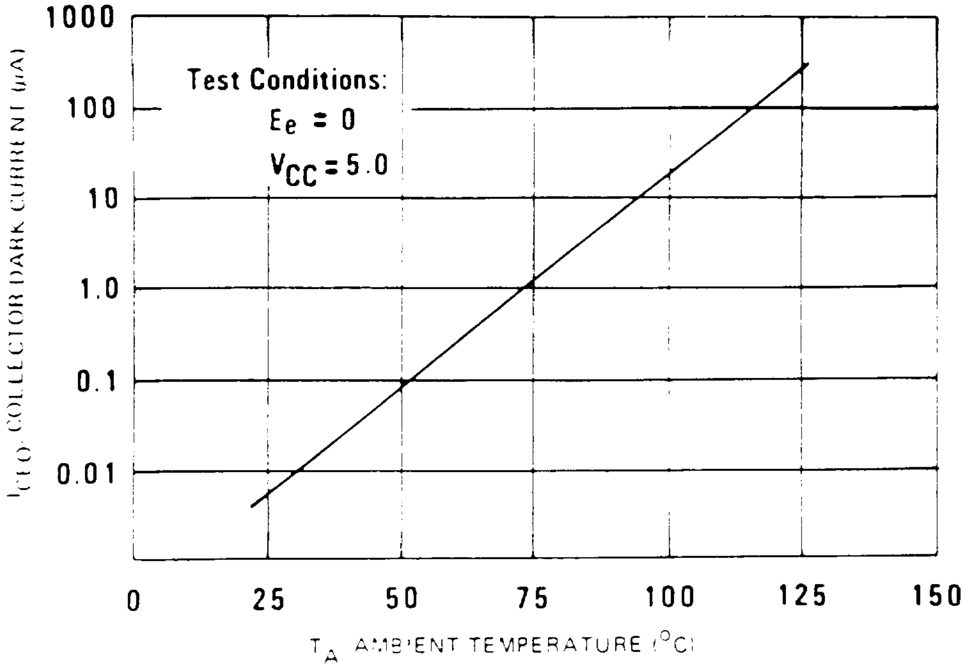

FIGURE 5.18. Collector dark current for a photodarlington transistor versus ambient temperature. Refer to endnote 18 in the Endnotes section.

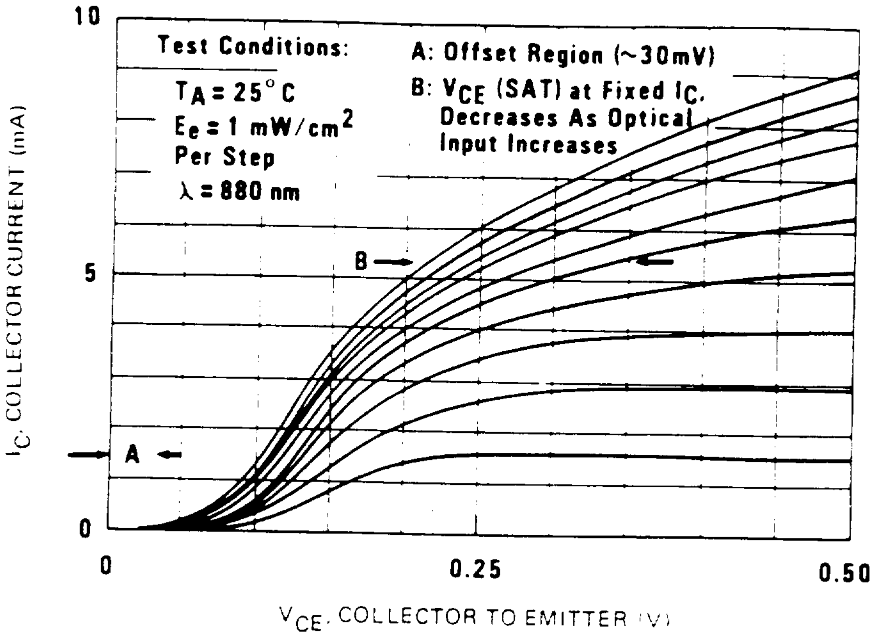

FIGURE 5.19. Collector current versus collector to emitter voltage under test conditions for a typical phototransistor.

## The Final Selection Of Photo Cells

The final selection for the photo cells for the tracker consists of four phototransisters from the old 1993 tracking device and four infrared photodiodes. The phototransisters will be used inside the tube while the diodes will be mounted on the outside as the secondary part of the tracker. The photodiodes were purchased from Centronic Inc. and are known by the company as BP-65 photodiodes. The sensitivity curve for these photodiodes are shown in Figure 5.20 below. The sensitivity for these diodes peaks at about 870 nanometers.

FIGURE 5.20 Sensitivity Curve for the Centronic BP-65 Photodiodes.

## Infrared Diode Boxes And Hot Mirrors

In order to work without interference from outside wavelength emissions, a hot mirror with a cutoff range of 800 nanometers and greater must be bought and used over these diodes. The active range of tracking then would be between the Visible spectra and 800 nanometers when once mounted. Each diode should be mounted inside a shallow box container of less than one inch by one inch by 3/4 inch dimensions. The box can be metal or plastic and should be painted white on the outside to reflect infrared and reduce heat build up inside the box. If not done this way the devices may be fooled by errant wavelengths from the walls of the boxes. These hot mirrors can be bought in a two inch by two inch sheet and be cut down to size by the Optical Sciences Machine Shop. The estimated cost for this approach is between $40-$50. If not done this way and bought elsewhere, they will cost up to $400 to get.

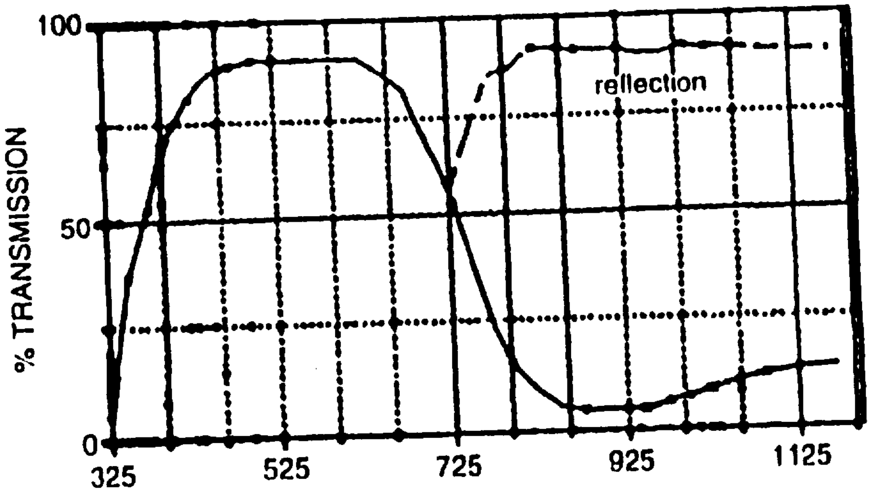

FIGURE 5.21 Sensitivity Curve for The Hot Mirrors.

# SOLAR TRACKER TESTING

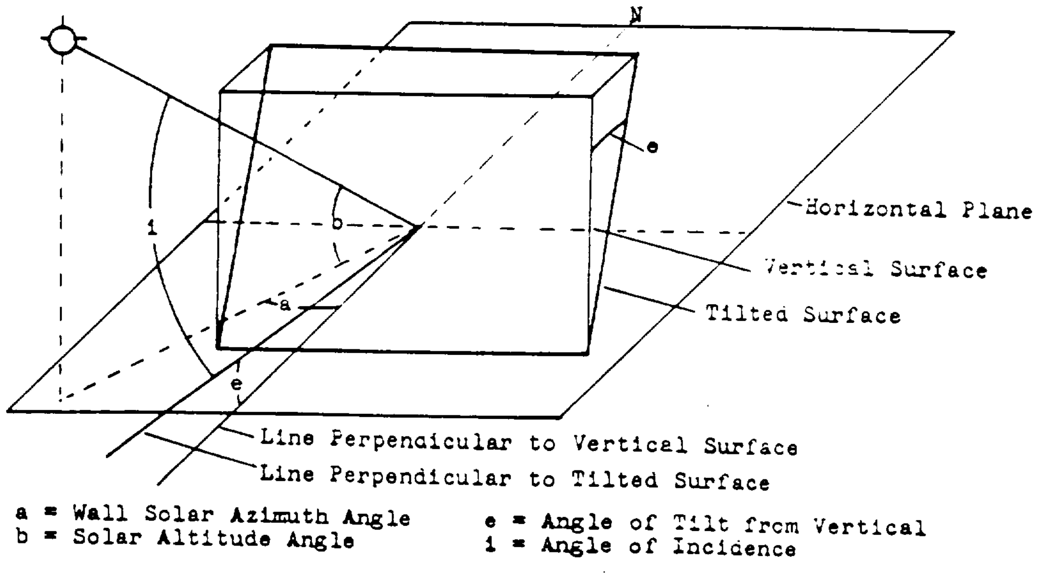
N
e
Horizontal Plane
Vertical Surface
Tilted Surface
i
b
a
e
Line Perpendicular to Vertical Surface
Line Perpendicular to Tilted Surface
a = Wall Solar Azimuth Angle
b = Solar Altitude Angle
e = Angle of Tilt from Vertical
i = Angle of Incidence

FIGURE 6.0. Definition of Solar Angles. For Diagram reference information refer to endnote 20 in the Endnote Section of this report.

Once the building of the Solar Tracker is accomplished, it will need to be tested for accuracy. The tracker as stated must track within ±1 degree of the sun. A test must be developed that can accurately measure the solar altitude and azimuth angles. These angles are shown and defined in Figure 6.0. Additional information on solar tracking is provided in Figures 6.2, 6.3, 6.4, and 6.5. These Figures are provided to give comparison data to the test. To do the test, a lab from the Solar Engineering Class will be modified and used to test the equipment. The lab materials to be used are a built test stand for the solar tracker, the solar tracker, the motors and controls for tracker and a solar sundial. The design for the test stand is shown in Figure 6.1.

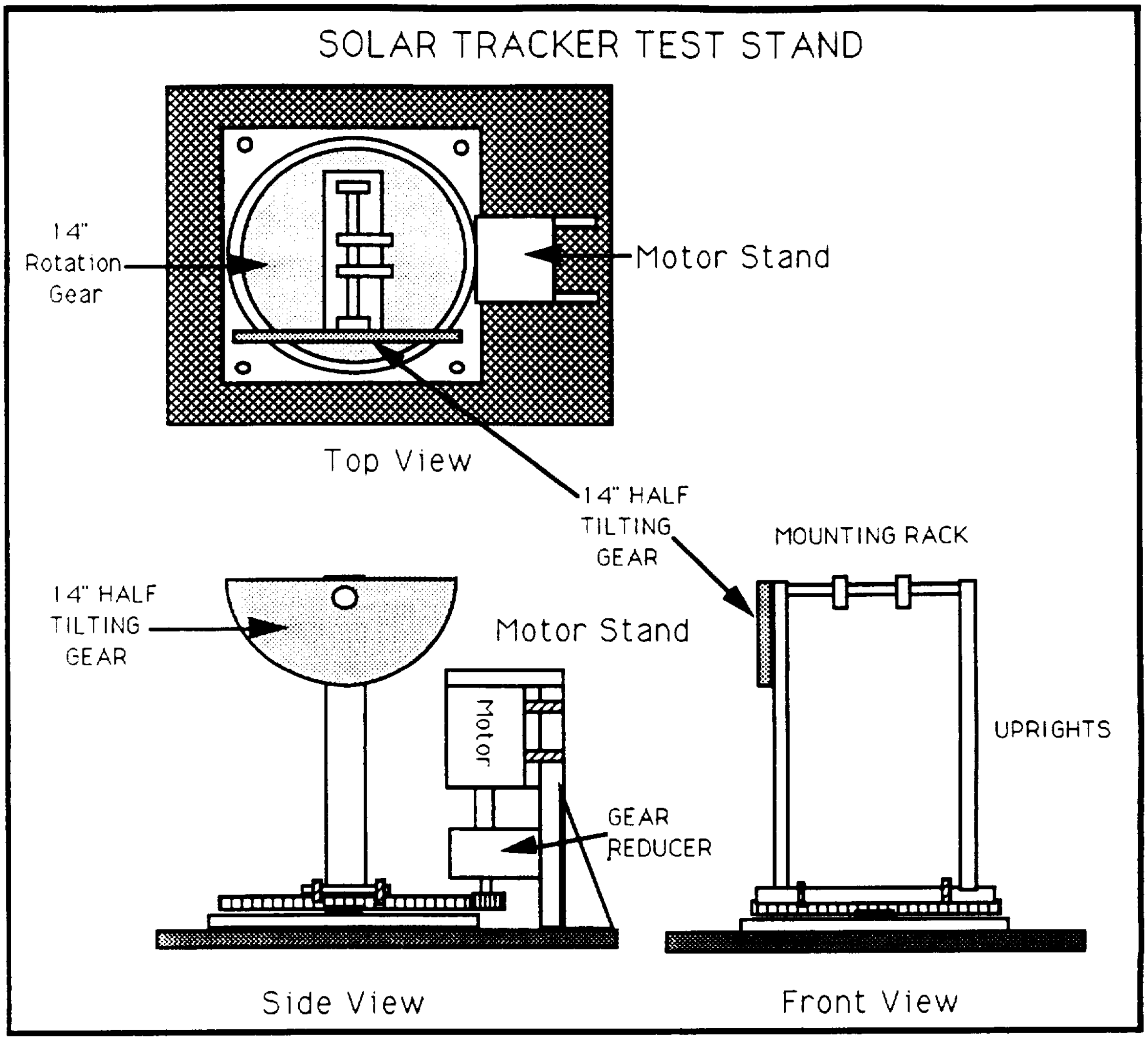
SOLAR TRACKER TEST STAND
14" Rotation Gear
Motor Stand
Top View
14" HALF TILTING GEAR
MOUNTING RACK
14" HALF TILTING GEAR
Motor Stand
Motor
UPRIGHTS
GEAR REDUCER
Side View
Front View

FIGURE 6.1

The Test Stand

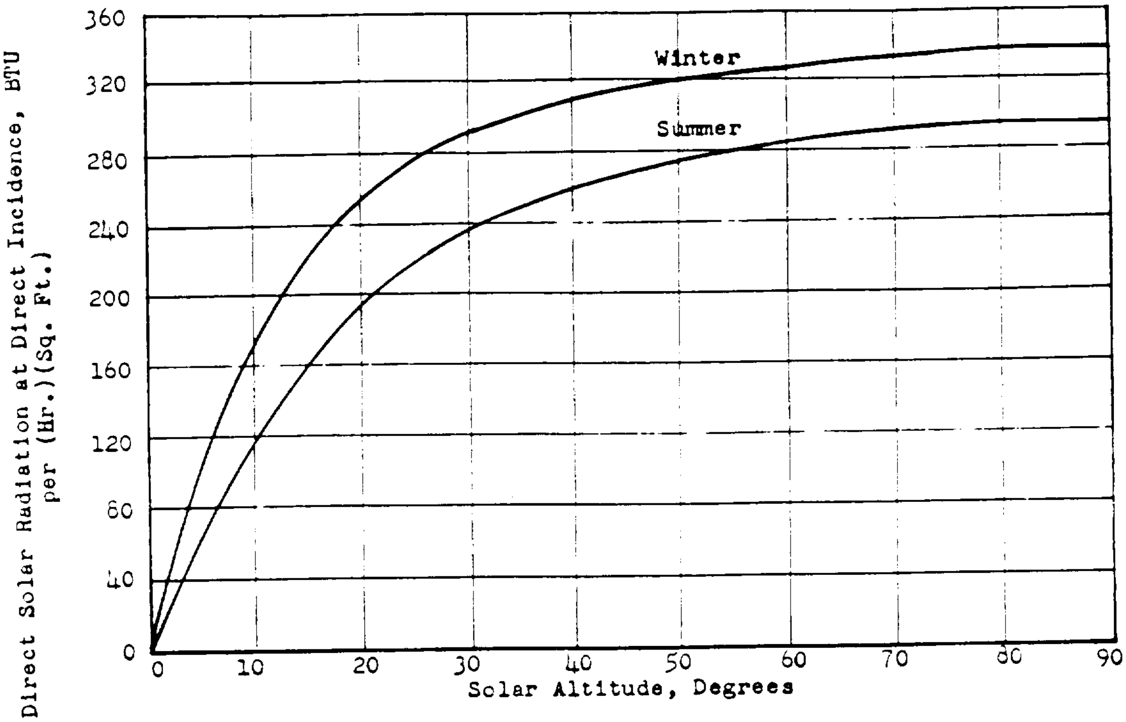

FIGURE 6.2. Direct solar radiation incident upon a surface perpendicular to the sun's rays at sea level on the earth during cloudy days. Refer to endnote 21 for reference in Endnote section of this report.

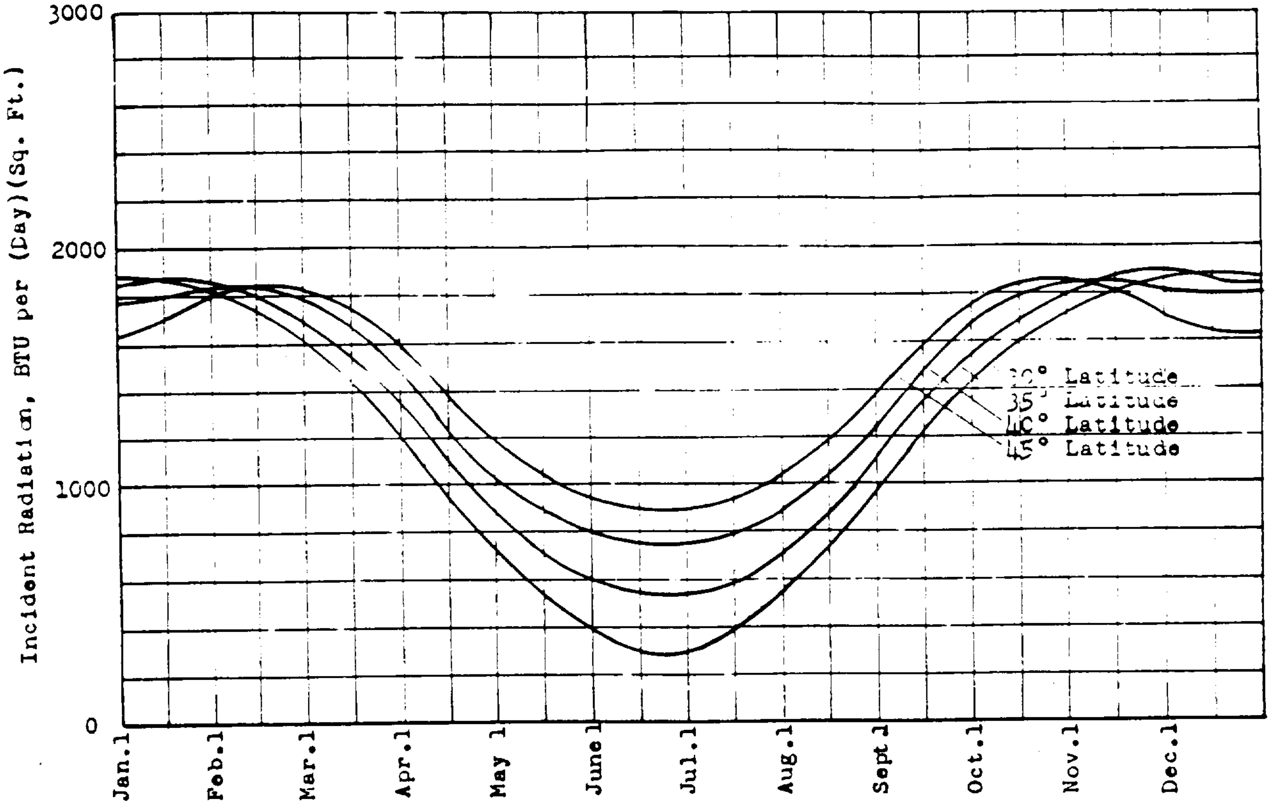

FIGURE 6.3. Daily total direct and sky radiation incident upon a vertical south-facing surface at various north latitudes during cloudless days. Refer to endnote 22 for reference in Endnote section of this report.

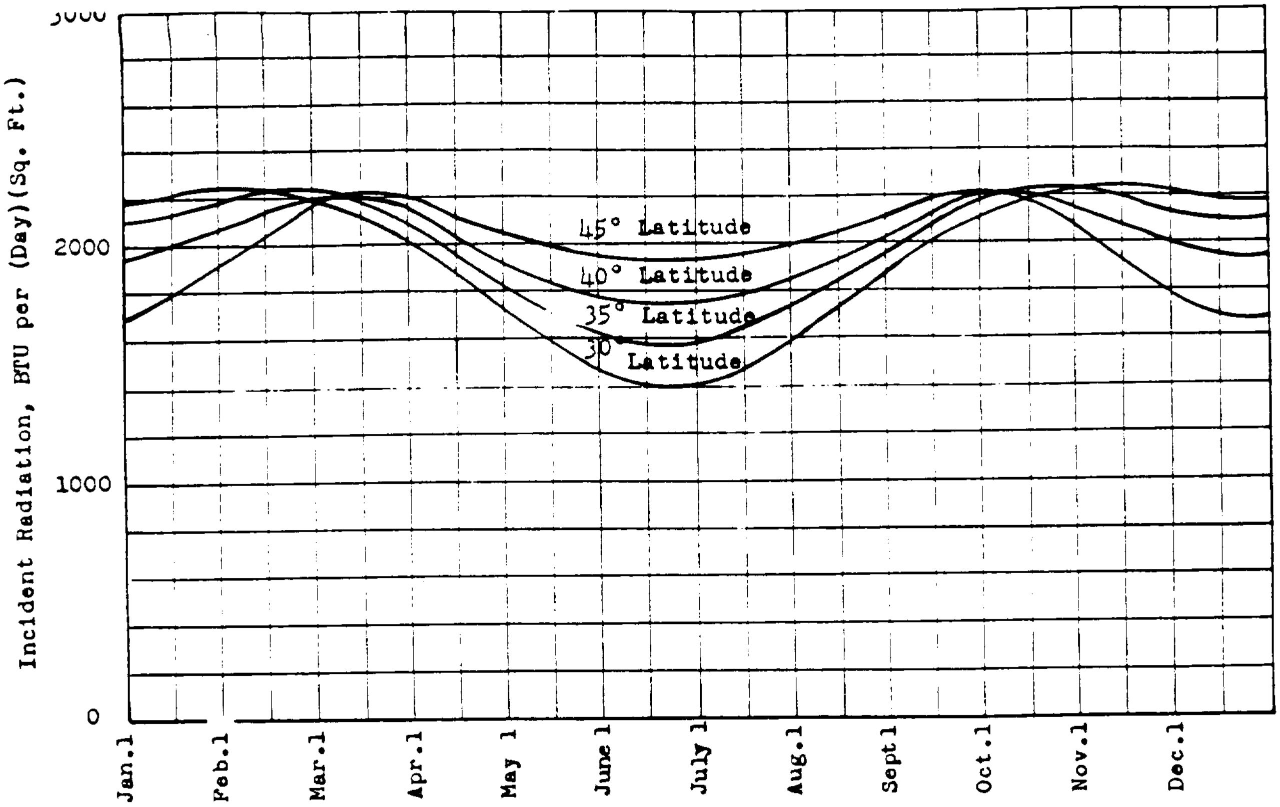

FIGURE 6.4. Daily total direct and sky radiation incident upon a vertical south-facing surface tilted 30 degrees from the vertical at various north latitudes during cloudless days. Refer to endnote 23 for reference in Endnote section of this report.

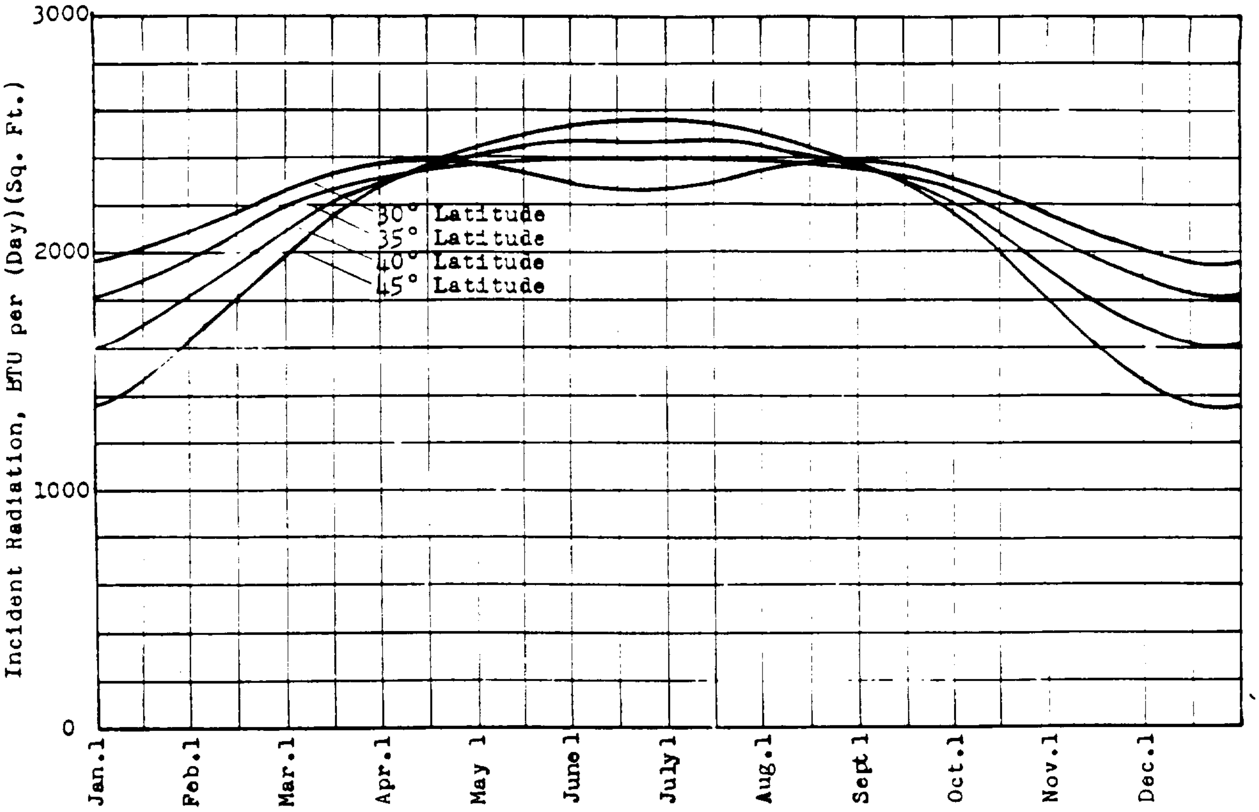

FIGURE 6.5. Daily total direct and sky radiation incident upon a vertical south-facing surface tilted 60 degrees from the vertical at various north latitudes during cloudless days. Refer to endnote 24 for reference in Endnote section of this report.

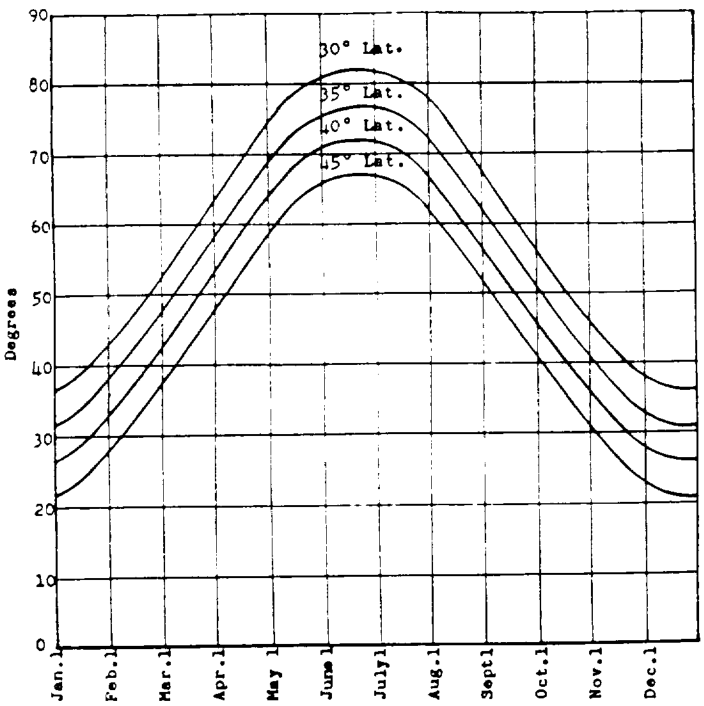

FIGURE 6.6 Number of degrees to tilt a south-facing surface from the vertical to make it perpendicular to the sun's rays at solar noon. Refer to endnote 25 for reference in Endnote section of this report.

## The Test

A copy of the Solar Engineering Lab has been inserted in the appendix and the test that follows is a modified version of it. The steps for this test are as follows:

1. Arrive at the west side of the Old Engineering Building and set up equipment before 11 A.M near the stairway and plaza. Align the Equipment facing south along a north-south axis. The steps are aligned this way and will be used to facilitate this set up.

2. Record the start time as Mountain Standard Time.

3. Start the solar tracker and at 10 minute intervals record the time, the solar altitude and solar azimuth for the tracker and sundial. The experiment will be run for two hours from 11 A. M. to 1 P.M. Record the end time.

4. From the data, you can calculate the Solar Noon time and will calculate the actual altitude and azimuth for each recording and the Standard Time.

5. Taking an average of this data, you can determine the deviation of the tracker for the secondary and primary systems. This will give the accuracy of the tracker.

## CONCLUSION

The design proposed in this report should satisfy the criteria needed for ASPOD's solar tracker. At present from the data and research, I have found a photodiode sensitive to a specific wavelengths up to 0.8 micrometers and beyond. Through the use of a hot mirror all wavelengths above 0.8 micrometers will be cut off allowing for a visible to near IR range upto 0.8 micrometers on the secondaries. The phototransistors will stay the same and the tracker has been made from available parts found in the Aerospace-Mechanical Lab Building machine shop. This design has been made to be snap together for easy maintenance. All wavelengths used will be functional in space as well as on Earth.

### Items To Be Completed

The tracker platform has been built and the controls started by Bruce in the AME Electronics Shop. Unfortunately due to lack of funds for buying the necessary components and the lack of remaining time in the Spring 1994 Semester, this project cannot be completed by myself and must be passed on to a new group for completion. Having graduated and being that I shall not be going to school at the University of Arizona for graduate studies, I can no longer complete this project. I only wish that money for this project had been allocated more readily and sooner. I wish to leave behind some advice to complete this project.

For the completion of this project, there will need to be at least two to three individuals. The work can be divided up as follows:

1. Controls: It is recommended that an individual be selected who has taken the Mechanical Engineering controls class. It is also highly recommended that the two existing one speed motors be replaced with variable speed motors that vary between 15 and 30 degrees per hour rotating speed. The design of the controls as I have initially designed them on paper incorporate an automatic sense of "intelligence". The wide viewing angle of the secondary tracking system makes this intelligence work. Theoretically, using variable speed motors, this tracker can be placed in any direction and automatically find the sun using its secondary tracking system. Once it finds the sun, then the primary system takes over and completes the most accurate part of the tracking.

The secondary system is not as accurate as the primary system. It is not meant to be. Its job is only to find the sun, then switch to the primary system once it finds it. The primary system only turns off when it is aligned precisely. If the primaries are blinded then the secondaries turn on. In essence, this is an "on or on or off" logic control system.

2. Solar Tracker: This can be done by one or two people. What is needed here is to design a test stand that is accurate. Also needed is to finish mounting the photocells to the tracker platform. The individuals will need to have taken the Solar Engineering technical elective class in order to test the tracker. See Solar Tracker Test in this report. The test stand can be a stand alone or, as I recommend, be permanently attached to the ASPOD Base using two pointers and two wide protractors to measure the Azimuth and the Altitude angles.

## Design Troubleshooting Hints

This section has been inserted to try to help those following in my footsteps a way to possibly complete this project and overcome any problems with my design. I urge the person who may do this to first stick with my design. It has been well thought out. Please complete the project as defined in this section.

1. The four primary phototransisters should be mounted no more than 1.1 inches from the center of the tube and at ninety degrees to one another. This should give at least ±0.125 degrees tracking ability for the primary tracker. This is according to the solar tracker calculations found in the appendix. Holes must be drilled through the plastic to bring the necessary wires through for connections.

   If problems develop in tracking on the primaries, first increase the size of the tube hole in increments of an 0.125 inches to no more than 0.5 inches. At present, the hole is at 0.125 inches. If these methods do not work, try increasing the length of the tube to up to 12 inches. By trial and error, the right sizing can be found.
2. The secondary tracker should have its photodiodes mounted within 0.125 inches of the dividers. They should be mounted along the trackers center line and at ninety degrees to one another. They need to be mounted in 1"x1"x0.75" boxes to help mount the hot mirrors over them. The boxes can be made of aluminum or plastic. They should be coated on the outside with a reflective

white surface to reduce heat build up in the boxes. This heat build up could fool the secondaries if not done this way.

If tracking problems develop on the secondaries, then increase the height of the dividers until the desired accuracy is reached. Theoretically, this could be as high as the tube itself but should be no higher.

3. Controls need to be finished as stated above. This is one area which needs to be checked for possible sources of error. The quality of the primary phototransisters is questionable since I have no idea what their manufacturing specifications say about them. They are borrowed from previous design work on ASPOD.

4. If the controls and its design check out and everything above has been tried and the design still gives some trouble then by all means at this point try another design. This tracking concept is sound in theory but has not been tried before.

ENDNOTES

1. Diagram taken from Solar Engineering of Thermal Processes, Duffie, John A. and Beckman, William A., John Wiley and Sons, Inc., 1991, P.148.

2. Diagram taken from Solar Radiation, Robinson, N., Elsevier Publishing Company, New York 1966, p. 81.

3. Picture taken from Photovoltaics, Seippel, Robert G., Reston Publishing Company Inc., Reston, Virginia 1983, p.184.

4. Figure taken from "On the Diurnal Properties From Geostationary Satellite Observations", Hunt, Garry E., Clouds: Their Formation, Optical Properties, and Effects, Academic Press Inc., New York 1981, p.283.

5. Kreith, Frank and Kreider, Jan F., Principles of Solar Engineering, Hemisphere Publishing Corporation 1978, p.15.

6. Figure taken from Solar Radiation, Robinson, N., Elsevier Publishing Company, New York 1966, p. 81.

7. Table information taken from Solar Radiation, Robinson, N., Elsevier Publishing Company, New York 1966, p. 66-67.

8. Table information taken from Solar and Terrestrial Radiation: Methods and Measurements, Coulson, Kinsell L., Academic Press Inc., New York 1975, pp.265-268.

9. Table taken from "Radiation Characteristics Of Clouds In the Solar Spectrum", Cox, Stephen K., Clouds: Their Formation, Optical Properties, and Effects, Academic Press Inc., New York 1981, p. 269.

10. Figure taken from Assorted Solar Energy Engineering Classnotes, John Peck, University of Arizona 1992.

11. Figure taken from A Guide to Remote Sensing: Interpreting Images of the Earth, Drury, S.A., Oxford University Press, Oxford, England 1990, p. 33 .

12. Table information taken from Photovoltaics, Seippel, Robert G., Reston Publishing Company Inc., Reston, Virginia 1983, p.131.

13. Figure taken from Photovoltaics, Seippel, Robert G., Reston Publishing Company Inc., Reston, Virginia 1983, p.131.

14. Figure taken from Solar and Terrestrial Radiation: Methods and Measurements, Coulson, Kinsell L., Academic Press Inc., New York 1975, p. 122.

15. Figure taken from Infrared Optoelectronics: Devices and Applications, Nunley, William and Bechtel, J. Scott, Marcel Dekker Inc., New York 1987, p. 43.

16. Figure taken from Infrared Optoelectronics: Devices and Applications, Nunley, William and Bechtel, J. Scott, Marcel Dekker Inc., New York 1987, p. 92.

17. Figure taken from Infrared Optoelectronics: Devices and Applications, Nunley, William and Bechtel, J. Scott, Marcel Dekker Inc., New York 1987, p. 92.

18. Figure taken from Infrared Optoelectronics: Devices and Applications, Nunley, William and Bechtel, J. Scott, Marcel Dekker Inc., New York 1987, p. 91.

19. Figure taken from Infrared Optoelectronics: Devices and Applications, Nunley, William and Bechtel, J. Scott, Marcel Dekker Inc., New York 1987, p. 91.

20. Figure taken from "Solar Radiation Availability On Surfaces In the United States As Affected By Season, Orientation, Latitude, Altitude and Cloudiness", Becker, Clarence Frederick, Energy in The American Economy, Arno Press, New York 1979, p.13.

21. Figure taken from "Solar Radiation Availability On Surfaces In the United States As Affected By Season, Orientation, Latitude, Altitude and Cloudiness", Becker, Clarence Frederick, Energy in The American Economy, Arno Press, New York 1979, p.12.

22. Figure taken from "Solar Radiation Availability On Surfaces In the United States As Affected By Season, Orientation, Latitude, Altitude and Cloudiness", Becker, Clarence Frederick, Energy in The American Economy, Arno Press, New York 1979, p.25-27.

23. Figure taken from "Solar Radiation Availability On Surfaces In the United States As Affected By Season, Orientation, Latitude, Altitude and Cloudiness", Becker, Clarence Frederick, Energy in The American Economy, Arno Press, New York 1979, p.25-27.

24. Figure taken from "Solar Radiation Availability On Surfaces In the United States As Affected By Season, Orientation, Latitude, Altitude and Cloudiness", Becker, Clarence Frederick, Energy in The American Economy, Arno Press, New York 1979, p.25-27.

25. Figure taken from "Solar Radiation Availability On Surfaces In the United States As Affected By Season, Orientation, Latitude, Altitude and Cloudiness", Becker, Clarence Frederick, Energy in The American Economy, Arno Press, New York 1979, p.30.

## REFERENCES

1. Peck, John, Assorted Solar Energy Engineering Classnotes, University of Arizona 1992.

2. Solar Energy Research Institute, Solar Thermal: Technical Information Guide, May 1985.

3. Kreith, Frank and Kreider, Jan F., Principles of Solar Engineering, Hemisphere Publishing Corporation 1978.

4. Coulson, Kinsell L., Solar and Terrestrial Radiation: Methods and Measurements, Academic Press Inc., New York 1975.

5. Robinson, N., Solar Radiation, Elsevier Publishing Company, New York 1966.

6. Becker, Clarence Frederick, "Solar Radiation Availability On Surfaces In the United States As Affected By Season, Orientation, Latitude, Altitude and Cloudiness", Energy in The American Economy, Arno Press, New York 1979.

7. Duffie, John A. and Beckman, William A., Solar Engineering of Thermal Processes, John Wiley and Sons, Inc., 1991

8. Reagan, J. A., Thorne, K. J. and Herman, B. M., "A Simple Instrument and Technique for Measuring Columnar Water Vapor via Near-IR Differential Solar Transmission Measurements", IEEE Transactions On Geoscience and Remote Sensing, Volume 30, No. 4, July 1992.

9. Biberman, Lucien M., Reticles In Electro-Optical Devices Pergamon Press Inc. New York 1966.

10. Cox, Stephen K., "Radiation Characteristics Of Clouds In the Solar Spectrum", Clouds: Their Formation, Optical Properties, and Effects, Academic Press Inc., New York 1981

11. Drury, S.A., A Guide to Remote Sensing: Interpreting Images of the Earth, Oxford University Press, Oxford, England 1990.

12. Nunley, William and Bechtel, J. Scott, Infrared Optoelectronics: Devices and Applications, Marcel Dekker Inc., New York 1987.

13. Seippel, Robert G., Photovoltaics, Reston Publishing Company Inc., Reston, Virginia 1983.

14. High Performance Silicon Photodetectors, Second Edition, Centronic Inc. Newbury, California

# APPENDIX

A. Calculations

B. Completed Design Diagrams

C. Material Receipts

D. Phototransister and Mirror Information

# TUBE CALCULATION EQUATIONS

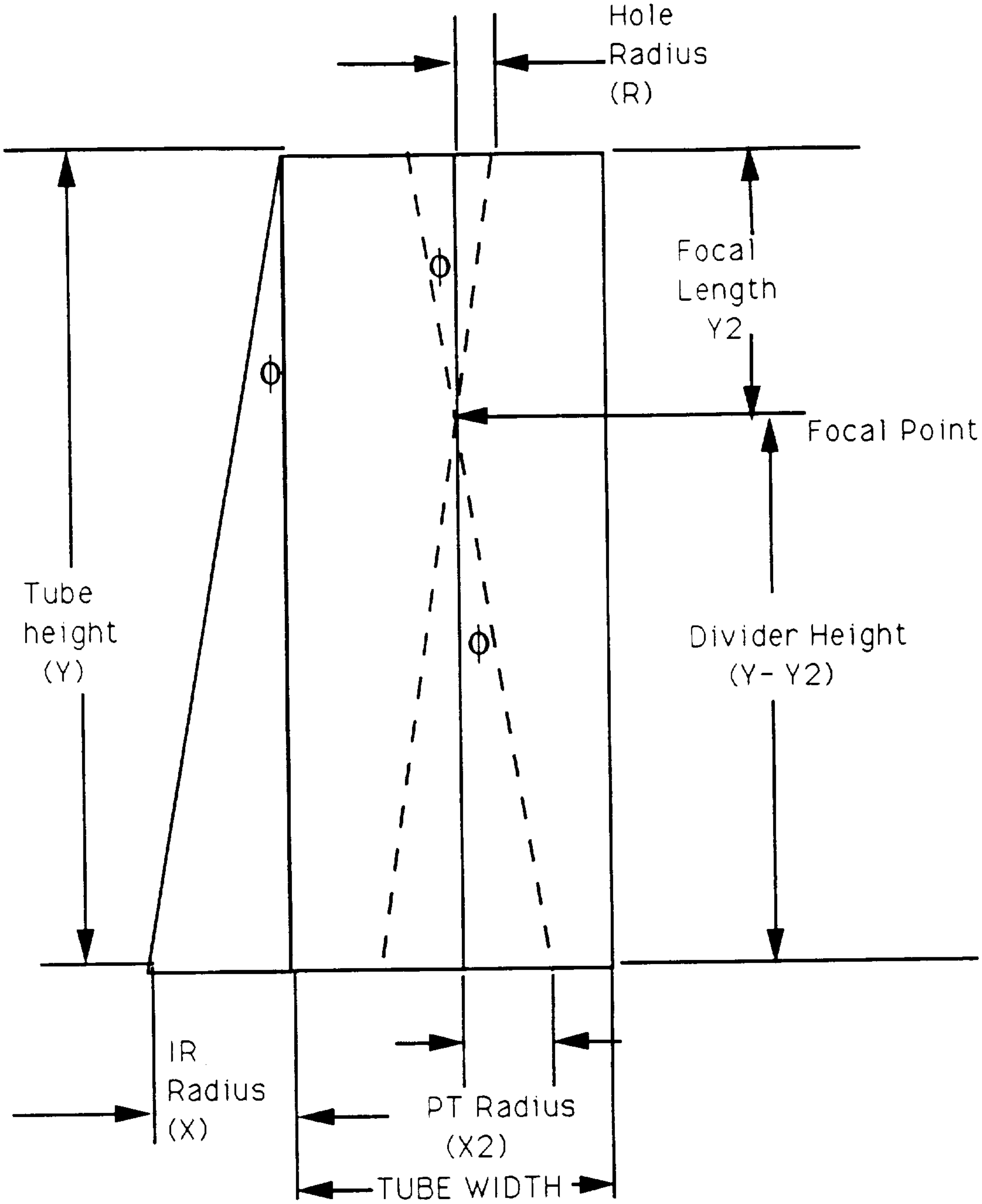
Hole
Radius
(R)
ϕ
ϕ
Focal
Length
Y2
Focal Point
Tube
height
(Y)
ϕ
Divider Height
(Y- Y2)
IR
Radius
(X)
PT Radius
(X2)
TUBE WIDTH

KNOWN VALUES ARE R, Y, ϕ
UNKNOWNS ARE X,Y2, X2 AND
THE TUBE RADIUS

PT- PHOTOTRANSISTORS
IR- INFRARED DIODES

EQUATIONS USED

EQUATION 1
X= Y* TAN (ϕ)

EQUATION 2
Y2=R/TAN (ϕ)

EQUATION 3
X2=(Y-Y2)*TAN (ϕ)

TUBE WIDTH= 2*X2 + 1 INCH

# SOLAR TRACKER CALCULATIONS

| Tube Height Inches | Hole Diameter Inches | Hole Radius r Inches | Angle (Theta) Degrees | Angle (Theta) Arcmin. | Focal Length y Inches | Transister Radius Inches | Needed Tube Radius Inches | IR Distance Inches |
|---|---|---|---|---|---|---|---|---|
| 4 | 1.00000 | 0.50000 | 1.000 | 60.0 | 0.321 | 5.730 | 6.230 | 6.230 |
| 4 | 0.75000 | 0.37500 | 1.000 | 60.0 | 0.241 | 5.855 | 6.355 | 6.230 |
| 4 | 0.50000 | 0.25000 | 1.000 | 60.0 | 0.161 | 5.980 | 6.480 | 6.230 |
| 4 | 0.25000 | 0.12500 | 1.000 | 60.0 | 0.080 | 6.105 | 6.605 | 6.230 |
| 4 | 0.12500 | 0.06250 | 1.000 | 60.0 | 0.040 | 6.167 | 6.667 | 6.230 |
| 4 | 0.06250 | 0.03125 | 1.000 | 60.0 | 0.020 | 6.198 | 6.698 | 6.230 |
| 4 | 0.03125 | 0.01563 | 1.000 | 60.0 | 0.010 | 6.214 | 6.714 | 6.230 |
| 4 | 0.01563 | 0.00781 | 1.000 | 60.0 | 0.005 | 6.222 | 6.722 | 6.230 |
| 4 | 0.00781 | 0.00391 | 1.000 | 60.0 | 0.003 | 6.226 | 6.726 | 6.230 |
| 4 | 0.00391 | 0.00195 | 1.000 | 60.0 | 0.001 | 6.228 | 6.728 | 6.230 |
| 4 | 0.00195 | 0.00098 | 1.000 | 60.0 | 0.001 | 6.229 | 6.729 | 6.230 |
| 4 | 0.00098 | 0.00049 | 1.000 | 60.0 | 0.000 | 6.229 | 6.729 | 6.230 |
| 4 | 0.00049 | 0.00024 | 1.000 | 60.0 | 0.000 | 6.229 | 6.729 | 6.230 |

| Tube Height Inches | Hole Diameter Inches | Hole Radius r Inches | Angle (Theta) Degrees | Angle (Theta) Arcmin. | Focal Length y Inches | Transister Radius Inches | Needed Tube Radius Inches | IR Distance Inches |
|---|---|---|---|---|---|---|---|---|
| 4 | 1.00000 | 0.50000 | 0.500 | 30.0 | 0.915 | 1.685 | 2.185 | 2.185 |
| 4 | 0.75000 | 0.37500 | 0.500 | 30.0 | 0.686 | 1.810 | 2.310 | 2.185 |
| 4 | 0.50000 | 0.25000 | 0.500 | 30.0 | 0.458 | 1.935 | 2.435 | 2.185 |
| 4 | 0.25000 | 0.12500 | 0.500 | 30.0 | 0.229 | 2.060 | 2.560 | 2.185 |
| 4 | 0.12500 | 0.06250 | 0.500 | 30.0 | 0.114 | 2.123 | 2.623 | 2.185 |
| 4 | 0.06250 | 0.03125 | 0.500 | 30.0 | 0.057 | 2.154 | 2.654 | 2.185 |
| 4 | 0.03125 | 0.01563 | 0.500 | 30.0 | 0.029 | 2.170 | 2.670 | 2.185 |
| 4 | 0.01563 | 0.00781 | 0.500 | 30.0 | 0.014 | 2.177 | 2.677 | 2.185 |
| 4 | 0.00781 | 0.00391 | 0.500 | 30.0 | 0.007 | 2.181 | 2.681 | 2.185 |
| 4 | 0.00391 | 0.00195 | 0.500 | 30.0 | 0.004 | 2.183 | 2.683 | 2.185 |
| 4 | 0.00195 | 0.00098 | 0.500 | 30.0 | 0.002 | 2.184 | 2.684 | 2.185 |
| 4 | 0.00098 | 0.00049 | 0.500 | 30.0 | 0.001 | 2.185 | 2.685 | 2.185 |
| 4 | 0.00049 | 0.00024 | 0.500 | 30.0 | 0.000 | 2.185 | 2.685 | 2.185 |

| Tube Height Inches | Hole Diameter Inches | Hole Radius r Inches | Angle (Theta) Degrees | Angle (Theta) Arcmin. | Focal Length y Inches | Transister Radius Inches | Needed Tube Radius Inches | IR Distance Inches |
|---|---|---|---|---|---|---|---|---|
| 4 | 1.00000 | 0.50000 | 0.250 | 15.0 | 1.958 | 0.521 | 1.021 | 1.021 |
| 4 | 0.75000 | 0.37500 | 0.250 | 15.0 | 1.469 | 0.646 | 1.146 | 1.021 |
| 4 | 0.50000 | 0.25000 | 0.250 | 15.0 | 0.979 | 0.771 | 1.271 | 1.021 |
| 4 | 0.25000 | 0.12500 | 0.250 | 15.0 | 0.490 | 0.896 | 1.396 | 1.021 |
| 4 | 0.12500 | 0.06250 | 0.250 | 15.0 | 0.245 | 0.959 | 1.459 | 1.021 |
| 4 | 0.06250 | 0.03125 | 0.250 | 15.0 | 0.122 | 0.990 | 1.490 | 1.021 |
| 4 | 0.03125 | 0.01563 | 0.250 | 15.0 | 0.061 | 1.006 | 1.506 | 1.021 |
| 4 | 0.01563 | 0.00781 | 0.250 | 15.0 | 0.031 | 1.014 | 1.514 | 1.021 |
| 4 | 0.00781 | 0.00391 | 0.250 | 15.0 | 0.015 | 1.017 | 1.517 | 1.021 |
| 4 | 0.00391 | 0.00195 | 0.250 | 15.0 | 0.008 | 1.019 | 1.519 | 1.021 |
| 4 | 0.00195 | 0.00098 | 0.250 | 15.0 | 0.004 | 1.020 | 1.520 | 1.021 |
| 4 | 0.00098 | 0.00049 | 0.250 | 15.0 | 0.002 | 1.021 | 1.521 | 1.021 |
| 4 | 0.00049 | 0.00024 | 0.250 | 15.0 | 0.001 | 1.021 | 1.521 | 1.021 |

| Tube Height Inches | Hole Diameter Inches | Hole Radius r Inches | Angle (Theta) Degrees | Angle (Theta) Arcmin. | Focal Length y Inches | Transister Radius Inches | Needed Tube Radius Inches | IR Distance Inches |
|---|---|---|---|---|---|---|---|---|
| 4 | 1.00000 | 0.50000 | 0.125 | 7.5 | 3.979 | 0.003 | 0.503 | 0.503 |
| 4 | 0.75000 | 0.37500 | 0.125 | 7.5 | 2.984 | 0.128 | 0.628 | 0.503 |
| 4 | 0.50000 | 0.25000 | 0.125 | 7.5 | 1.990 | 0.253 | 0.753 | 0.503 |
| 4 | 0.25000 | 0.12500 | 0.125 | 7.5 | 0.995 | 0.378 | 0.878 | 0.503 |
| 4 | 0.12500 | 0.06250 | 0.125 | 7.5 | 0.497 | 0.440 | 0.940 | 0.503 |
| 4 | 0.06250 | 0.03125 | 0.125 | 7.5 | 0.249 | 0.471 | 0.971 | 0.503 |
| 4 | 0.03125 | 0.01563 | 0.125 | 7.5 | 0.124 | 0.487 | 0.987 | 0.503 |
| 4 | 0.01563 | 0.00781 | 0.125 | 7.5 | 0.062 | 0.495 | 0.995 | 0.503 |
| 4 | 0.00781 | 0.00391 | 0.125 | 7.5 | 0.031 | 0.499 | 0.999 | 0.503 |
| 4 | 0.00391 | 0.00195 | 0.125 | 7.5 | 0.016 | 0.501 | 1.001 | 0.503 |
| 4 | 0.00195 | 0.00098 | 0.125 | 7.5 | 0.008 | 0.502 | 1.002 | 0.503 |
| 4 | 0.00098 | 0.00049 | 0.125 | 7.5 | 0.004 | 0.502 | 1.002 | 0.503 |
| 4 | 0.00049 | 0.00024 | 0.125 | 7.5 | 0.002 | 0.502 | 1.002 | 0.503 |

| Tube Height Inches | Hole Diameter Inches | Hole Radius r Inches | Angle (Theta) Degrees | Angle (Theta) Arcmin. | Focal Length y Inches | Transister Radius Inches | Needed Tube Radius Inches | IR Distance Inches |
|---|---|---|---|---|---|---|---|---|
| 4 | 1.00000 | 0.50000 | 0.083 | 5.0 | 5.986 | -0.166 | 0.334 | 0.334 |
| 4 | 0.75000 | 0.37500 | 0.083 | 5.0 | 4.490 | -0.041 | 0.459 | 0.334 |
| 4 | 0.50000 | 0.25000 | 0.083 | 5.0 | 2.993 | 0.084 | 0.584 | 0.334 |
| 4 | 0.25000 | 0.12500 | 0.083 | 5.0 | 1.497 | 0.209 | 0.709 | 0.334 |
| 4 | 0.12500 | 0.06250 | 0.083 | 5.0 | 0.748 | 0.272 | 0.772 | 0.334 |
| 4 | 0.06250 | 0.03125 | 0.083 | 5.0 | 0.374 | 0.303 | 0.803 | 0.334 |
| 4 | 0.03125 | 0.01563 | 0.083 | 5.0 | 0.187 | 0.318 | 0.818 | 0.334 |
| 4 | 0.01563 | 0.00781 | 0.083 | 5.0 | 0.094 | 0.326 | 0.826 | 0.334 |
| 4 | 0.00781 | 0.00391 | 0.083 | 5.0 | 0.047 | 0.330 | 0.830 | 0.334 |
| 4 | 0.00391 | 0.00195 | 0.083 | 5.0 | 0.023 | 0.332 | 0.832 | 0.334 |
| 4 | 0.00195 | 0.00098 | 0.083 | 5.0 | 0.012 | 0.333 | 0.833 | 0.334 |
| 4 | 0.00098 | 0.00049 | 0.083 | 5.0 | 0.006 | 0.334 | 0.834 | 0.334 |
| 4 | 0.00049 | 0.00024 | 0.083 | 5.0 | 0.003 | 0.334 | 0.834 | 0.334 |

## SOLAR TRACKER CALCULATIONS

| Tube Height Inches | Hole Diameter Inches | Hole Radius r Inches | Angle (Theta) Degrees | Angle (Theta) Arcmin. | Focal Length y Inches | Transister Radius Inches | Needed Tube Radius Inches | IR Distance Inches |
|---|---|---|---|---|---|---|---|---|
| 6 | 1.00000 | 0.50000 | 1.000 | 60.0 | 0.321 | 8.844 | 9.344 | 9.344 |
| 6 | 0.75000 | 0.37500 | 1.000 | 60.0 | 0.241 | 8.969 | 9.469 | 9.344 |
| 6 | 0.50000 | 0.25000 | 1.000 | 60.0 | 0.161 | 9.094 | 9.594 | 9.344 |
| 6 | 0.25000 | 0.12500 | 1.000 | 60.0 | 0.080 | 9.219 | 9.719 | 9.344 |
| 6 | 0.12500 | 0.06250 | 1.000 | 60.0 | 0.040 | 9.282 | 9.782 | 9.344 |
| 6 | 0.06250 | 0.03125 | 1.000 | 60.0 | 0.020 | 9.313 | 9.813 | 9.344 |
| 6 | 0.03125 | 0.01563 | 1.000 | 60.0 | 0.010 | 9.329 | 9.829 | 9.344 |
| 6 | 0.01563 | 0.00781 | 1.000 | 60.0 | 0.005 | 9.337 | 9.837 | 9.344 |
| 6 | 0.00781 | 0.00391 | 1.000 | 60.0 | 0.003 | 9.341 | 9.841 | 9.344 |
| 6 | 0.00391 | 0.00195 | 1.000 | 60.0 | 0.001 | 9.342 | 9.842 | 9.344 |
| 6 | 0.00195 | 0.00098 | 1.000 | 60.0 | 0.001 | 9.343 | 9.843 | 9.344 |
| 6 | 0.00098 | 0.00049 | 1.000 | 60.0 | 0.000 | 9.344 | 9.844 | 9.344 |
| 6 | 0.00049 | 0.00024 | 1.000 | 60.0 | 0.000 | 9.344 | 9.844 | 9.344 |

| Tube Height Inches | Hole Diameter Inches | Hole Radius r Inches | Angle (Theta) Degrees | Angle (Theta) Arcmin. | Focal Length y Inches | Transister Radius Inches | Needed Tube Radius Inches | IR Distance Inches |
|---|---|---|---|---|---|---|---|---|
| 6 | 1.00000 | 0.50000 | 0.500 | 30.0 | 0.915 | 2.778 | 3.278 | 3.278 |
| 6 | 0.75000 | 0.37500 | 0.500 | 30.0 | 0.686 | 2.903 | 3.403 | 3.278 |
| 6 | 0.50000 | 0.25000 | 0.500 | 30.0 | 0.458 | 3.028 | 3.528 | 3.278 |
| 6 | 0.25000 | 0.12500 | 0.500 | 30.0 | 0.229 | 3.153 | 3.653 | 3.278 |
| 6 | 0.12500 | 0.06250 | 0.500 | 30.0 | 0.114 | 3.215 | 3.715 | 3.278 |
| 6 | 0.06250 | 0.03125 | 0.500 | 30.0 | 0.057 | 3.247 | 3.747 | 3.278 |
| 6 | 0.03125 | 0.01563 | 0.500 | 30.0 | 0.029 | 3.262 | 3.762 | 3.278 |
| 6 | 0.01563 | 0.00781 | 0.500 | 30.0 | 0.014 | 3.270 | 3.770 | 3.278 |
| 6 | 0.00781 | 0.00391 | 0.500 | 30.0 | 0.007 | 3.274 | 3.774 | 3.278 |
| 6 | 0.00391 | 0.00195 | 0.500 | 30.0 | 0.004 | 3.276 | 3.776 | 3.278 |
| 6 | 0.00195 | 0.00098 | 0.500 | 30.0 | 0.002 | 3.277 | 3.777 | 3.278 |
| 6 | 0.00098 | 0.00049 | 0.500 | 30.0 | 0.001 | 3.277 | 3.777 | 3.278 |
| 6 | 0.00049 | 0.00024 | 0.500 | 30.0 | 0.000 | 3.278 | 3.778 | 3.278 |

| Tube Height Inches | Hole Diameter Inches | Hole Radius r Inches | Angle (Theta) Degrees | Angle (Theta) Arcmin. | Focal Length y Inches | Transister Radius Inches | Needed Tube Radius Inches | IR Distance Inches |
|---|---|---|---|---|---|---|---|---|
| 6 | 1.00000 | 0.50000 | 0.250 | 15.0 | 1.958 | 1.032 | 1.532 | 1.532 |
| 6 | 0.75000 | 0.37500 | 0.250 | 15.0 | 1.469 | 1.157 | 1.657 | 1.532 |
| 6 | 0.50000 | 0.25000 | 0.250 | 15.0 | 0.979 | 1.282 | 1.782 | 1.532 |
| 6 | 0.25000 | 0.12500 | 0.250 | 15.0 | 0.490 | 1.407 | 1.907 | 1.532 |
| 6 | 0.12500 | 0.06250 | 0.250 | 15.0 | 0.245 | 1.470 | 1.970 | 1.532 |
| 6 | 0.06250 | 0.03125 | 0.250 | 15.0 | 0.122 | 1.501 | 2.001 | 1.532 |
| 6 | 0.03125 | 0.01563 | 0.250 | 15.0 | 0.061 | 1.516 | 2.016 | 1.532 |
| 6 | 0.01563 | 0.00781 | 0.250 | 15.0 | 0.031 | 1.524 | 2.024 | 1.532 |
| 6 | 0.00781 | 0.00391 | 0.250 | 15.0 | 0.015 | 1.528 | 2.028 | 1.532 |
| 6 | 0.00391 | 0.00195 | 0.250 | 15.0 | 0.008 | 1.530 | 2.030 | 1.532 |
| 6 | 0.00195 | 0.00098 | 0.250 | 15.0 | 0.004 | 1.531 | 2.031 | 1.532 |
| 6 | 0.00098 | 0.00049 | 0.250 | 15.0 | 0.002 | 1.532 | 2.032 | 1.532 |
| 6 | 0.00049 | 0.00024 | 0.250 | 15.0 | 0.001 | 1.532 | 2.032 | 1.532 |

| Tube Height Inches | Hole Diameter Inches | Hole Radius r Inches | Angle (Theta) Degrees | Angle (Theta) Arcmin | Focal Length y Inches | Transister Radius Inches | Needed Tube Radius Inches | IR Distance Inches |
|---|---|---|---|---|---|---|---|---|
| 6 | 1.00000 | 0.50000 | 0.125 | 7.5 | 3.979 | 0.254 | 0.754 | 0.754 |
| 6 | 0.75000 | 0.37500 | 0.125 | 7.5 | 2.984 | 0.379 | 0.879 | 0.754 |
| 6 | 0.50000 | 0.25000 | 0.125 | 7.5 | 1.990 | 0.504 | 1.004 | 0.754 |
| 6 | 0.25000 | 0.12500 | 0.125 | 7.5 | 0.995 | 0.629 | 1.129 | 0.754 |
| 6 | 0.12500 | 0.06250 | 0.125 | 7.5 | 0.497 | 0.691 | 1.191 | 0.754 |
| 6 | 0.06250 | 0.03125 | 0.125 | 7.5 | 0.249 | 0.723 | 1.223 | 0.754 |
| 6 | 0.03125 | 0.01563 | 0.125 | 7.5 | 0.124 | 0.738 | 1.238 | 0.754 |
| 6 | 0.01563 | 0.00781 | 0.125 | 7.5 | 0.062 | 0.746 | 1.246 | 0.754 |
| 6 | 0.00781 | 0.00391 | 0.125 | 7.5 | 0.031 | 0.750 | 1.250 | 0.754 |
| 6 | 0.00391 | 0.00195 | 0.125 | 7.5 | 0.016 | 0.752 | 1.252 | 0.754 |
| 6 | 0.00195 | 0.00098 | 0.125 | 7.5 | 0.008 | 0.753 | 1.253 | 0.754 |
| 6 | 0.00098 | 0.00049 | 0.125 | 7.5 | 0.004 | 0.753 | 1.253 | 0.754 |
| 6 | 0.00049 | 0.00024 | 0.125 | 7.5 | 0.002 | 0.754 | 1.254 | 0.754 |

| Tube Height Inches | Hole Diameter Inches | Hole Radius r Inches | Angle (Theta) Degrees | Angle (Theta) Arcmin. | Focal Length y Inches | Transister Radius Inches | Needed Tube Radius Inches | IR Distance Inches |
|---|---|---|---|---|---|---|---|---|
| 6 | 1.00000 | 0.50000 | 0.083 | 5.0 | 5.986 | 0.001 | 0.501 | 0.501 |
| 6 | 0.75000 | 0.37500 | 0.083 | 5.0 | 4.490 | 0.126 | 0.626 | 0.501 |
| 6 | 0.50000 | 0.25000 | 0.083 | 5.0 | 2.993 | 0.251 | 0.751 | 0.501 |
| 6 | 0.25000 | 0.12500 | 0.083 | 5.0 | 1.497 | 0.376 | 0.876 | 0.501 |
| 6 | 0.12500 | 0.06250 | 0.083 | 5.0 | 0.748 | 0.439 | 0.939 | 0.501 |
| 6 | 0.06250 | 0.03125 | 0.083 | 5.0 | 0.374 | 0.470 | 0.970 | 0.501 |
| 6 | 0.03125 | 0.01563 | 0.083 | 5.0 | 0.187 | 0.486 | 0.986 | 0.501 |
| 6 | 0.01563 | 0.00781 | 0.083 | 5.0 | 0.094 | 0.493 | 0.993 | 0.501 |
| 6 | 0.00781 | 0.00391 | 0.083 | 5.0 | 0.047 | 0.497 | 0.997 | 0.501 |
| 6 | 0.00391 | 0.00195 | 0.083 | 5.0 | 0.023 | 0.499 | 0.999 | 0.501 |
| 6 | 0.00195 | 0.00098 | 0.083 | 5.0 | 0.012 | 0.500 | 1.000 | 0.501 |
| 6 | 0.00098 | 0.00049 | 0.083 | 5.0 | 0.006 | 0.501 | 1.001 | 0.501 |
| 6 | 0.00049 | 0.00024 | 0.083 | 5.0 | 0.003 | 0.501 | 1.001 | 0.501 |

## SOLAR TRACKER CALCULATIONS

| Tube Height Inches | Hole Diameter Inches | Hole Radius r Inches | Angle (Theta) Degrees | Angle (Theta) Arcmin. | Focal Length y Inches | Transister Radius Inches | Needed Tube Radius Inches | IR Distance Inches |
|---|---|---|---|---|---|---|---|---|
| 8 | 1.00000 | 0.50000 | 1.000 | 60.0 | 0.321 | 11.959 | 12.459 | 12.459 |
| 8 | 0.75000 | 0.37500 | 1.000 | 60.0 | 0.241 | 12.084 | 12.584 | 12.459 |
| 8 | 0.50000 | 0.25000 | 1.000 | 60.0 | 0.161 | 12.209 | 12.709 | 12.459 |
| 8 | 0.25000 | 0.12500 | 1.000 | 60.0 | 0.080 | 12.334 | 12.834 | 12.459 |
| 8 | 0.12500 | 0.06250 | 1.000 | 60.0 | 0.040 | 12.397 | 12.897 | 12.459 |
| 8 | 0.06250 | 0.03125 | 1.000 | 60.0 | 0.020 | 12.428 | 12.928 | 12.459 |
| 8 | 0.03125 | 0.01563 | 1.000 | 60.0 | 0.010 | 12.444 | 12.944 | 12.459 |
| 8 | 0.01563 | 0.00781 | 1.000 | 60.0 | 0.005 | 12.451 | 12.951 | 12.459 |
| 8 | 0.00781 | 0.00391 | 1.000 | 60.0 | 0.003 | 12.455 | 12.955 | 12.459 |
| 8 | 0.00391 | 0.00195 | 1.000 | 60.0 | 0.001 | 12.457 | 12.957 | 12.459 |
| 8 | 0.00195 | 0.00098 | 1.000 | 60.0 | 0.001 | 12.458 | 12.958 | 12.459 |
| 8 | 0.00098 | 0.00049 | 1.000 | 60.0 | 0.000 | 12.459 | 12.959 | 12.459 |
| 8 | 0.00049 | 0.00024 | 1.000 | 60.0 | 0.000 | 12.459 | 12.959 | 12.459 |

| Tube Height Inches | Hole Diameter Inches | Hole Radius r Inches | Angle (Theta) Degrees | Angle (Theta) Arcmin | Focal Length y Inches | Transister Radius Inches | Needed Tube Radius Inches | IR Distance Inches |
|---|---|---|---|---|---|---|---|---|
| 8 | 1.00000 | 0.50000 | 0.500 | 30.0 | 0.915 | 3.870 | 4.370 | 4.370 |
| 8 | 0.75000 | 0.37500 | 0.500 | 30.0 | 0.686 | 3.995 | 4.495 | 4.370 |
| 8 | 0.50000 | 0.25000 | 0.500 | 30.0 | 0.458 | 4.120 | 4.620 | 4.370 |
| 8 | 0.25000 | 0.12500 | 0.500 | 30.0 | 0.229 | 4.245 | 4.745 | 4.370 |
| 8 | 0.12500 | 0.06250 | 0.500 | 30.0 | 0.114 | 4.308 | 4.808 | 4.370 |
| 8 | 0.06250 | 0.03125 | 0.500 | 30.0 | 0.057 | 4.339 | 4.839 | 4.370 |
| 8 | 0.03125 | 0.01563 | 0.500 | 30.0 | 0.029 | 4.355 | 4.855 | 4.370 |
| 8 | 0.01563 | 0.00781 | 0.500 | 30.0 | 0.014 | 4.363 | 4.863 | 4.370 |
| 8 | 0.00781 | 0.00391 | 0.500 | 30.0 | 0.007 | 4.367 | 4.867 | 4.370 |
| 8 | 0.00391 | 0.00195 | 0.500 | 30.0 | 0.004 | 4.368 | 4.868 | 4.370 |
| 8 | 0.00195 | 0.00098 | 0.500 | 30.0 | 0.002 | 4.369 | 4.869 | 4.370 |
| 8 | 0.00098 | 0.00049 | 0.500 | 30.0 | 0.001 | 4.370 | 4.870 | 4.370 |
| 8 | 0.00049 | 0.00024 | 0.500 | 30.0 | 0.000 | 4.370 | 4.870 | 4.370 |

| Tube Height Inches | Hole Diameter Inches | Hole Radius r Inches | Angle (Theta) Degrees | Angle (Theta) Arcmin | Focal Length y Inches | Transister Radius Inches | Needed Tube Radius Inches | IR Distance Inches |
|---|---|---|---|---|---|---|---|---|
| 8 | 1.00000 | 0.50000 | 0.250 | 15.0 | 1.958 | 1.543 | 2.043 | 2.043 |
| 8 | 0.75000 | 0.37500 | 0.250 | 15.0 | 1.469 | 1.668 | 2.168 | 2.043 |
| 8 | 0.50000 | 0.25000 | 0.250 | 15.0 | 0.979 | 1.793 | 2.293 | 2.043 |
| 8 | 0.25000 | 0.12500 | 0.250 | 15.0 | 0.490 | 1.918 | 2.418 | 2.043 |
| 8 | 0.12500 | 0.06250 | 0.250 | 15.0 | 0.245 | 1.980 | 2.480 | 2.043 |
| 8 | 0.06250 | 0.03125 | 0.250 | 15.0 | 0.122 | 2.011 | 2.511 | 2.043 |
| 8 | 0.03125 | 0.01563 | 0.250 | 15.0 | 0.061 | 2.027 | 2.527 | 2.043 |
| 8 | 0.01563 | 0.00781 | 0.250 | 15.0 | 0.031 | 2.035 | 2.535 | 2.043 |
| 8 | 0.00781 | 0.00391 | 0.250 | 15.0 | 0.015 | 2.039 | 2.539 | 2.043 |
| 8 | 0.00391 | 0.00195 | 0.250 | 15.0 | 0.008 | 2.041 | 2.541 | 2.043 |
| 8 | 0.00195 | 0.00098 | 0.250 | 15.0 | 0.004 | 2.042 | 2.542 | 2.043 |
| 8 | 0.00098 | 0.00049 | 0.250 | 15.0 | 0.002 | 2.042 | 2.542 | 2.043 |
| 8 | 0.00049 | 0.00024 | 0.250 | 15.0 | 0.001 | 2.042 | 2.542 | 2.043 |

| Tube Height Inches | Hole Diameter Inches | Hole Radius r Inches | Angle (Theta) Degrees | Angle (Theta) Arcmin | Focal Length y Inches | Transister Radius Inches | Needed Tube Radius Inches | IR Distance Inches |
|---|---|---|---|---|---|---|---|---|
| 8 | 1.00000 | 0.50000 | 0.125 | 7.5 | 3.979 | 0.505 | 1.005 | 1.005 |
| 8 | 0.75000 | 0.37500 | 0.125 | 7.5 | 2.984 | 0.630 | 1.130 | 1.005 |
| 8 | 0.50000 | 0.25000 | 0.125 | 7.5 | 1.990 | 0.755 | 1.255 | 1.005 |
| 8 | 0.25000 | 0.12500 | 0.125 | 7.5 | 0.995 | 0.880 | 1.380 | 1.005 |
| 8 | 0.12500 | 0.06250 | 0.125 | 7.5 | 0.497 | 0.943 | 1.443 | 1.005 |
| 8 | 0.06250 | 0.03125 | 0.125 | 7.5 | 0.249 | 0.974 | 1.474 | 1.005 |
| 8 | 0.03125 | 0.01563 | 0.125 | 7.5 | 0.124 | 0.990 | 1.490 | 1.005 |
| 8 | 0.01563 | 0.00781 | 0.125 | 7.5 | 0.062 | 0.997 | 1.497 | 1.005 |
| 8 | 0.00781 | 0.00391 | 0.125 | 7.5 | 0.031 | 1.001 | 1.501 | 1.005 |
| 8 | 0.00391 | 0.00195 | 0.125 | 7.5 | 0.016 | 1.003 | 1.503 | 1.005 |
| 8 | 0.00195 | 0.00098 | 0.125 | 7.5 | 0.008 | 1.004 | 1.504 | 1.005 |
| 8 | 0.00098 | 0.00049 | 0.125 | 7.5 | 0.004 | 1.005 | 1.505 | 1.005 |
| 8 | 0.00049 | 0.00024 | 0.125 | 7.5 | 0.002 | 1.005 | 1.505 | 1.005 |

| Tube Height Inches | Hole Diameter Inches | Hole Radius r Inches | Angle (Theta) Degrees | Angle (Theta) Arcmin. | Focal Length y Inches | Transister Radius Inches | Needed Tube Radius Inches | IR Distance Inches |
|---|---|---|---|---|---|---|---|---|
| 8 | 1.00000 | 0.50000 | 0.083 | 5.0 | 5.986 | 0.168 | 0.668 | 0.668 |
| 8 | 0.75000 | 0.37500 | 0.083 | 5.0 | 4.490 | 0.293 | 0.793 | 0.668 |
| 8 | 0.50000 | 0.25000 | 0.083 | 5.0 | 2.993 | 0.418 | 0.918 | 0.668 |
| 8 | 0.25000 | 0.12500 | 0.083 | 5.0 | 1.497 | 0.543 | 1.043 | 0.668 |
| 8 | 0.12500 | 0.06250 | 0.083 | 5.0 | 0.748 | 0.606 | 1.106 | 0.668 |
| 8 | 0.06250 | 0.03125 | 0.083 | 5.0 | 0.374 | 0.637 | 1.137 | 0.668 |
| 8 | 0.03125 | 0.01563 | 0.083 | 5.0 | 0.187 | 0.653 | 1.153 | 0.668 |
| 8 | 0.01563 | 0.00781 | 0.083 | 5.0 | 0.094 | 0.660 | 1.160 | 0.668 |
| 8 | 0.00781 | 0.00391 | 0.083 | 5.0 | 0.047 | 0.664 | 1.164 | 0.668 |
| 8 | 0.00391 | 0.00195 | 0.083 | 5.0 | 0.023 | 0.666 | 1.166 | 0.668 |
| 8 | 0.00195 | 0.00098 | 0.083 | 5.0 | 0.012 | 0.667 | 1.167 | 0.668 |
| 8 | 0.00098 | 0.00049 | 0.083 | 5.0 | 0.006 | 0.668 | 1.168 | 0.668 |
| 8 | 0.00049 | 0.00024 | 0.083 | 5.0 | 0.003 | 0.668 | 1.168 | 0.668 |

## SOLAR TRACKER CALCULATIONS

| Tube Height Inches | Hole Diameter Inches | Hole Radius r Inches | Angle (Theta) Degrees | Angle (Theta) Arcmin. | Focal Length y Inches | Transister Radius Inches | Needed Tube Radius Inches | IR Distance Inches |
|---|---|---|---|---|---|---|---|---|
| 10 | 1.00000 | 0.50000 | 1.000 | 60.0 | 0.321 | 15.074 | 15.574 | 15.574 |
| 10 | 0.75000 | 0.37500 | 1.000 | 60.0 | 0.241 | 15.199 | 15.699 | 15.574 |
| 10 | 0.50000 | 0.25000 | 1.000 | 60.0 | 0.161 | 15.324 | 15.824 | 15.574 |
| 10 | 0.25000 | 0.12500 | 1.000 | 60.0 | 0.080 | 15.449 | 15.949 | 15.574 |
| 10 | 0.12500 | 0.06250 | 1.000 | 60.0 | 0.040 | 15.512 | 16.012 | 15.574 |
| 10 | 0.06250 | 0.03125 | 1.000 | 60.0 | 0.020 | 15.543 | 16.043 | 15.574 |
| 10 | 0.03125 | 0.01563 | 1.000 | 60.0 | 0.010 | 15.558 | 16.058 | 15.574 |
| 10 | 0.01563 | 0.00781 | 1.000 | 60.0 | 0.005 | 15.566 | 16.066 | 15.574 |
| 10 | 0.00781 | 0.00391 | 1.000 | 60.0 | 0.003 | 15.570 | 16.070 | 15.574 |
| 10 | 0.00391 | 0.00195 | 1.000 | 60.0 | 0.001 | 15.572 | 16.072 | 15.574 |
| 10 | 0.00195 | 0.00098 | 1.000 | 60.0 | 0.001 | 15.573 | 16.073 | 15.574 |
| 10 | 0.00098 | 0.00049 | 1.000 | 60.0 | 0.000 | 15.574 | 16.074 | 15.574 |
| 10 | 0.00049 | 0.00024 | 1.000 | 60.0 | 0.000 | 15.574 | 16.074 | 15.574 |

| Tube Height Inches | Hole Diameter Inches | Hole Radius r Inches | Angle (Theta) Degrees | Angle (Theta) Arcmin. | Focal Length y Inches | Transister Radius Inches | Needed Tube Radius Inches | IR Distance Inches |
|---|---|---|---|---|---|---|---|---|
| 10 | 1.00000 | 0.50000 | 0.500 | 30.0 | 0.915 | 4.963 | 5.463 | 5.463 |
| 10 | 0.75000 | 0.37500 | 0.500 | 30.0 | 0.686 | 5.088 | 5.588 | 5.463 |
| 10 | 0.50000 | 0.25000 | 0.500 | 30.0 | 0.458 | 5.213 | 5.713 | 5.463 |
| 10 | 0.25000 | 0.12500 | 0.500 | 30.0 | 0.229 | 5.338 | 5.838 | 5.463 |
| 10 | 0.12500 | 0.06250 | 0.500 | 30.0 | 0.114 | 5.401 | 5.901 | 5.463 |
| 10 | 0.06250 | 0.03125 | 0.500 | 30.0 | 0.057 | 5.432 | 5.932 | 5.463 |
| 10 | 0.03125 | 0.01563 | 0.500 | 30.0 | 0.029 | 5.447 | 5.947 | 5.463 |
| 10 | 0.01563 | 0.00781 | 0.500 | 30.0 | 0.014 | 5.455 | 5.955 | 5.463 |
| 10 | 0.00781 | 0.00391 | 0.500 | 30.0 | 0.007 | 5.459 | 5.959 | 5.463 |
| 10 | 0.00391 | 0.00195 | 0.500 | 30.0 | 0.004 | 5.461 | 5.961 | 5.463 |
| 10 | 0.00195 | 0.00098 | 0.500 | 30.0 | 0.002 | 5.462 | 5.962 | 5.463 |
| 10 | 0.00098 | 0.00049 | 0.500 | 30.0 | 0.001 | 5.463 | 5.963 | 5.463 |
| 10 | 0.00049 | 0.00024 | 0.500 | 30.0 | 0.000 | 5.463 | 5.963 | 5.463 |

| Tube Height Inches | Hole Diameter Inches | Hole Radius r Inches | Angle (Theta) Degrees | Angle (Theta) Arcmin. | Focal Length y Inches | Transister Radius Inches | Needed Tube Radius Inches | IR Distance Inches |
|---|---|---|---|---|---|---|---|---|
| 10 | 1.00000 | 0.50000 | 0.250 | 15.0 | 1.958 | 2.053 | 2.553 | 2.553 |
| 10 | 0.75000 | 0.37500 | 0.250 | 15.0 | 1.469 | 2.178 | 2.678 | 2.553 |
| 10 | 0.50000 | 0.25000 | 0.250 | 15.0 | 0.979 | 2.303 | 2.803 | 2.553 |
| 10 | 0.25000 | 0.12500 | 0.250 | 15.0 | 0.490 | 2.428 | 2.928 | 2.553 |
| 10 | 0.12500 | 0.06250 | 0.250 | 15.0 | 0.245 | 2.491 | 2.991 | 2.553 |
| 10 | 0.06250 | 0.03125 | 0.250 | 15.0 | 0.122 | 2.522 | 3.022 | 2.553 |
| 10 | 0.03125 | 0.01563 | 0.250 | 15.0 | 0.061 | 2.538 | 3.038 | 2.553 |
| 10 | 0.01563 | 0.00781 | 0.250 | 15.0 | 0.031 | 2.546 | 3.046 | 2.553 |
| 10 | 0.00781 | 0.00391 | 0.250 | 15.0 | 0.015 | 2.550 | 3.050 | 2.553 |
| 10 | 0.00391 | 0.00195 | 0.250 | 15.0 | 0.008 | 2.551 | 3.051 | 2.553 |
| 10 | 0.00195 | 0.00098 | 0.250 | 15.0 | 0.004 | 2.552 | 3.052 | 2.553 |
| 10 | 0.00098 | 0.00049 | 0.250 | 15.0 | 0.002 | 2.553 | 3.053 | 2.553 |
| 10 | 0.00049 | 0.00024 | 0.250 | 15.0 | 0.001 | 2.553 | 3.053 | 2.553 |

| Tube Height Inches | Hole Diameter Inches | Hole Radius r Inches | Angle (Theta) Degrees | Angle (Theta) Arcmin. | Focal Length y Inches | Transister Radius Inches | Needed Tube Radius Inches | IR Distance Inches |
|---|---|---|---|---|---|---|---|---|
| 10 | 1.00000 | 0.50000 | 0.125 | 7.5 | 3.979 | 0.757 | 1.257 | 1.257 |
| 10 | 0.75000 | 0.37500 | 0.125 | 7.5 | 2.984 | 0.882 | 1.382 | 1.257 |
| 10 | 0.50000 | 0.25000 | 0.125 | 7.5 | 1.990 | 1.007 | 1.507 | 1.257 |
| 10 | 0.25000 | 0.12500 | 0.125 | 7.5 | 0.995 | 1.132 | 1.632 | 1.257 |
| 10 | 0.12500 | 0.06250 | 0.125 | 7.5 | 0.497 | 1.194 | 1.694 | 1.257 |
| 10 | 0.06250 | 0.03125 | 0.125 | 7.5 | 0.249 | 1.225 | 1.725 | 1.257 |
| 10 | 0.03125 | 0.01563 | 0.125 | 7.5 | 0.124 | 1.241 | 1.741 | 1.257 |
| 10 | 0.01563 | 0.00781 | 0.125 | 7.5 | 0.062 | 1.249 | 1.749 | 1.257 |
| 10 | 0.00781 | 0.00391 | 0.125 | 7.5 | 0.031 | 1.253 | 1.753 | 1.257 |
| 10 | 0.00391 | 0.00195 | 0.125 | 7.5 | 0.016 | 1.255 | 1.755 | 1.257 |
| 10 | 0.00195 | 0.00098 | 0.125 | 7.5 | 0.008 | 1.256 | 1.756 | 1.257 |
| 10 | 0.00098 | 0.00049 | 0.125 | 7.5 | 0.004 | 1.256 | 1.756 | 1.257 |
| 10 | 0.00049 | 0.00024 | 0.125 | 7.5 | 0.002 | 1.256 | 1.756 | 1.257 |

| Tube Height Inches | Hole Diameter Inches | Hole Radius r Inches | Angle (Theta) Degrees | Angle (Theta) Arcmin. | Focal Length y Inches | Transister Radius Inches | Needed Tube Radius Inches | IR Distance Inches |
|---|---|---|---|---|---|---|---|---|
| 10 | 1.00000 | 0.50000 | 0.083 | 5.0 | 5.986 | 0.335 | 0.835 | 0.835 |
| 10 | 0.75000 | 0.37500 | 0.083 | 5.0 | 4.490 | 0.460 | 0.960 | 0.835 |
| 10 | 0.50000 | 0.25000 | 0.083 | 5.0 | 2.993 | 0.585 | 1.085 | 0.835 |
| 10 | 0.25000 | 0.12500 | 0.083 | 5.0 | 1.497 | 0.710 | 1.210 | 0.835 |
| 10 | 0.12500 | 0.06250 | 0.083 | 5.0 | 0.748 | 0.773 | 1.273 | 0.835 |
| 10 | 0.06250 | 0.03125 | 0.083 | 5.0 | 0.374 | 0.804 | 1.304 | 0.835 |
| 10 | 0.03125 | 0.01563 | 0.083 | 5.0 | 0.187 | 0.820 | 1.320 | 0.835 |
| 10 | 0.01563 | 0.00781 | 0.083 | 5.0 | 0.094 | 0.827 | 1.327 | 0.835 |
| 10 | 0.00781 | 0.00391 | 0.083 | 5.0 | 0.047 | 0.831 | 1.331 | 0.835 |
| 10 | 0.00391 | 0.00195 | 0.083 | 5.0 | 0.023 | 0.833 | 1.333 | 0.835 |
| 10 | 0.00195 | 0.00098 | 0.083 | 5.0 | 0.012 | 0.834 | 1.334 | 0.835 |
| 10 | 0.00098 | 0.00049 | 0.083 | 5.0 | 0.006 | 0.835 | 1.335 | 0.835 |
| 10 | 0.00049 | 0.00024 | 0.083 | 5.0 | 0.003 | 0.835 | 1.335 | 0.835 |

SOLAR TRACKER CALCULATIONS

| Tube Height Inches | Hole Diameter Inches | Hole Radius r Inches | Angle (Theta) Degrees | Angle (Theta) Arcmin. | Focal Length y Inches | Transister Radius Inches | Needed Tube Radius Inches | IR Distance Inches |
|---|---|---|---|---|---|---|---|---|
| 12 | 1.00000 | 0.50000 | 1.000 | 60.0 | 0.321 | 18.189 | 18.689 | 18.689 |
| 12 | 0.75000 | 0.37500 | 1.000 | 60.0 | 0.241 | 18.314 | 18.814 | 18.689 |
| 12 | 0.50000 | 0.25000 | 1.000 | 60.0 | 0.161 | 18.439 | 18.939 | 18.689 |
| 12 | 0.25000 | 0.12500 | 1.000 | 60.0 | 0.080 | 18.564 | 19.064 | 18.689 |
| 12 | 0.12500 | 0.06250 | 1.000 | 60.0 | 0.040 | 18.626 | 19.126 | 18.689 |
| 12 | 0.06250 | 0.03125 | 1.000 | 60.0 | 0.020 | 18.658 | 19.158 | 18.689 |
| 12 | 0.03125 | 0.01563 | 1.000 | 60.0 | 0.010 | 18.673 | 19.173 | 18.689 |
| 12 | 0.01563 | 0.00781 | 1.000 | 60.0 | 0.005 | 18.681 | 19.181 | 18.689 |
| 12 | 0.00781 | 0.00391 | 1.000 | 60.0 | 0.003 | 18.685 | 19.185 | 18.689 |
| 12 | 0.00391 | 0.00195 | 1.000 | 60.0 | 0.001 | 18.687 | 19.187 | 18.689 |
| 12 | 0.00195 | 0.00098 | 1.000 | 60.0 | 0.001 | 18.688 | 19.188 | 18.689 |
| 12 | 0.00098 | 0.00049 | 1.000 | 60.0 | 0.000 | 18.688 | 19.188 | 18.689 |
| 12 | 0.00049 | 0.00024 | 1.000 | 60.0 | 0.000 | 18.689 | 19.189 | 18.689 |
| | | | | | | | | |
| | | | | | | | | |
| Tube Height Inches | Hole Diameter Inches | Hole Radius r Inches | Angle (Theta) Degrees | Angle (Theta) Arcmin. | Focal Length y Inches | Transister Radius Inches | Needed Tube Radius Inches | IR Distance Inches |
| 12 | 1.00000 | 0.50000 | 0.500 | 30.0 | 0.915 | 6.056 | 6.556 | 6.556 |
| 12 | 0.75000 | 0.37500 | 0.500 | 30.0 | 0.686 | 6.181 | 6.681 | 6.556 |
| 12 | 0.50000 | 0.25000 | 0.500 | 30.0 | 0.458 | 6.306 | 6.806 | 6.556 |
| 12 | 0.25000 | 0.12500 | 0.500 | 30.0 | 0.229 | 6.431 | 6.931 | 6.556 |
| 12 | 0.12500 | 0.06250 | 0.500 | 30.0 | 0.114 | 6.493 | 6.993 | 6.556 |
| 12 | 0.06250 | 0.03125 | 0.500 | 30.0 | 0.057 | 6.524 | 7.024 | 6.556 |
| 12 | 0.03125 | 0.01563 | 0.500 | 30.0 | 0.029 | 6.540 | 7.040 | 6.556 |
| 12 | 0.01563 | 0.00781 | 0.500 | 30.0 | 0.014 | 6.548 | 7.048 | 6.556 |
| 12 | 0.00781 | 0.00391 | 0.500 | 30.0 | 0.007 | 6.552 | 7.052 | 6.556 |
| 12 | 0.00391 | 0.00195 | 0.500 | 30.0 | 0.004 | 6.554 | 7.054 | 6.556 |
| 12 | 0.00195 | 0.00098 | 0.500 | 30.0 | 0.002 | 6.555 | 7.055 | 6.556 |
| 12 | 0.00098 | 0.00049 | 0.500 | 30.0 | 0.001 | 6.555 | 7.055 | 6.556 |
| 12 | 0.00049 | 0.00024 | 0.500 | 30.0 | 0.000 | 6.555 | 7.055 | 6.556 |
| | | | | | | | | |
| | | | | | | | | |
| Tube Height Inches | Hole Diameter Inches | Hole Radius r Inches | Angle (Theta) Degrees | Angle (Theta) Arcmin. | Focal Length y Inches | Transister Radius Inches | Needed Tube Radius Inches | IR Distance Inches |
| 12 | 1.00000 | 0.50000 | 0.250 | 15.0 | 1.958 | 2.564 | 3.064 | 3.064 |
| 12 | 0.75000 | 0.37500 | 0.250 | 15.0 | 1.469 | 2.689 | 3.189 | 3.064 |
| 12 | 0.50000 | 0.25000 | 0.250 | 15.0 | 0.979 | 2.814 | 3.314 | 3.064 |
| 12 | 0.25000 | 0.12500 | 0.250 | 15.0 | 0.490 | 2.939 | 3.439 | 3.064 |
| 12 | 0.12500 | 0.06250 | 0.250 | 15.0 | 0.245 | 3.002 | 3.502 | 3.064 |
| 12 | 0.06250 | 0.03125 | 0.250 | 15.0 | 0.122 | 3.033 | 3.533 | 3.064 |
| 12 | 0.03125 | 0.01563 | 0.250 | 15.0 | 0.061 | 3.048 | 3.548 | 3.064 |
| 12 | 0.01563 | 0.00781 | 0.250 | 15.0 | 0.031 | 3.056 | 3.556 | 3.064 |
| 12 | 0.00781 | 0.00391 | 0.250 | 15.0 | 0.015 | 3.060 | 3.560 | 3.064 |
| 12 | 0.00391 | 0.00195 | 0.250 | 15.0 | 0.008 | 3.062 | 3.562 | 3.064 |
| 12 | 0.00195 | 0.00098 | 0.250 | 15.0 | 0.004 | 3.063 | 3.563 | 3.064 |
| 12 | 0.00098 | 0.00049 | 0.250 | 15.0 | 0.002 | 3.064 | 3.564 | 3.064 |
| 12 | 0.00049 | 0.00024 | 0.250 | 15.0 | 0.001 | 3.064 | 3.564 | 3.064 |
| | | | | | | | | |
| | | | | | | | | |
| Tube Height Inches | Hole Diameter Inches | Hole Radius r Inches | Angle (Theta) Degrees | Angle (Theta) Arcmin. | Focal Length y Inches | Transister Radius Inches | Needed Tube Radius Inches | IR Distance Inches |
| 12 | 1.00000 | 0.50000 | 0.125 | 7.5 | 3.979 | 1.008 | 1.508 | 1.508 |
| 12 | 0.75000 | 0.37500 | 0.125 | 7.5 | 2.984 | 1.133 | 1.633 | 1.508 |
| 12 | 0.50000 | 0.25000 | 0.125 | 7.5 | 1.990 | 1.258 | 1.758 | 1.508 |
| 12 | 0.25000 | 0.12500 | 0.125 | 7.5 | 0.995 | 1.383 | 1.883 | 1.508 |
| 12 | 0.12500 | 0.06250 | 0.125 | 7.5 | 0.497 | 1.445 | 1.945 | 1.508 |
| 12 | 0.06250 | 0.03125 | 0.125 | 7.5 | 0.249 | 1.477 | 1.977 | 1.508 |
| 12 | 0.03125 | 0.01563 | 0.125 | 7.5 | 0.124 | 1.492 | 1.992 | 1.508 |
| 12 | 0.01563 | 0.00781 | 0.125 | 7.5 | 0.062 | 1.500 | 2.000 | 1.508 |
| 12 | 0.00781 | 0.00391 | 0.125 | 7.5 | 0.031 | 1.504 | 2.004 | 1.508 |
| 12 | 0.00391 | 0.00195 | 0.125 | 7.5 | 0.016 | 1.506 | 2.006 | 1.508 |
| 12 | 0.00195 | 0.00098 | 0.125 | 7.5 | 0.008 | 1.507 | 2.007 | 1.508 |
| 12 | 0.00098 | 0.00049 | 0.125 | 7.5 | 0.004 | 1.507 | 2.007 | 1.508 |
| 12 | 0.00049 | 0.00024 | 0.125 | 7.5 | 0.002 | 1.508 | 2.008 | 1.508 |
| | | | | | | | | |
| | | | | | | | | |
| Tube Height Inches | Hole Diameter Inches | Hole Radius r Inches | Angle (Theta) Degrees | Angle (Theta) Arcmin. | Focal Length y Inches | Transister Radius Inches | Needed Tube Radius Inches | IR Distance Inches |
| 12 | 1.00000 | 0.50000 | 0.083 | 5.0 | 5.986 | 0.502 | 1.002 | 1.002 |
| 12 | 0.75000 | 0.37500 | 0.083 | 5.0 | 4.490 | 0.627 | 1.127 | 1.002 |
| 12 | 0.50000 | 0.25000 | 0.083 | 5.0 | 2.993 | 0.752 | 1.252 | 1.002 |
| 12 | 0.25000 | 0.12500 | 0.083 | 5.0 | 1.497 | 0.877 | 1.377 | 1.002 |
| 12 | 0.12500 | 0.06250 | 0.083 | 5.0 | 0.748 | 0.940 | 1.440 | 1.002 |
| 12 | 0.06250 | 0.03125 | 0.083 | 5.0 | 0.374 | 0.971 | 1.471 | 1.002 |
| 12 | 0.03125 | 0.01563 | 0.083 | 5.0 | 0.187 | 0.987 | 1.487 | 1.002 |
| 12 | 0.01563 | 0.00781 | 0.083 | 5.0 | 0.094 | 0.995 | 1.495 | 1.002 |
| 12 | 0.00781 | 0.00391 | 0.083 | 5.0 | 0.047 | 0.998 | 1.498 | 1.002 |
| 12 | 0.00391 | 0.00195 | 0.083 | 5.0 | 0.023 | 1.000 | 1.500 | 1.002 |
| 12 | 0.00195 | 0.00098 | 0.083 | 5.0 | 0.012 | 1.001 | 1.501 | 1.002 |
| 12 | 0.00098 | 0.00049 | 0.083 | 5.0 | 0.006 | 1.002 | 1.502 | 1.002 |
| 12 | 0.00049 | 0.00024 | 0.083 | 5.0 | 0.003 | 1.002 | 1.502 | 1.002 |

# Solar Tracking Device
# Completed Design

Top View

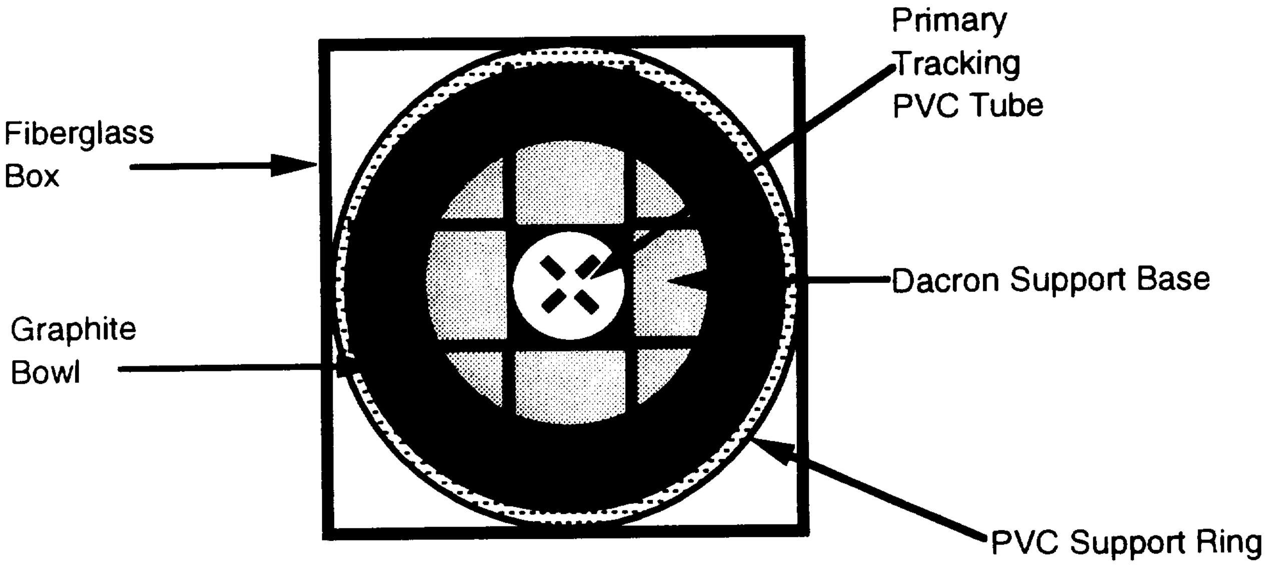
Primary
Tracking
PVC Tube
Fiberglass
Box
Dacron Support Base
Graphite
Bowl
PVC Support Ring

Side View

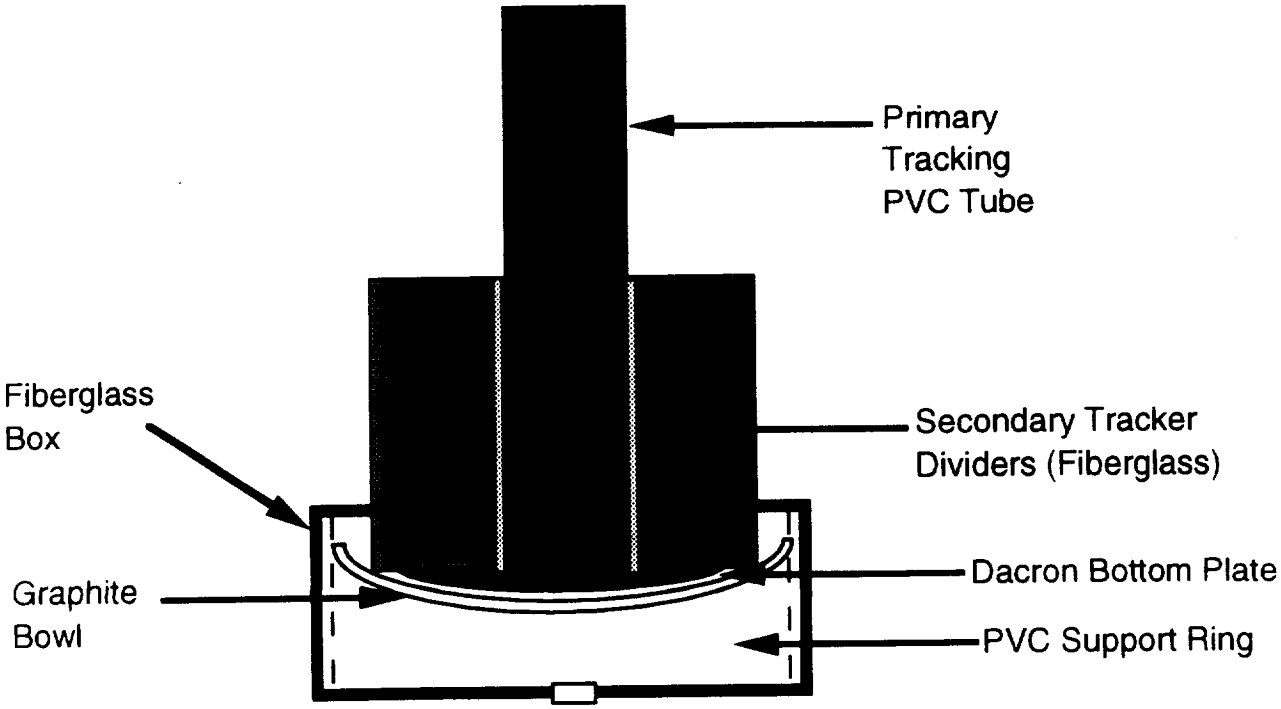
Primary
Tracking
PVC Tube
Fiberglass
Box
Secondary Tracker
Dividers (Fiberglass)
Dacron Bottom Plate
Graphite
Bowl
PVC Support Ring

# Final Completed Spring 1994 Design

## Primary Tracking System

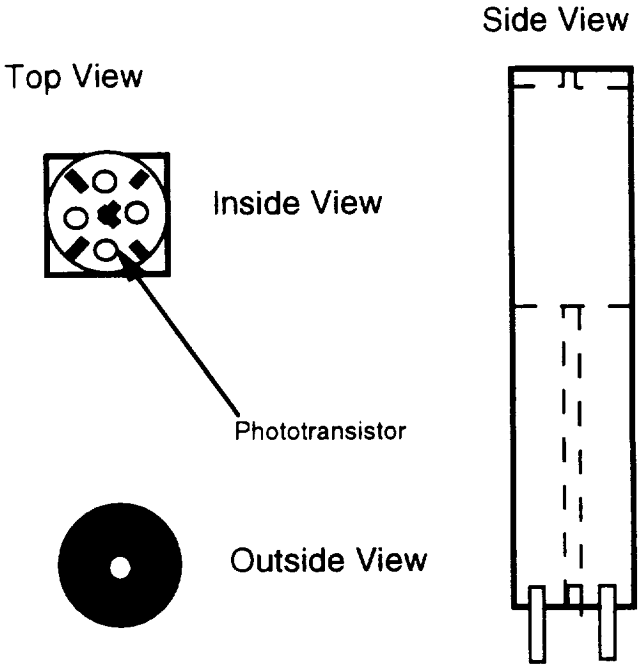
Side View
Top View
Inside View
Phototransistor
Outside View

## Secondary Tracking System

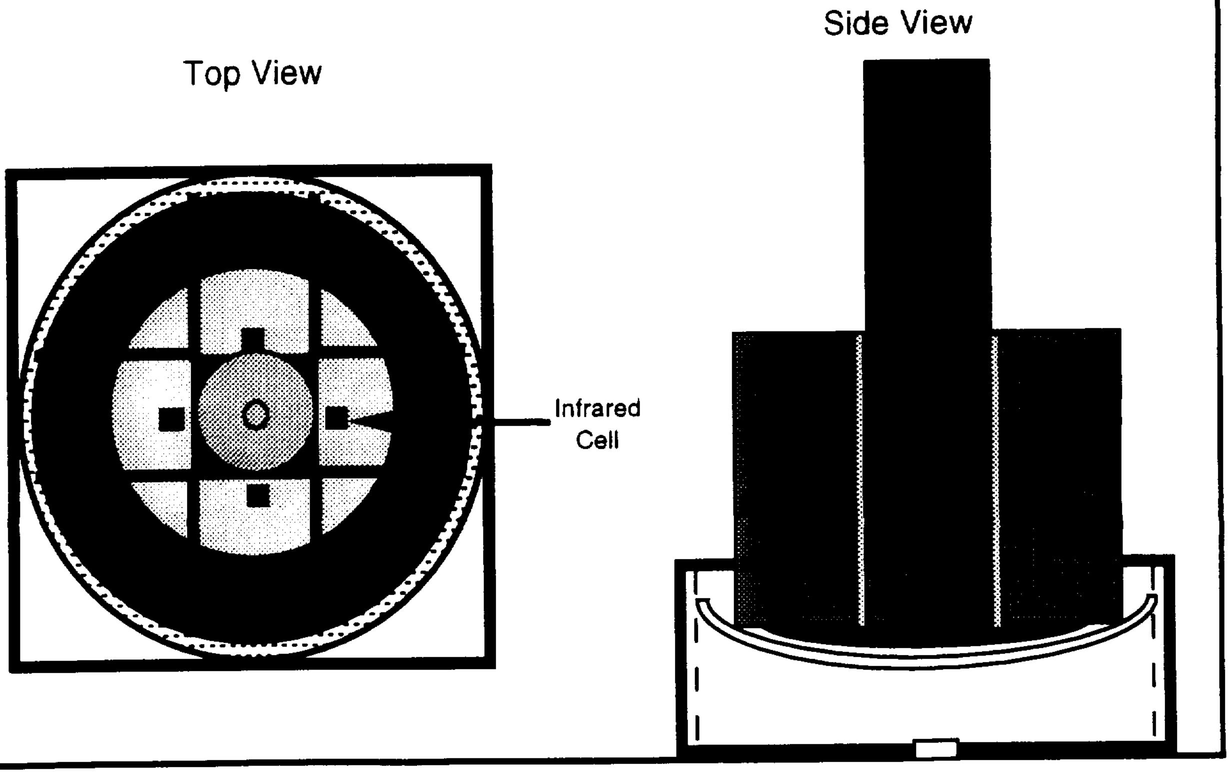
Side View
Top View
Infrared
Cell

# Solar Tracking Device
# Completed Design
# Dimensions

Top View

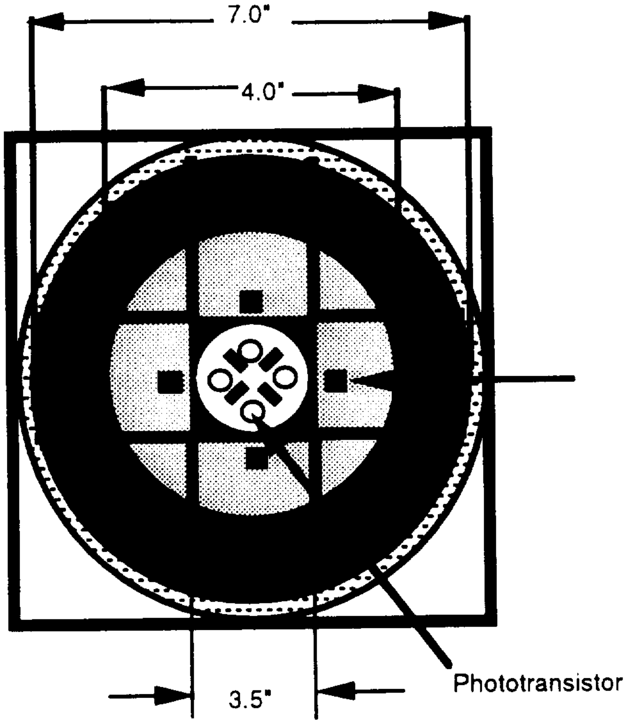

7.0"
4.0"
Phototransistor
3.5"

Side View

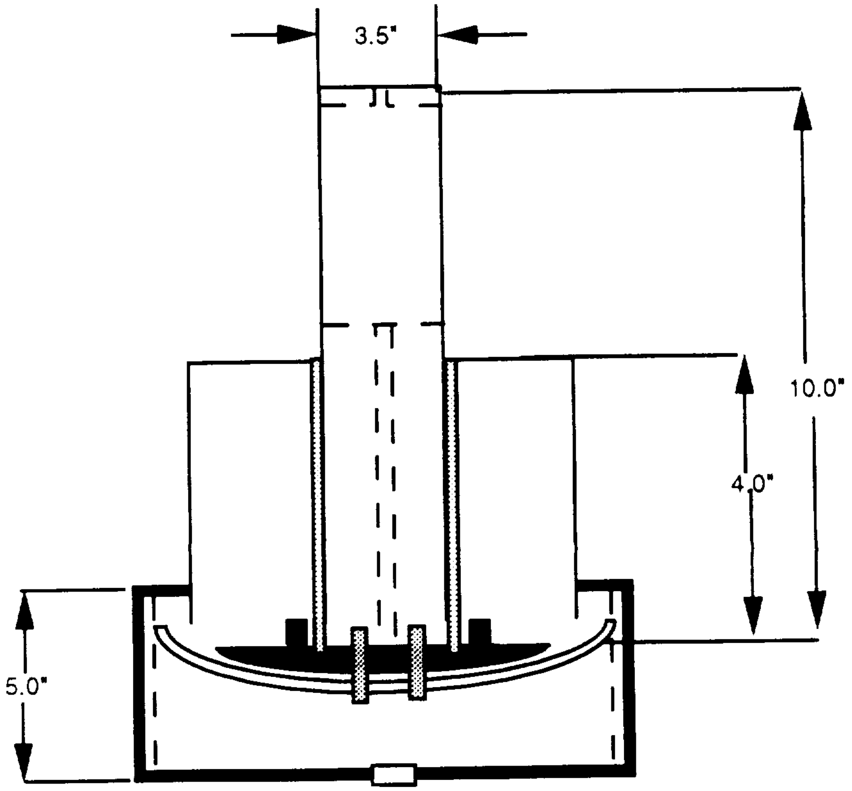

# Primary Tracker Plug Diagram and Dimensions

Top View

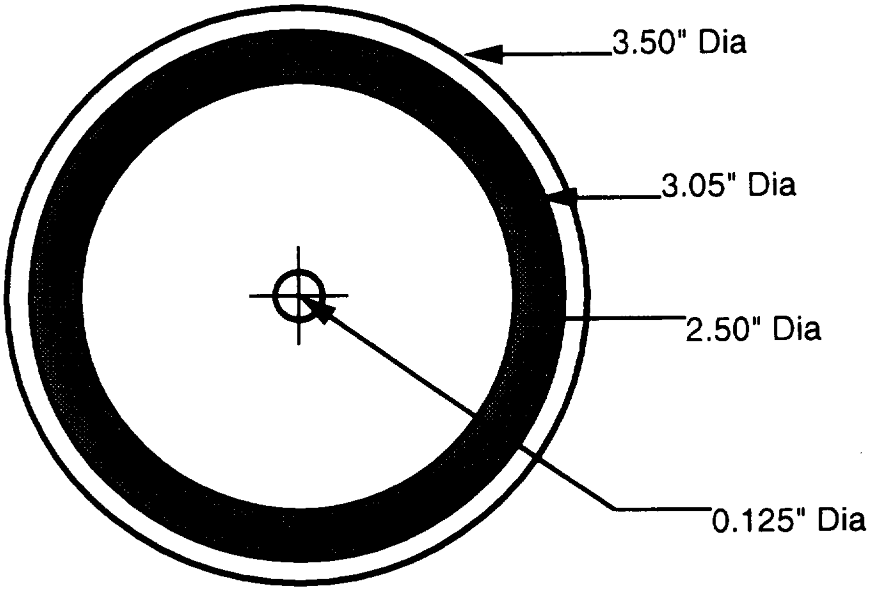
3.50" Dia
3.05" Dia
2.50" Dia
0.125" Dia

Side View

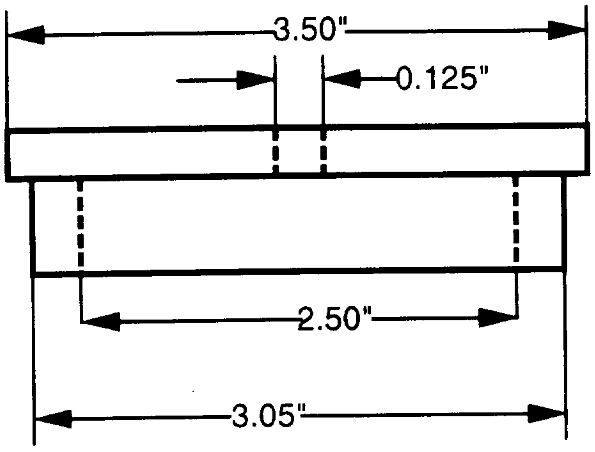
3.50"
0.125"
2.50"
3.05"

# Bottom Plate Design Dimensions

Top View

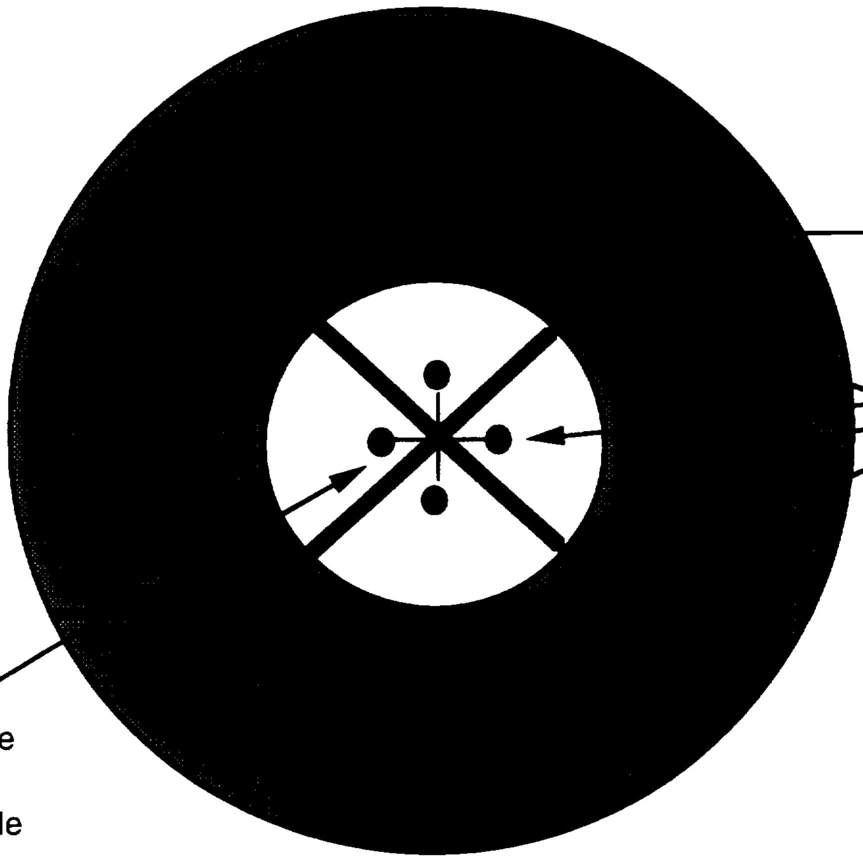

Divider Slots
0.125" Wide

Drill Holes
Evenly Spaced

Set Primary
Photocells
0.773" From
Center of
Tracker.

3.0" Dia
Inner Circle
6.0" Dia
Outer Circle

Side View

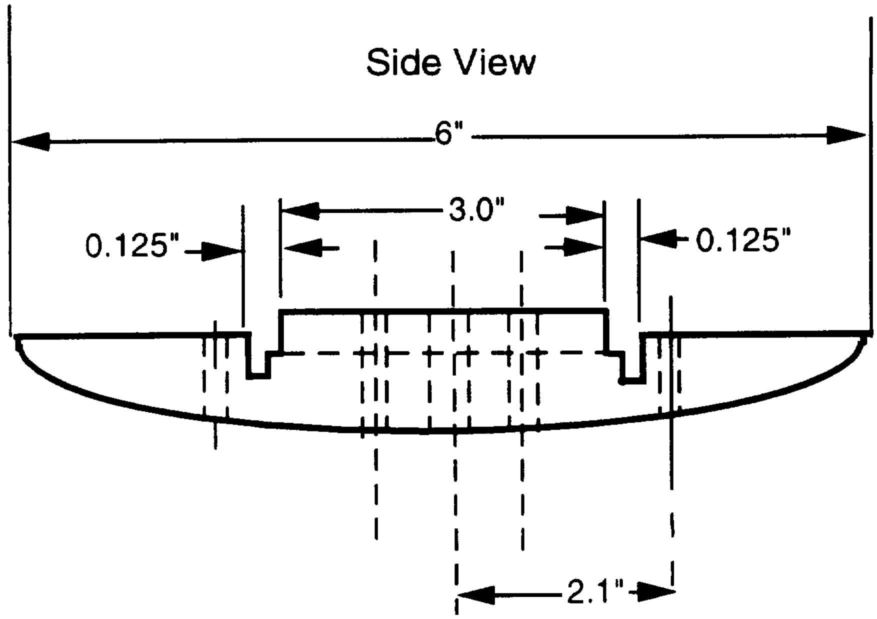

4201 SOUTH SANTA RITA

TUCSON, AZ 85714

602/741 1900

| FEDERAL I D NO | | |
|---|---|---|
| [illegible] | | |
| SHIP ORDER NO. | DATE | |
| 92 12601 11 | 11/16/93 | |
| TOTAL WEIGHT | TIME | P.C. |
| | 11:25 | 1 |

WE'VE COMPUTERIZED TO BETTER SERVE YOU!

SOLD TO
UNIVERSITY OF ARIZONA
STORES DEPT
P O BOX 40370
TUCSON AZ 85717

SHIP TO
AME DEPT
FUND# 407740
JEN JACKSON 621-6092

| ORDER TYPE | OUTSIDE SALESMAN NO. | CUSTOMER NUMBER | COPIES | CUSTOMER ORDER NO. | INSIDE S'MAN NO | CREDIT APPROVAL | TAX CODE | DATE SHIPPED | SHIPPED VIA |
|---|---|---|---|---|---|---|---|---|---|
| X | 82A0 | 82-460153-000 | 3 | 955771 | NZ | | T | 11/16/93 | CUSTOMER P U |

| LINE NO. | PART NUMBER | QUANTITY ORDERED | QUANTITY SHIPPED | QUANTITY BACK ORDERED | CATALOG NUMBER AND DESCRIPTION | TX | | UNIT OF MEAS. | |
|---|---|---|---|---|---|---|---|---|---|
| 1 | | 1 | [✓ 1] | | BLACK PLEX .250 X 16¼" X 28"<br>MANUAL-PCK 1 ____ $11.75 | | [redacted] | PC | [redacted] |
| 2 | | 1 | [✓ 1] | | BLACK PLEX .125 X 15.25" X 17" $3.10<br>MANUAL-PCK 1 ____ | | [redacted] | PC | [redacted] |
| 3 | | 1 | [✓ 1] | | BLACK DELRIN 1.00 X 11.75" X 12.50"<br>MANUAL-PCK 1 ____ $60.63 | | [redacted] | PC | [redacted] |

75.48

Tx 5.29

Tot. 80.77

THANK YOU FOR YOUR ORDER.
ANDREW SPIEL

1 PROMISE: 11 16/93 1208

[redacted]

RECEIVED BY X Jennifer J Jackson

PACKING LIST

I N V O I C E

| INVOICE NO. | PAGE |
|---|---|
| 2262 | 1 |

INVOICE DATE
04/05/94

**INVOICE**

Morgan

# CENTRONIC INC.
CENTRONIC
E-O DIVISION

2088 Anchor Court • Newbury Park, California 91320
(805) 499-5902 • FAX: (805) 499-7770

SOLD TO
UNIVERSITY OF ARIZONA
AERO/MECHANICAL ENGINEERING
AERONAUTICAL BLDG - ROOM 301
TUCSON, AZ 85721
USA

UNIVERSITY OF ARIZONA
AERO/MECHANICAL ENGINEERING
AERONAUTICAL BLDG - ROOM 30
TUCSON AZ 85721

ATTN: DAVID ROWNEY
JENNIFER JACKSON

UPS GROUND

| ORDER NO. | ORDER DATE | CUSTOMER | LOC. | REP | |
|---|---|---|---|---|---|
| 7117 | 04/05/94 | UOFAZ | NB | 999 | C7[illegible] |

| QTY. ORDER/B.O. | QTY. SHIPPED | ITEM NO./ DESCRIPTION | UNIT PRICE | UNIT | TOTAL PRICE |
|---|---|---|---|---|---|
| 4 | 4 | BPX-65<br>HIGH SPEED PHOTODIODE<br><br>DAVID ROWNEY / JENIFER JACKSON<br>602 621 6092 | 6.6000 | EA<br>.00 | 26.40 |

OK
M.S.

| | |
|---|---|
| TOTAL | 26.4 |
| MISC. CHARGES | .0 |
| FREIGHT | 8.0 |
| SALES TAX | .0 |
| TOTAL | 34.4 |
| PREPAID AMOUNT | 34.4 |
| BALANCE DUE | .0 |

COMMENTS

ORIGINAL PAGE IS OF POOR QUALITY

22

TERMS: Credit Card

FOB - NEWBURY PARK, CA

# Ultra High Speed Photodiodes BPX-65, AX65-R2F

The BPX65 is a high speed, high quality silicon photodetector which is manufactured in large quantity and offers an excellent price-to-performance ratio. Its high frequency response, sensitivity and low cost make the BPX65 suitable for applications including fiber optic communications, shaft encoders, computer light pens, and laser instrumentation.

The photodetector consists of a 1mm² active element mounted in a hermetically sealed TO-18 equivalent package. The cathode is connected to the case, although a special isolated version, the BPX65R, is available upon request. This device however utilizes a three-lead TO-18 package, unlike the two-lead version shown in the diagram.

This device is available in a special package for fiber optic applications (the AX65-R2F), with an epoxy covering (the X65-EB), or even in die form. Centronic can also supply the die in a special custom-designed package and manufacture the device to MIL SPEC.

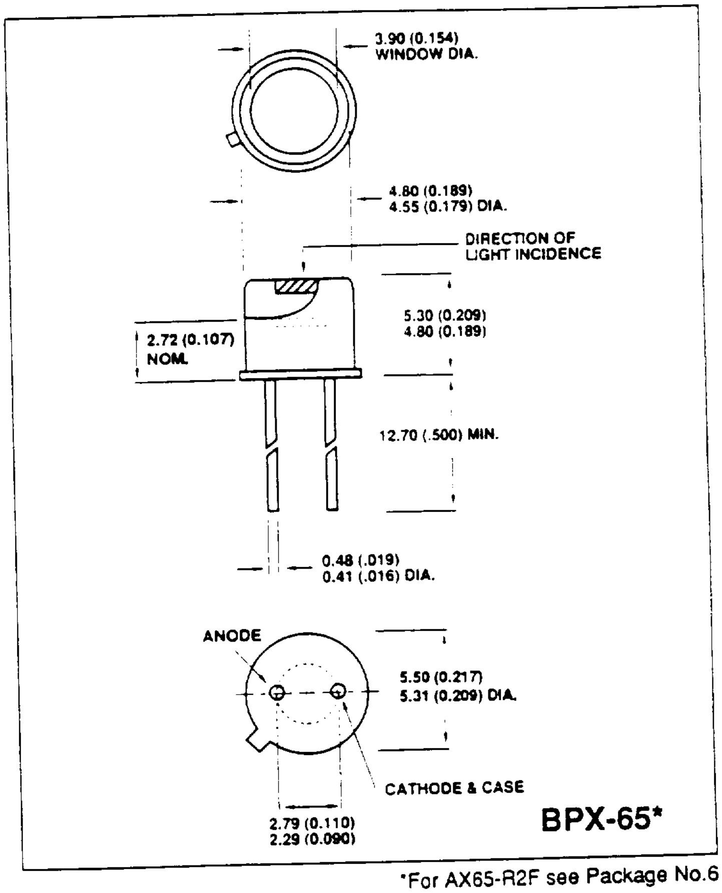

*For AX65-R2F see Package No.6

## ABSOLUTE MAXIMUM RATINGS

| | Max. Rating | Unit |
|---|---|---|
| Storage Temperature | -55 to +100 | °C |
| Operating Temperature | -40 to +80 | °C |
| Active Element Dimensions | 1 x 1 | mm |
| Recommended Wavelength Range | 400 to 1000 | nm |
| High Frequency Response | up to 100 | MHz |
| Field of View (BPX-65) | 74 | ° |

| ELECTRO-OPTICAL SPECIFICATIONS* | | MIN. | TYPICAL | MAX. | UNITS |
|---|---|---|---|---|---|
| Peak Sensitivity | | | | 850 | nm |
| Operating Voltage | | | | 30 | V |
| Power Dissipation (at 25°C) | | | | 250 | mW |
| Response Linearity (to better than 1%) | | | up to 7.5 | | mW/cm² |
| Responsivity at | 450nm | | 0.20 | | A/W |
| | at 900nm | 0.52 | 0.55 | | A/W |
| | at 1064nm | | 0.15 | | A/W |
| Risetime (measured at 900nm) (Vr-20V) | | | 3.5 | | ns |
| Capacitance (Vr = 0V) | | | 15 | | pF |
| Capacitance (Vr = 20V) | | | 3.5 | 4.0 | pF |
| Dark Current (Vr = 20V) | | | 1.0 | 5.0 | nA |
| NEP at 900nm (Vr = 20V) | | | $3.3 \times 10^{-14}$ | | $WHz^{-1/2}$ |
| Photosensitivity (at color temp of 2856°K) (Vr = 20V) | | | 6 | | nA/LUX |

*All the parameters are characteristic of a photodiode operating at 23°C, and connected to a load resistance of 50 ohms (where appropriate).

CENTRONIC INC.
2088 Anchor Court
Newbury Park, CA 91320
805-499-5902 • FAX: 805-499-7770

*For Sales and Technical Assistance Please Call:*
**805-499-5902**

ORIGINAL PAGE IS OF POOR QUALITY

D1

# Low Light Level Sensors OSD35-LR

Centronic low light level sensors are special large area silicon photodiodes (35mm$^2$) designed for circuits requiring a very high shunt resistance. These photodiodes are used with scintillation crystals for radiation detectors and for measuring fluorescence in gas and liquid analysis.

## ABSOLUTE MAXIMUM RATINGS

| | Max. Rating | Unit |
|---|---|---|
| DC Reverse Voltage | 50 | V |
| Storage Temperature Range | -45 to +100 | °C |
| Operating Temperature Range | -25 to +75 | °C |

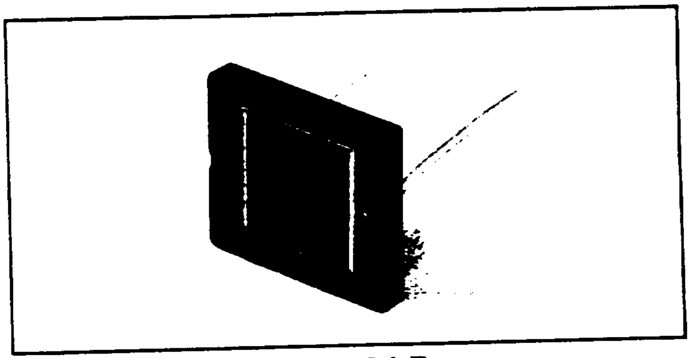

OSD35-LR

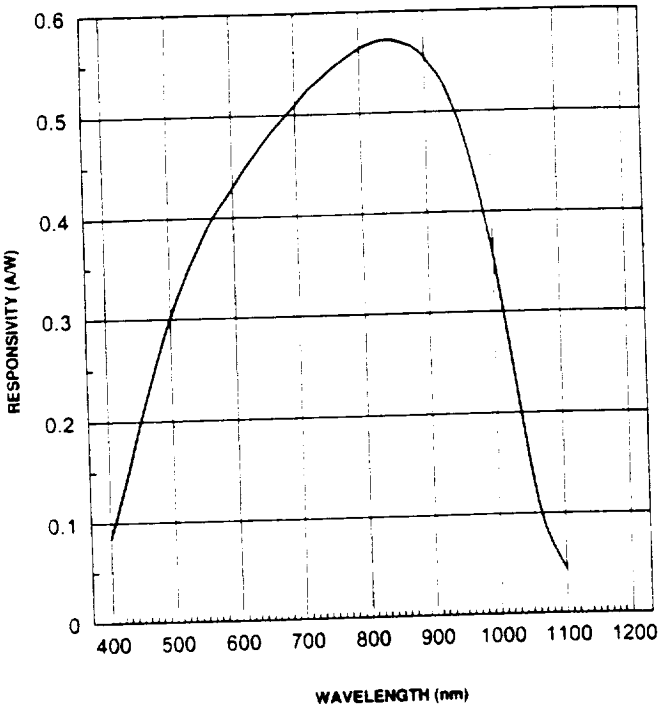

OSD35-LR - TYPICAL SPECTRAL RESPONSE

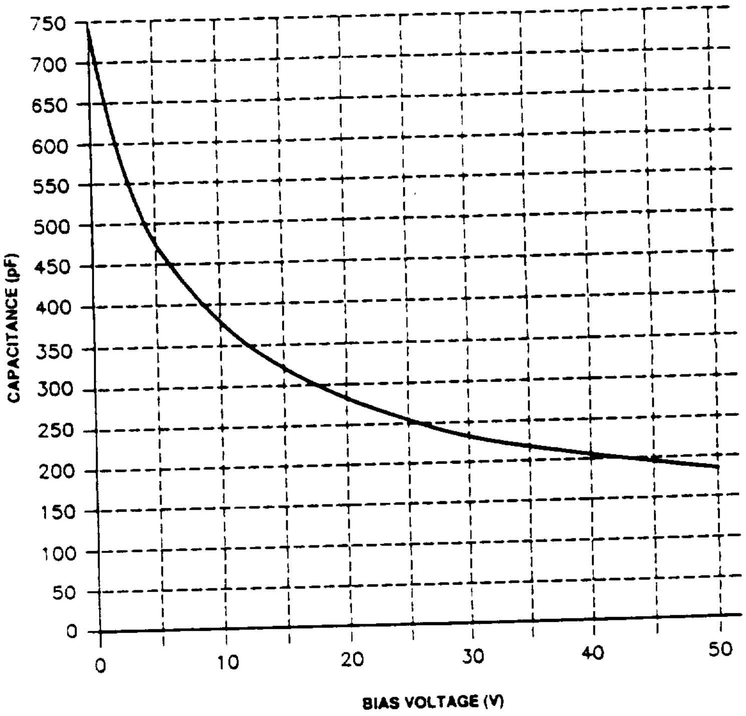

OSD35-LR - TYPICAL JUNCTION CAPACITANCE

## Electrical / Optical Specifications

Characteristics measured at 22° C (±2) ambient, unless otherwise stated.

**OSD35-LR responsivity tested at 900nm is .47A/W min., typical .54 A/W**

| Type No. | Active Area | | Dark Current pA at .010 Volts Max. | NEP WHz$^{-1/2}$ 900 nm | Capacitance pF | | Shunt Resistance Gigohms | | Package |
|---|---|---|---|---|---|---|---|---|---|
| | mm² | mm | | Typ. | Vr=0V Typ. | Vr=12V Max. | Min. | Typ. | |
| OSD35-LR-A | 35 | 6 x 6 | 5 | 1.0 x 10$^{-13}$ | 1000 | 400 | 2 | 5 | 32 |
| OSD35-LR-B | 35 | 6 x 6 | 10 | 1.0 x 10$^{-13}$ | 1000 | 400 | 1 | 3 | 32 |
| OSD35-LR-C | 35 | 6 x 6 | 20 | 1.0 x 10$^{-13}$ | 1000 | 400 | .5 | 1 | 32 |
| OSD35-LR-D | 35 | 6 x 6 | 100 | 1.0 x 10$^{-13}$ | 1000 | 400 | .1 | .5 | 32 |

CENTRONIC

CENTRONIC INC.
2088 Anchor Court
Newbury Park, CA 91320
805-499-5902 • FAX: 805-499-7770

*For Sales and Technical Assistance Please Call:*

**805-499-5902**

For use in Allowing in Infrared

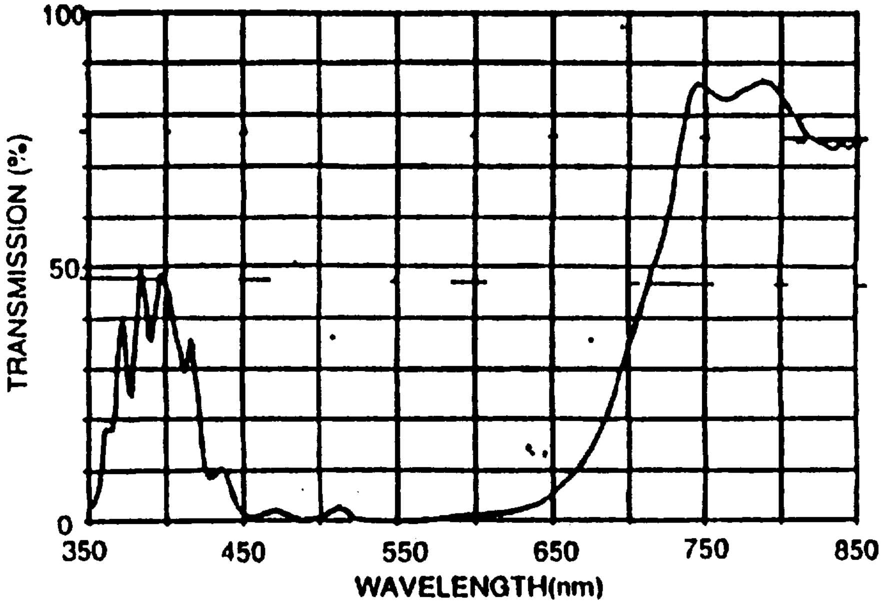

## HOW TO REFLEC
## WITHOUT THE HE
## USE A “COLD” M

Now you can safely b
systems without worry
build-up. This 4" x 5" gl
reflect 90% of visib
allowing 80% trans
waves to pass throug
the reflected beam.
thick glass to allow cu
size, the “cold” mirr
microscopy, specime
lighting systems, or any other application where high temperature lighting
Mirror will function satisfactorily and will not be damaged by exposure
temperature of -50°F and +450°F.

**Cold Mirror** **D4**

ORIGINAL PAGE IS
OF POOR QUALITY

PRECEDING PAGE BLANK NOT FILMED

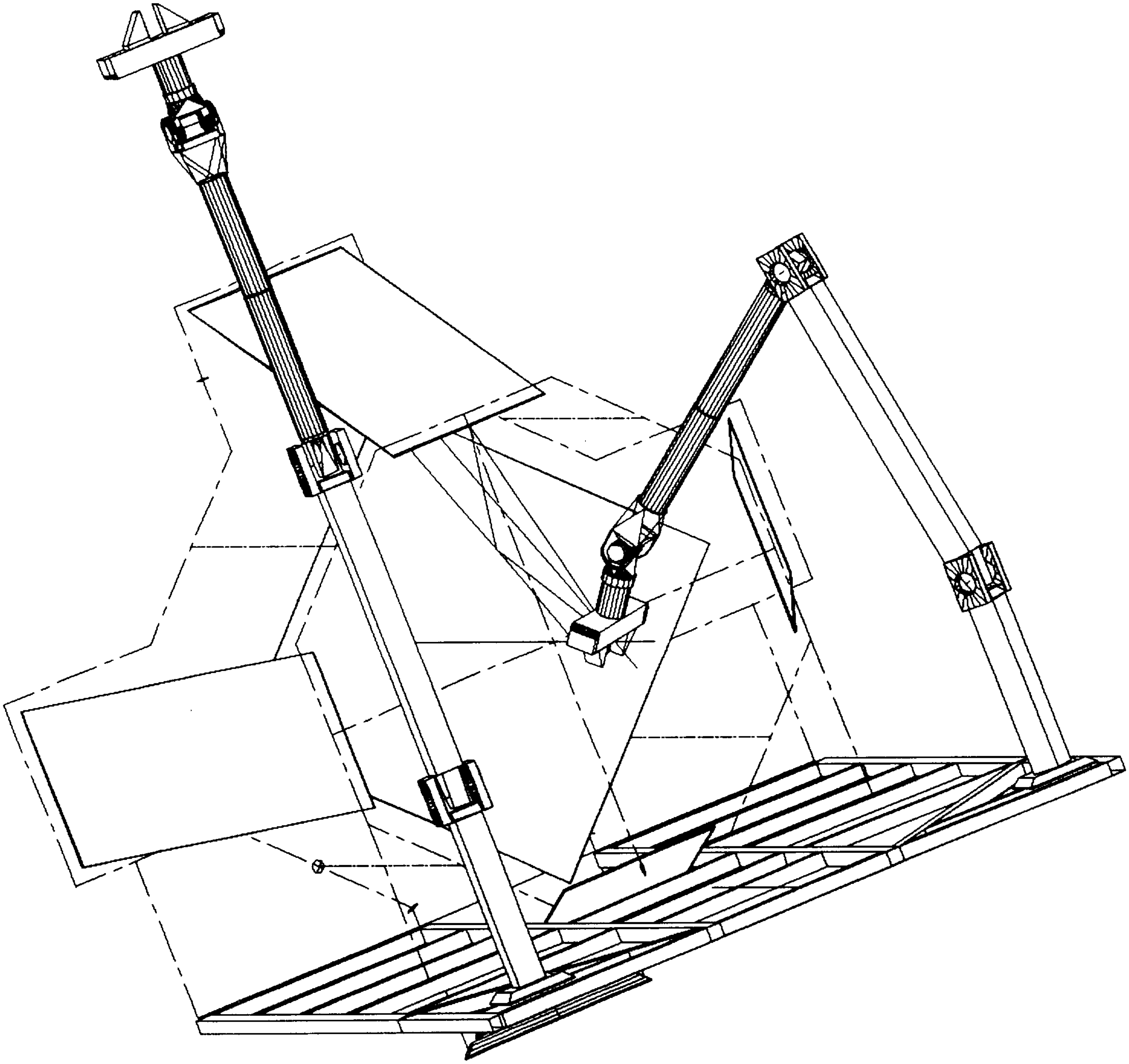

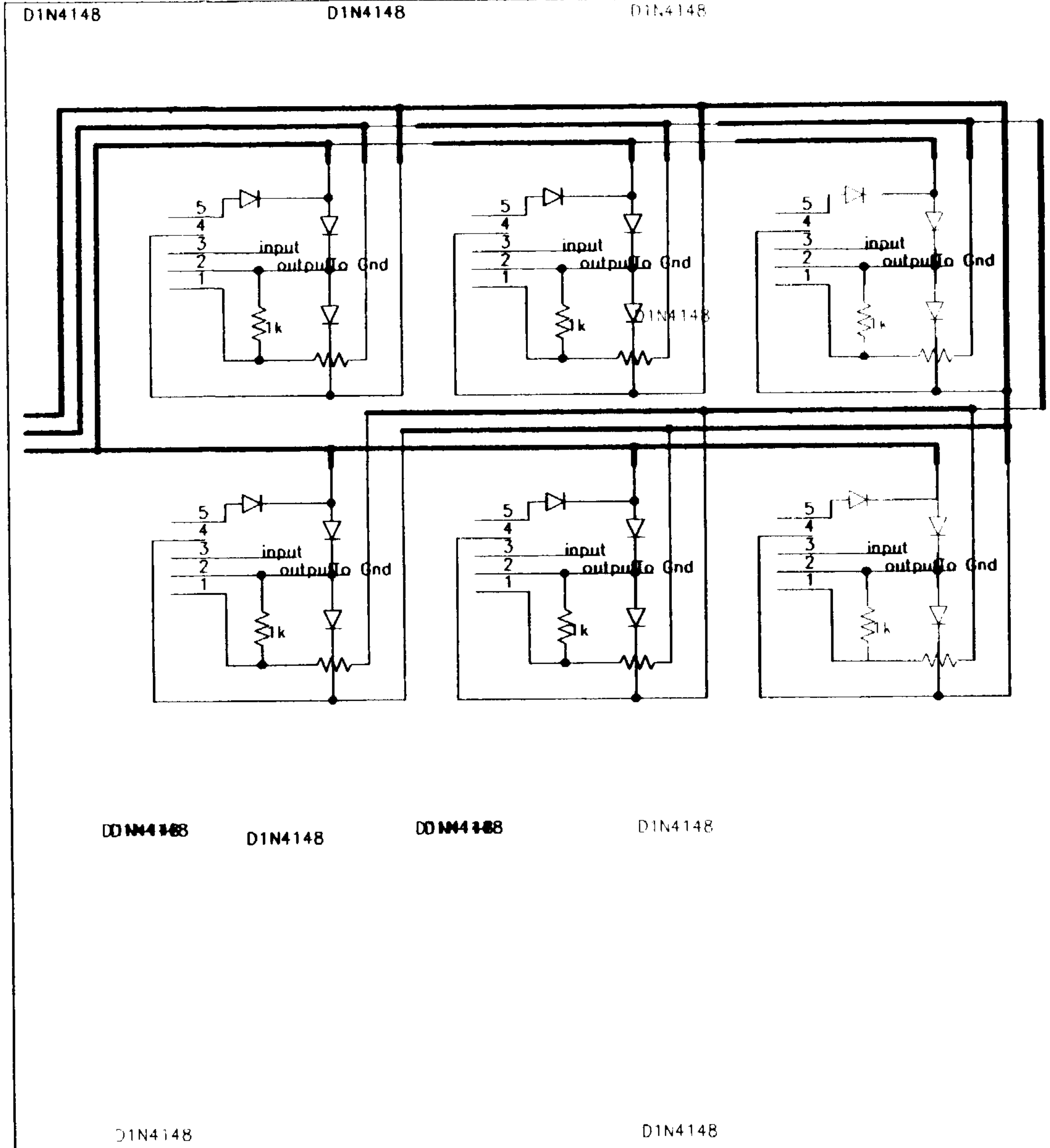
D1N4148
D1N4148
D1N4148
5
4
3
2
1
input
output
To Gnd
1k
D1N4148
D1N4148
D1N4148
D1N4148
D1N4148
D1N4148
D1N4148

University of Arizona Mechanical Engr.
Tucson, Arizona 85711
Irvine, CA 92718
Project: AME 302 Operational Amps

**Page Size:** **A**

**Revision:** –

**January** 1990 **Page** 1 of 1

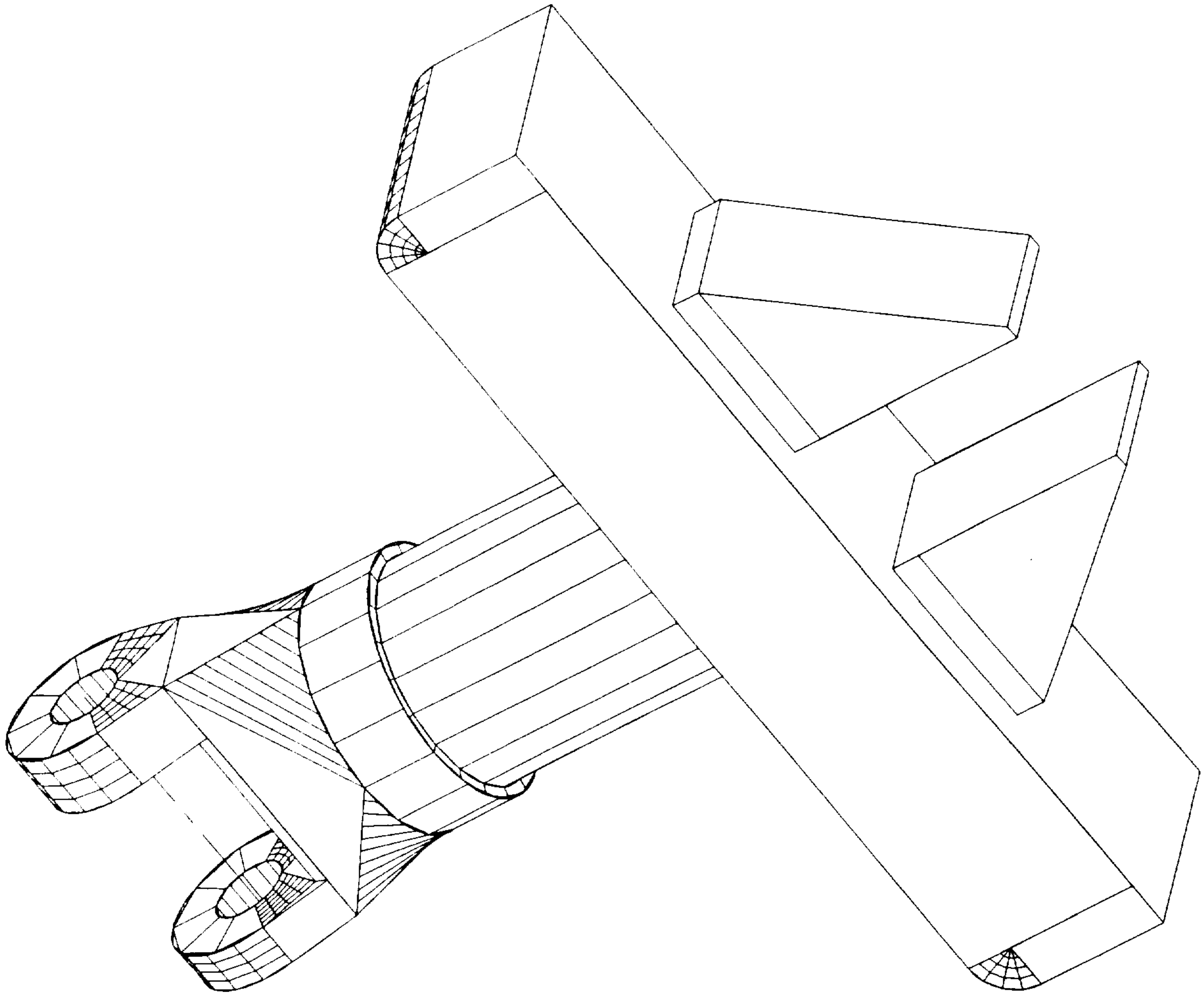

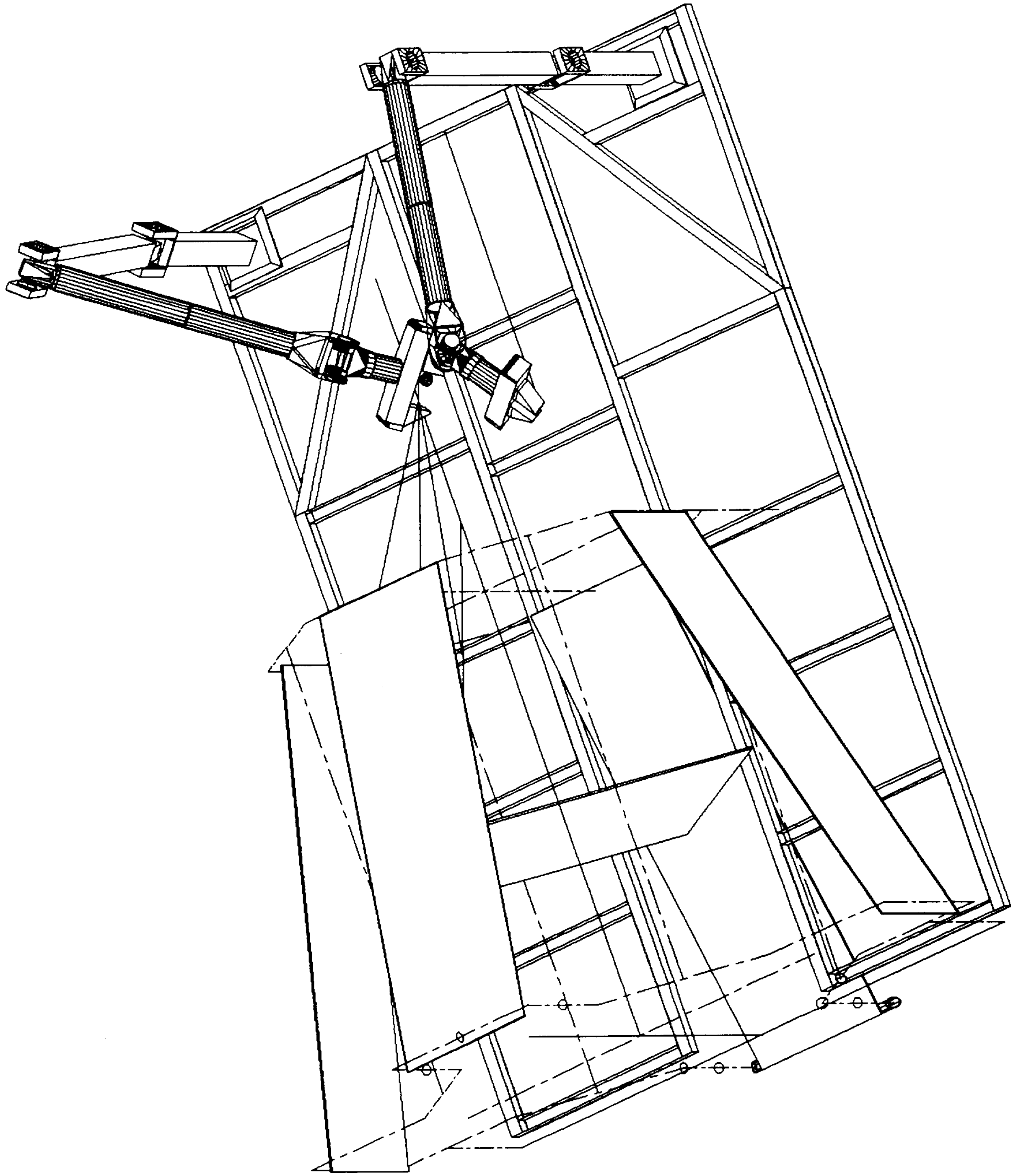

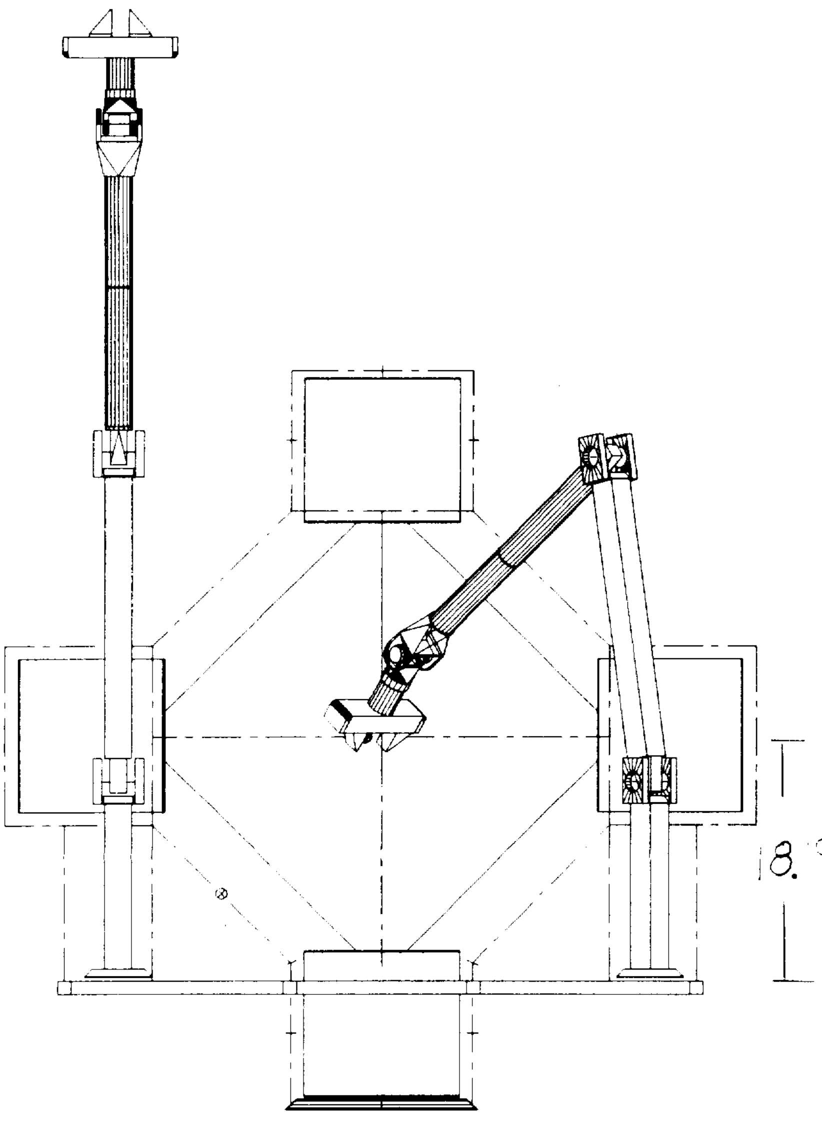
18.9"

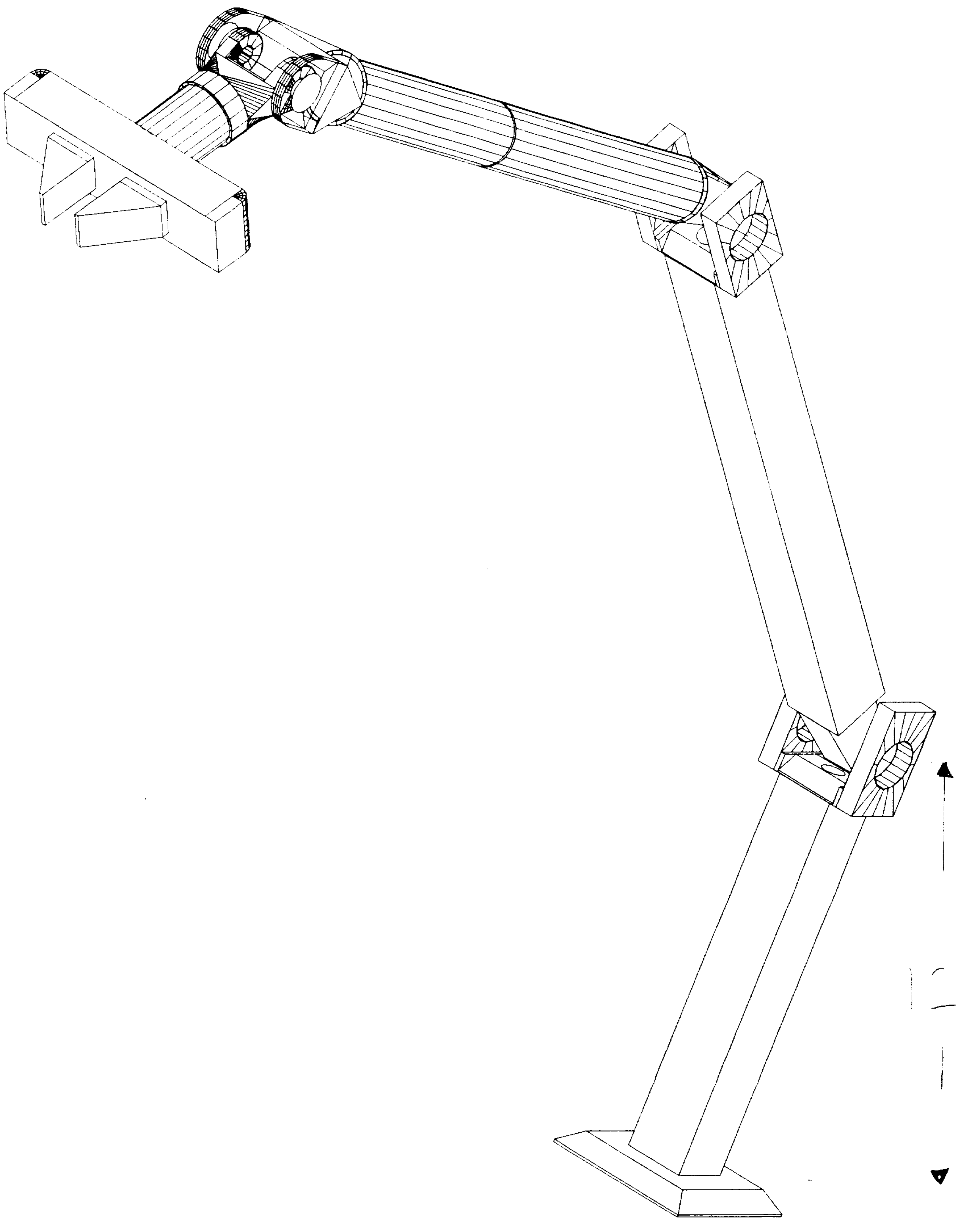
12"

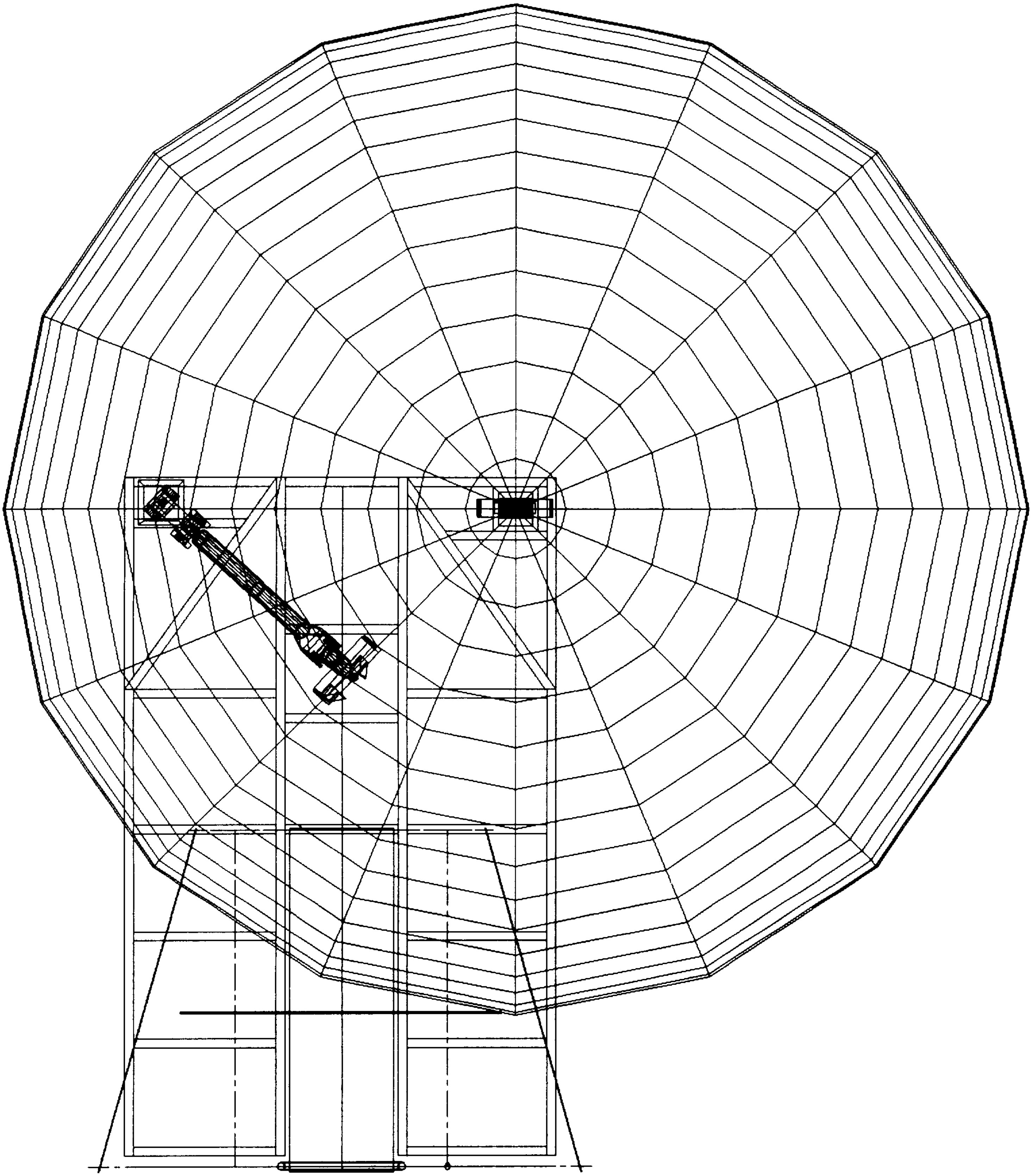

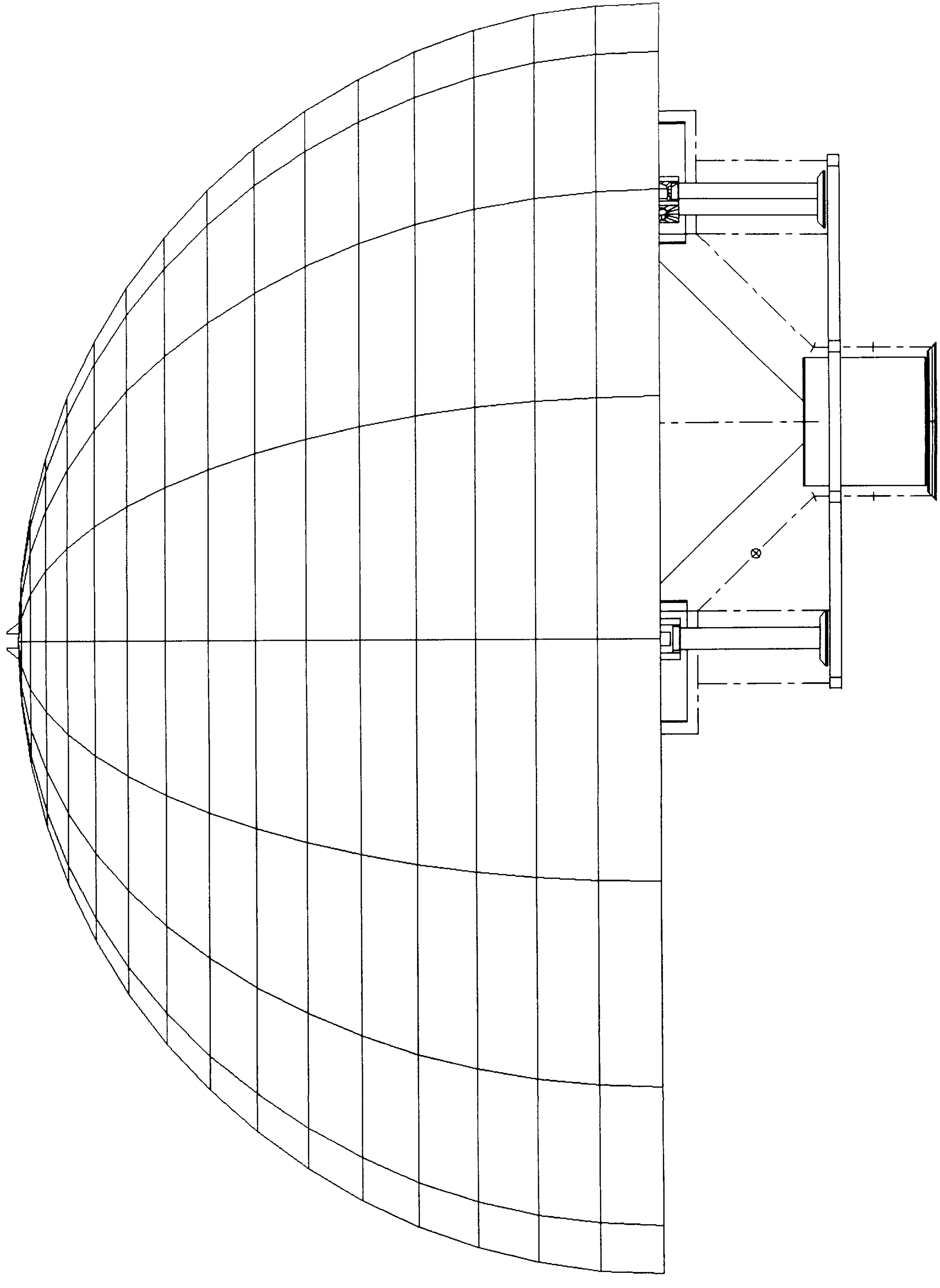

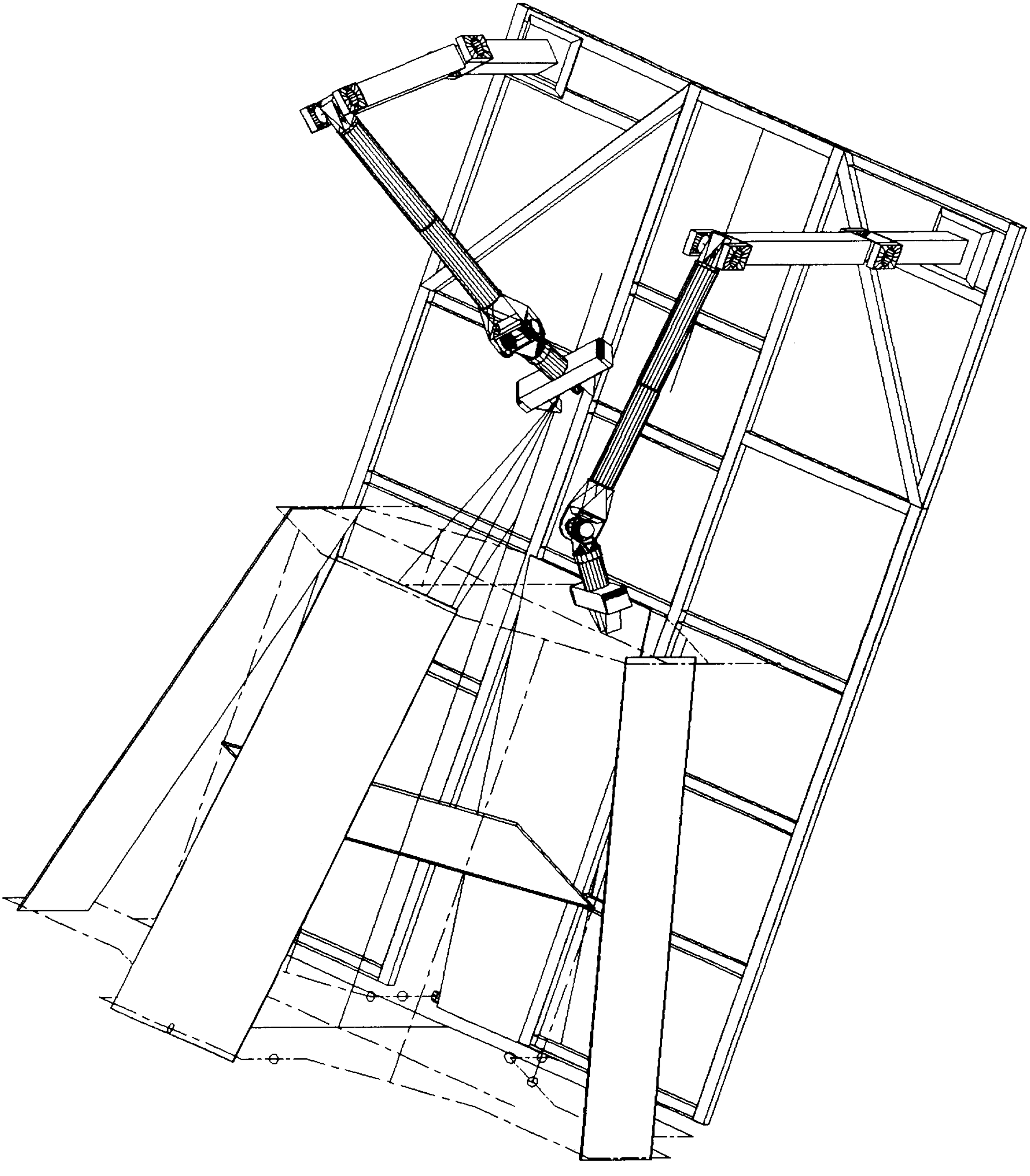

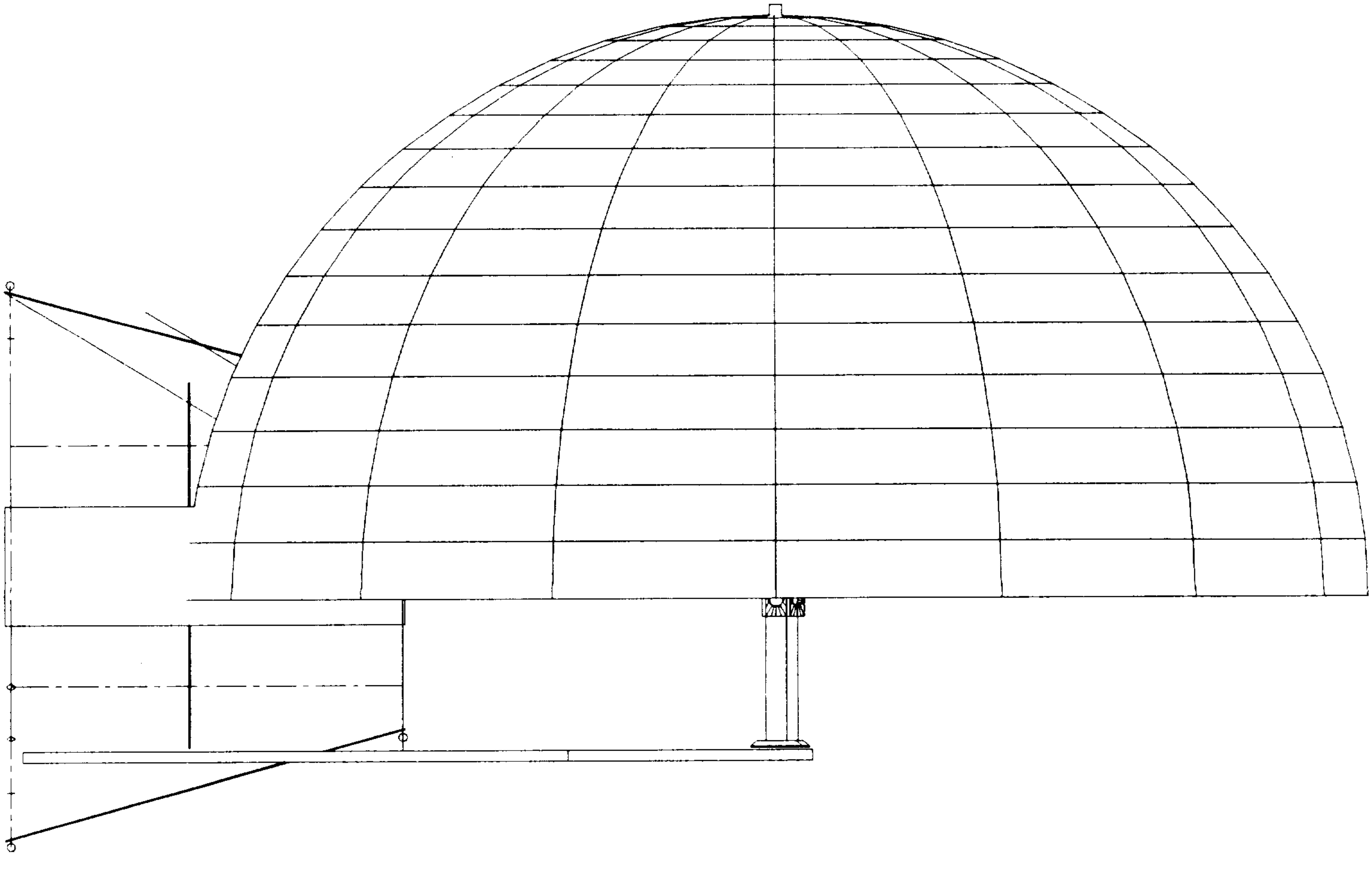

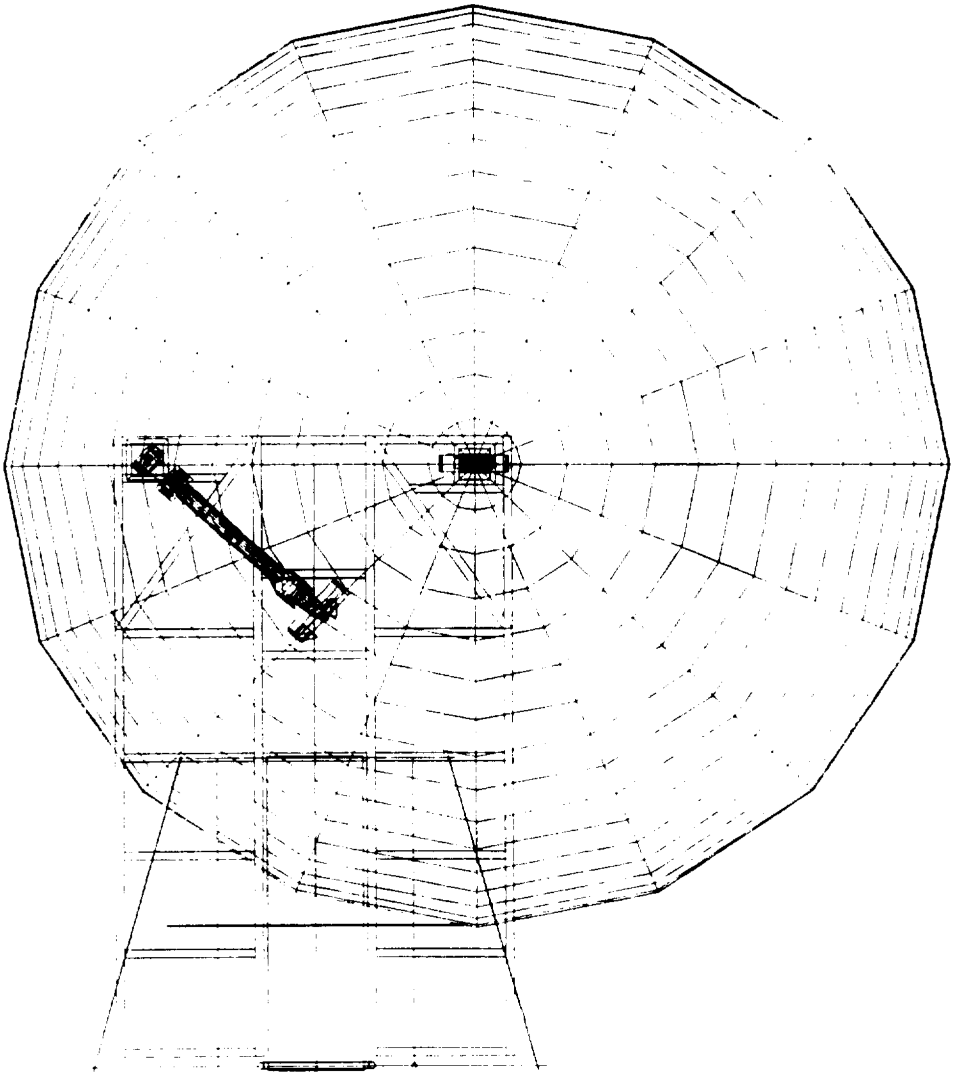

ORIGINAL PAGE IS
OF POOR QUALITY

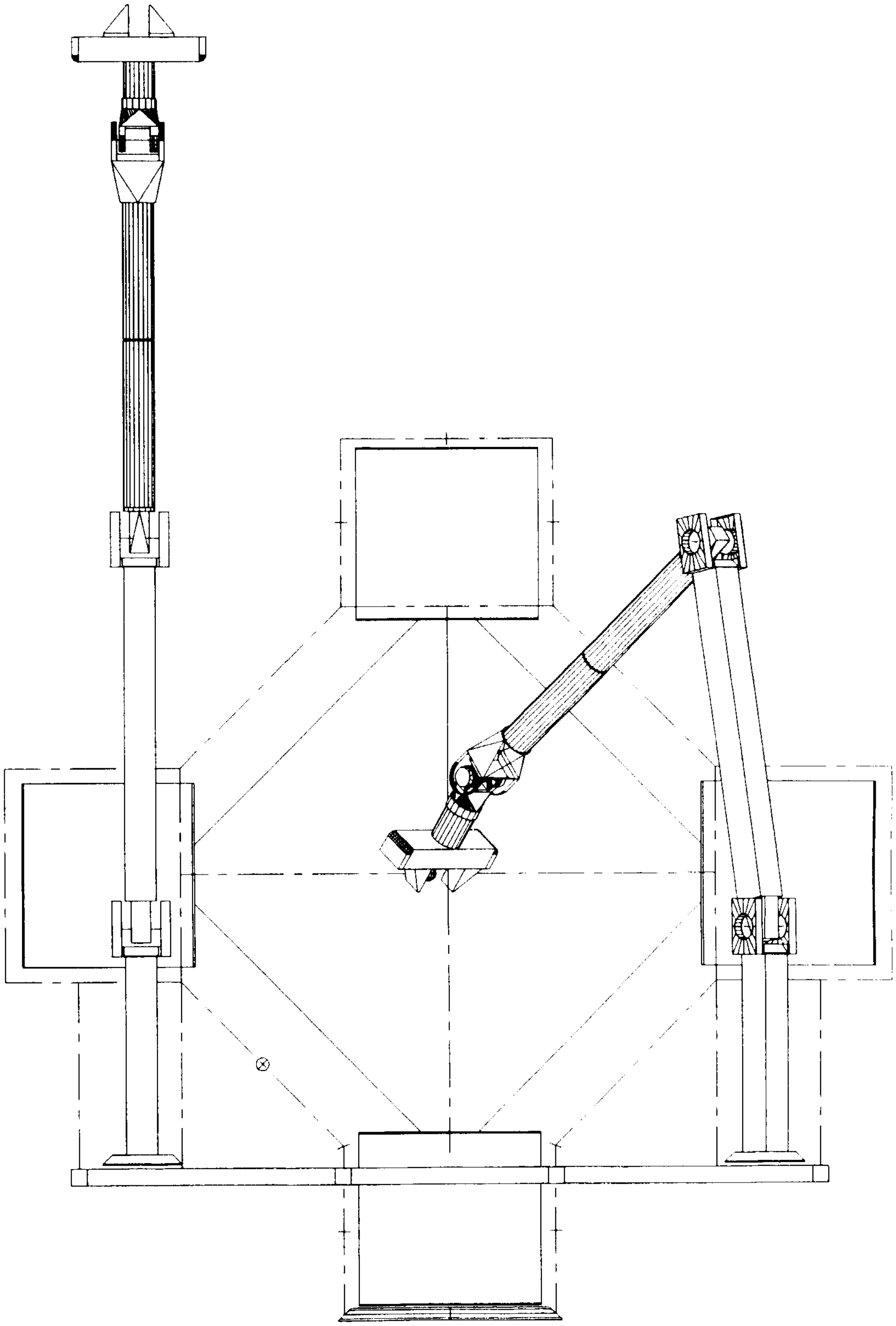

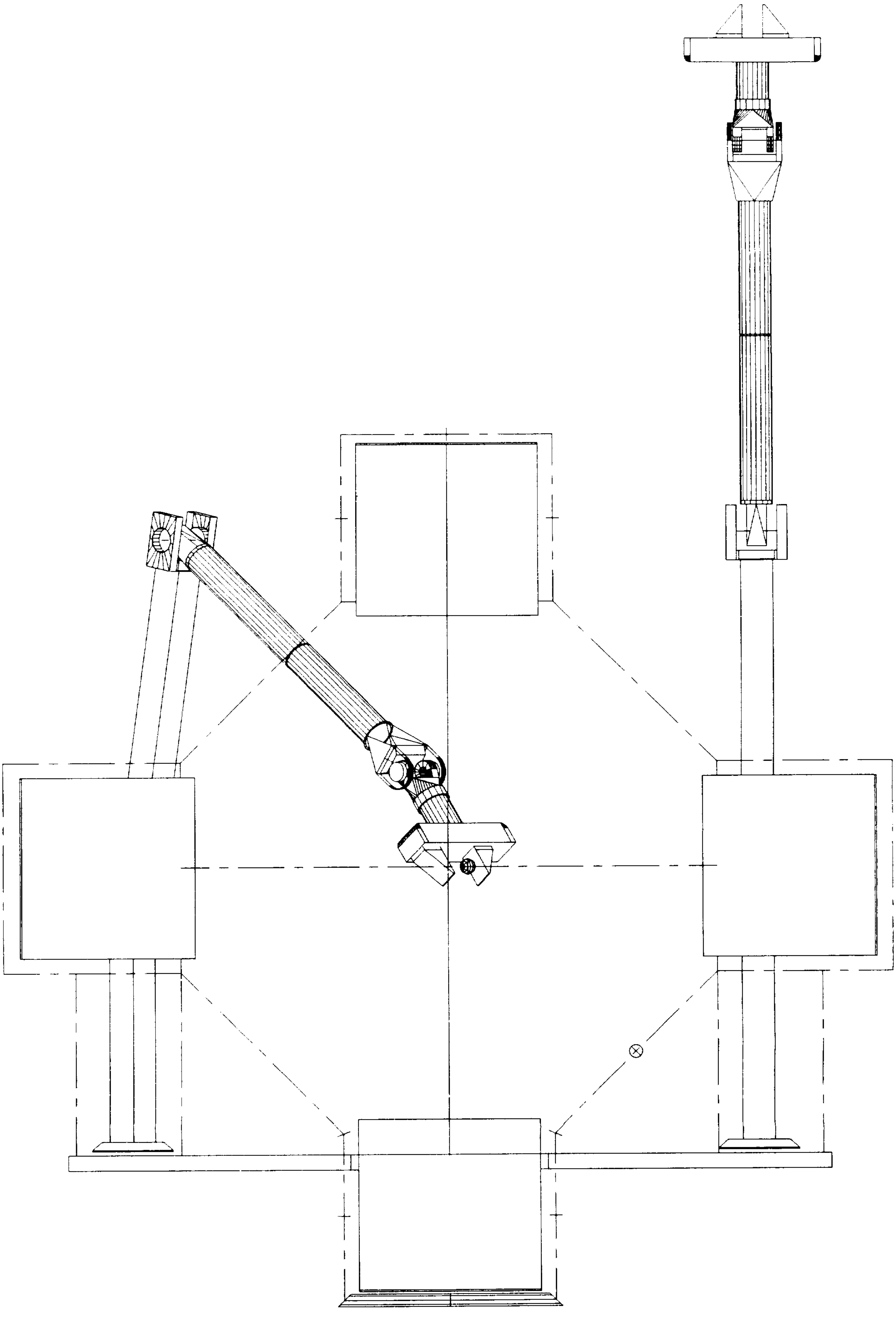

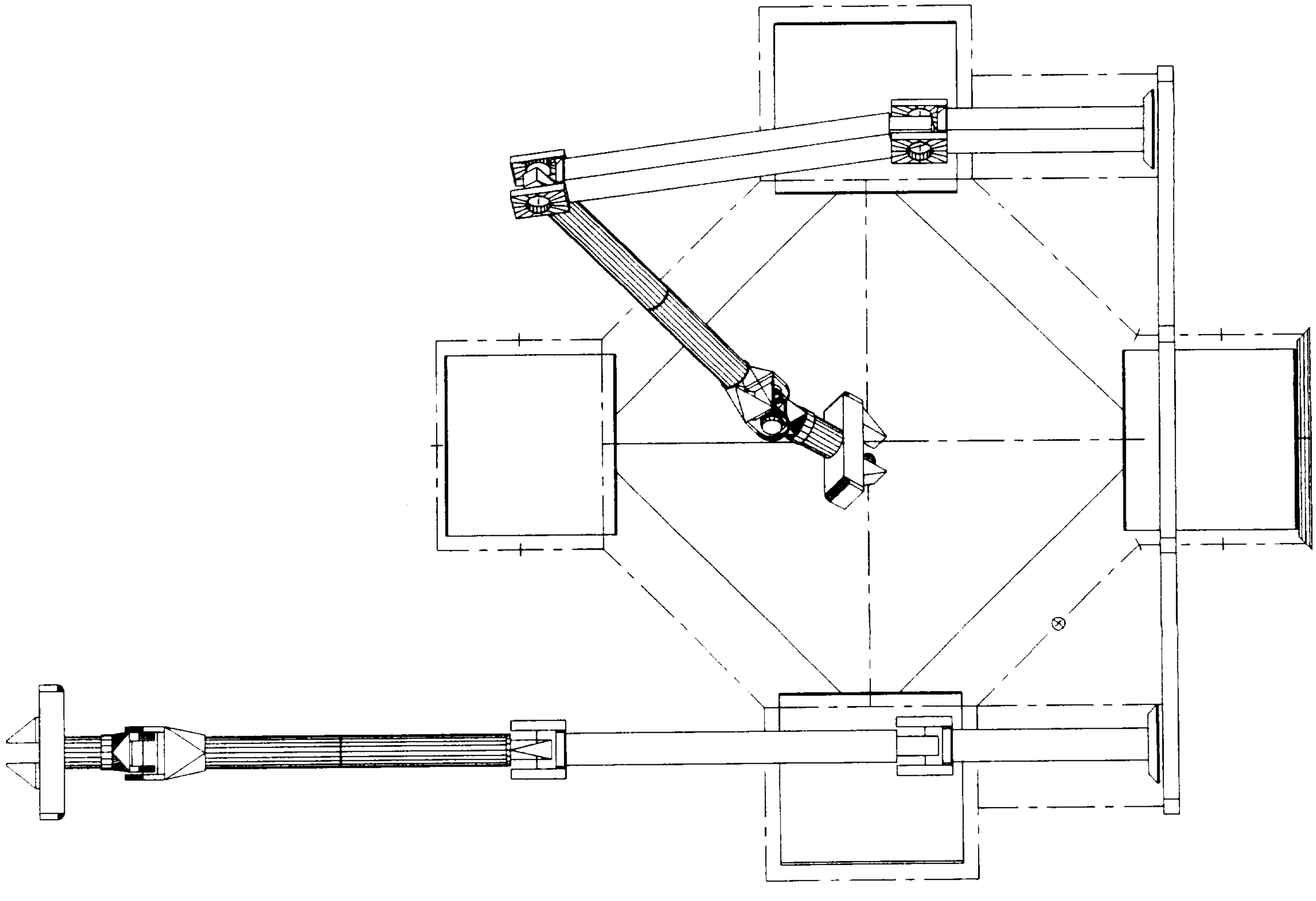

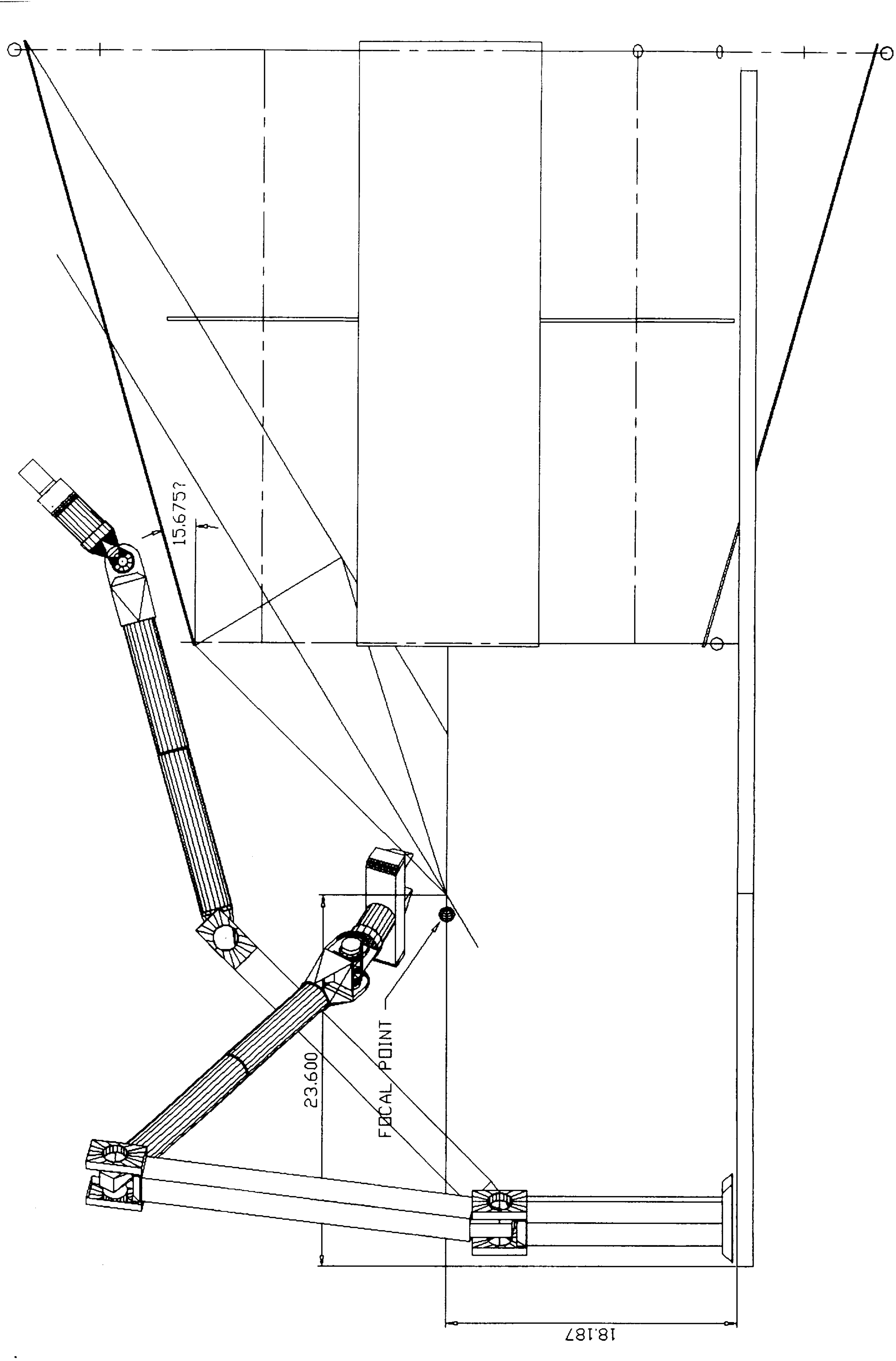
15.675?
23.600
FOCAL POINT
18.187

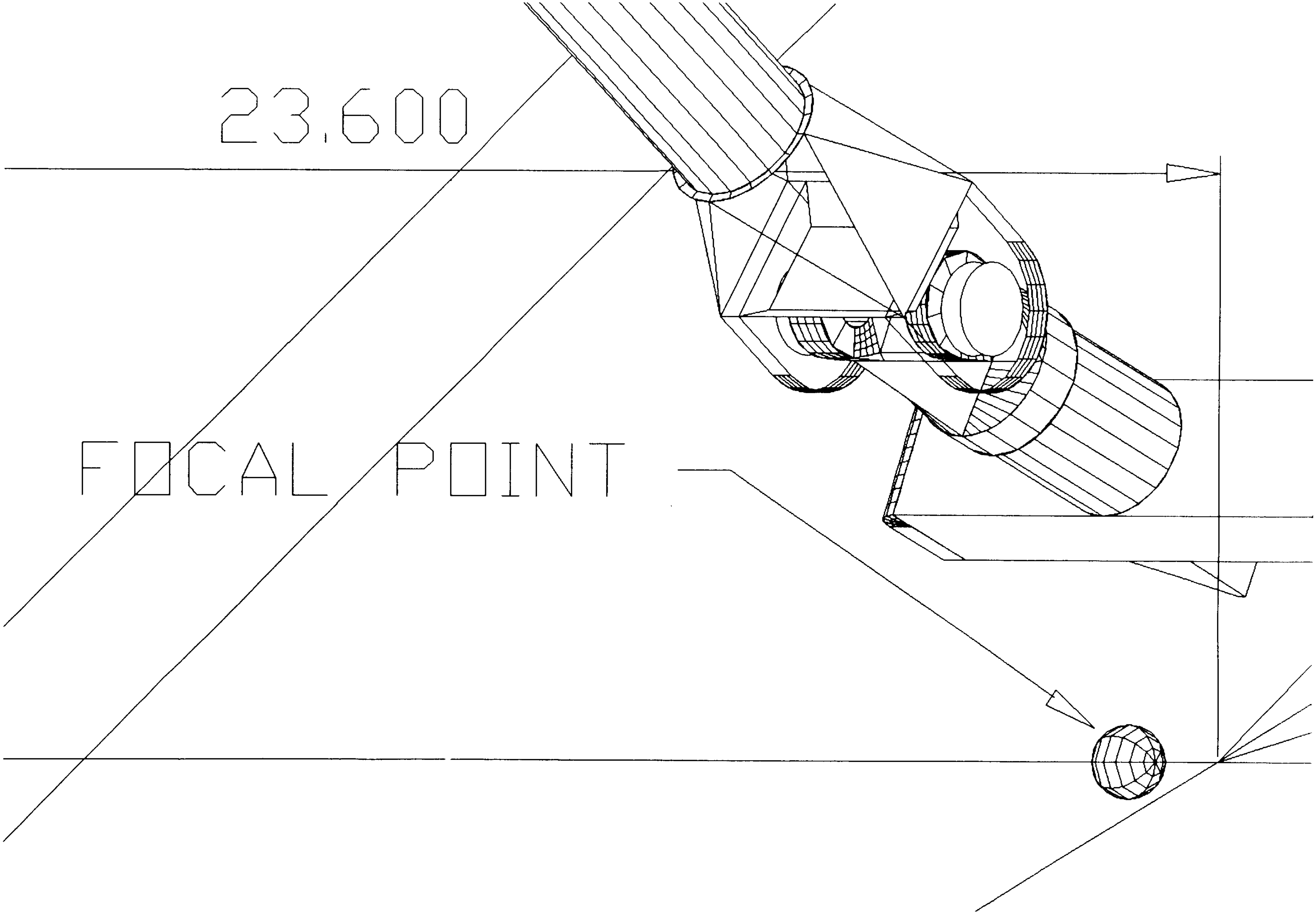
23.600
FOCAL POINT

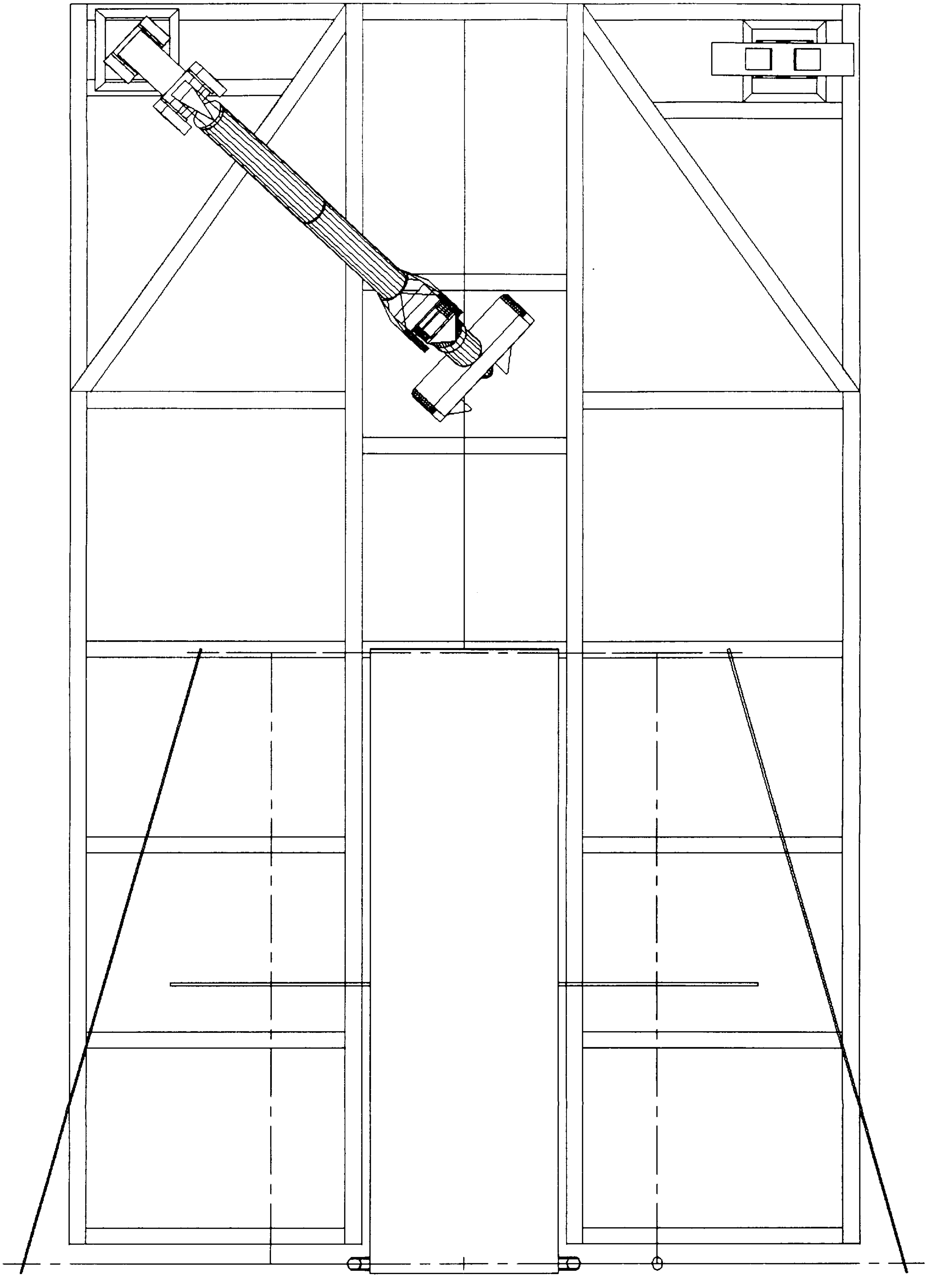

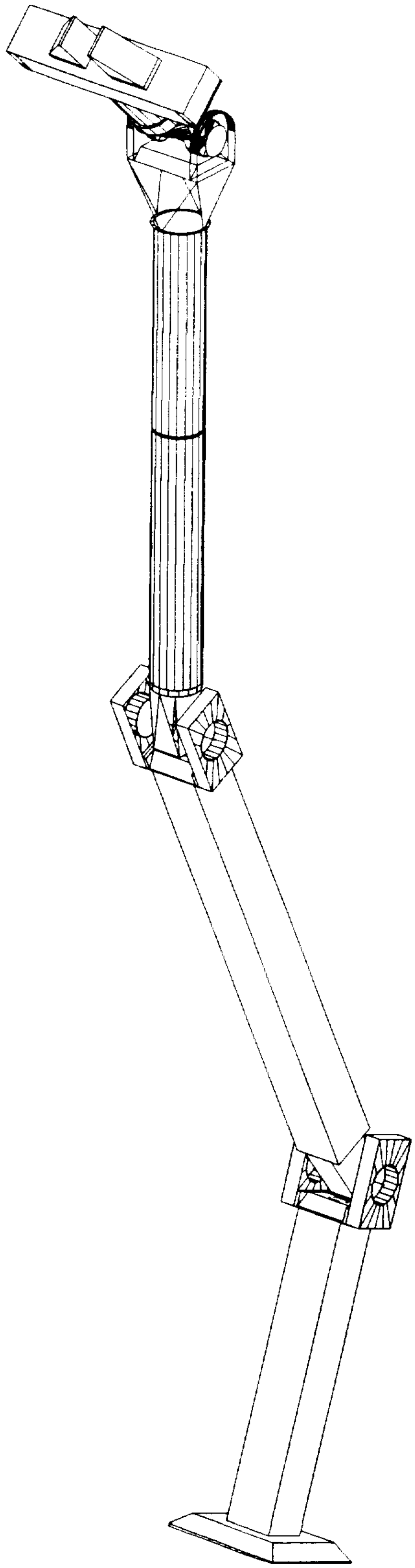

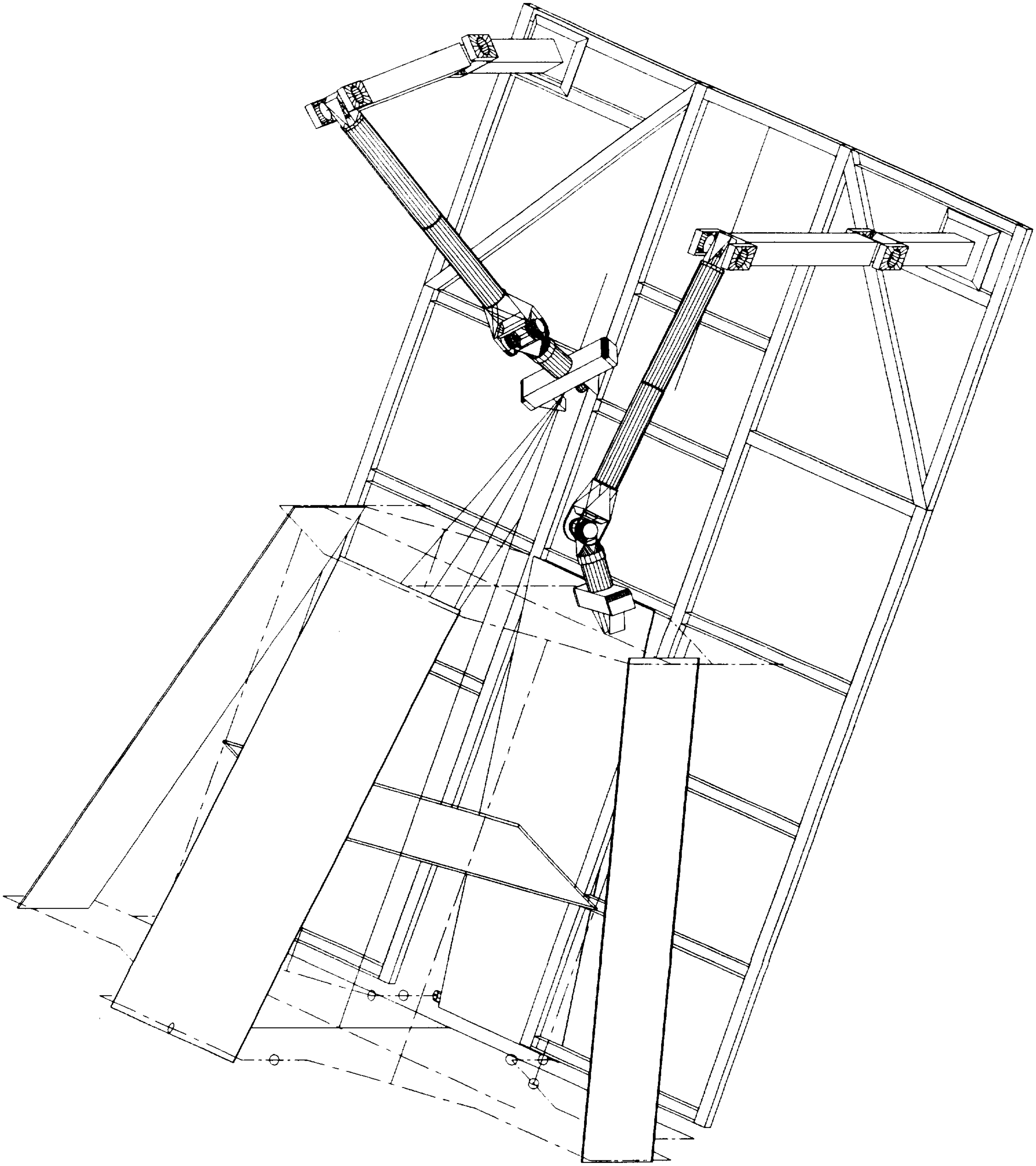

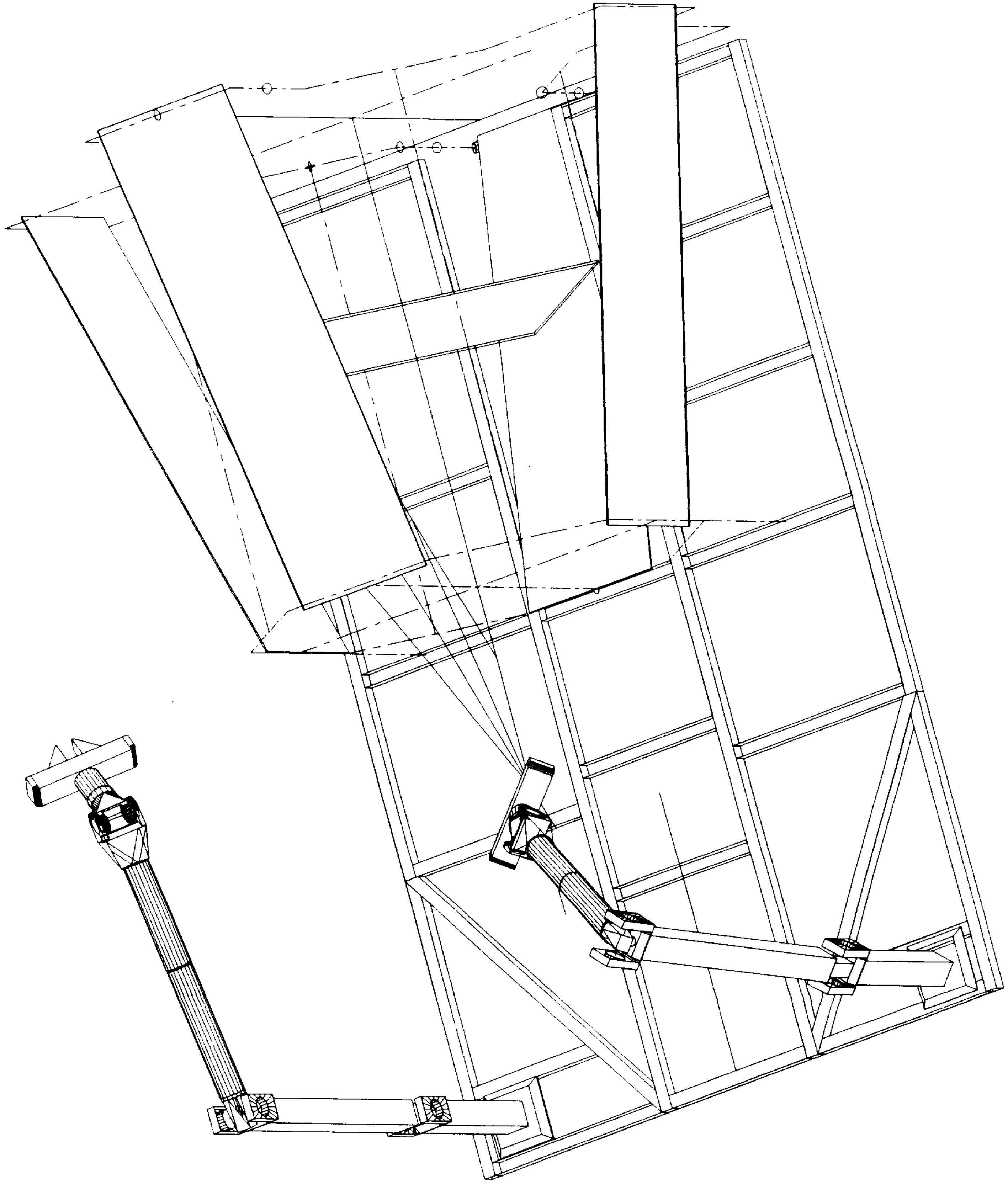

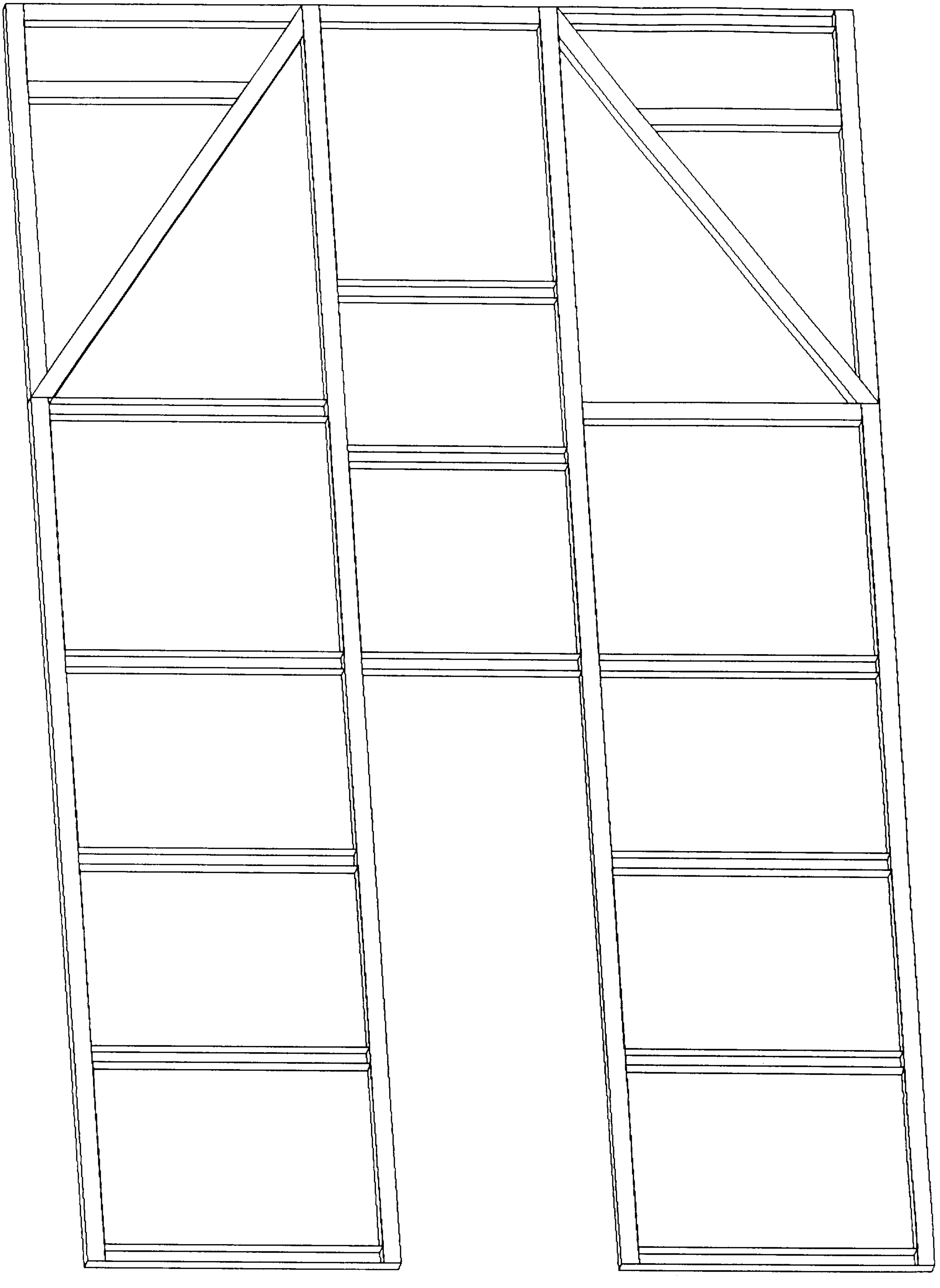

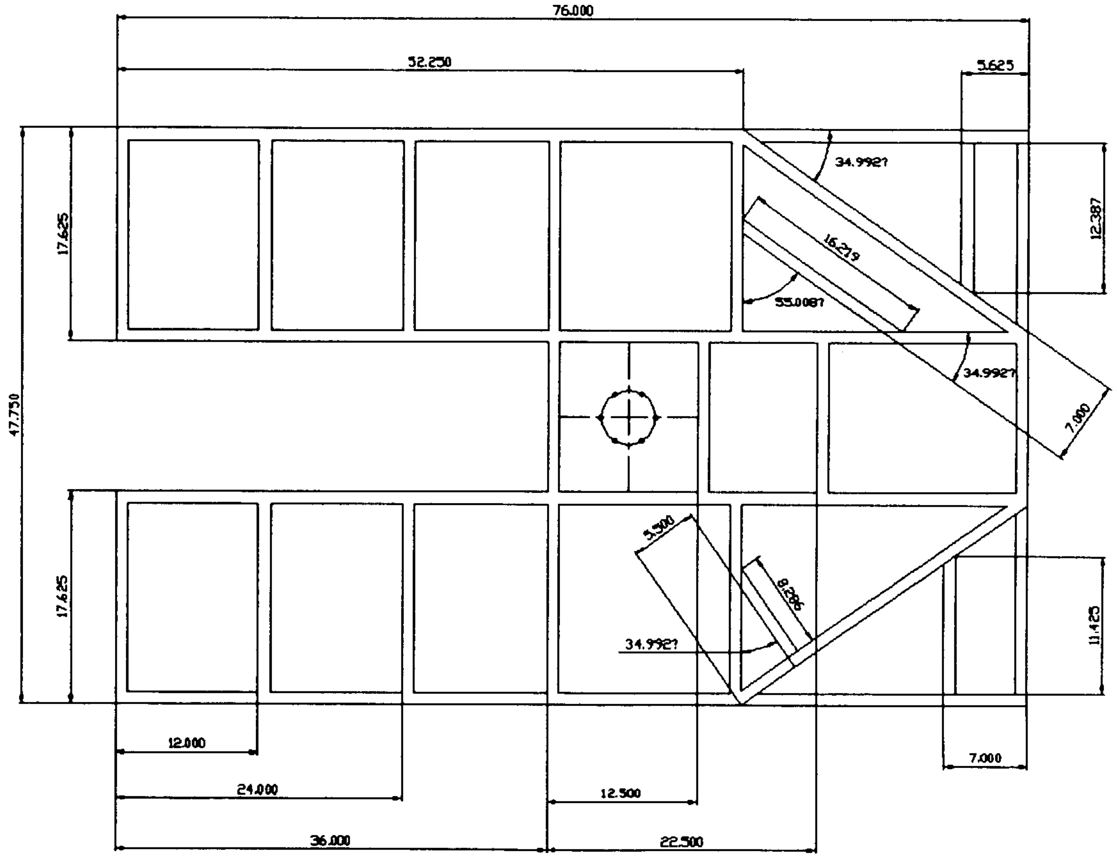
76.000
52.250
5.625
34.9927
12.387
16.219
55.0087
34.9927
7.000
47.750
17.625
17.625
5.500
8.286
34.9927
11.425
12.000
24.000
12.500
7.000
36.000
22.500

UNIVERSITY OF ARIZONA

DATE NAME

PROJECT:
AUTONOMOUS SPACE PROCESSOR
FOR ORBITAL DEBRIS (ASPOD).

TITLE:
STRUCTURE, WELDED ALUMINUM

MATERIAL:

Part No.:

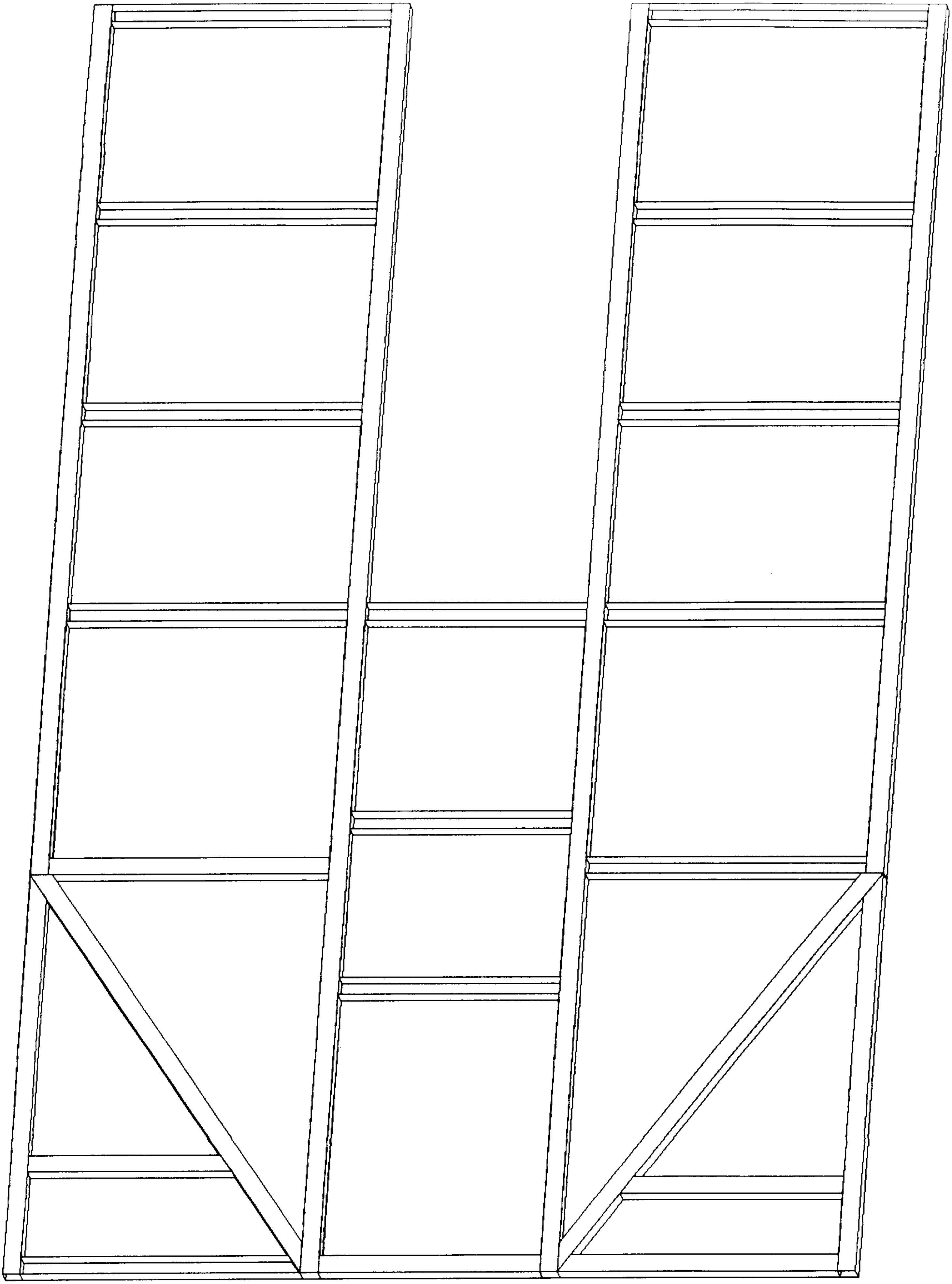FORMAT:
A1